NKS-476
ISBN 978-87-7893-571-7

COMBMORC - Combined analysis of primary and scattered components in mobile gamma spectrometric data for detection of materials out of regulatory control, NKS-B COMBMORC Report 2022

Christopher L. Rääf[1] (chair), Robert R. Finck[1] (co-chair)
Vikas C. Baranwal[5], Marius-Catalin Dinca[1]
Jon Drefvelin[6], Charlotte Alfast Espensen[2]
Kjartan Guðnason[4], Per Otto Hetland[6]
Gísli Jónsson[4], Mattias Jönsson[1]
Marie Lundgaard Davidsdóttir[2], Bredo Møller[6]
Frode Ofstad[5], Jan Gert Olsen[2]
Petri Smolander[3]

[1]Medical Radiation Physics, ITM, Lund University, Sweden
[2]Danish Emergency Management Agency, Denmark
[3]Radiation and Nuclear Safety Authority, Finland
[4]Icelandic Radiation Safety Authority, Iceland
[5]Geological Survey of Norway, Norway
[6]Norwegian Radiation and Nuclear Safety Authority, Norway

August 2023

Abstract

The NKS-supported research project COMBMORC 2021-2022 aimed to develop combined methods within mobile gamma spectrometry to search for radiation sources that have come out of the authorities' control (Material Out of Regulatory Control, MORC). In 2022, mobile gamma spectrometry teams from the Nordic countries conducted a joint field experiment in southern Sweden. The experiment was to test region-of-interest (ROI) based methods to determine ratios between detector recordings from Compton scattered and primary radiation along a road past a Cs-137 source to determine the distance, shielding and activity of the source. The assessment used two newly developed Excel applications (SSC and SODAC). On average, the distance determination was underestimated by 20 ± 3 per cent at source-detector distances of 30 - 90 m. The shield thickness determination was overestimated on average by 4 ± 9 per cent for building material thicknesses 0 - 330 kg/m^2.

Key words

Mobile gamma spectrometry, orphan sources, shielding

NKS-476
ISBN 978-87-7893-571-7
Electronic report, August 2023
NKS Secretariat
P.O. Box 49
DK - 4000 Roskilde, Denmark
Phone +45 4677 4041
www.nks.org
e-mail nks@nks.org

COMBMORC - Combined analysis of primary and scattered components in mobile gamma spectrometry for detection of materials out of regulatory control

NKS-B COMBMORC 2022
Contract: AFT/B(22)2
June 10, 2023

Coordinating organisation:

Medical Radiation Physics, ITM, Lund University, Sweden [Christopher L. Rääf (chair), Robert R. Finck (co-chair)]

Participating organisations and contact persons:

Danish Emergency Management Agency (DEMA), Denmark [Marie Lundgaard Davidsdóttir]
Radiation and Nuclear Safety Authority (STUK), Finland [Petri Smolander]
Icelandic Radiation Safety Authority (IRSA, GR), Iceland [Gísli Jónsson]
Geological Survey of Norway (NGU), Norway [Vikas Baranwal]
Norwegian Radiation and Nuclear Safety Authority (DSA), Norway [Bredo Møller]
Swedish Radiation Safety Authority, Sweden (as stakeholder)

Abstract

The NKS-supported research project COMBMORC 2021-2022 aimed to develop combined methods within mobile gamma spectrometry to search for radiation sources that have come out of the authorities' control (Material Out of Regulatory Control, MORC). In 2022, mobile gamma spectrometry teams from the Nordic countries conducted a joint field experiment in southern Sweden. The experiment was to test region-of-interest (ROI) based methods to determine ratios between detector recordings from Compton scattered and primary radiation along a road past a Cs-137 source to determine the distance, shielding and activity of the source. The assessment used two newly developed Excel applications (SSC and SODAC). On average, the distance determination was underestimated by 20 ± 3 per cent at source-detector distances of 30 - 90 m. The shield thickness determination was overestimated on average by 4 ± 9 per cent for building material thicknesses 0 - 330 kg/m^2.

Table of contents

Summary

The NKS activity COMBMORC dealt with problems in mobile search for radioactive material out of authorities' regulatory control (MORC). In particular, COMBMORC developed and explored methods to determine distance, shielding, and activity for lost gamma-ray sources by mobile gamma spectrometry. Mobile measurement teams from the Nordic countries have jointly conducted real-environment experiments with Cs-137 sources to test the methods. The activities have been ongoing during 2021 - 2022. An NKS report on results from 2021 exists. The present report describes field experiments carried out in 2022 and the results obtained.

There may be hazards around an uncontrolled radiation source that limit the possibility of a search team getting close to the source. Finding methods to determine the location and activity of a radiation source during a first search effort at a distance from the source is, therefore, essential. In a previous NKS-supported project, AUTOMORC 2018, Lund University developed a method based on Bayesian inference to determine the location and activity of unshielded gamma-ray sources when passing by a source. However, the method was computationally demanding and did not consider shielded sources in houses. Within the framework of the current project, Lund University has developed alternate methods that deal with the shielding problem and calculate distance and activity from measurement data. The Nordic mobile gamma spectrometry teams experimentally tested the methods and now report the outcome here.

The previous NKS-supported SHIELDMORC 2019 - 2020 project showed that registration of Compton scattered photons in a gamma spectrometer could form a method to determine the mass thickness of a shield positioned in front of a point-shaped gamma-ray source. The count rate from Compton photons produced in a shield (for example, a house wall) increases exponentially as the mass thickness of the shield increases linearly. By calibrating a detector's count rate for Compton photons registered in defined energy intervals (region of interest, ROI) relative to primary photons from the source for different shield thicknesses, the parameters of the exponential function can be determined. In the present COMBMORC 2022 experiments, all teams performed such a calibration. Next, the teams tested to determine shield thicknesses for five unknown irradiation geometries with Cs-137 sources at three different distances 30, 60 and 90 meters from the mobile gamma spectrometers. An Excel application developed by Lund University, called SSC (Source Shielding Calculator), handled the calibration data and the shield mass thickness assessments. The exponential model overestimated the shield mass thicknesses for all five setups on average by 1.6 ± 10 per cent. The overestimation was 4 ± 9 per cent when combined with a polynomial model. However, single measurements could show over- or underestimations of several tens per cent, depending on counting statistics, background subtraction correctness, and spectrometer gain drift.

The distance to a point-shaped gamma-ray source can be determined based on geometrical assumptions and physical laws for attenuating gamma rays in matter. Suppose that measurements of a radiation source's primary photon fluence rate occur along a straight road that passes the source. Then a mathematical relationship exists between the source's distance to the road and the distribution of primary fluence

measurements along the road. An Excel routine developed by Lund University, called SODAC, uses this relationship to determine the distance to a radiation source. The SSC routine mentioned above can determine the shielding of the radiation source from the pulse height distribution of the gamma spectrometer. When the distance and shielding are known, SODAC can calculate the radiation source's activity from the gamma spectrometer's count rate for the primary fluence. The Teams made semi-stationary measurements for 5 - 10 minutes at each point along the road past a source to obtain enough statistical accuracy in the recorded pulse height distribution. Then, the teams combined SODAC and SSC to determine distance, shielding, and activity for the five unknown irradiation geometries with Cs-137 point sources.

The SODAC estimated distances were, on average, underestimated by 20 ± 3 per cent. The calculated activity deviation from the actual values was, on average, 0 ± 13 per cent when the estimated distances to the source were applied and overestimated by 83 ± 17 per cent when the actual distances were applied. Unfortunately, vegetation shielded part of the measurements, which may have contributed to the observed underestimation of the distance to the source. Another reason for underestimating the distance may be that some teams did not possess sufficient angular efficiency correction data for their detector types.

SSC and SODAC methods enable the determination of the distance, shielding and activity of unknown Cs-137 sources by mobile gamma spectrometry making semi-stationary measurements along a straight road past the source. There are limitations in the methods that need further investigation. The COMBMORC experiments were the first of their kind, and it would be desirable to carry out complementary, carefully controlled experimental investigations to determine the practical applicability of the methods in search of lost gamma-ray sources.

1. Introduction

Lost radioactive sources (material out of regulatory control, MORC) can expose people to radiation hazards. Since human senses cannot detect ionising radiation, measuring instruments must be used to search for and identify a lost radiation source. Mobile gamma spectrometry is one method of searching for lost radiation sources (e.g. Hjerpe *et al.* 2001; Aage and Korsbech, 2003; Kock, 2012; Nilsson, 2016). The Nordic radiation safety authorities have equipment and personnel trained in mobile search of radiation sources. Exercises with radiation source search have been performed in the Nordic countries. (Finck and Ulvsand, 2003; Finck *et al.* 2008; Östlund *et al.* 2012). Experiences from the exercises show that locating lost radiation sources over large areas is a challenge. False positive signals due to natural variations in the background radiation are one of the problems that prevent the detection of weak signals from a distant source. Another problem is that sources may be hidden in buildings where the radiation is shielded, which makes it challenging to discover sources even when they are closer to the detection equipment.

Methods to detect gamma-emitting sources with mobile gamma spectrometry have been developed and experimentally tested by mobile teams from the Nordic countries in a series of NKS-funded research projects MOMORC 2016 (Finck *et al.* 2017), AUTOMORC 2017-2018 (Rääf *et al.* 2019) and SHIELDMORC (Rääf *et al.* 2020, 2021). The results of the experiments have shown that the signals obtained in different parts of a mobile gamma spectrometer's pulse height distribution are unique for the distance and shielding of the radiation source and for the detector used. By experimentally calibrating[1] a mobile detector's response in different photon energy intervals (regions-of-interest, ROIs) for known shield thicknesses and distances, it is possible to create a ”knowledge library” that can be used to determine the shielding of a gamma ray source. (Rääf *et al.* 2021). The method has so far mainly been tested for Cs-137 point sources and, to a lesser extent, for Co-60. However, it should reasonably apply to other radionuclides with a few primary gamma energies.

In order to calculate the activity of a radiation source, it is necessary to know the distance to the source, in addition to knowledge of the shield thickness. Lund University has developed a method to determine the distance to a radiation source from a series of measurements when the measuring device passes along the road past the source. (Bukartas *et al.* 2019). The method is based on Markov Chain Monte Carlo simulation and Bayesian inference, where the physical radiation field from a point source constitutes an invariant assumption. The method is computationally demanding. A more straightforward method to determine the distance to a radiation source can be applied by comparing a series of measurements along the path past the source with theoretically calculated photon fluence rates from radiation sources at different distances. The most probable distance is where the difference between measured data along the route and theoretically calculated data shows a minimum, which is the method applied in this experimental investigation.

Aim of COMBMORC 2022

The aim of COMBMORC 2022 was to carry out joint Nordic field experiments with mobile gamma spectrometry to verify ROI-based methods using combined analysis of

[1] The word “calibration” is used here as a broader concept of determining parameters in a model than in its strict sense of correcting a measuring instrument's deviation according to traceable standards.

registrations from scattered and primary radiation to determine the distance to radiation sources and estimate shielding thickness and source activity.

2. Theory

When a mobile gamma spectrometer passes a radiation source and acquires measurements at short intervals, the recorded pulse height distributions will contain information that is characteristic of the distance to the radiation source and the shielding of the source. Below is a brief account of how this information can be used to determine distance, shielding and activity for the radiation source.

2.1 Determining the shielding of a source by Compton photons

The method of determining shield mass thicknesses based on registrations of single and multiple scattered Compton photons from the shield has been described in detail in the NKS SHIELDMORC report 2020 (Rääf *et al.* 2021). It is valid for shield material having atomic numbers below 25, which is common in building materials. The method is based on net (background subtracted) count rate ratios for specified energy intervals in the pulse height distribution, called regions of interest (ROI). Count rates in energy regions below the primary radiation represent single or multiple Compton scattered photons. Three energy regions were defined for Compton scattered radiation (ROI A, B and C) and two for primary photons from the source (ROI PR and P). ROI P represents the entire energy range around the full energy peak, and ROI PR represents the right half of the full energy peak. The net count rate ratios ROI A/PR, B/PR, C/PR and ROI A/P, B/P and C/P from scattered to primary photons are calculated from the registered pulse height distributions.

2.1.1 Exponential model

The SHIELDMORC experiment found that background subtracted count rate ratios $q = q_g - q_b$ increase nearly exponentially with increasing shield mass thickness $z\rho$.

$$q = a\,e^{b\,z\,\rho} \tag{1}$$

where q_g represents the gross count rate ratios A/PR, B/PR … C/P, respectively and q_b represents the background count rate ratios for the same regions. ρ is the shield density, and z is the linear shield thickness. The coefficients a and b are determined by fitting experimental calibration data to the exponential equation.

The mass thickness $z\rho$ is obtained by solving Eqn(1):

$$z\,\rho = \frac{\ln(q/a)}{b} \tag{2}$$

Each measured net count rate ratio provides a value of the shield mass thickness $z\rho$, so using the six ROI ratios above provides six solutions for the shield mass thickness, all of which should give approximately the same value. The six solutions to the problem showing individual variations, which may be due to statistical fluctuations in the net count rate data, will indicate the accuracy in the shield thickness determination.

2.1.2 Polynomial model

When looking at a plot of mass shield thickness versus ROI net count rate ratios for the exponential model, the fitted exponential function does not perfectly follow the measured data. Some systematic deviations seem to occur. To test whether a better fit could be made with a function that follows the measurement data more closely, a five-degree polynomial function has been tested:

$$z\rho = a_5 (\ln q)^5 + a_4 (\ln q)^4 + a_3 (\ln q)^3 + a_2 (\ln q)^2 + a_1 (\ln q) + a_0 \qquad (3)$$

where a_0 - a_5 are the polynomial coefficients obtained by fitting the five-degree polynomial to the calibration net count rate ratios q for the known mass shield thicknesses.

With the polynomial function, it is possible to better adapt the function to the measurement data in a limited range for the net count rate ratios. Outside the range, however, the fit is completely derailed. It is, therefore, essential to identify the minimum and maximum values for the background subtracted count rate ratio within which the polynomial function applies. In this work, the maximum and minimum borders have been set to 15 per cent beyond the background subtracted count rate values obtained for the thickest and thinnest shields in the calibration measurements.

2.1.3 Regions of interest (ROI) for shield thickness determination

Defining regions of interest (ROI) instead of using the entire pulse height distribution channel by channel facilitates the implementation of the background subtracted count rate ratio method to determine shield mass thickness. It is relatively easy to implement because all software for gamma spectrometry can output sums of count rates for selectable energy intervals.

For COMBMORC, six ROIs are used, which represents Compton scattered and primary radiation from a Cs-137 point source. Table 1 gives the selected ROI subdivisions into energy intervals and which photon interaction they generally represent.

Table 1. Energy regions for NaI(Tl) spectrometers in the COMBMORC experiments, assuming a channel width of 3 keV. The energy regions may have to be adjusted to the channel division for other channel widths.

Region designation	Energy interval (keV)	Detected photons from the source are mainly…
ROI A	77 – 239	Compton scattered 110 - 180 degrees and multiple scattered
ROI B	245 – 407	Compton scattered 27 - 58 degrees
ROI C	413 – 575	Compton scattered 0 - 27 degrees
ROI PL	581 – 659	Primary and small angle Compton scattered
ROI PR	665 – 743	Primary
ROI P	581 – 743	Primary and small angle Compton scattered

For a NaI(Tl) spectrometer, there is always a substantial overlap of photon energies into adjacent ROIs because of the spectrometers’ low energy resolution.

For an HPGe spectrometer, the higher energy resolution produces less overlap between primary and Compton scattered photons. The full energy peak ROI P is used in its entity and not divided. The NaI(Tl) energy region ROI PL contains only scattered photons and is for HPGe spectrometers called ROI PLN or ROI D.

More information on individual teams' selection of ROI channels is provided in Appendix I.

2.2 Determining the shielding of a source by primary photons

There is a way to estimate the shield thickness using only the registrations of primary photons from the shielded radiation source, assuming the shield is of the slab type. (Fig 1). The primary photon fluence $\phi(\theta)$ passing through the shield at an angle θ will be attenuated more than the photon fluence $\phi(0)$ passing straight through the shield at $\theta = 0$. The photon fluence ratio can be expressed:

$$\frac{\phi(\theta)}{\phi(0)} = \frac{e^{-\mu z(\theta)}}{e^{-\mu z}} \tag{4}$$

where μ is the linear attenuation coefficient of the shield, which can be replaced by the mass attenuation coefficient μ/ρ of the shield if multiplied by the shield density ρ. For common building material (with atomic numbers 3 - 25) the mass attenuation coefficient for 662 keV photons is approximately 0.008 m^2/kg. The path length through the shield $z(\theta)$ at an angle θ can also be expressed as:

$$z(\theta) = z/\cos(\theta) \tag{5}$$

From Eqs 1 and 2, the shield thickness can be solved from a measured ratio $\phi(\theta)/\phi(0)$ or the corresponding full energy peak count rate ratio, corrected for the detector's varying angular efficiency.

The typical situation in mobile gamma spectrometry is to measure along a road that passes the radiation source. The photon fluence along the road varies according to Eqn 7. The photon fluence generates a near bell-shaped curve with a maximum centred just opposite the source. (Fig 2). The curve's width is a function of the distance x between the source and the nearest point on the road. For an unshielded source, the photon fluence function can be used to determine the distance to the source, assuming the road past the source is straight (described in Section 2.3).

If the source has a slab-type shield, the width of the photon fluence curve will decrease because the attenuation for oblique penetration through the shield increases relative to straight penetration. (Fig 2). Suppose the distance to the source is known (other than by photon fluence measurement). In that case, it is theoretically possible to determine the thickness of the shield by making photon fluence measurements at a few points along the road and finding the photon fluence function for shielded sources that best fits the measurement data.

In practice, however, this method requires measurement data with low statistical uncertainty, which is challenging to meet. The detector angular efficiency needs to be well known so that correction for the efficiency as a function of the angle of incidence θ can be made when calculating the photon fluence from the source.

Suppose both the distance to the source and the angular efficiency of the detector are unknown. In that case, the method of primary photon fluence cannot be used to determine the shield thickness because there are too many unknown factors.

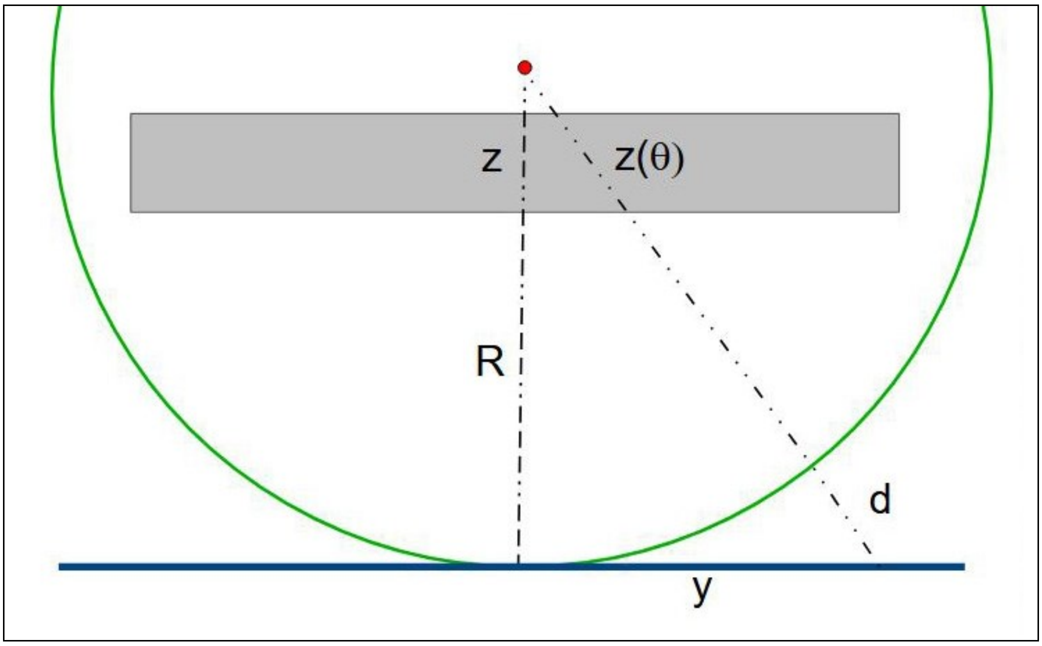

Fig 1. Principle sketch of the geometry of a point-shaped photon source, a shield and the location of measuring instruments along a circular periphery (green) or along a straight road past the source (blue). $R = x$ at $y = 0$ in Eqn 7.

2.3 Determining the distance and activity of a source

Information about the distance to a radiation source is necessary to calculate the source's activity from measurements of the photon fluence rate. Since the primary photon fluence in air monotonically decreases with increasing distance to the source (provided free sight between the source and the detector), gamma spectrometric measurements of the primary fluence represented in the full energy peak at a few (at least two) locations can, in principle, provide information of the source-detector distance.

2.3.1 Distance to an unshielded point source

The primary (unscattered) photon fluence rate $\dot{\phi}$ in the air at a distance R from a point source emitting $\dot{S}$ photons per second can be expressed by the "point kernel" equation:

$$\dot{\phi}\left(R,\dot{S}\right) = \frac{\dot{S}\, e^{-\frac{\mu_a}{\rho_a}\rho_a R}}{4\pi R^2} \tag{6}$$

where $\frac{\mu_a}{\rho_a}$ is the mass attenuation coefficient of air and ρ_a is the air density.

Dividing R into two distances, x and y, where y is the distance along a straight road past the source, $-\infty < y < +\infty$, and x is the perpendicular distance from the road to the source defined at the point $y = 0$, the primary fluence rate can be expressed:

$$\dot{\varphi}\left(x, y, \dot{S}\right) = \frac{\dot{S}\, e^{-\frac{\mu_a}{\rho_a}\rho_a\sqrt{x^2 + y^2}}}{4\pi\left(x^2 + y^2\right)} \tag{7}$$

For each chosen source distance x, the primary photon fluence rate along the road $\dot{\varphi}(y, \dot{S})$ forms a type of Lorentzian curve with exponential tails subtracted aroundthe location $y = 0$ (but not a Gaussian shape). This photon fluence rate curve is sometimes called the "intensity curve" along the road. Fig 2 shows an example of curve shapes for source distances $x = 50$ and $x = 100$ m. Curves widen as the distance x from the road to the source increases. The curve shape (the width relative to the height) depends on the distance x, but it is independent of the photon emission rate $\dot{S}$ (or the source activity).

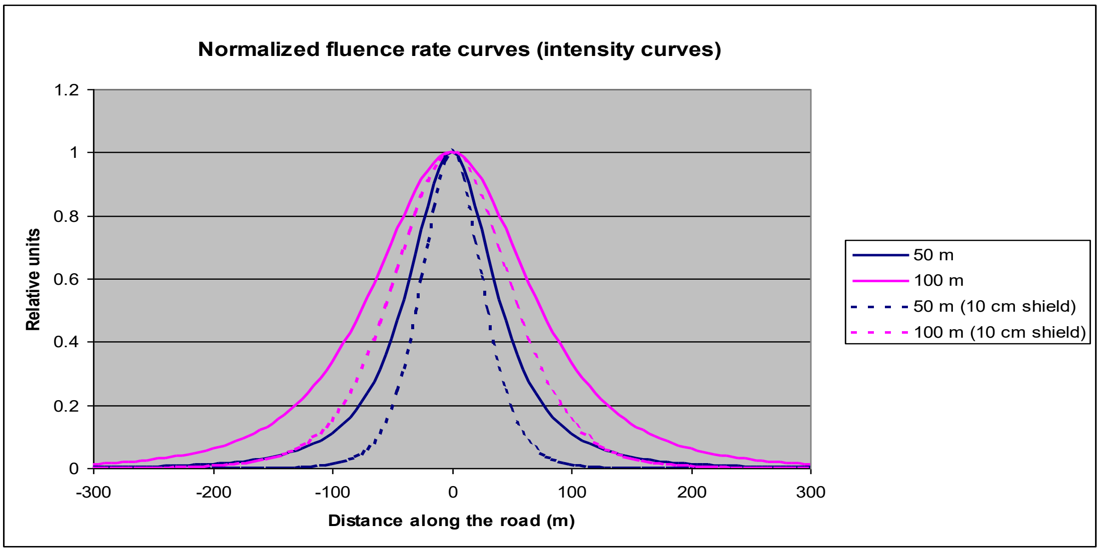

Fig 2. Normalized fluence rate curves from a Cs-137 point source at 50 m (blue line) and 100 m (magenta line) from the measurement route. Solid lines are valid for an unshielded source. Dotted lines are valid for a source with a 10 cm thick concrete slab shield in front of the source. The shielding produces reduced tails in the fluence rate curves.

The distance x in Eqn (7) cannot be solved as a simple analytical expression, but x could be solved using a numerical method (Finck *et al*. 2022). However, this work choose a different "knowledge library-type" approach. By comparing measured photon fluence rates at different locations, y, along the road with a library of theoretically calculated photon fluence rates for different road-source distances, x, it is possible to identify which library curve best corresponds to the measured data. If the measurement statistics are good, the distance to the source can be easily determined. Lund University has developed software (the Excel application SODAC) to determine distances.

2.3.2 Correcting for the detector's varying angular efficiency

Using a pre-computed library of photon fluence ("intensity") curves for different distances assumes the detector's efficiency for recording photons with different incidence angles does not vary. The assumption is correct if the detector has a spherical shape and approximately correct if it has a cylindrical shape where the height and diameter of the cylinder are equal. Equal dimensions are the case for 3"x3" NaI(Tl) crystals but not for 4-litre NaI(Tl) crystals which have an oblong shape. Suppose a 4-litre NaI(Tl) crystal is placed horizontally in the measuring vehicle. In that case it exhibits a significant reduction in efficiency for photons incident at angles of 30 - 90 degrees relative to the long side of the detector (90 degrees is the short side of the detector). When measured count rates are converted to fluence rates, the varying angular detector efficiency must be considered before searching "the knowledge library" for the closest resembling fluence function $\dot{\varphi}\left(x,y,\dot{S}\right)$ in Eqn 7. However, the angle to the radiation source is unknown because the distance y to the source is unknown. There are two unknown variables and theoretically, no solution can be found to match Eqn. 7 for a detector with varying angular efficiency. This difficulty is partially overcome in the Excel routine SODAC, where an iterative process has been introduced for the searched distance x, which, with knowledge of the detector angular efficiency, searches for the x value that gives the best fit between the measured count rates in the full energy peak and theoretically calculated photon fluence rates in the measurement points along the road passing the source.

Lund University measured the angular efficiency for a 4-litre NaI(Tl) detector in connection with the NKS AUTOMORC research project (Rääf *et al.* 2019). Fig 3 shows the variation in angular efficiency due to the detector's elongated shape. Table 2 provides the correction coefficients applied in the SODAC routine when the detector is oriented horizontally with its long side to the side of the vehicle.

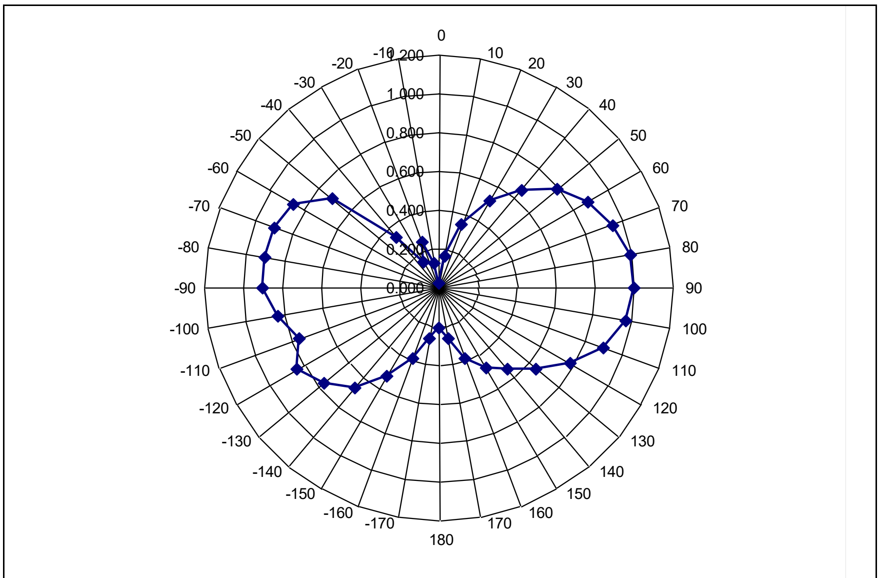

Fig 3. Relative angular efficiency for a mobile 4-litre NaI(Tl) detector at 662 keV. The detector is mounted in its long direction along the vehicle. Efficiency values are normalised to 90 degrees to the right of the forward direction. The photomultiplier tube is oriented to the back. The detector is shielded by another NaI(Tl) detector in the front direction - 10 to +10 degrees.

Table 2. Angular correction coefficients used in SODAC for a 4-litre NaI(Tl) detector mounted along the measuring vehicle. Values are normalised to 90 degrees to the right of the forward direction.

Angle degrees	Correction coefficient	Angle degrees	Correction coefficient
0	0.206	90	1.000
10	0.236	95	0.996
20	0.342	100	0.984
30	0.479	110	0.936
40	0.621	120	0.858
50	0.751	130	0.751
60	0.858	140	0.621
70	0.936	150	0.479
80	0.984	160	0.341
85	0.996	170	0.236
90	1.000	180	0.206

2.3.3 Activity of an unshielded point source

The primary fluence rate from the point source can be calculated from the measured full energy peak count rate $\dot{N}$ by:

$$\dot{\phi} = \frac{\dot{N}}{\varepsilon} \tag{8}$$

where ε is the effective detector area (m^2) for the primary photon energy in question (662 keV for Cs-137), also called the detector field efficiency.

The maximum full energy peak count rate along the road is obtained at the location with the shortest distance between the road and the source (location y = 0). At that point, the distance to the source is known from the calculation procedure mentioned above. Then the activity, A, of the source can be calculated from the maximum count rate $\dot{N}$:

$$A = \frac{\dot{N}}{\beta\ \dot{\phi}(x)\ \varepsilon} \tag{9}$$

where β is the transition's branching ratio (photons per decay). The SODAC application software does this calculation automatically from the measured count rate.

2.3.4 Distance to a shielded point source

For a point source with a slab shield, an additional exponential term for the attenuation in the shield must be included in Eqn 7, becoming:

$$\dot{\varphi}\left(x,y,\dot{S}\right) = \frac{\dot{S}\ e^{-\frac{\mu_a}{\rho_a}\rho_a\sqrt{x^2+y^2}}\ e^{-\frac{\mu_s}{\rho_s}\rho_s\ z_s\ \sec\theta}}{4\pi\left(x^2+y^2\right)} \tag{10}$$

where $\frac{\mu_s}{\rho_s}$ is the mass attenuation coefficient of the shield, ρ_s is the density of the shield material, and z_s is the linear thickness of the shield (m). The product $\rho_s z_s$ is the mass thickness of the shield (kg/m^2). The term sec θ = 1/cos θ considers the penetration angle for primary photons through the shield in the direction of the measurement point (x,y). If layers of different shielding materials are present, Eqn 10 should be multiplied with further exponential terms. In this case, it is assumed that the thickness z_s of the shield is much smaller than the distance x.

The presence of additional exponential terms in Eqn 10, describing the attenuation in the shield, leads to narrowing the width of the photon fluence rate curve along the road. The narrowing can be seen in Fig 2, where the dotted lines represent the x = 50 and x = 100 m curves, with a 10 cm concrete slab shield in front of the source. Such curve narrowing can be detected in the primary count rate region of the spectrometer if measurements are made far enough along the road from the maximum count rate point y = 0. Measurements should be made at least as far away from y = 0 along the road as the distance x to the source, giving the penetration angle θ = 45 degrees of the primary photons through the shield. Because of the longer distance to the source and the increased shielding, measurement times at these locations must be long enough to obtain sufficient counting statistics. As a rule of thumb, measurement times should be at least four times longer at $\theta = 45$ degrees than at $\theta = 0$ degrees (y = 0).

Theoretically, it would be possible to determine whether the radiation source has a shield using the shape of the "intensity" curve along the road passing the source. In practice, however, getting good statistical measurement accuracy can be difficult. The narrower "intensity" curve resulting from a shielded radiation source can easily be confused with the narrower curve that applies to a radiation source closer to the road.

The best method to determine the possible shielding of the radiation source is to use the regions-of-interest (ROI) method described above with net ratios between scattered and primary radiation registrations. It may require a longer stationary measurement to be made at the point y = 0. However, it should be noted that the ROI method assumes that the source shield is made of building material, is of a homogeneous slab type and is extended perpendicular to the line between the source and the detector. Otherwise, the ROI method may give incorrect values for the shield thickness.

2.3.5 Activity of a shielded point source

If a radiation source is shielded, part of the primary photon fluence will be attenuated in the shield. The count rate in the spectrometer's full energy peak is then reduced compared to what would be obtained if the source was unshielded. Using Eqs 8 and 9 to calculate the source activity will provide a value that is too low, i.e. the source gets a virtually lower activity value. To obtain the source's real activity, the mass thickness of the shield $\rho_s z_s$ and its mass attenuation coefficient μ_s/ρ_s must be known. Then the actual activity A can be obtained from the virtual activity A_v by the relation:

$$A = \frac{A_v}{e^{-\frac{\mu_s}{\rho_s}\rho_s z_s}} \tag{11}$$

If the actual composition of the radiation shield is unknown, but if it can be assumed that it consists of standard building material, then the mass attenuation coefficient can be set to 0.008 m^2/kg for the gamma energy 662 keV (Cs-137) because the mass attenuation coefficient for materials with atomic numbers 2 - 25 varies little (Rääf *et al.* 2020).

3. Experimental method

The COMBMORC 2022 field experiments occurred outside the decommissioned Barsebäck nuclear power station in Sweden on October 11 – 13, 2022. Six teams from Denmark (1), Finland (1), Norway (2), Iceland (1), and Sweden (1) participated in the mobile gamma spectrometric measurements.

3.1 Location of the field experiments

Fig 4 shows the location of the experiments at the Barsebäck nuclear power station.

Fig 4. The location of the COMBMORC 2022 experiment is near the former Barsebäck NPP. Site C was the parking lot used for the shielding calibration measurements. Site M was the crossroad (red line) where the five setups of shielded sources in a trailer were located. Semi-stationary measurements were made along Kraftverksvägen to determine the source's distance, shielding and activity. Dotted (blue) markings indicate approximate positions for the semi-stationary measurements. Site G (the meeting place Grevinnan) was the headquarters for the COMBMORC experiments. Map from Open Street Maps 2022.

3.2 Field experiment main parts

The field experiment in COMBMORC 2022 consisted of two parts:

(1) ***Shield thickness calibration measurements.*** The detectors' response to primary radiation (recorded in ROI PL, PR and P) and scattered radiation (recorded in ROI A, B, C) from Cs-137 sources for different shield thicknesses was measured. Data from the measurements were input to the Excel application SSC, where the coefficients for the exponential and polynomial shield thickness determination models were automatically calculated. The SSC application was then used to assess shield mass thicknesses for the five experimental setups in part (2) of the experiment.

(2) ***Experimental distance, shielding and activity determination*** for Cs-137 sources. The teams performed semi-stationary measurements against five setups of shielded Cs-137 sources at locations 30 - 90 m from the road passing the source. The aim was to test the method of determining distance, shielding and activity from gamma spectrometric measurements along a road passing the source. The evaluation of source shielding was made using the SSC application. The source distance and activity were determined using the Excel application SODAC.

3.3 Generic regions of interest (ROI)

Each team had to select the ROI channel intervals for their detector(s) corresponding to the photon energy interval principles in Table 1. Table 3 provides examples of ROI selections for different conversion gains and energy width per channel. The exact ROI selections for each team and detector are listed in Appendix I.

Table 3. Suggested ROI energy intervals in keV for detecting primary and scattered photons by a gamma spectrometer having 1024, 512 or 256 channels corresponding to channel widths of 3, 6 or 12 keV/channel. The full energy peak area is suitable for NaI(Tl) spectrometers and is divided into three intervals: left peak area (PL), centre channel (PC) and right peak area (PR), which together constitute the full energy peak area (P).

ROI	Energy node (keV)	Compton scattered degree	3 keV/ch (keV)	ROI width chs	6 keV/ch (keV)	ROI width chs	12 keV/ch (keV)	ROI width ch
	74							
A			77-239	55	80-236	27	86-230	13
	242	110						
B			245-407	55	248-404	27	254-398	13
	410	58						
C			413-575	55	416-572	27	422-566	13
	578	27						
PL			581-659	27	584-656	13	590-650	6
PC			662	1	662	1	662	1
PR			665-743	27	668-740	13	674-734	6
P			581-743	55	584-740	27	590-734	13

3.4 Shield mass thickness assessment by Compton scattered radiation

3.4.1 Method steps

The previous NKS-funded project SHIELDMORC (Rääf *et al.* 2021) has described the theory for determining shield thicknesses by detecting Compton photons that have interacted in the radiation shield and registered in the pulse height distribution of a gamma spectrometer. The ratio of Compton photons to primary photons measures the radiation shield thickness. As described in theory, we have used three regions of interest for Compton photons (ROI A, B, C) and three for primary photons (ROI PL, PR and P).

The method of determining shield mass thickness involves two steps:

(1) Calibration of the detector response for shield geometries. The calibration data forms entries in the ”knowledge library”. Gamma spectrometric measurements are made for point sources with well-known shield thicknesses. The count rates in ROI A, B, C, PL, PR, and P for measurements in shield geometry and the background are entered into the Excel application SSC. SSC calculates the parameters of the exponential relations (ROI A/PR, B/PR, C/PR, PL/PR, A/P, B/P, C/P) as functions of shield mass thickness.

(2) Measurements on unknown shielded radiation sources. Gamma spectrometric measurement is made on the unknown source geometry. The count rates in ROIs A, B, C, PL, PR and P are entered into SSC. An estimated background count rate is entered into SSC for the same ROIs. SSC uses the parameters from the calibration and calculates seven versions of the shield mass thickness (from the net count rates (ROI A/PR, B/PR, C/PR PL/PR, A/P, B/P, C/P) and the mean value of the mass thickness.

3.4.2 Calibration setup

A car trailer was used at site C (Fig 4) for setting up the shielded sources in the calibration measurements (Table 4). The shielding geometries were built with wood and concrete blocks of varying thicknesses (wood 23.5 - 70.5 kg/m^2, Fig 5 and concrete 119 - 715 kg/m^2, Fig 6 and 7). Three Cs-137 sources with different activities (60, 200 and 600 MBq, approximate values), chosen depending on shield thickness, were placed behind the shields. The setup was built with shields in two opposite directions, allowing two teams to make the calibration measurements simultaneously. (Fig 5 - 7).

Fig 5. Setup C3 for shield thickness calibration mounted on a trailer. View from the side behind. The source is placed inside the clay brick cave. The shield consists of three layers of 4.5 cm wooden beams producing a wall thickness of 135 mm in two directions, left and right. The sidewalls of the trailer consist of 1 mm steel. The mass thickness of the wooden wall is 70.5 kg/m^2.

Fig 6. Setup C10 for shield thickness calibration mounted on a trailer. View from the side behind. The source is placed inside the clay brick cave. The shield consists of six layers of 5 cm concrete blocks producing a wall thickness of 300 mm in two directions, left and right. The mass thickness of the concrete wall is 714.6 kg/m^2.

Fig 7. Setup C10 for shield thickness calibration mounted on a trailer. View obliquely from behind and above. The source is placed in the cave below the clay bricks. The shield consists of six layers of 5 cm concrete blocks producing a wall thickness of 300 mm in two directions, left and right.

Table 4. Setup data for calibration of mobile gamma spectrometers for shield mass thickness determination. The source-detector distance was 10 m. The shielding was built in a car trailer (Fig 5 - 7). The trailer sidewall was 1 mm sheet steel, the shielding of which was corrected by adding the mass thickness of 6 m air. The steel walls are included in the mass thickness given in the table below.

Setup number	Material	Mass thickness (kg/m^2)
C1	Air only	19.89
C2	4.5 cm wood	43.38
C3	9 cm wood	66.87
C4	13.5 cm wood	90.36
C5	5 cm concrete	139.0
C6	10 cm concrete	258.1
C7	15 cm concrete	377.2
C8	20 cm concrete	496.3
C9	25 cm concrete	615.4
C10	30 cm concrete	734.5

3.4.3 SSC - Source shielding calculator

SSC is used in mobile gamma spectrometry to calculate the mass thickness of a shield in front of a Cs-137 point source from count rates in regions of interest (ROI) in a pulse height distribution (measured gamma spectrum). The gamma spectrometer can be of type NaI(Tl) or HPGe. As previously mentioned SSC is an Excel application developed by Lund University for the NKS COMBMORC activity. The application can run on all Windows systems from Windows XP to Windows 10 with any Excel version, and it can also run on all open-source applications Libre Office Calc versions.

SSC calculates and stores the function parameters for the exponential model. The updated version from May 2023 also stores the parameters for a five-degree polynomial model. SSC is programmed for calibration input from three NaI(Tl) spectrometers and one HPGe spectrometer. The storage of the experimentally obtained parameters for the various NaI(Tl) and HPGe detectors is called the “knowledge library”. In addition, calibration parameters from previous measurements on shielded sources in the SHIELDMORC project are also stored in the “knowledge library”.

A description and short tutorial for SSC can be found in Appendix J.

3.4.4 Limitations of the SSC shielding assessment method

Shield thickness assessment presumes that the shield is of slab type with atomic numbers between 3 and 25, where Compton scattering is the dominating effect for gamma radiation with energies between 100 and 1000 keV. The method does not work for lead shields.

If a source is placed far from a slab shield that is not uniform in lateral extent, SSC may give wrong shield thickness values, for example, if a source is placed in the middle of a house with windows toward the detector. Gamma radiation passing through the windows will not be Compton scattered to the same extent as in the thicker walls, and SSC will underestimate the wall thickness.

3.5 Shield mass thickness assessment by primary radiation

As described in Section 2.2, it is theoretically possible to determine the thickness of a slab shield in front of a gamma-ray source from measurements of primary photon fluence at different angles to the source. When measuring along a straight road that passes the source, it will be necessary to know the distance to the source, and the angular efficiency of the detector. Measurement data from the full energy peaks (ROI PL, PR and P) at semi-stationary points along the road past the source collected by the various teams could be analysed for shield thickness. However, the uncertainty in the measurement data is so great (to short measurement time, not fully mapped angular efficiency for some detectors, and possible shielding by trees) that it is not feasible in this work to draw any conclusions about the method from experimental data. It would, however, be possible to design a new experiment that could test the method.

3.6. Determination of distance, shielding and activity of Cs-137 point sources

3.6.1 Measurement setup

A car trailer with a shielded Cs-137 source was placed on a minor side road from the main road Kraftverksvägen. (Fig 4). The trailer was placed at 30, 60 and 90 m distance from the main road, and three shielding variants were used (air only, wood and wood in combination with concrete). Details of the setups are given in Table 5. A sketch of the concrete shield in the trailer is shown in Fig 8. The main road was marked at 10 m intervals. The mobile units made measurements along the road, standing still for short times (some minutes) at marked places of their own choice. The recommendations from the experimental management were to measure at least in six marked places along the main road for each setup.

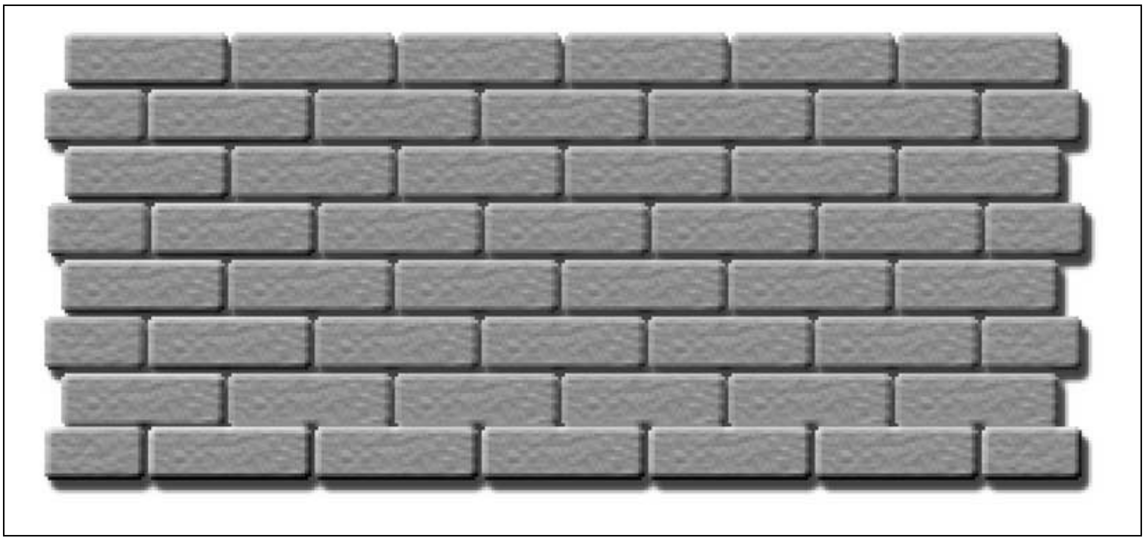

Fig 8. Sketch of the 13 cm thick concrete wall used in set-up M2, M4, M7 and M9. In addition, a 4.5 cm wooden layer was placed on the outer part of the wall. The width of the concrete wall was 118 cm. The height was 40 cm. The source was placed 5.75 cm behind the wall in the middle at a height of 22.5 cm.

Each team measured the background at the road crossing when no source was placed in the trailer on the side road. For all measurements, teams calculated the ROI A, B, C, PL, PR, and P count rates.

Teams used about a day and a half to make the measurements along the main road for the five setups. For each setup, approximately two hours were used for measurements.

Table 5. Setup data for the experiments, determining distance, shielding and activity of a 606 MBq Cs-137 point source at site M.

Setup	Distance (m)	Shield material	Mass thickness (kg/m^2)	Activity* (MBq)
M1, M6	60	60 m air	74.58	606
M2, M7	30	13 cm concrete 4.5 cm wood 30 m air	309.7 23.5 37.3 Σ 370.5	606
M3, M8	60	18 cm wood 60 m air	94.0 74.6 Σ 168.6	606
M4, M9	60	13 cm concrete 4.5 cm wood 60 m air	309.7 23.5 74.6 Σ 407.8	606
M5, M10	90	18 cm wood 90 m air	94.0 111.9 Σ 205.9	606

* The activity includes the shielding effect of the source capsule.

3.6.2 SODAC - Source distance and activity calculator

Teams were provided with the aforementioned Excel application SODAC, Source Distance and Activity Calculator for immediate assessment of distance, shielding and activity after each measurement setup. SODAC accepts ROI A, B, C, PL, PR and P count rate data and calculates the distance to the source based on the input data.

Lund University developed SODAC for the NKS COMBMORC activity. The application is written in Excel 2000, and it can run on all Windows systems from Windows XP to Windows 10 with any Excel version. It can also run on all open-source applications Libre Office Calc versions. A description of the SODAC application is given in Appendix K.

At least three measurements at different marked places along the main road are needed for meaningful results with SODAC. Additional measurements at places along the road provide more data for the distance assessment. As a rule of thumb for measurements along the main road, measurement locations should be chosen up to 1.5 times, preferably twice the estimated distance between the main road and the radiation source.

3.6.3 Activity calculation

SODAC also stores the efficiencies of the detectors and calculates the apparent activity of the (shielded) source from the distance information. Apparent activity is calculated based on the count rate in the full energy peak and the detector's efficiency. If the source is shielded, the actual activity is higher. SODAC recalculates to the actual activity, using Eqn 11, if the shield thickness and density are input into the application.

The source's shield thickness is obtained with the SSC application by measuring in the location along the main road where the maximum count rate in the full energy peak is obtained. In all setups, the maximum occurs at the intersection between the side road and the main road. Results from the teams' SSC calculations are given in the respective Appendix for the individual teams.

4. Results and discussion

Six mobile gamma spectrometry teams from the Nordic countries, using 14 detectors, carried out measurements in 15 setups. Together, the teams made approximately 350 gamma spectrometric measurements. A selection of analysis results is presented here as examples. The SSC application for determining shield mass thickness and the SODAC application for determining distance and activity for Cs-137 point sources were used in the analysis. Appendix A - F contains the detailed report of analysis results from all teams.

4.1 Determining shield mass thickness with the SSC application

The experiments to determine shield thicknesses were done in two steps. First, calibration measurements were made against known shield thicknesses (Setup C1 - C10). Next, shield thicknesses were determined for five combinations of distance and shielding (Setup M1 - M5).

4.1.1 Example of calibration data for shield thickness assessment (STUK data)

Example results from the shield thickness calibration measurements are shown here for the STUK 4-litre NaI(Tl) detector (vertically mounted, right side). Fig 9 shows shield thickness as a function of net count rate ratios for the exponential and polynomial models' different ROI areas. Tables 6 and 7 show the coefficients for the exponential and polynomial models after the model functions have been fitted to the measurement data.

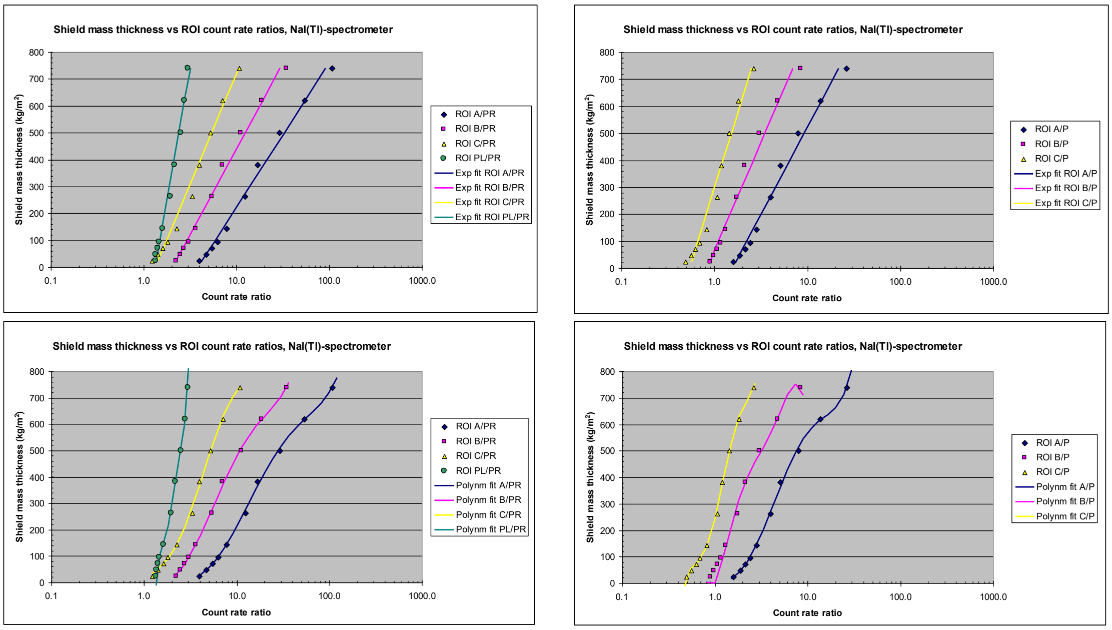

Fig 9. SSC analyzed data from calibration measurements for shield thickness determination with the STUK 4-litre NaI(Tl) (right side) spectrometer. Curves show shield mass thickness as a function of ROI net count rate ratio obtained from fitting measured data to exponential functions (top diagrams) and five-degree polynomial functions (bottom diagrams), valid for Cs-137 point sources behind shields of standard building material (wood and concrete) with mass thickness between 20 and 730 kg/m^2. The source-detector distance is 10 m.

Table 6. Coefficients *a* and *b* in an exponential model for determining shield mass thickness according to the description in section 2.1.1, and valid for the STUK 4-litre NaI(Tl) detector vertically mounted on the right side of the measuring vehicle. The unit of *b* is m^2/kg.

ROI ratio	*a*	*b*
ROI A/PR	3.85	0.00430
ROI B/PR	2.05	0.00361
ROI C/PR	1.33	0.00281
ROI PL/PR	1.33	0.00118
ROI A/P	1.56	0.00356
ROI B/P	0.833	0.00287
ROI C/P	0.540	0.00208

Table 7. Coefficients $a_0 \ldots a_5$ in the five-degree polynomial model for determining shield mass thickness according to the description in section 2.1.2, and valid for the STUK4-litre NaI(Tl) detector vertically mounted on the right side of the measuring vehicle. The unit of the coefficients is kg/m^2.

ROI ratio	a_5	a_4	a_3	a_2	a_1	a_0
ROI A/PR	5.614	-68.74	281.4	-392.9	186.0	0
ROI B/PR	9.2284	-73.09	155.4	30.94	-55.02	0
ROI C/PR	33.344	-248.1	573.0	-367.3	213.7	0
ROI PL/PR	12700	-44400	59760	-37980	11930	-1409
ROI A/P	21.59	-155.00	321.4	-90.32	36.16	0
ROI B/P	-202.2	1036	-1815	1146	294.7	0
ROI C/P	602.83	-504.9	-683.4	450.1	645.7	244.39

The count rate ratio functions ROI A/PR, B/PR, C/PR, A/P, B/P and C/P have slopes that clearly show an increase in shield thickness with increasing count rate ratios, while ROI PL/PR has a very sharp slope. Uncertainty in the ratio ROI PL/PR will then significantly impact on the value for shield thickness determination. The ratio is also susceptible to gain drifts. Thus, the ratio PL/PR is less suitable for determining shield thickness, a general observation for all NaI(Tl)-detectors.

4.1.2 Example of shield thickness assessment (STUK data)

The SSC routine made the determination of shield thicknesses for the unknown source geometries at the M site based on the calibrated functions. Figs 10 - 13 show results for obtained shield thicknesses plotted along the respective function curves. The assessment can be considered reasonably representative if all obtained values become approximately the same, for example, the case in Fig 11 (Setup M2), where the spread in obtained thickness is small for all ROI ratios. Obtained shield thicknesses range between 320 and 400 kg/m^2, and the average value for the four diagrams is between 360 and 400 kg/m^2. The actual value is 372 kg/m^2, including the air thickness between the source and the detector.

The determination is more uncertain if the spread in the obtained shield thickness is significant, as seen in Fig 13 (Setup M5). The individual values lie between 200 and 380 kg/m^2, and the average values are between 300 and 360 kg/m^2. The ROI ratio PL/PR contributes significantly to the uncertainty. The real value is 207 kg/m^2. Here, the SSC method has overestimated the shield thickness. The reason for the overestimation needs to be investigated through additional experiments.

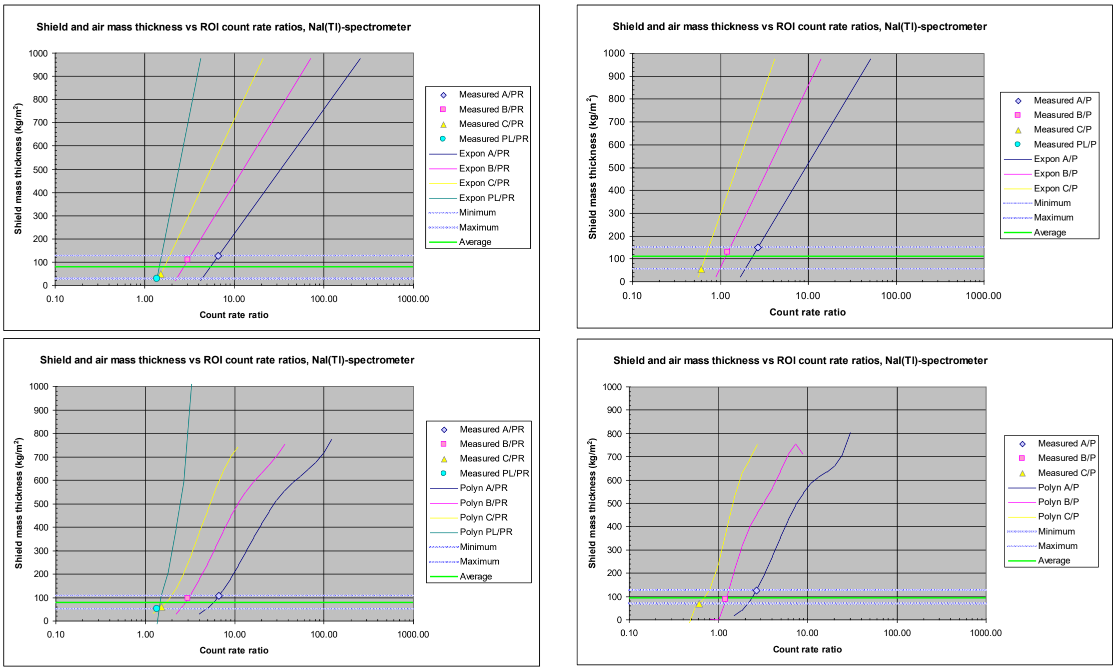

Fig 10. Setup M1. Shield mass thickness determination by the STUK 4 litre NaI(Tl) spectrometer using the ROI count rate ratio method with exponential (top diagrams) and polynomial (bottom diagrams) models. The distance to the source is 61 m. The models show an average shield mass thickness of 80 - 100 kg/m^2. The true shield mass thickness is 75.8 kg/m^2, including the air between the source and the detector.

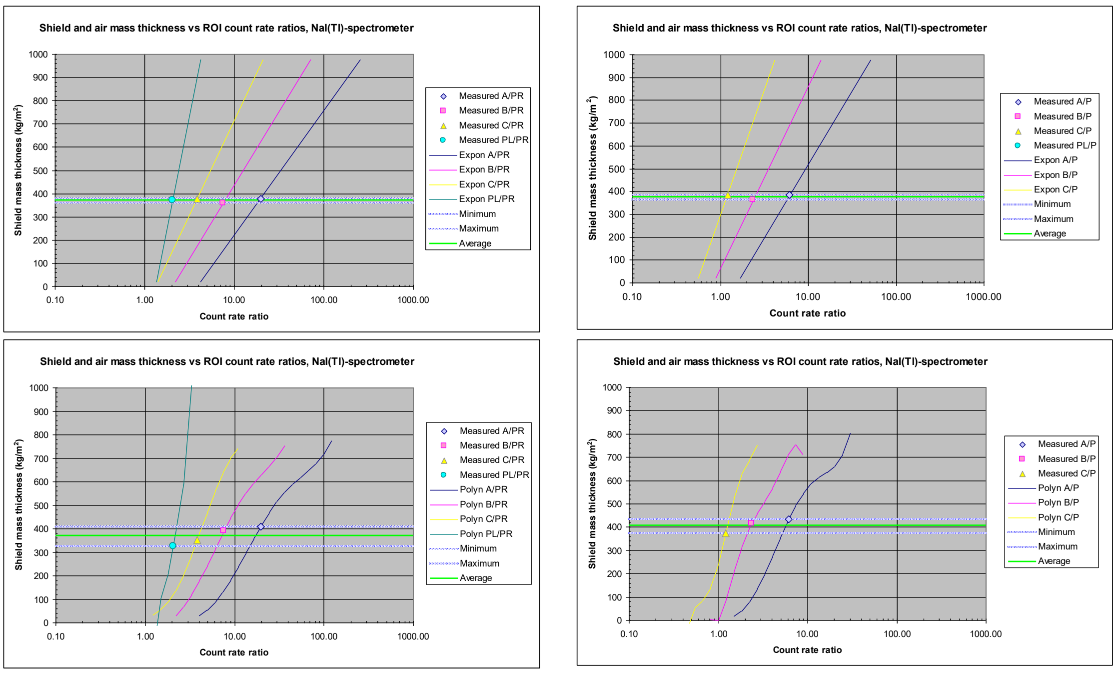

Fig 11. Setup M2. Shield mass thickness determination by the STUK 4 litre NaI(Tl) spectrometer using the ROI count rate ratio method with exponential (top diagrams) and polynomial (bottom diagrams) models. The distance to the source is 31 m. The models show an average shield mass thickness of 360 - 400 kg/m^2. The true shield mass thickness is 372 kg/m^2, including the air between the source and the detector.

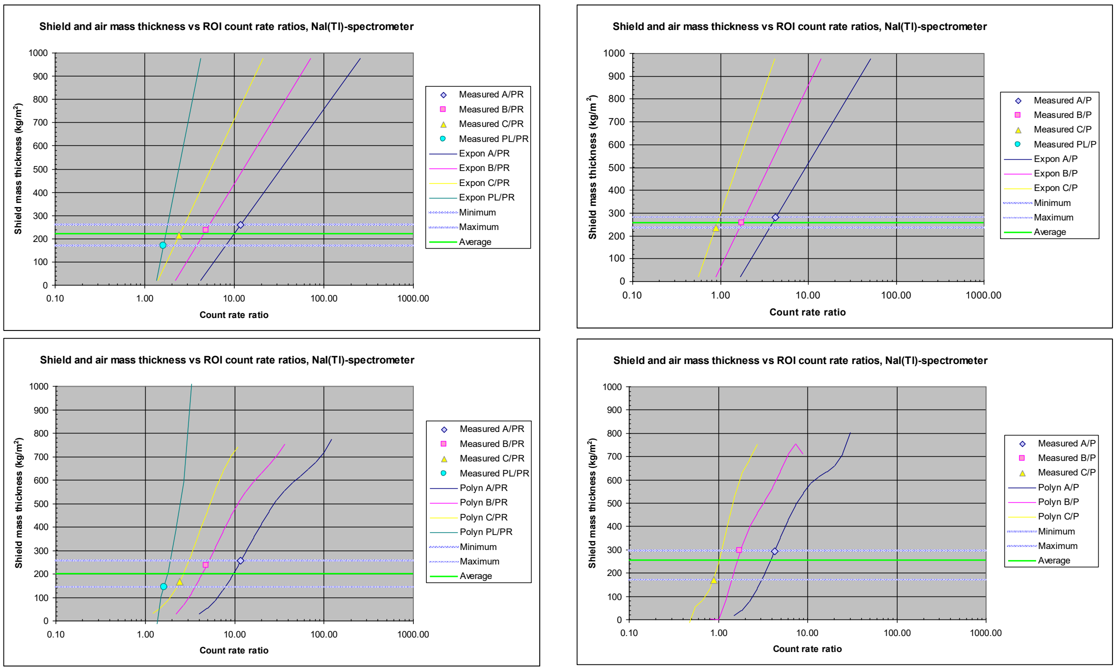

Fig 12. Setup M3. Shield mass thickness determination by the STUK 4 litre NaI(Tl) spectrometer using the ROI count rate ratio method with exponential (top diagrams) and polynomial (bottom diagrams) models. The distance to the source is 61 m. The models show an average shield mass thickness of 200 - 260 kg/m^2. The true shield mass thickness is 170 kg/m^2, including the air between the source and the detector.

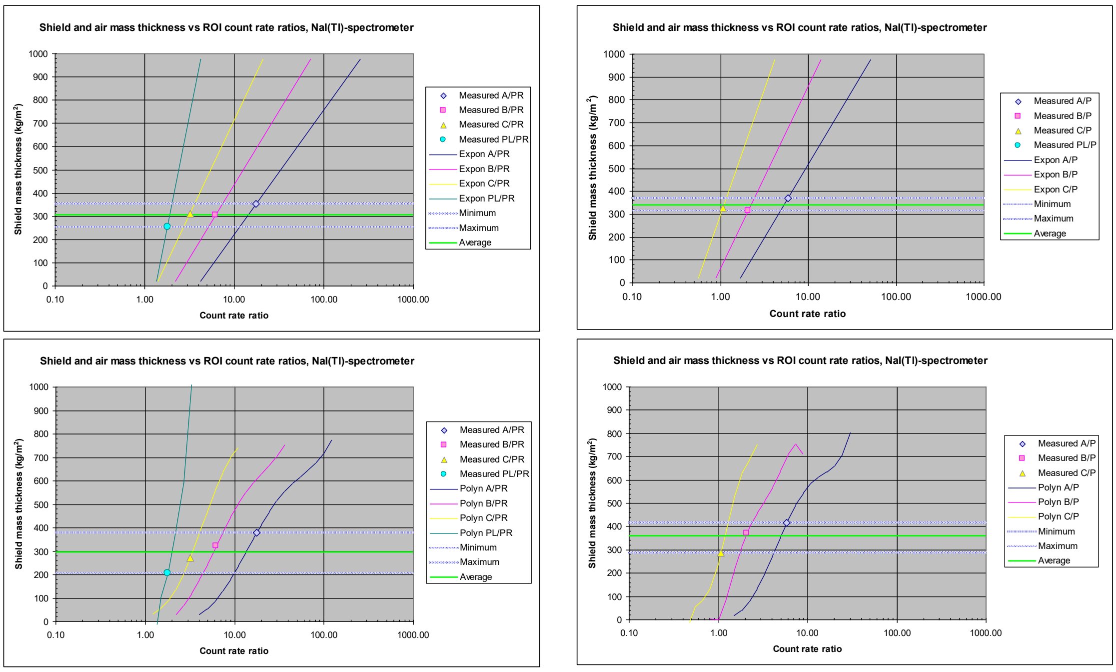

Fig 13. Setup M5. Shield mass thickness determination by the STUK 4 litre NaI(Tl) spectrometer using the ROI count rate ratio method with exponential (top diagrams) and polynomial (bottom diagrams) models. The distance to the source is 91 m. The models show an average shield mass thickness of 300 - 360 kg/m^2. The true shield mass thickness is 207 kg/m^2, including the air between the source and the detector.

4.1.3 Shield thickness assessment with a HPGe detector (Lund University)

In the experiment, an HPGe detector from Lund University was used. It is an electrically cooled portable detector named DetectiveX. Fig 14 shows the calibrated exponential and polynomial functions. The five-degree polynomial functions appear to follow the experimental data well.

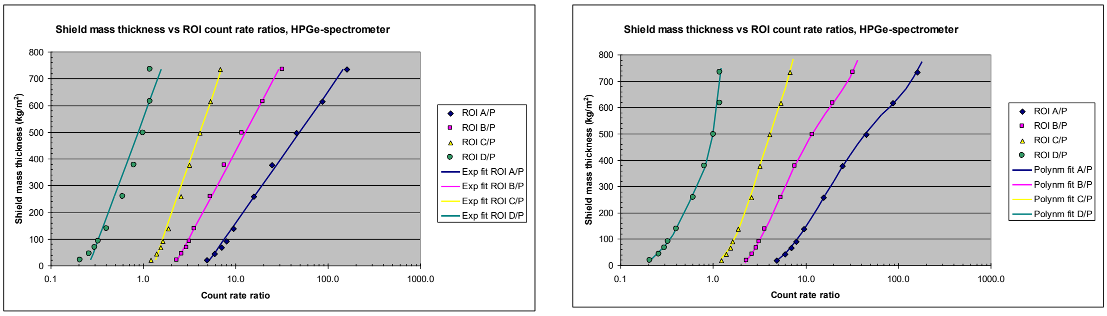

Fig 14. SSC analyzed data from calibration measurements for shield thickness determination with the Lund University HPGe detector (DetectiveX). Curves show shield mass thickness as a function of ROI net count rate ratio obtained from fitting measured data to exponential functions (left) and five-degree polynomial functions (right), valid for Cs-137 point sources behind shields of standard building material (wood and concrete) with mass thickness between 20 and 730 kg/m^2. The source-detector distance is 10 m.

An example of determining the shield thickness with the HPGe detector is shown in Fig. 15 for setup M2 with the source at a distance of 31 m. For the exponential model, there is a spread in the result. Above all, the value for ROI PL/PR is deviant. The exponential model gives an average value of 440 kg/m^2 for the shield mass thickness. The actual value is 372 kg/m^2, including the air between the source and the detector. The polynomial model gives more consistent values, but still too high, on average 420 kg/m^2. The reason for the overestimation of the shield thickness is not apparent. Further research into the method is needed to obtain an explanation.

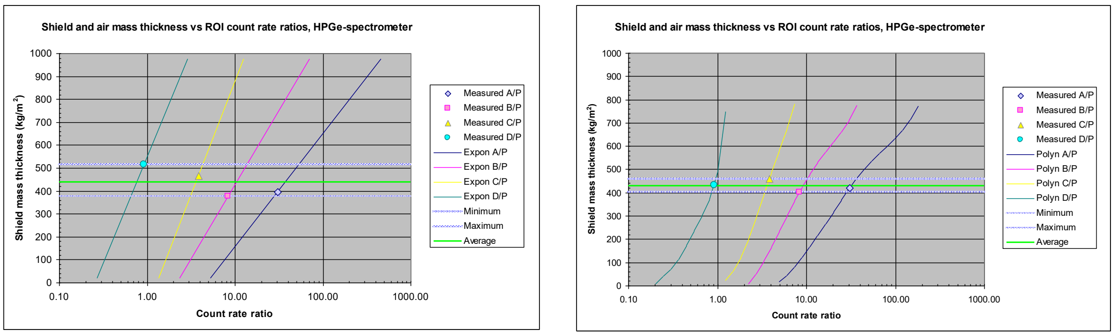

Fig 15. Setup M2. Shield mass thickness determination by the Lund University HPGe detector (DetectiveX) using the ROI count rate ratio method with exponential (left) and polynomial (right) models. The distance to the source is 31 m. The models show an average shield mass thickness of 430 - 440 kg/m^2. The true shield mass thickness is 372 kg/m^2, including the air between the source and the detector.

4.1.4 Summary of shield thickness assessments for all teams and detectors

A list of all calibration coefficients obtained for all teams' detectors for the exponential model for determining shield mass thicknesses is given in Table 8.

A compilation of average values over all determinations of shield thicknesses for the five combinations of distance to the radiation source and shielding of the source (setup M1 - M5) for all teams and detectors is given in Table 9.

No significant difference in results between the exponential and the polynomial model can be noted. The polynomial model is more complicated to use than the exponential model, as it requires maximum and minimum values to be defined within which the model is valid. Outside the valid range, the polynomial model can produce results entirely out of bonds. Since the exponential model is more straightforward, it is preferable.

Individual determinations of shield mass thicknesses can show overestimations and underestimations in several tens of per cent. The variations may be due to statistical uncertainty in the count rate data, not sufficiently determined background measurement data and gain drift that causes the ROI energy range to shift. NaI(Tl) detectors are sensitive to temperature changes that may cause gain drift. Gain drift can lead to significant errors in determining shield thicknesses if the full energy peak drifts.

The exponential model overestimated the shield mass thicknesses for all five setups (M1 - M5) on average by 1.6 ± 10%. The polynomial model overestimated the mass thickness on average by 6.4 ± 9 %. For both models together the shield mass thickness was overestimated by 4 ± 9%.

In summary, for a slab-type radiation shield made of commonly used building materials, the SSC method gives average values for the mass thickness of radiation shields that do not significantly differ from actual values. However, depending on statistical uncertainty in measurement data and possible gain drift in the registration of pulse height distributions, individually determined shield mass thickness values may exhibit significant variations.

Table 8. Experimentally determined calibration coefficients in the function $a\, e^{b\, z\, \rho}$ to obtain shield mass thickness from gamma spectrometric count rate ratios in regions of interest ROI A, B, C, PL, PR, and P, valid for a source emitting 662 keV photons.

	a			
Detector	ROI A/ PR	ROI B/PR	ROI C/PR	ROI PL/PR
LU 3x3" NaI(Tl)	6.14	2.59	1.43	1.22
DSA 3x3" NaI(Tl)	15.2	5.29	2.63	1.37
DEMA 4L NaI(Tl)	3.90	2.00	1.40	1.53
DSA 4 L NaI(Tl)	4.58	2.15	1.52	1.41
GR 2x2 L NaI(Tl)	4.28	2.16	1.38	1.21
LU 4 L NaI(Tl) (F)	3.69	1.98	1.35	1.21
LU 4 L NaI(Tl) ®	3.45	1.90	1.33	1.30
STUK 4 L NaI(Tl)	3.85	2.05	1.33	1.33
NGU 16 L NaI(Tl)	3.54	2.16	1.57	1.53
	ROI A/P	ROI B/P	ROI C/P	
LU 3x3" NaI(Tl)	2.65	1.11	0.616	
DSA 3x3" NaI(Tl)	6.18	2.15	1.07	
DEMA 4L NaI(Tl)	1.47	0.758	0.529	
DSA 4 L NaI(Tl)	1.83	0.858	0.605	
GR 2x2 L NaI(Tl)	1.89	0.953	0.612	
LU 4 L NaI(Tl) (F)	1.61	0.862	0.590	
LU 4 L NaI(Tl) ®	1.43	0.787	0.552	
STUK 4 L NaI(Tl)	1.56	0.833	0.540	
NGU 16 L NaI(Tl)	1.34	0.822	0.597	
LU Detective HPGe	4.80	2.20	1.30	

	b (m^2/kg)			
Detector	ROI A/ PR	ROI B/PR	ROI C/PR	ROI PL/PR
LU 3x3" NaI(Tl)	0.00400	0.00309	0.00230	0.000599
DSA 3x3" NaI(Tl)	0.00444	0.00341	0.00220	0.00120
DEMA 4L NaI(Tl)	0.00501	0.00402	0.00295	0.000996
DSA 4 L NaI(Tl)	0.00479	0.00397	0.00278	0.00118
GR 2x2 L NaI(Tl)	0.00516	0.00448	0.00355	0.00169
LU 4 L NaI(Tl) (F)	0.00398	0.00334	0.00231	0.000392
LU 4 L NaI(Tl) ®	0.00416	0.00349	0.00247	0.000560
STUK 4 L NaI(Tl)	0.00430	0.00361	0.00281	0.00118
NGU 16 L NaI(Tl)	0.00454	0.00366	0.00256	0.000879
	ROI A/P	ROI B/P	ROI C/P	
LU 3x3" NaI(Tl)	0.00367	0.00276	0.00197	
DSA 3x3" NaI(Tl)	0.00366	0.00263	0.00142	
DEMA 4L NaI(Tl)	0.00437	0.00338	0.00231	
DSA 4 L NaI(Tl)	0.00401	0.00320	0.00201	
GR 2x2 L NaI(Tl)	0.00401	0.00333	0.00240	
LU 4 L NaI(Tl) (F)	0.00377	0.00313	0.00210	
LU 4 L NaI(Tl) ®	0.00384	0.00318	0.00215	
STUK 4 L NaI(Tl)	0.00356	0.00287	0.00208	
NGU 16 L NaI(Tl)	0.00397	0.00310	0.00199	
LU Detective HPGe	0.00467	0.00354	0.00231	

Table 9. Summary of deviations (%) in shield mass thickness determination from actual (true) values for the ROI A, B, C, PL /PR method and the ROI A, B, C /P method when using exponential and the five-degree polynomial models. Uncertainties are given as the standard error of the mean.

Model type		Exponential model		Polynomial model	
ROI ratio method		A,B,C,PL/PR	A,B,C/P	A,B,C,PL/PR	A,B,C/P
Team	Detector				
DEMA	4L NaI(Tl)	18.8 ± 9.2	17.1 ± 8.5	15.6 ± 7.7	16.5 ± 9.6
DSA	4L NaI(Tl)	-16.5 ± 11.1	-23.8 ± 16.8	-15.5 ± 7.6	-23.9 ± 16.6
GR	2x2L NaI(Tl)	11.9 ± 10.8	20.4 ± 12.6	18.2 ± 11.3	30.0 ± 13.1
LU	4L NaI(Tl) (F)	-12.6 ± 23.9	-8.3 ± 10.7	-12.1 ± 17.2	-10.0 ± 12.5
LU	4L NaI(Tl) (R)	-56.6 ± 31.6	-25.5 ± 11.3	36.4 ± 26.0	-29.3 ± 16.8
LU	3"x3" NaI(Tl)	-1.3 ± 27.8	9.0 ± 3.7	-16.8 ± 40.5	8.95 ± 3.30
LU	HPGe	-	46.7 ± 18.5	-	39.5 ± 19.7
STUK	4L NaI(Tl)	19.9 ± 8.9	31.9 ± 14.0	8.52 ± 10.6	31.6 ± 13.1
Average		-5.2 ± 10.1	8.4 ± 9.2	4.9 ± 7.7	7.9 ± 9.3

4.2 Determining distance and activity with the SODAC application

The experiments to determine the distance to a source and its activity were made in five setups (M1 - M5). The setups are described in section 3.6. In all setups, a 606 MBq Cs-137 point source was used. Here examples of the results are shown. The full descriptions of all teams' results are given in Appendix A - F. In addition, teams should determine the shield mass thicknesses, the results of which examples are given above in section 4.1 and the full descriptions in Appendix A to F.

4.2.1 Example of SODAC assessment, 4 litre NaI(Tl) detector (DEMA)

The DEMA 4-litre NaI(Tl) detector was mounted on the rooftop of the measuring vehicle. Calibration of the detector efficiency needed for activity determination was made in a previous experiment AUTOMORC, where all teams attended. Calibration data was stored in the SODAC application.

Unfortunately, some trees were in the line of sight between the source and some of the detector measurement positions along the main road, which tends SODAC to produce shorter distance estimates. The positions and angles where the source is shielded have been identified, and their measurement data has been removed from the analysis.

During the initial evaluation of the measurements to determine the distance to the radiation source, all measurements made with the 4-litre NaI(Tl) detectors *showed too short distances*, which is due to the uneven angular efficiency that arises due to the oblong shape of the detector. It appears when the detector is oriented horizontally in the longitudinal direction of the vehicle and results in the photon fluence from the source when it falls obliquely towards the detector giving a lower count rate. It then looks as if the bell-shaped curve over the photon fluence along the road past the source becomes narrower, interpreted as the source is closer to the road. It is thus necessary to correct the count rate in the detector for the uneven angular efficiency, which has been done in an updated version of SODAC. The data reported here is from the updated version.

Figs 16 - 20 show the photon fluence curve, and the distance and activity calculation results with SODAC for setup M1 - M5. The activity calculation highly depends on the calculated distance and the assumed shield thickness.

In order to assess SODAC's accuracy, the actual shield thickness has been used as an input value. The teams did make measurements and calculations of the shield thickness with SSC, which could be used as the assumed shield thickness in SODAC. However, since those values contain significant uncertainties, the SSC values have not been used in SODAC.

The figure captions indicate the calculated activity for the distance obtained from SODAC, although it is not the actual distance. The activity values for the actual distances are given in the detailed report from the teams' measurements in Appendix A - F.

The SODAC estimated distances were, on average, underestimated by 10 ± 4%. The calculated activity was, on average, overestimated by 88 ± 23% when the estimated distances to the source were applied and by 88 ± 35% when the actual distances were applied. The reason for these deviations is not apparent. Further experimental investigations of the detector's response at longer source distances and thicker shielding are needed to investigate the reason more in-depth.

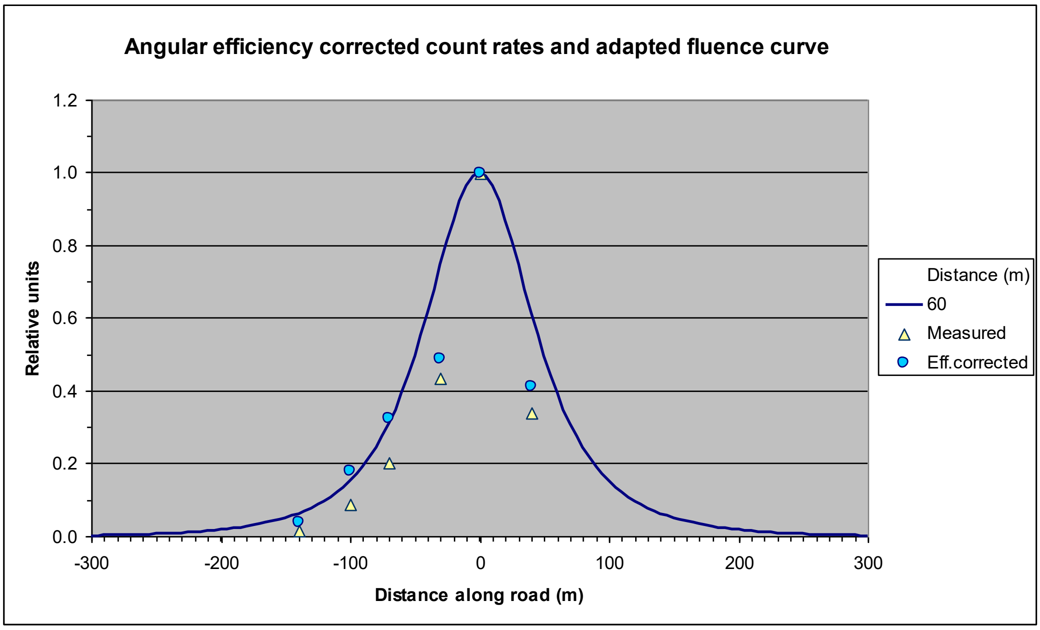

Fig 16. Setup M1 (Table 5). SODAC calculated photon fluence curve from the recorded full energy peak in a 4-litre NaI(Tl) detector, corrected for the varying angular efficiency of the detector. (DEMA results). Yellow triangles are measured data. Blue circles are corrected data. The estimated source distance is 60 m, and the actual distance is 61 m. The estimated activity of the unshielded Cs-137 point source (applying the estimated distance) is 702 MBq, and the actual activity is 606 MBq. Trees shield the source at -40 m and + 40 m along the road, resulting in count rates below the fluence curve.

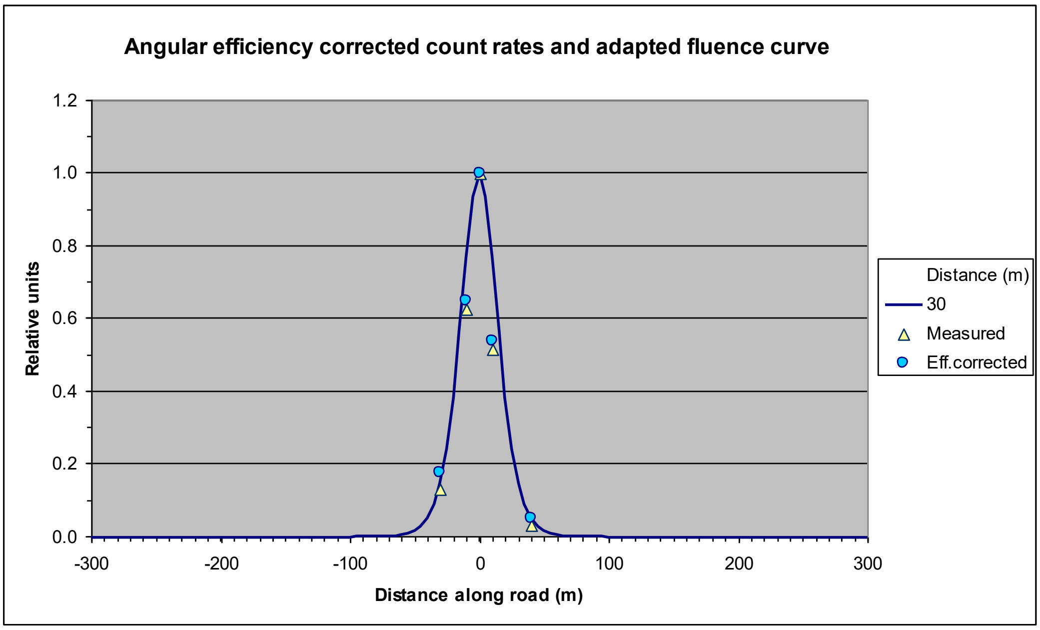

Fig 17. Setup M2. SODAC calculated photon fluence curve from the recorded full energy peak in a 4-litre NaI(Tl) detector, corrected for the varying angular efficiency of the detector. (DEMA results). Yellow triangles are measured data. Blue circles are corrected data. The estimated source distance is 30 m, and the actual distance is 31 m. The estimated activity of the shielded Cs-137 point source (applying the estimated distance and the actual shielding) is 1157 MBq, and the actual activity is 606 MBq.

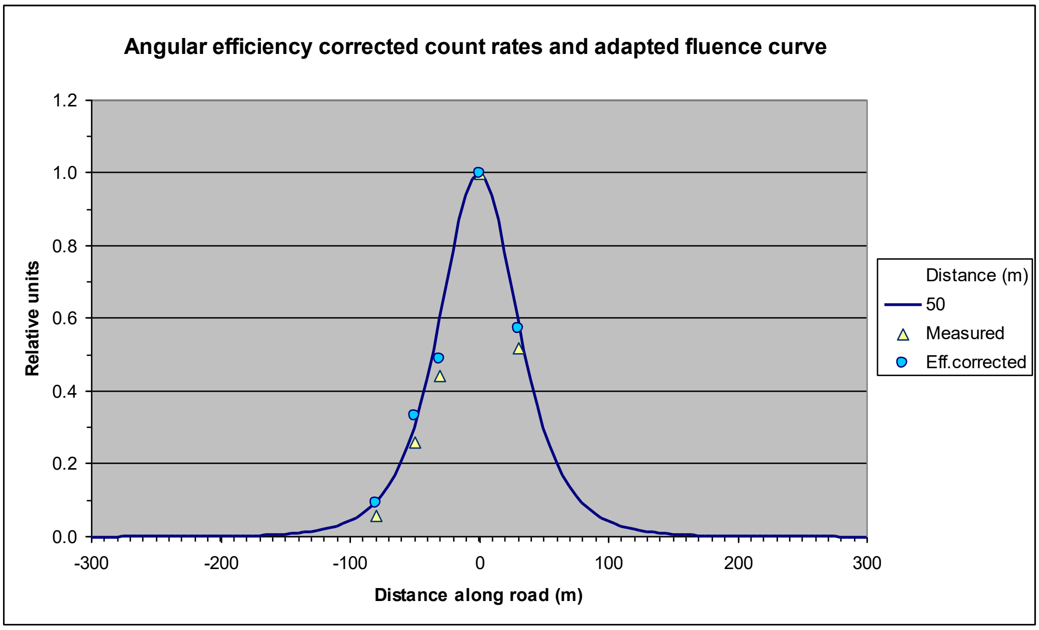

Fig 18. Setup M3. SODAC calculated photon fluence curve from the recorded full energy peak in a 4-litre NaI(Tl) detector, corrected for the varying angular efficiency of the detector. (DEMA results). Yellow triangles are measured data. Blue circles are corrected data. The estimated source distance is 50 m, and the actual distance is 61 m. The estimated activity of the shielded Cs-137 point source (applying the estimated distance and the actual shielding) is 511 MBq, and the actual activity is 606 MBq.

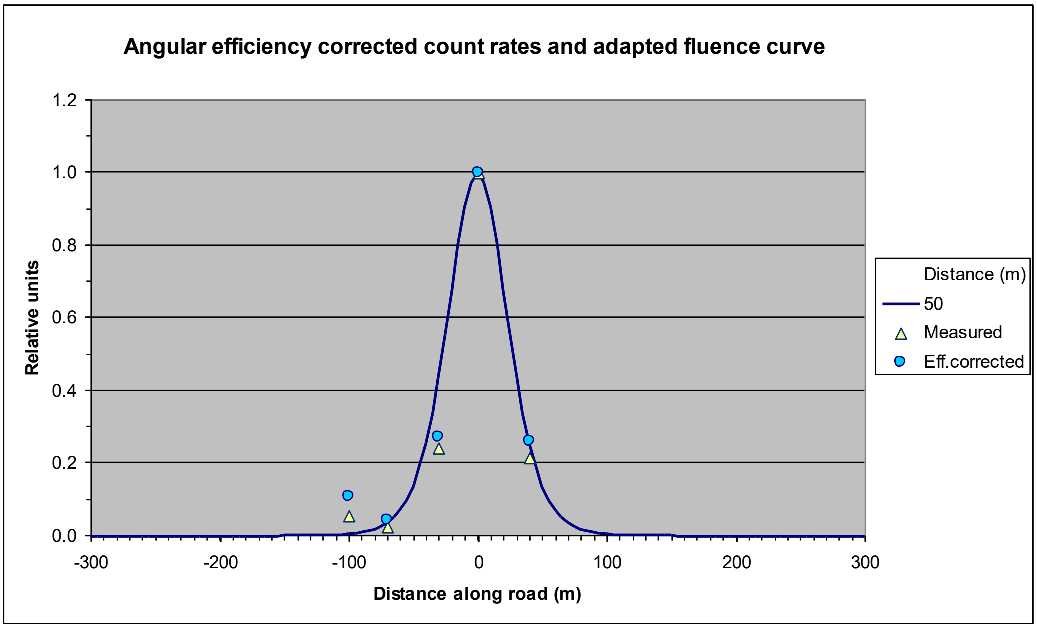

Fig 19. Setup M4. SODAC calculated photon fluence curve from the recorded full energy peak in a 4-litre NaI(Tl) detector, corrected for the varying angular efficiency of the detector. (DEMA results). Yellow triangles are measured data. Blue circles are corrected data. The estimated source distance is 50 m, and the actual distance is 61 m. The estimated activity of the shielded Cs-137 point source (applying the estimated distance and the actual shielding) is 1201 MBq, and the actual activity is 606 MBq.

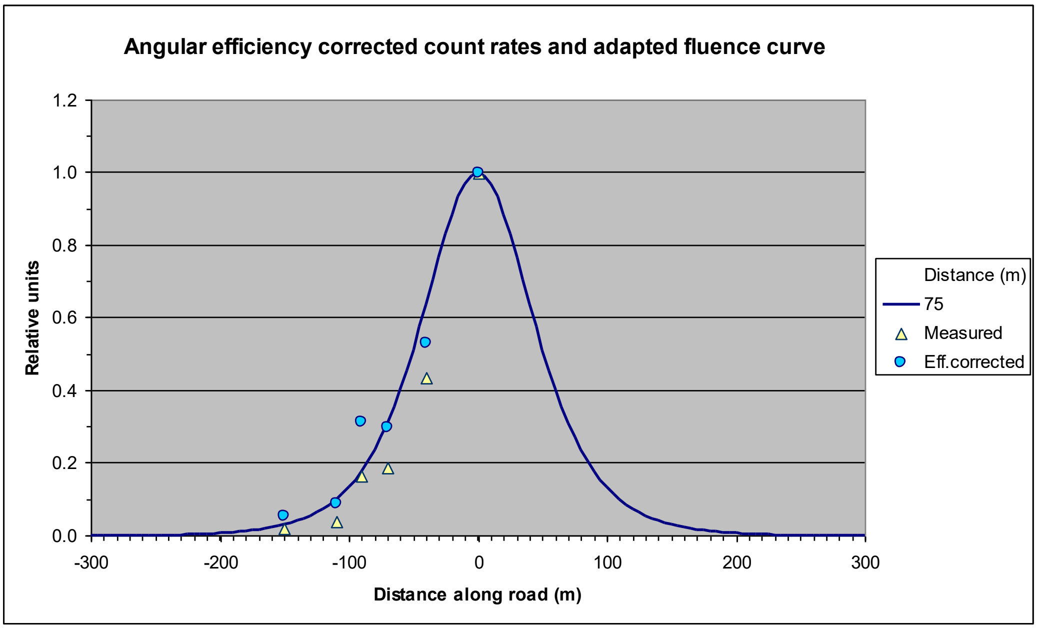

Fig 20. Setup M5. SODAC calculated photon fluence curve from the recorded full energy peak in a 4-litre NaI(Tl) detector, corrected for the varying angular efficiency of the detector. (DEMA results). Yellow triangles are measured data. Blue circles are corrected data. The estimated source distance is 75 m, and the actual distance is 91 m. The estimated activity of the shielded Cs-137 point source (applying the estimated distance and the actual shielding) is 675 MBq, and the actual activity is 606 MBq.

4.2.2 Example of SODAC assessment, HPGe detector (Lund University)

The Lund University HPGe detector (DetectivX) was mounted inside the measuring vehicle's right side and with its sensitive volume pointed backwards. Calibration of the detector efficiency needed for activity determination was done previously. Calibration data was stored in the SODAC application.

The angular efficiency of the HPGe detector increased by about 10% from the direction towards the mantle surface to the direction towards the central axis from the back side. The efficiency decreased significantly in the direction of the forward central axis (where the cryostat shields the detector). However, the current version has not incorporated the correction for the varying angular efficiency into SODAC. Thus, the distance determinations are affected for the HPGe detector, and too short source distances can be expected when analyzing measurement data with the current version of SODAC

Figs 21 - 24 show the photon fluence curve, and the distance and activity calculations results with SODAC for setups M1, M2, M3 and M5. The activity calculation highly depends on the calculated distance and the assumed shield thickness. The actual shield thickness has been input into the SODAC application.

The figure captions indicate the calculated activity for the distance obtained from SODAC, although it is not the actual distance. The detailed report in Appendix D gives the activity values for the actual distances.

The SODAC estimated distances were, on average, underestimated by 13 ± 6%. The calculated activity was, on average, underestimated by 17 ± 15% when the estimated distances to the source were applied and overestimated by 18 ± 7% when the actual distances were applied. As mentioned above, one reason for the underestimation of the source distances may be the lack of correction for the varying angular efficiency.

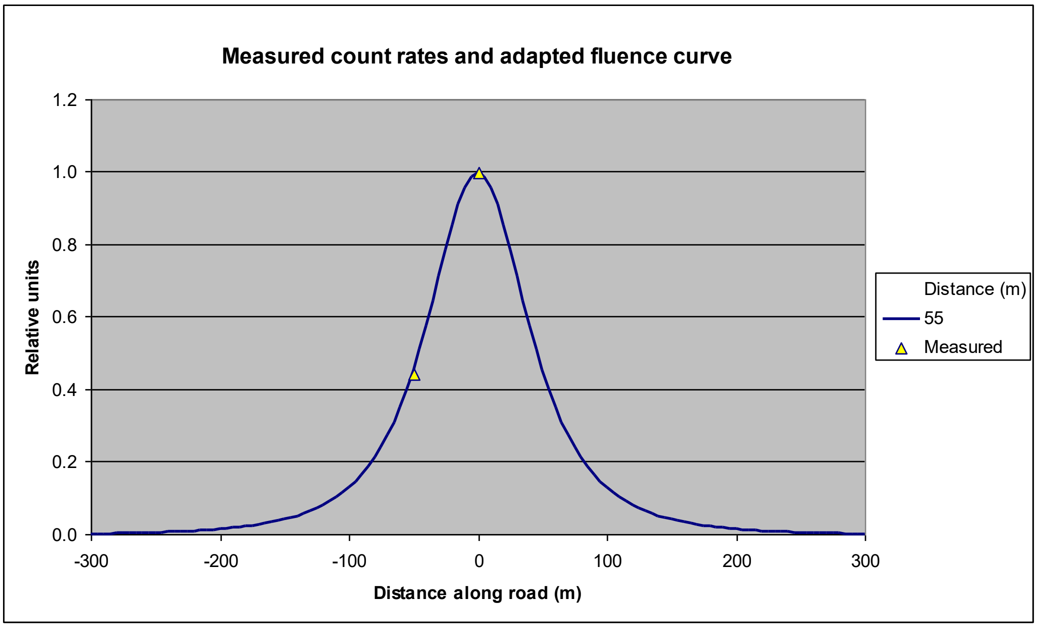

Fig 21. Setup M1. SODAC calculated photon fluence curve from the recorded full energy peak in an HPGe detector (Lund University). The estimated source distance is 55 m, and the actual distance is 61 m. The estimated activity of the unshielded Cs-137 point source (applying the estimated distance) is 531 MBq, and the actual activity is 606 MBq. Measurement data in locations along the road where trees shield the source have been removed.

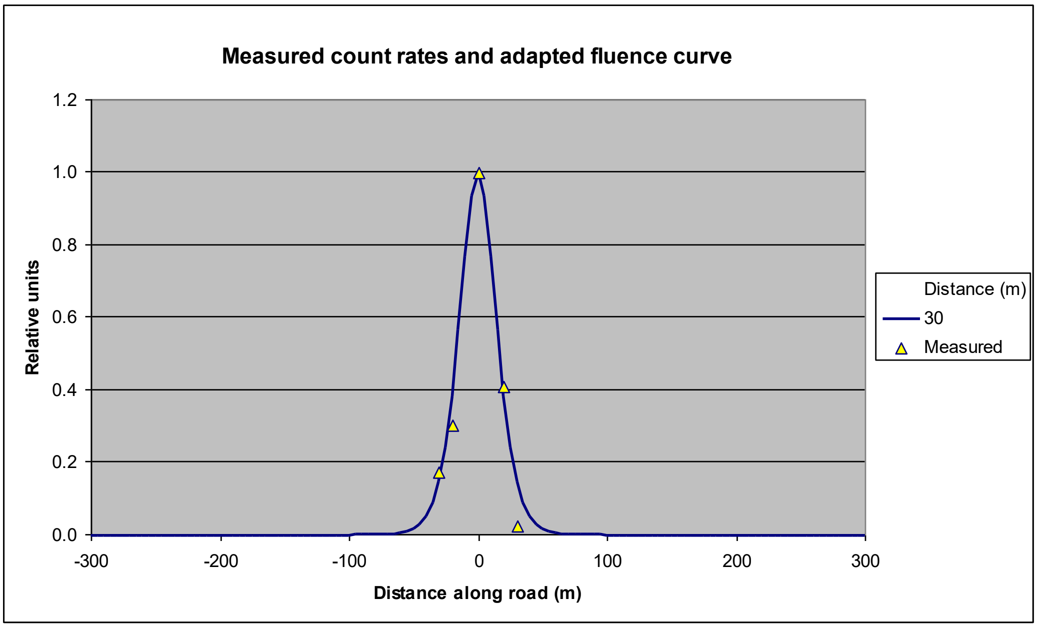

Fig 22. Setup M2. SODAC calculated photon fluence curve from the recorded full energy peak in an HPGe detector (Lund University). The estimated source distance is 30 m, and the actual distance is 31 m. The estimated activity of the shielded Cs-137 point source (applying the estimated distance and the actual shielding) is 745 MBq, and the actual activity is 606 MBq.

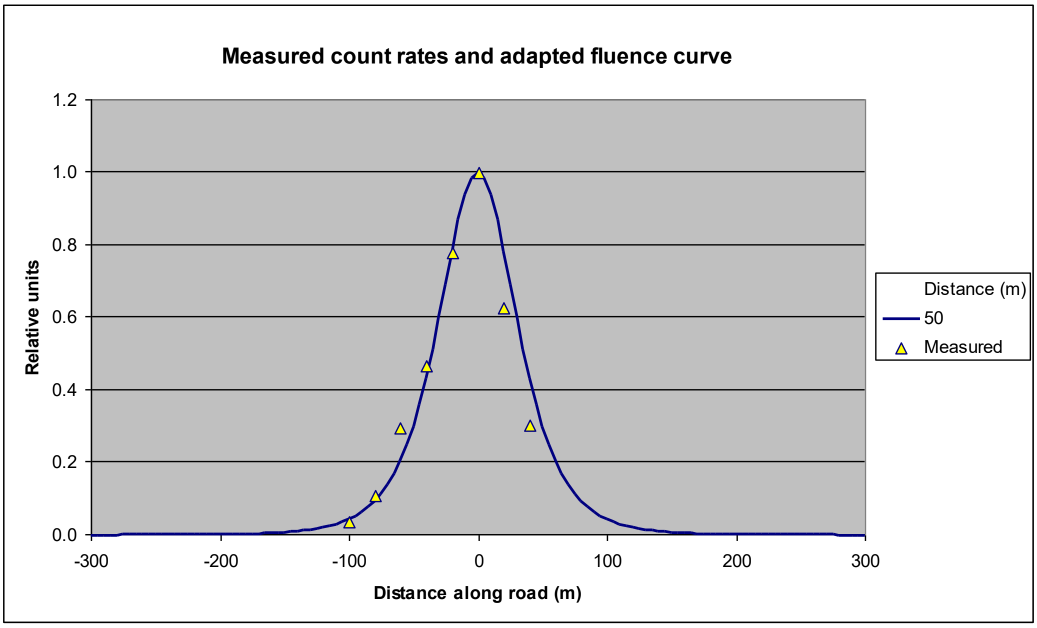

Fig 23. Setup M3. SODAC calculated photon fluence curve from the recorded full energy peak in an HPGe detector (Lund University). The estimated source distance is 50 m, and the actual distance is 61 m. The estimated activity of the shielded Cs-137 point source (applying the estimated distance and the actual shielding) is 397 MBq, and the actual activity is 606 MBq.

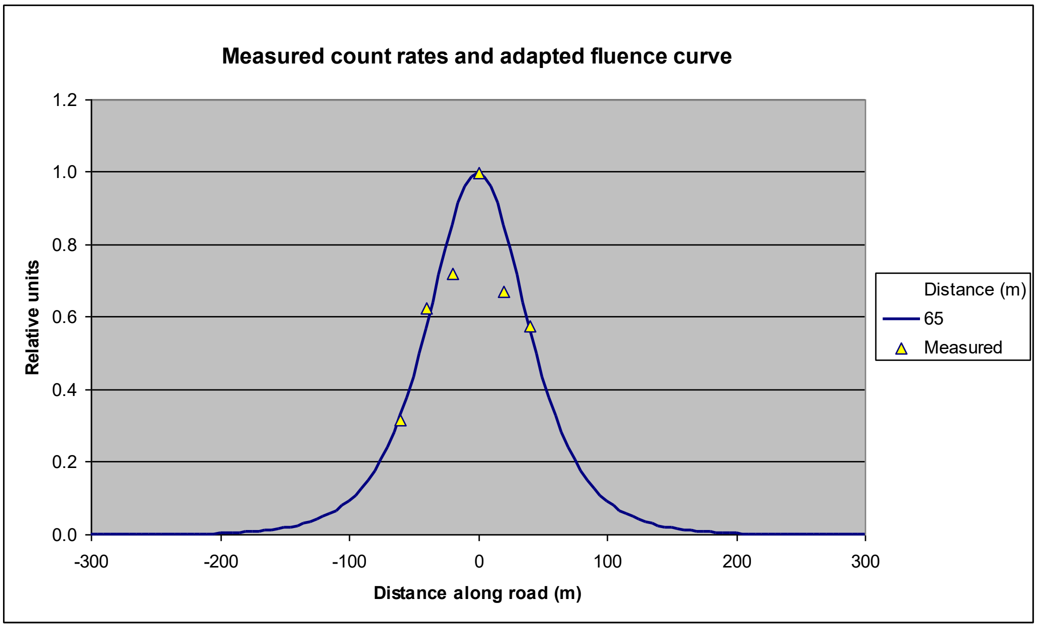

Fig 24. Setup M5. SODAC calculated photon fluence curve from the recorded full energy peak in an HPGe detector (Lund University). The estimated source distance is 65 m, and the actual distance is 91 m. The estimated activity of the shielded Cs-137 point source (applying the estimated distance and the actual shielding) is 333 MBq, and the actual activity is 606 MBq.

4.2.3 Summary of distance and activity results from all teams

A compilation of SODAC-calculated source distances and activity values is given in Table 10 for all teams' NaI(Tl) detectors and Table 11 for the HPGe detector from Lund University.

The SODAC calculation generally underestimates of the source distance by 20 ± 3 per cent. It indicates that the count rates in the full energy peak with the conversion to photon fluence rate give too low values when the distance of the detector along the path increases from the point right in front of the source. The underestimation may be due to insufficient correction for the varying angular efficiency of the detector. Whether this or some other reason contributes to the underestimation of the distance should be further investigated in well-controlled experiments.

When determining the activity of the source, the actual shield thickness was used so that the attenuation of primary photons in the shield could be calculated correctly. For the shorter, underestimated distances, SODAC gave an average deviation in source activity of 0 ± 13% from the actual activity, which in reality means that SODAC somewhat overestimated the activity of the source. *For the actual distances, the average overestimation of the activity is 83 ± 17%* (Table 10). Why this discrepancy exists needs to be investigated through further well-controlled experiments.

Table 10. Summary of deviations (%) in source distance determination and source activity determination from actual (true) values when using the SODAC method with NaI(Tl) detectors. Uncertainties are given as the standard error of the mean.

Team	Detector	Distance deviation from actual value %	Activity deviation from actual value at obtained distance %	Activity deviation from actual value at actual distance %
DEMA	4L NaI(Tl)	-10 ± 4	40 ± 23	88 ± 35
DSA	4L NaI(Tl)	-18 ± 4	-18 ± 13	51 ± 19
GR	2x2L NaI(Tl)	-23 ± 6	-34 ± 16	22 ± 12
LU	4L NaI(Tl) (F)	-10 ± 10	-15 ± 24	86 ± 24
LU	4L NaI(Tl) (R)	-32 ± 11	-36 ± 22	54 ± 22
LU	3"x3" NaI(Tl)	-34 ± 11	-30 ± 25	81 ± 30
NGU	4x4L NaI(Tl)	-17 ± 6	33 ± 34	104 ± 41
STUK	4L NaI(Tl)	-18 ± 7	57 ± 32	181 ± 70
Average		-20 ± 3	0 ± 13	83 ± 17

Table 11. Summary of deviations (%) in source distance determination and source activity determination from actual (true) values when using the SODAC method with a HPGe detector. Uncertainties are given as the standard error of the mean.

Team	Detector	Distance deviation from actual value %	Activity deviation from actual value at obtained distance %	Activity deviation from actual value at actual distance %
LU	HPGe	-13 ± 6	-17 ± 15	18 ± 7

5. Conclusions

SSC and SODAC methods enable the determination of the distance, shielding and activity of an unknown Cs-137 source by mobile gamma spectrometry by making semi-stationary measurements along a straight road past the source. The uncertainty in the determinations depends on the statistical uncertainty in the measurement data, which, among other things, depends on the measurement time at each location along the road. Experiments carried out with the Nordic countries' mobile measuring equipment using 4-litre NaI(Tl) detectors show that radiation sources located at distances within 90 m, with activities within 500 - 1000 MBq and shielding by building material up to 330 kg/m^2 *can be located with a distance uncertainty of 20 - 30% and an activity uncertainty within a factor of two*.

The above conclusion applies under the assumption that the road past the source is straight. If the source is in a building, the walls must be of ordinary homogenous building material and parallel to the road. If a source is in a house, it is not certain that these conditions are met. Windows and doors make the shielding inhomogeneous, and walls may be oriented with an angle to the road from which measurements are made. Such uncontrolled conditions increase the uncertainty in determining an unknown source's distance, shielding and activity.

Some circumstances are essential to consider in the application of the SSC and SODAC methods:

- *A detector should preferably have equal angular efficiency* in all directions from which a sought-after radiation source may be detected. For a 4-litre NaI(Tl) detector, uniform angular efficiency in car-borne search can be obtained by mounting the detector vertically. Detectors with a cylindrical sensitive volume should be mounted so that the central axis of the cylinder is vertical.
- If a detector has uneven angular efficiency, the measured count rate must be *corrected for the varying angular efficiency* assuming the direction of the source.
- Any shielding structures between a possible source and the measuring equipment should be observed so that corrections to the measurement data can be made. It should be noted that shielded structures could also help determine the direction of a radiation source.
- Semi-stationary measurements *along a road should be distributed to cover the entire photon fluence curve (also termed the intensity curve)*. As far as possible, one should strive to also make measurements at the "tail" of the photon fluence curve. These measurements require longer measurement time intervals. More reliable values are obtained in the source distance calculation by adequately identifying the entire width of the photon fluence curve.
- When using NaI(Tl) detectors, monitoring the gain is essential to avoid gain drift that would change the energy intervals for the regions of interest used by SSC and SODAC. *Uncorrected gain drift may lead to a great loss of accuracy in determining the distance*, shielding and activity of a sought-after source.

References

H. K. Aage, U. Korsbech, Search for lost orphan radioactive sources based on NaI gamma spectrometry. Applied Radiation and Isotopes, 58, pp 103-113, 2003. https://doi.org/10.1016/S0969-8043(02)00222-1

Antanas Bukartas, Robert Finck, Jonas Wallin, Christopher L. Rääf. A Bayesian method to localize lost gamma sources, Applied Radiation and Isotopes, 145 pp 142-147. March 2019. https://doi.org/10.1016/j.apradiso.2018.11.008

R.R. Finck, T. Ulvsand. Search for orphan gamma radiation sources, Experiences from the Barents Rescue 2001 exercise. Proceedings, Security of Radioactive Sources held at IAEA, Vienna, Austria, 10-13 March 2003. IAEA, Vienna, pp 123 – 137, 2003.

Robert Finck, Jan Johansson, B. Åke Persson, Christer Samuelsson, Karl Östlund. Close Reality in Radiological Emergency Exercises, in Proceedings of the *12th Congress of the International Radiation Protection Association (IRPA)* in Buenos Aires, on October 19 –24, 2008.

Robert R. Finck, Vikas C. Baranwal, Therése Geber Bergstrand, Jonas Jarneborn, Gísli Jónsson, Mattias Jönsson, Sune Juul Krogh, Simon Karlsson, F. Osftad, Jonas Nilsson, Marcus Persson, Per Reppenhagen Grim, Christopher L. Rääf, Morten Sickel, Petri Smolander, Robin Watson, Karl Östlund. Mobile search of material out of regulatory control (MORC) – Detection limits assessed by field experiments. Final report from the NKS-B MOMORC activity Contract: AFT/B(16)1, 2017.

Finck, R., Bukartas, A., Jönsson, M., Rääf, C., Maximum detection distances for gamma emitting point sources in mobile gamma spectrometry, Applied Radiation and Isotopes, 184; pp 2022. 11019. https://doi.org/10.1016/j.apradiso.2022.1101

Thomas Hjerpe, Robert R. Finck, and Christer Samuelsson. 2001. Statistical Data Evaluation in Mobile Gamma Spectrometry: An Optimization of On-Line Search Strategies in the Scenario of Lost Point Sources, Health Physics Vol 80 No 6, pp 563 – 570, 2001.

Peder Kock. Orphan source detection in mobile gamma-ray spectrometry - Improved techniques for background assessment. Doctoral thesis, Department of Medical Radiation Physics, Lund University, 2012.

Jonas Nilsson. Mobile Gamma Spectrometry. Development and Optimisation of Methods for Locating and Mapping Lost Radioactive Sources. Doctoral thesis, Medical Radiation Physics, Malmö, Lund University. 2016.

Christopher L. Rääf (chair), Robert R. Finck (co-chair), Antanas Bukartas, Gísli Jónsson, Sune Juul Krogh, Simon Karlsson, Morten Sickel, Petri Smolander, Jonas Wallin, Robin Watson. AUTOMORC – Improvement of automatic methods for identification of radioactive material out of regulatory control (MORC) by mobile gamma spectrometric search experiments. Nordic Nuclear Safety Research, Report NKS-422, March 2019.

Christopher L. Rääf (chair), Robert R. Finck (co-chair), Vikas C. Baranwal, Antanas Bukartas, Marie-Andrée Dumais, Kjartan Guðnason, Yvonne Hinrichsen, Gísli Jónsson, Mattias Jönsson, Peder Kock, Sune Juul Krogh, Simon Karlsson, Frode Ofstad, Jan Steinar Rønning, Petri Smolander, Kasra Tazmani, Mikael Westin, SHIELDMORC – Detection distances and methods to locate orphan gamma radiation sources in shielded building geometries by mobile gamma spectrometry, Nordic Nuclear Safety Research, Report NKS-433, March 2020.

Christopher L. Rääf, Robert R. Finck, Vikas C. Baranwal, Jonas Boson, Antanas Bukartas, Marie-Andrée Dumais, Kjartan Guðnason, Marjan Ilkov, Gísli Jónsson, Mattias Jönsson, Simon Karlsson, Marie Lundgaard Davidsdóttir, Frode Ofstad, Jan Steinar Rønning, Petri Smolander, Mikael Westin, Detection of orphan gamma radiation sources in shielded building geometries by mobile gamma spectrometry. A method of using Compton scattered radiation to estimate the shielding mass thickness of common building material, Nordic Nuclear Safety Research Report NKS-448, June 2021.

Karl Östlund, Therese Geber-Bergstrand, Mattias Jönsson, Jonas Nilsson, Matthew J F Healy, Magnus Linde, Sigurður Emil Pálsson, Christer Samuelsson, Robert Finck, REFOX - Outline and preliminary evaluation of a joint Nordic radiological emergency response exercise conducted in Sweden, CBRNe Convergence Conference Norfolk, 2012.

Acknowledgement

The authors thank Barsebäck Kraft AB for the access to the zones for certain parts of the experimental measurements.

The experiments made by Lund University were carried out with measuring equipment financed by the former Swedish Radiation Protection Authority (SSI) and The Swedish Radiation Safety Authority (SSM).

NKS conveys its gratitude to all organizations and persons who by means of financial support or contributions in kind have made the work presented in this report possible.

Appendix A. Results from team DEMA, Danish Emergency Management Agency, Denmark

A1. Measuring equipment

The DEMA mobile spectrometry unit used in the experiments was a converted VW Multivan with room for a driver, a co-driver and two operators. One driver and one operator typically operate the car (Fig A1-1).

The car was equipped with a Radiation Solutions RSI RS-700 system with two detectors connected, an RSX 4 litre NaI(Tl) and an RSX 3"x3" NaI(Tl) crystal, but only the 4-litre detector was used in this experiment. The detector was placed in a box on the rooftop of the car. The detector system was connected to a computer inside the car, which runs RadAssist software with mapping and radionuclide identification capability.

Figure A1-1. DEMA´s mobile gamma spectrometry car used in the experiment**.**

A2. Detector efficiency calibration

The 4 litre NaI(Tl)-detector was calibrated for counting efficiency at 662 keV in an earlier NKS field experiment (NKS-AUTOMORC, 2018) using a Cs-137 point source with activity traceable to calibration sources from Eckert & Ziegler with 3% relative expanded uncertainty (k=2). When placed in the rooftop box, the detector efficiency for 662 keV photons from the right side (the apparent detector area for total photon absorption) was 0.0258 m^2 with 8% relative expanded uncertainty (k=2).

A3. Detector calibration for shield mass thickness determination, using SSC

The response of the 4 litre NaI(Tl) detector as net count rates in ROI A, B, C and PL relative to ROI PR and ROI P was measured for different shield mass thicknesses as described earlier in the report. The measurement data was entered into the Excel program SCC. The relationship between the net count rates for the ratios ROI A, B, C, and PL/PR for the exponential model is shown in Fig A3-1-a and the polynomial model in Fig A3-1-c. Corresponding relationships for the ratios ROI A, B, and C/ P are shown in Figs A3-1-b and A3-1-d.

The polynomial fit for the count rate ratio ROI PL/PR (Fig A3-1-c) shows a very sharp gradient, and the fit does not follow the measurement data particularly well at increased shield thickness. The misfit indicates that the ratio ROI PL/PR in the polynomial model cannot be expected to give reliable results for shield thicknesses.

The polynomial fit for the count rate ratio ROI B/P (Fig A3-1-d) is forced to 1.0 for zero shield thickness due to a trade-off that prioritizes better fitting of the polynomial model for thicker shields. For thin shields, a measured count rate ratio ROI C/P below 1.2 will show an unreliable low shield thickness.

The coefficients for fitting the exponential model to observed data are given in Table A3-1. The coefficients for fitting the five-degree polynomial model to observed data are given in Table A3-2.

Table A3-1. DEMA 4 litre NaI(Tl)-detector. Coefficients *a* and *b* in an exponential model for determining shield mass thickness according to the description in the main report. The unit of *b* is m^2/kg.

ROI ratio	*a*	*b*
ROI A/PR	3.90	0.00501
ROI B/PR	2.00	0.00402
ROI C/PR	1.40	0.00295
ROI PL/PR	1.53	0.000996
ROI A/P	1.47	0.00437
ROI B/P	0.758	0.00338
ROI C/P	0.529	0.00231

Table A3-2. DEMA 4 litre NaI(Tl)-detector. Coefficients a_0 - a_5 (kg/m^2) in the five-degree polynomial model for determining shield mass thickness according to Eqn 3 in the main report.

ROI ratio	a_5	a_4	a_3	a_2	a_1	a_0
ROI A/PR	5.99	-76.39	332.0	-530.3	301.6	0
ROI B/PR	20.97	-180.6	503.9	-443.5	165.0	0
ROI C/PR	118.0	-681.5	1326	-886.7	309.1	0
ROI PL/PR	-202600	668700	-850600	522800	-155100	17810
ROI A/P	19.39	-157.1	395.8	-274.5	133.3	0
ROI B/P	-144.2	864.9	-1752	1260	207.7	0
ROI C/P	904.3	-536.4	-944.0	437.9	644.8	229.1

A4. Results from shield thickness measurements, using SSC

In connection with the experiment determining the source distance with the SODAC routine, a determination of the shield mass thickness in front of the Cs-137 point source was made using the SSC routine when the measuring car was directly opposite the source, i.e. at the road location with the shortest distance to the source. The results are given in tables A4-1 to A4-4.

The deviation in the calculated mass thickness from the actual value was between -11% and 42% for the exponential model, and the polynomial model's deviation was between -14% and 44%. It is impossible to say that one model gives better values than the other. On average, the models overestimated the mass thickness by 17 ± 9%.

The detailed result from SSC is also reproduced in Figs A4-1 to A4-5, where the individual net count rate ratios ROI A/PR, ROI B/PR Etc., are plotted along the lines of the exponential model and the polynomial model. The measurement data show relatively good agreement for the different ROI ratios, except for the ROI PL/PR ratio. The misfit is likely because even a slight gain drift can significantly affect the area (net count rate) under the full energy peak that constitutes ROI PL and ROI PR, respectively.

Table A4-1. Result from the DEMA 4 litre NaI(Tl) detector determination of shield mass thickness by using ROI A, B, C, PL / PR net count rate ratios in an exponential model

Setup	Actual		Measured		Deviation
	Distance to source (m)	Shield mass thickness (kg/m^2)	Shield and air mass thickness (kg/m^2)	Shield mass thickness (kg/m^2)	of measured from actual value (%)
M1	61	0	108.2	32.4	42.8
M2	31	333	408	370	9.8
M3	61	94	217	142	28.2
M4	61	333	362	287	-11.3
M5	91	94	257	144	24.3
Average					18.8 ± 9.2

Table A4-2. Result from the DEMA 4 litre NaI(Tl) detector determination of shield mass thickness by using ROI A, B, C / P net count rate ratios in an exponential model

Setup	Actual		Measured		Deviation
	Distance to source (m)	Shield mass thickness (kg/m^2)	Shield and air mass thickness (kg/m^2)	Shield mass thickness (kg/m^2)	of measured from actual value (%)
M1	61	0	89.0	13.1	17.3
M2	31	333	375	336	0.8
M3	61	94	230	155	35.7
M4	61	333	390	314	-4.6
M5	91	94	283	170	36.5
Average					17.1 ± 8.5

Table A4-3. Result from the DEMA 4 litre NaI(Tl) detector determination of shield mass thickness by using ROI A, B, C, PL / PR net count rate ratios in a five-degree polynomial model

Setup	Actual		Measured		Deviation
	Distance to source (m)	Shield mass thickness (kg/m^2)	Shield and air mass thickness (kg/m^2)	Shield mass thickness (kg/m^2)	of measured from actual value (%)
M1	61	0	98.8	23.0	30.3
M2	31	333	482	442	29.5
M3	61	94	195	119	14.6
M4	61	333	359	283	-12.3
M5	91	94	240	127	15.7
Average					15.6 ± 7.7

Table A4-4. Result from the DEMA 4 litre NaI(Tl) detector determination of shield mass thickness by using ROI A, B, C / P net count rate ratios in a five-degree polynomial model

Setup	Actual		Measured		Deviation
	Distance to source (m)	Shield mass thickness (kg/m^2)	Shield and air mass thickness (kg/m^2)	Shield mass thickness (kg/m^2)	of measured from actual value (%)
M1	61	0	65.3	-10.5	-13.9
M2	31	333	430	391	15.6
M3	61	94	217	141	27.7
M4	61	333	448	372	9.6
M5	91	94	297	184	43.5
Average					16.5 ± 9.6

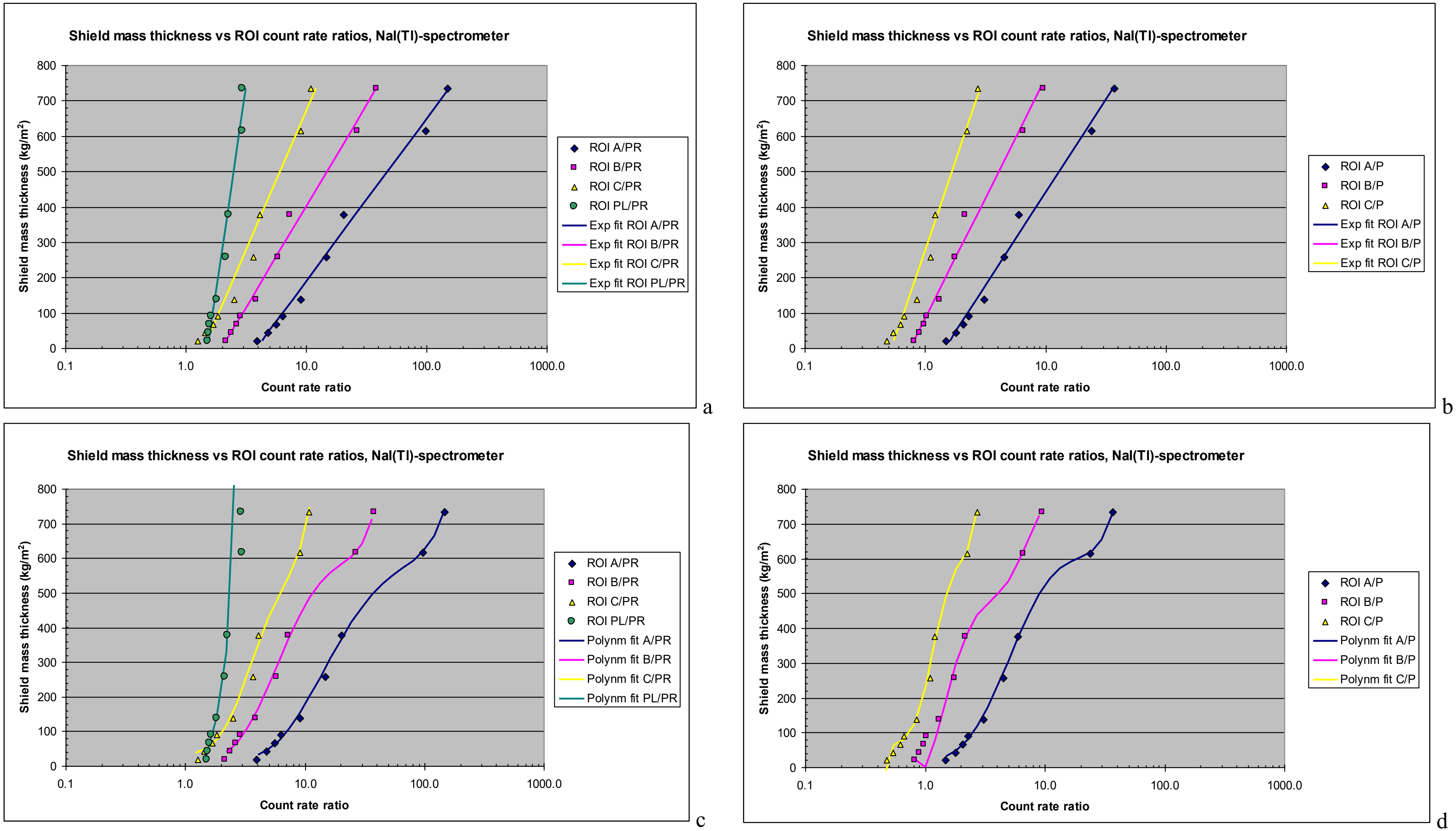

Fig A3-1-a-d. DEMA 4 litre NaI(Tl) spectrometer. Models of shield mass thickness as a function of ROI net count rate ratio obtained from fitting measured data to exponential functions (a, b) and five-degree polynomial functions (c, d), valid for Cs-137 point sources behind shields of standard building material (wood and concrete) with mass thickness between 20 and 730 kg/m^2. Values have been measured at a source-detector distance of 10 m.

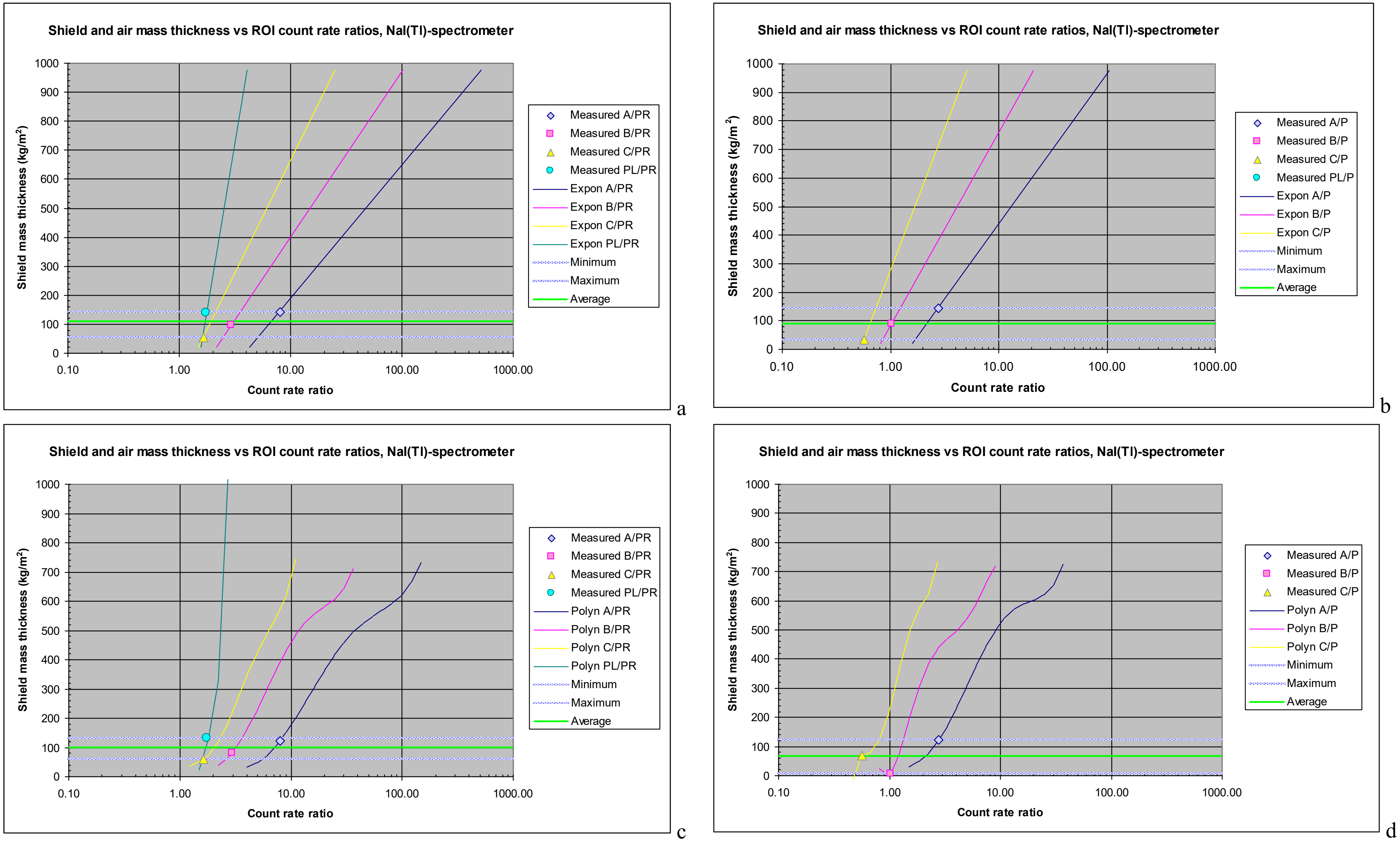

Fig A4-1-a-d (M1). Shield mass thickness determination by the DEMA 4 litre NaI(Tl) spectrometer using the ROI count rate ratio method with exponential (a, b) and polynomial (c, d) models. The true shield mass thickness is 75.8 kg/m2, including 61 m of air between the source and the detector.

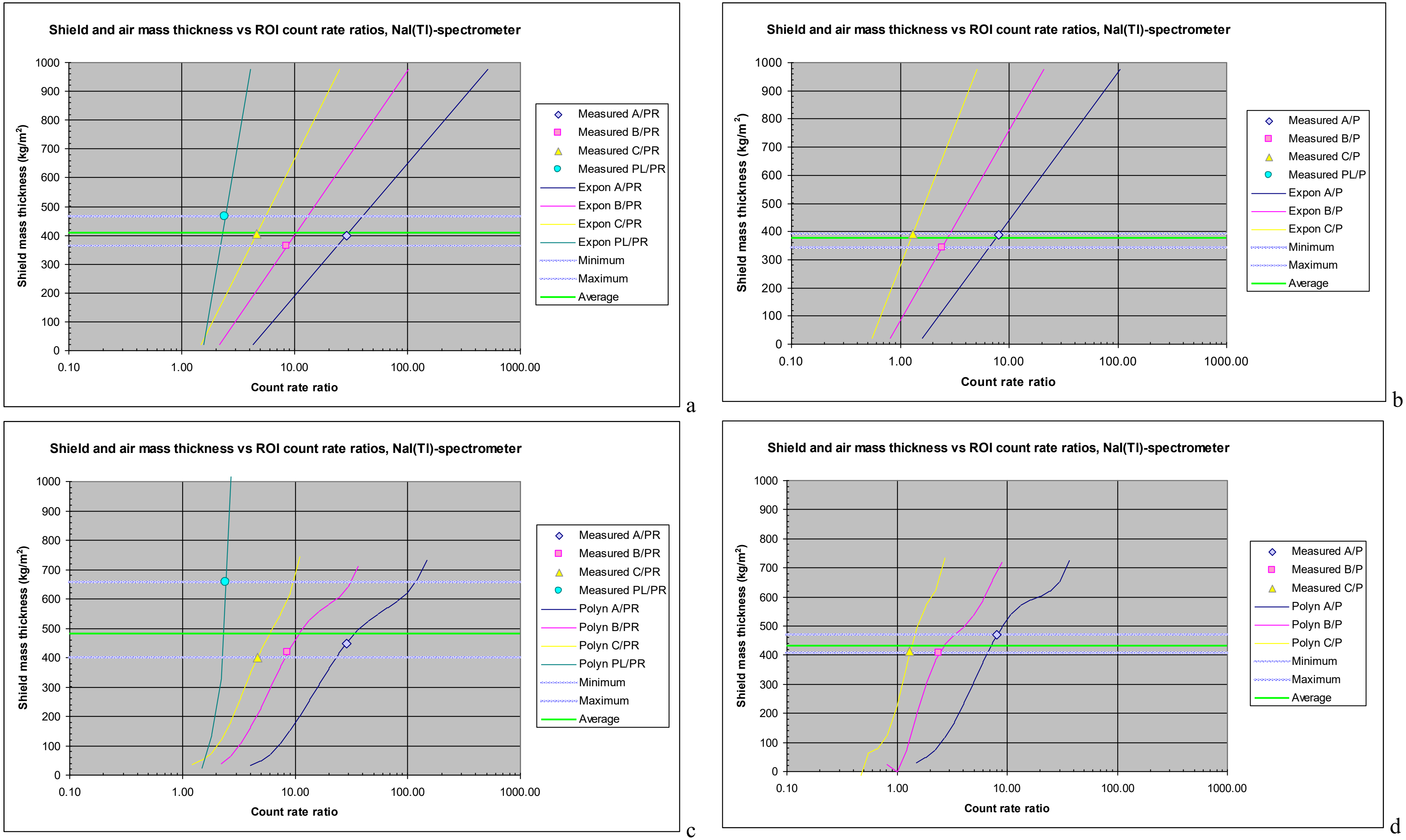

Fig A4-2-a-d (M2). Shield mass thickness determination by the DEMA 4 litre NaI(Tl) spectrometer using the ROI count rate ratio method with exponential (a, b) and polynomial (c, d) models. The true shield mass thickness is 372 kg/m2, including 31 m of air between the source and the detector.

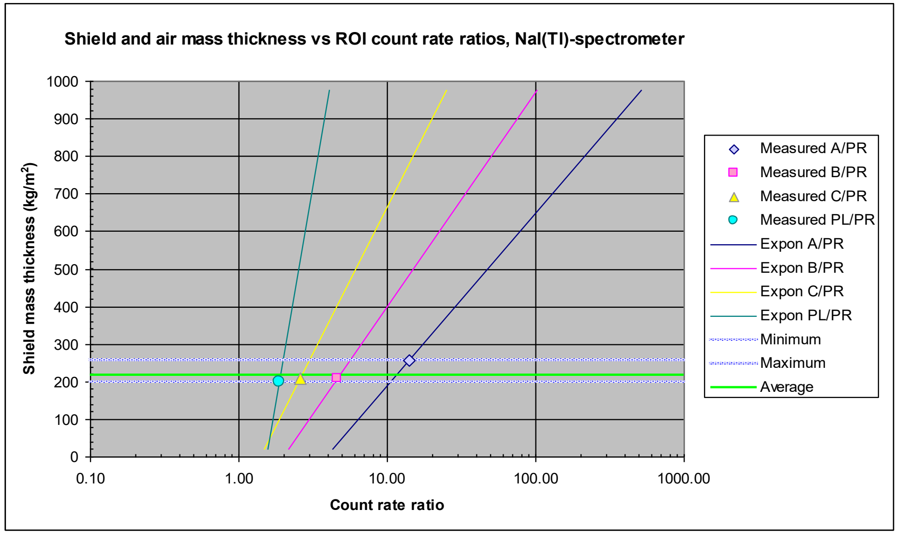

a

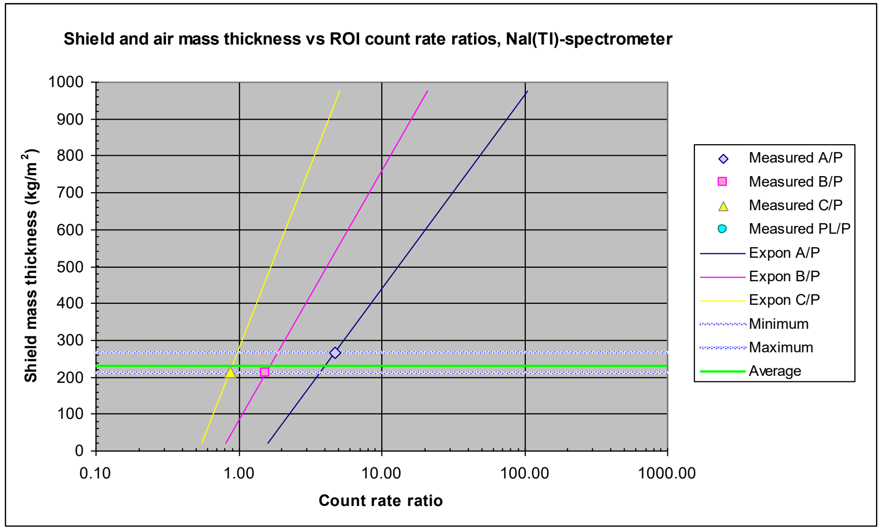

b

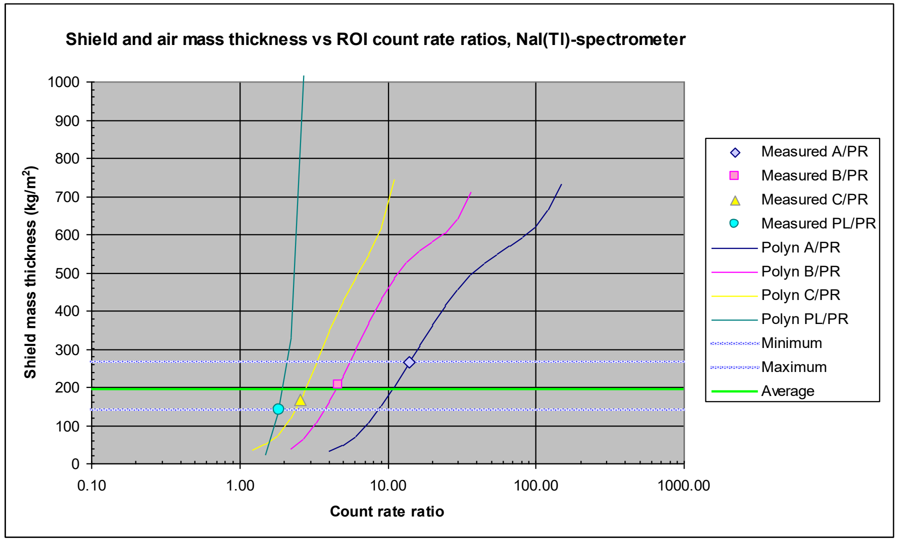

c

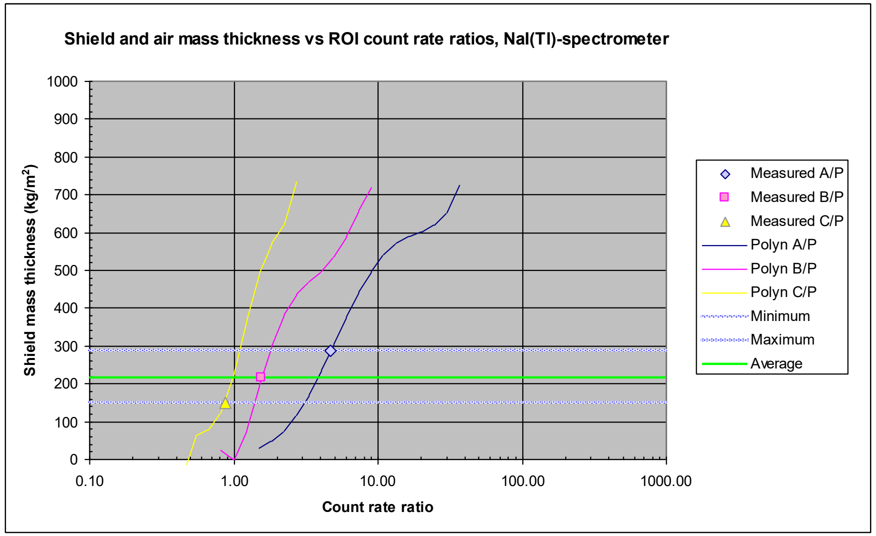

d

Fig A4-3-a-d (M3). Shield mass thickness determination by the DEMA 4 litre NaI(Tl) spectrometer using the ROI count rate ratio method with exponential (a, b) and polynomial (c, d) models. The true shield mass thickness is 170 kg/m2, including 61 m of air between the source and the detector.

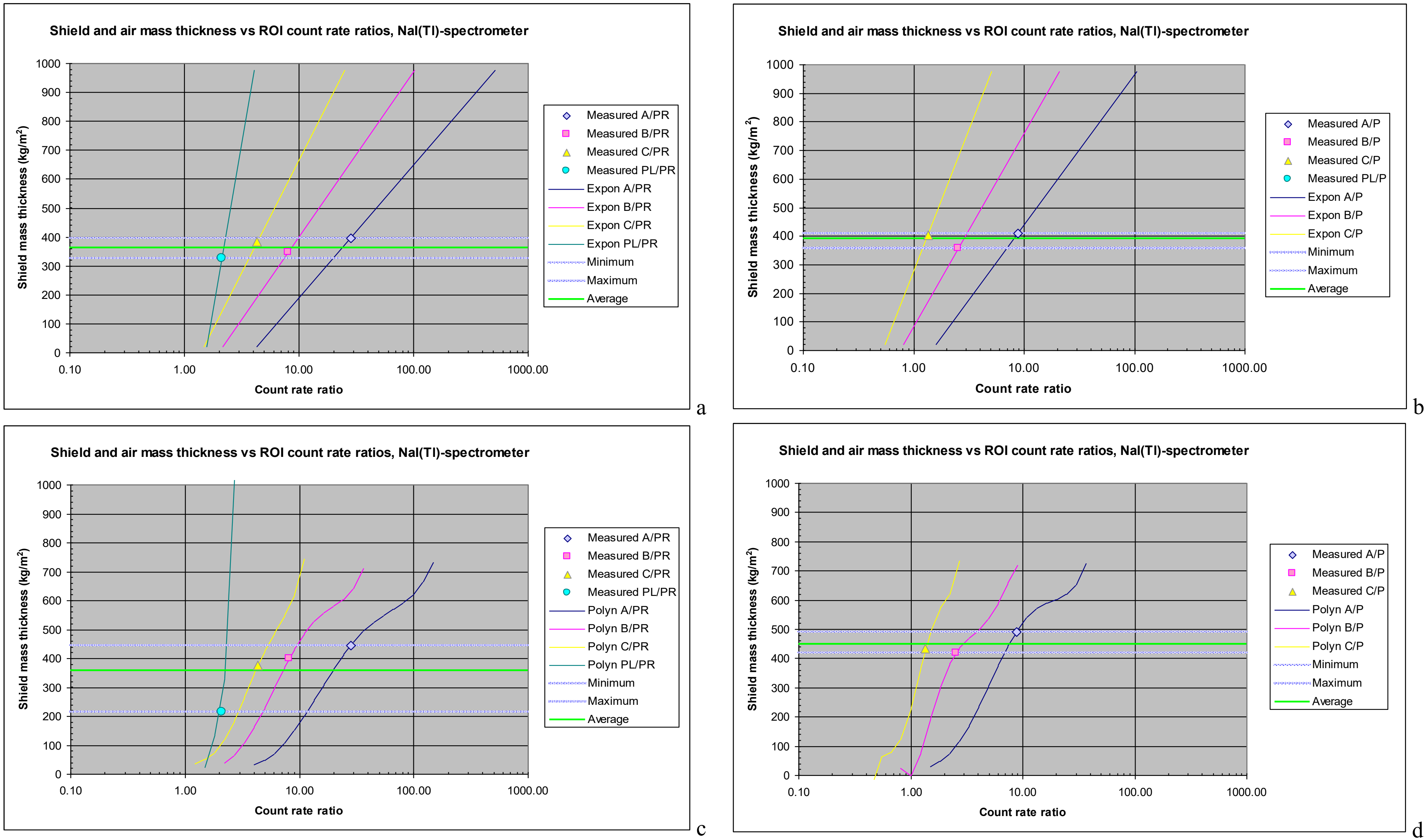

Fig A4-4-a-d (M4). Shield mass thickness determination by the DEMA 4 litre NaI(Tl) spectrometer using the ROI count rate ratio method with exponential (a, b) and polynomial (c, d) models. The true shield mass thickness is 409 kg/m2, including 61 m of air between the source and the detector.

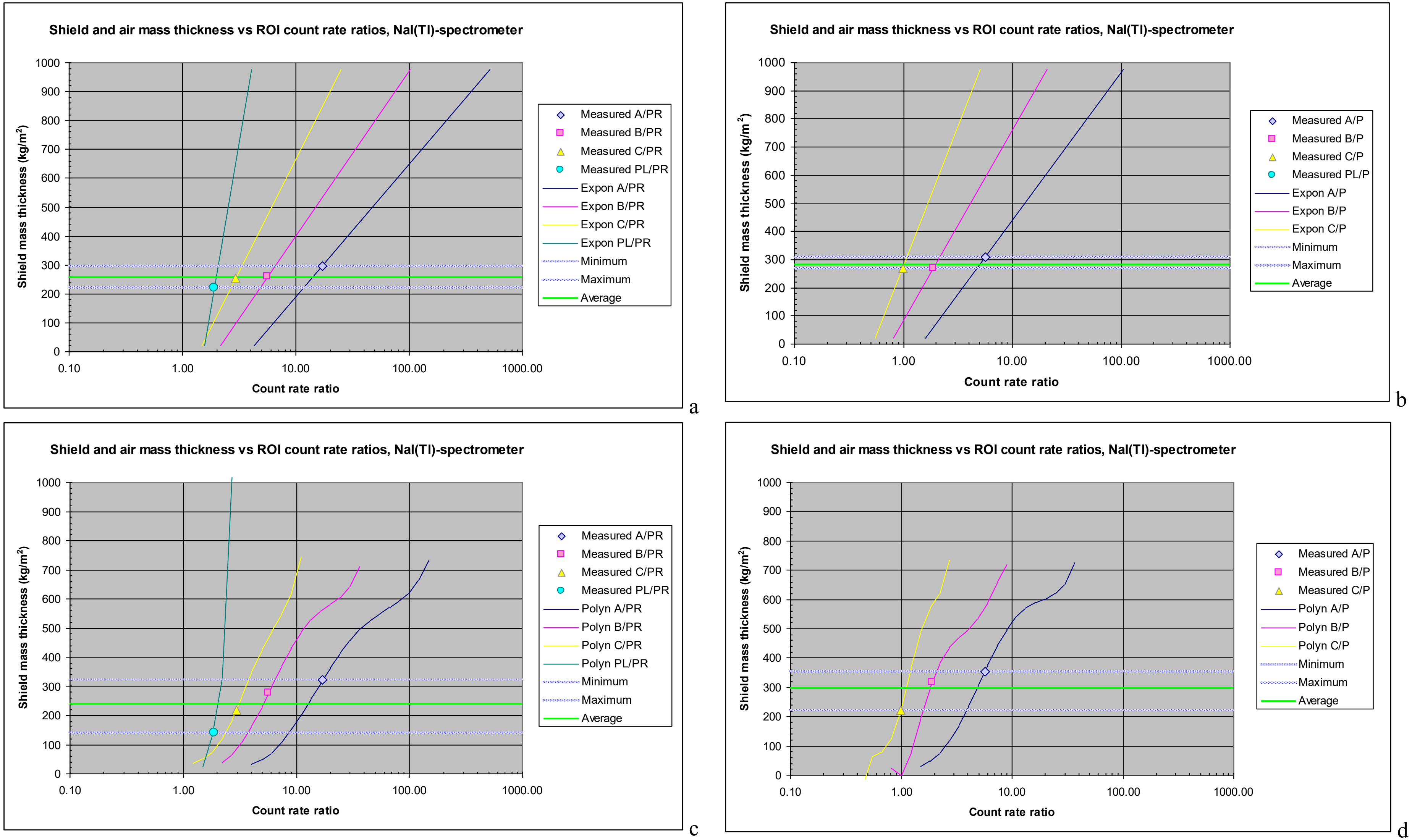

Fig A4-5-a-d (M5). Shield mass thickness determination by the DEMA 4 litre NaI(Tl) spectrometer using the ROI count rate ratio method with exponential (a, b) and polynomial (c, d) models. The true shield mass thickness is 207 kg/m^2, including 91 m of air between the source and the detector.

A5. Results from source distance measurements, using SODAC

The distance to a Cs-137 point source was determined using the Excel program SODAC for five different setups with different distances and shielding (M1 - M5), as described in the main report. All measurements were made standing still (semi-stationary) at various locations along the road that passes the radiation source. Unfortunately, it turned out that some trees between the radiation source and the measuring car shielded the photon fluence from the source at specific points along the road. These measurement points have been identified, and the data has been removed from the analysis.

Correcting the detector response for the angular dependence of the oblong detector for count rates from the source at different incident angles proved necessary during the analysis. How the correction is determined is reported in the text of the main report.

In the SODAC analysis, the actual shield thickness has been used in the distance determination (and not the one obtained through SSC) because it produces a more accurate picture of any distance determination deviations than a possibly distorted assumption of the shield thickness would do.

Results from the Excel program SODAC showing which "intensity curve" (primary photon fluence from the source as a function of distance along the road) best fits the measurement data along the road for the five setup distances are reproduced in Figs A5-1 to A5-5.

Results from the distance and activity determination with SODAC are summarized in Table A5-1. For setup M1 and M2, the distance determination agrees with the actual values, and the source activity is overestimated by 16% and 91% for these measurements, respectively. For setups M3, M4 and M5, the distance determination is underestimated by about 17%, and the activity determination is overestimated by 34% to 214% of the actual value.

On average, for five setups, the distance determinations are underestimated by 10 ± 4%, and the source activity is overestimated by 88 ± 35%.

The reason for the deviations from actual values is not fully known. It may be due to the low energy resolution in a NaI(Tl) detector and the increased distance to the source compared to the calibration distance for shield thickness. Photons scattered at small angles between the source and the detector are recorded as primary photons in the full-energy peak in the pulse height distribution of the detector. This photon scattering causes the count rate in ROI PR and ROI P to increase compared to primary-only photons, and it may affect distance and shield thickness determination at longer distances. Further experimental investigations of the detector's response at longer source distances and thicker shielding are needed to draw more definite conclusions.

Table A5-1. Results from the DEMA 4 litre NaI(Tl) detector, applying the SODAC routine to obtain the source distance and activity for a Cs-137 point source. The distance is adjusted for the varying angular efficiency for horizontally oriented 4 litre NaI(Tl) detectors. The activity is calculated from the full energy peak count rate for the adjusted and the actual distance, using the actual shield thickness. The actual point source activity is 606 MBq in all setups.

Setup	Actual		SODAC obtained				Deviation	
	Distance to source m	Shield mass thickness kg/m^2	Distance m	Distance angular efficiency adjusted m	Activity at adjusted distance MBq	Activity at actual distance MBq	Distance at adjusted rounded %	Activity at adjusted (at actual) distance %
M1	61	air only	35	60	702	702	0	15.8 (15.8)
M2	31	333	20	30	1157	1157	0	90.9 (90.9)
M3	61	94	45	50	511	810	-17	-15.7 (33.7)
M4	61	333	45	50	1201	1905	-17	98.2 (214)
M5	91	94	55	75	675	1123	-17	11.4 (85.3)
Average							-10 ± 4	40 ± 23 (88 ± 35)

SODAC source distance results, DEMA 4 litre NaI(Tl)-detector

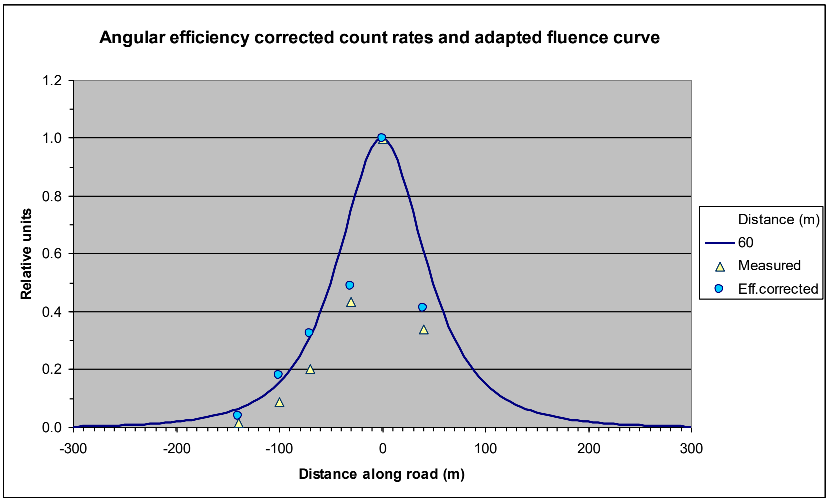

Fig A5-1. DEMA. Setup M1. The true source distance is 61 m

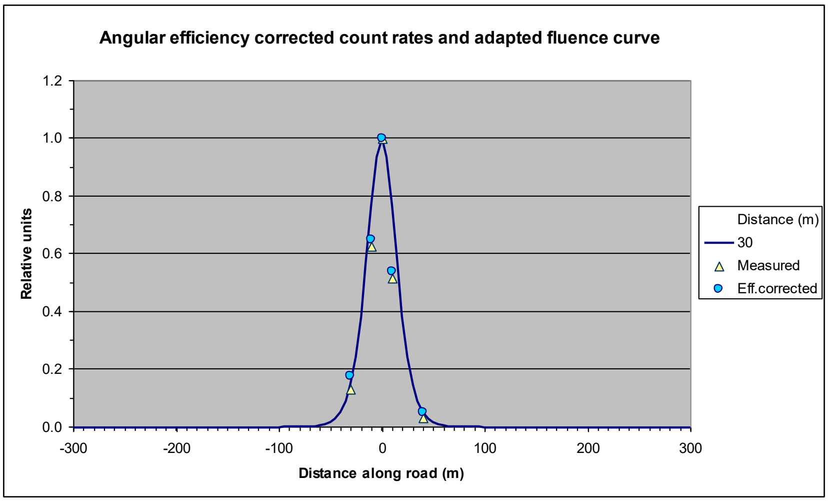

Fig A5-2. DEMA. Setup M2. The true source distance is 31 m

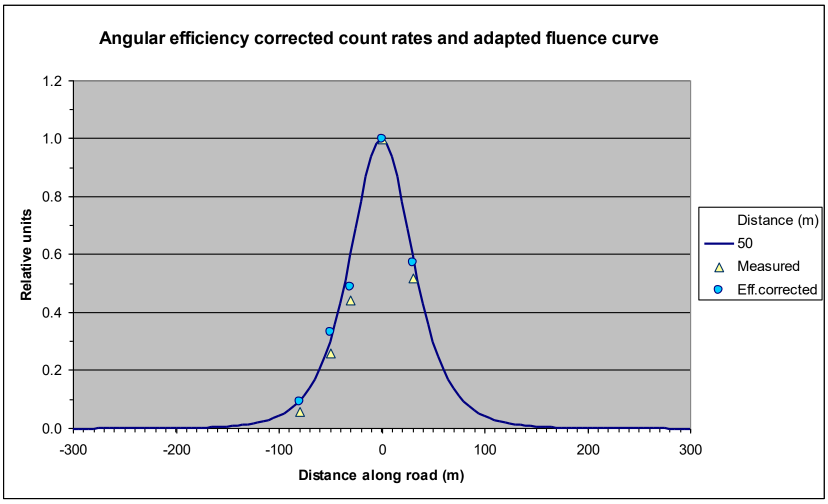

Fig A5-3. DEMA. Setup M3. The true source distance is 61 m

The figures show SODAC determined source distance results for the DEMA 4 litre NaI(Tl)-detector, corrected for varying angular efficiency. Tree-shielded measurement locations have been excluded.

SODAC source distance results, DEMA 4 litre NaI(Tl)-detector

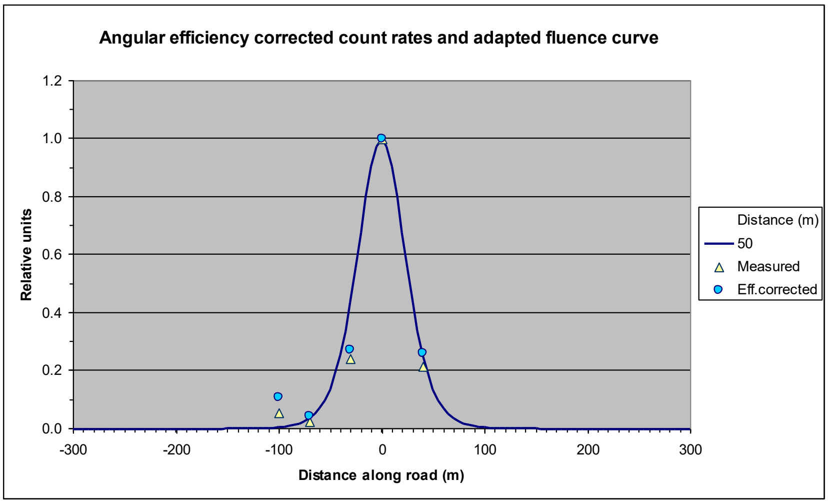

Fig A5-4. DEMA. Setup M4. The true source distance is 61 m

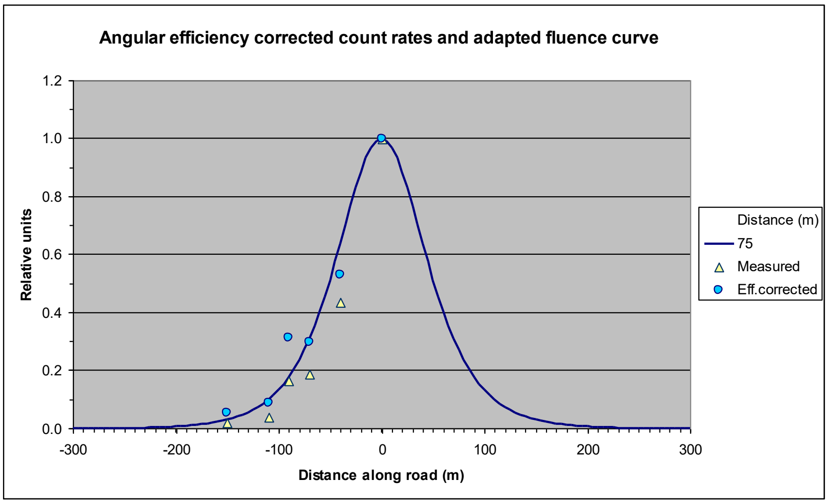

Fig A5-5. DEMA. Setup M5. The true source distance is 91 m

The figures show SODAC determined source distance results for the DEMA 4 litre NaI(Tl)-detector, corrected for varying angular efficiency. Tree-shielded measurement locations have been excluded.

A6. Summary and conclusion

In determining the mass thickness of the radiation shield with the SCC routine, two models have been used that describe the net count rate relationships between registrations from scattered radiation and primary radiation, an exponential model and a polynomial model. Both models give roughly the same results and overestimate the shield mass thickness by 17 ± 9%.

When determining the distance to a radiation source with the SODAC routine in five different cases with spacing from 30 to 90 m, the distances were, on average, underestimated by 10 ± 4%. The calculated activity was, on average, overestimated by 88 ± 35%. The reason for the deviations from actual values is not fully known. Further experimental investigations of the detector's response at longer source distances and thicker shielding are needed to investigate the reason more in-depth.

Appendix B. Results from team DSA, Norwegian Radiation and Nuclear Safety Authority, Norway

B1. Measuring equipment

The DSA mobile spectrometry unit used two 4 litre NaI(Tl)-detectors placed on each side of the car close to the roof, one 3"x3" NaI(Tl)-detector on the left side of the car close to the roof, and one He-3 neutron detector in the middle between the two 4 litre NaI(Tl)-detectors. All detectors and corresponding electronics were off the shelf from Radiation Solutions, RSI, and they worked fine.

One immediate observation was that the detectors on the left side of the car detected very few photons from the sources due to our fixed detector setup because the left detectors are somewhat shielded by the detectors placed on the right side of the car. Still, a shield mass thickness calibration for the 3"x3" NaI(Tl) detector was made. However, it was not possible to use this detector for distance, shielding and activity determination at road site M because the detector's relatively low efficiency produces too low count rates from the distance sources.

B2. Detector efficiency calibration

Only the right 4 litre NaI(Tl)-detector was used for distance shielding and activity determination. The detector's counting efficiency at 662 keV was determined in an earlier NKS field experiment (NKS-AUTOMORC, 2018) using a Cs-137 point source with activity traceable to calibration sources from Eckert & Ziegler with 3% relative expanded uncertainty (k=2). When placed on the right side in the car, the detector efficiency for 662 keV photons incident from the right side (the apparent detector area for total photon absorption) was 0.0252 m^2 with 8% relative expanded uncertainty (k=2).

B3. Detector calibration for shield mass thickness determination, using SSC

The response of the right side 4 litres NaI(Tl) detector as net count rates in ROI A, B, C and PL relative to ROI PR and ROI P was measured for different shield mass thicknesses described in the main report. The measurement data was entered into the Excel program SCC. The relationship between the net count rates for the ratios ROI A, B, C, and PL/PR for the exponential model is shown in Fig B3-1-a and the polynomial model in Fig B3-1-c. Corresponding relationships for the ratios ROI A, B, and C/P are shown in Figs B3-1-b and B3-1-d.

Response data for the 3"x3" NaI(Tl) detector is shown in Fig B3-2-a-d..

The coefficients for fitting the exponential model to observed data are given in Table B3-1 for the right side 4 litre NaI(Tl)-detector and in Table B3-3 for the 3"x3" NaI(Tl)-detector. The corresponding coefficients for fitting the five-degree polynomial model to observed data are given in Table B3-2 and B3-4.

The exponential model and the five-degree polynomial model represent the measured net count rate ratios for the different shield mass thicknesses quite well.

Table B3-1. DSA right side 4 litre NaI(Tl)-detector. Coefficients *a* and *b* in an exponential model for determining shield mass thickness according to the description in the main report. The unit of *b* is m^2/kg.

ROI ratio	*a*	*b*
ROI A/PR	4.58	0.00479
ROI B/PR	2.15	0.00397
ROI C/PR	1.52	0.00278
ROI PL/PR	1.41	0.00118
ROI A/P	1.83	0.00401
ROI B/P	0.858	0.00320
ROI C/P	0.605	0.00201

Table B3-2. DSA right side 4 litre NaI(Tl)-detector. Coefficients a_0 - a_5 (kg/m^2) in the five-degree polynomial model for determining shield mass thickness according to Eqn 3 in the main report.

ROI ratio	a_5	a_4	a_3	a_2	a_1	a_0
ROI A/PR	1.536	-18.77	65.94	-9.258	-74.90	0.000
ROI B/PR	-2.317	33.87	-190.5	484.7	-275.0	0.000
ROI C/PR	-8.375	33.35	-76.78	239.3	-12.15	0.000
ROI PL/PR	-2599	13000	-22410	17490	-5587	621.9
ROI A/P	3.403	-19.02	-18.11	241.4	-122.0	0.000
ROI B/P	12.04	-70.15	152.3	-217.4	523.8	0.000
ROI C/P	279.0	-421.2	-253.0	410.4	523.7	201.4

Table B3-3. DSA 3"x3" NaI(Tl)-detector. Coefficients *a* and *b* in an exponential model for determining shield mass thickness according to the description in the main report. The unit of *b* is m^2/kg.

ROI ratio	*a*	*b*
ROI A/PR	15.2	0.00444
ROI B/PR	5.29	0.00341
ROI C/PR	2.63	0.00220
ROI PL/PR	1.37	0.00120
ROI A/P	6.18	0.00366
ROI B/P	2.15	0.00263
ROI C/P	1.07	0.00142

Table B3-4. DSA 3"x3" NaI(Tl)-detector. Coefficients a_0 - a_5 (kg/m^2) in the five-degree polynomial model for determining shield mass thickness according to Eqn 3 in the main report.

ROI ratio	a_5	a_4	a_3	a_2	a_1	a_0
ROI A/PR	1.722	-31.45	199.2	-475.7	362.0	0.000
ROI B/PR	4.884	-59.13	227.8	-234.7	-3.571	0.000
ROI C/PR	-100.1	621.0	-1394	1538	-625.6	0.000
ROI PL/PR	-7177	23640	-29398	17690	-4637	449.2
ROI A/P	7.543	-95.14	405.5	-608.2	252.7	0.000
ROI B/P	14.68	-49.529	-167.0	816.1	-540.06	0.000
ROI C/P	-279.7	502.9	-956.9	1352	58.56	18.13

B4. Results from shield thickness measurements, using SSC

In connection with the experiment determining the source distance with the SODAC routine, a determination of the shield mass thickness in front of the Cs-137 point source was made using the SSC routine when the measuring car was directly opposite the source, i.e. at the road location with the shortest distance to the source. The results are given in tables B4-1 to B4-4.

The deviation in the calculated mass thickness from the actual value was between -87% and -1% for the exponential model, and the polynomial model's deviation was between -90% and -3%. Thus, both models seem to underestimate the mass shield thickness. On average, the models underestimated the mass thickness by 20 ± 13%. It remains to investigate the cause of the systematic underestimation.

The detailed result from SSC is also reproduced in Figs B4-1 to B4-5, where the individual net count rate ratios ROI A/PR, ROI B/PR Etc., are plotted along the lines of the exponential model and the polynomial model. The measurement data for the different ROIs showed mutually fairly good consistency for all shielding and distance setups (M1 to M5), although the mass shield thickness was systematically under-estimated.

Table B4-1. Result from the DSA 4 litre NaI(Tl) detector determination of shield mass thickness by using ROI A, B, C, PL / PR net count rate ratios in an exponential model

Setup	Actual		Measured		Deviation
	Distance to source (m)	Shield mass thickness (kg/m^2)	Shield and air mass thickness (kg/m^2)	Shield mass thickness (kg/m^2)	of measured from actual value (%)
M1	61	0	30.7	-45.1	-59.5
M2	31	333	361	323	-2.8
M3	61	94	168	91.9	-1.2
M4	61	333	345	269	-15.8
M5	91	94	201	87.7	-3.0
Average					-16.5 ± 11.1

Table B4-2. Result from the DSA 4 litre NaI(Tl) detector determination of shield mass thickness by using ROI A, B, C / P net count rate ratios in an exponential model

Setup	Actual		Measured		Deviation
	Distance to source (m)	Shield mass thickness (kg/m^2)	Shield and air mass thickness (kg/m^2)	Shield mass thickness (kg/m^2)	of measured from actual value (%)
M1	61	0	9.75	-66.1	-87.1
M2	31	333	346	306	-7.3
M3	61	94	156	80.5	-7.9
M4	61	333	349	274	-14.6
M5	91	94	203	90.1	-1.9
Average					-23.8 ± 16.8

Table B4-3. Result from the DSA 4 litre NaI(Tl) detector determination of shield mass thickness by using ROI A, B, C, PL / PR net count rate ratios in a five-degree polynomial model

Setup	Actual		Measured		Deviation
	Distance to source (m)	Shield mass thickness (kg/m^2)	Shield and air mass thickness (kg/m^2)	Shield mass thickness (kg/m^2)	of measured from actual value (%)
M1	61	0	42.2	-33.6	-44.4
M2	31	333	356	317	-4.3
M3	61	94	160	83.9	-5.9
M4	61	333	341	265	-16.6
M5	91	94	194	81.3	-6.1
Average					-15.5 ± 7.6

Table B4-4. Result from the DSA 4 litre NaI(Tl) detector determination of shield mass thickness by using ROI A, B, C / P net count rate ratios in a five-degree polynomial model

Setup	Actual		Measured		Deviation
	Distance to source (m)	Shield mass thickness (kg/m^2)	Shield and air mass thickness (kg/m^2)	Shield mass thickness (kg/m^2)	of measured from actual value (%)
M1	61	0	7.77	-68.1	-89.7
M2	31	333	360	321	-3.2
M3	61	94	149	73.0	-12.3
M4	61	333	364	288	-11.0
M5	91	94	200	87.1	-3.3
Average					-23.9 ± 16.6

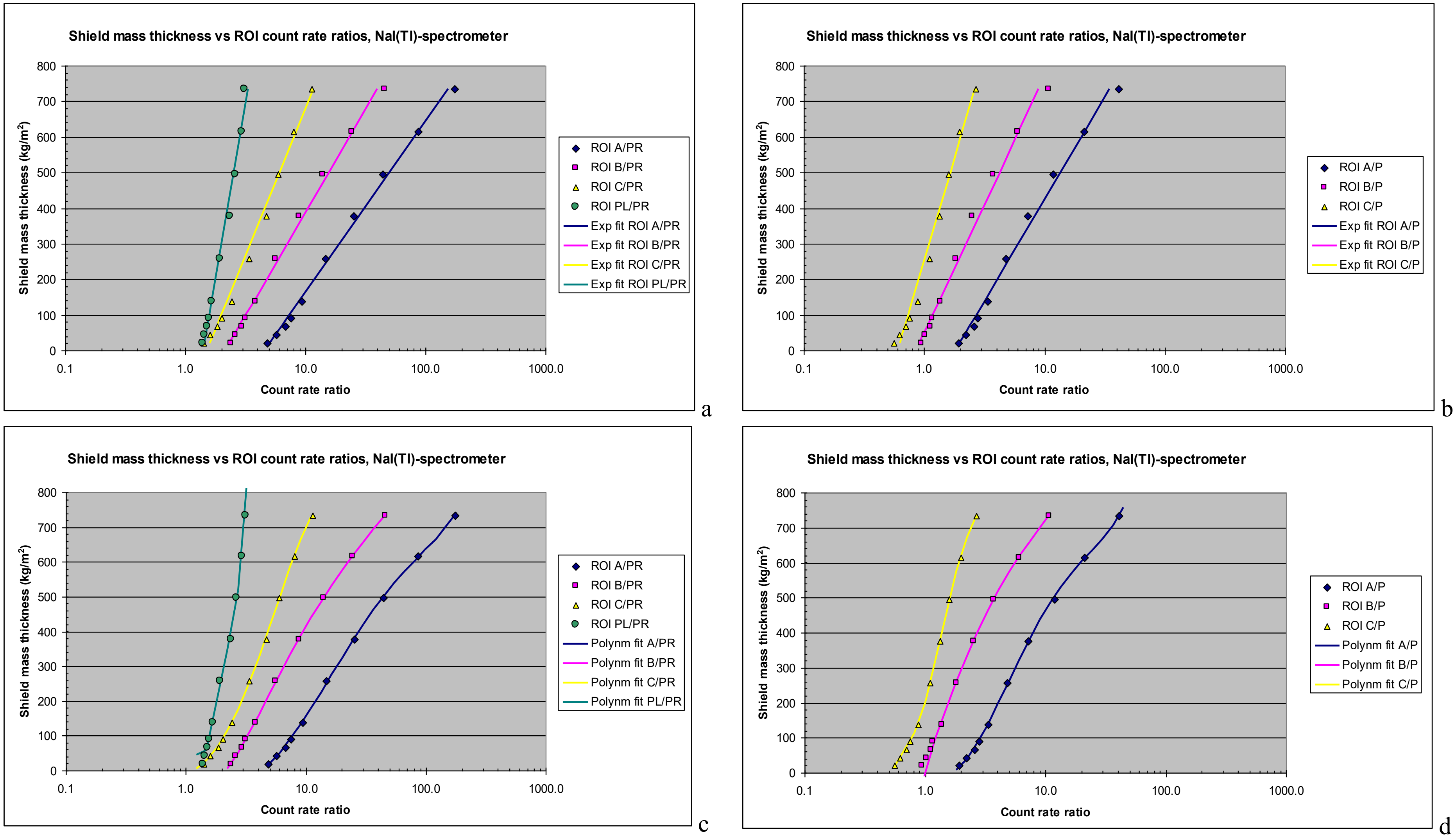

Fig B3-1-a-d. DSA 4 litre NaI(Tl) spectrometer. Models of shield mass thickness as a function of ROI net count rate ratio obtained from fitting measured data to exponential functions (a, b) and five-degree polynomial functions (c, d), valid for Cs-137 point sources behind shields of standard building material (wood and concrete) with mass thickness between 20 and 730 kg/m^2. Values have been measured at a source-detector distance of 10 m.

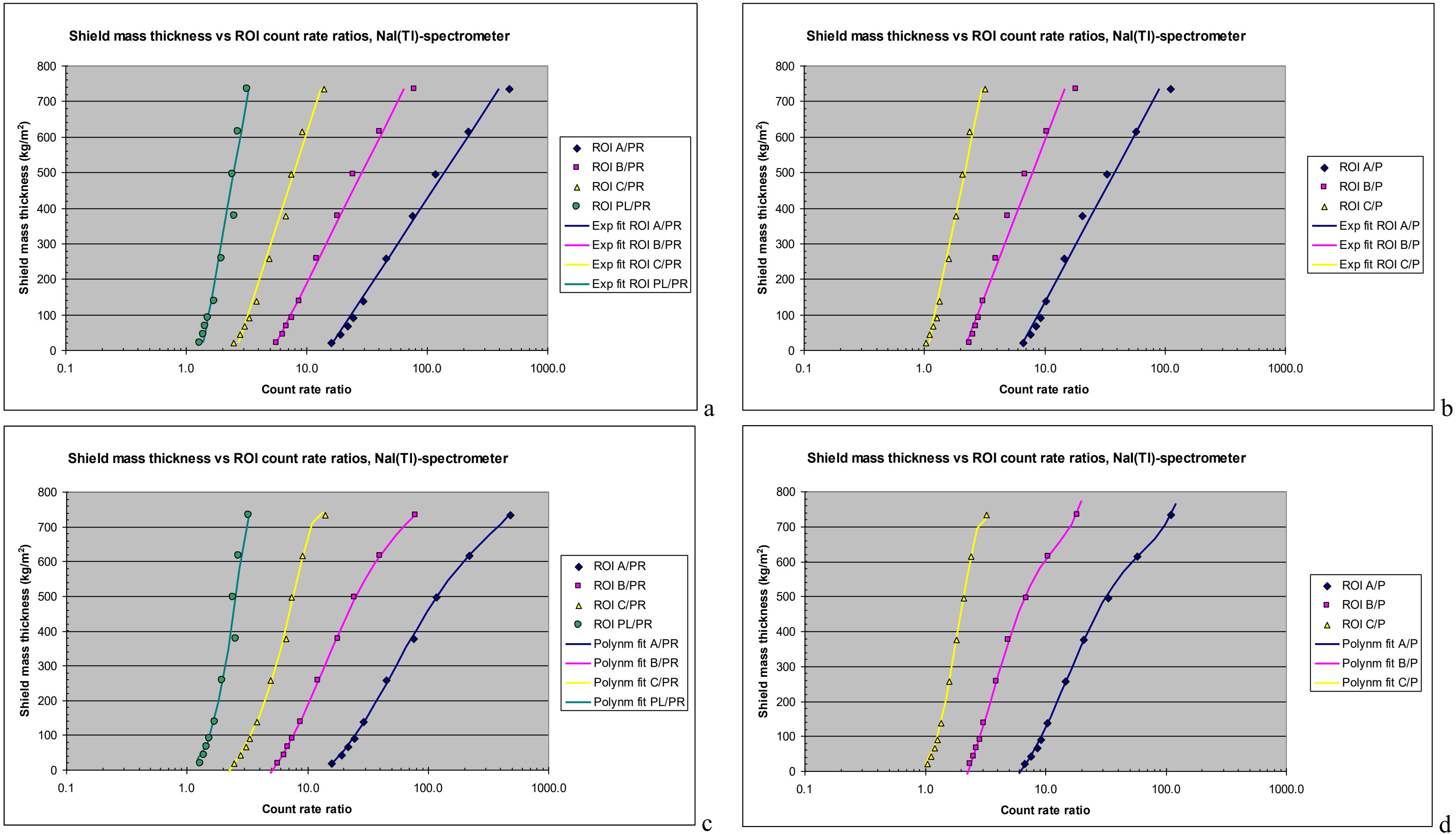

Fig B3-2-a-d. DSA 3"x3" NaI(Tl) spectrometer. Models of shield mass thickness as a function of ROI net count rate ratio obtained from fitting measured data to exponential functions (a, b) and five-degree polynomial functions (c, d), valid for Cs-137 point sources behind shields of standard building material (wood and concrete) with mass thickness between 20 and 730 kg/m^2. Values have been measured at a source-detector distance of 10 m.

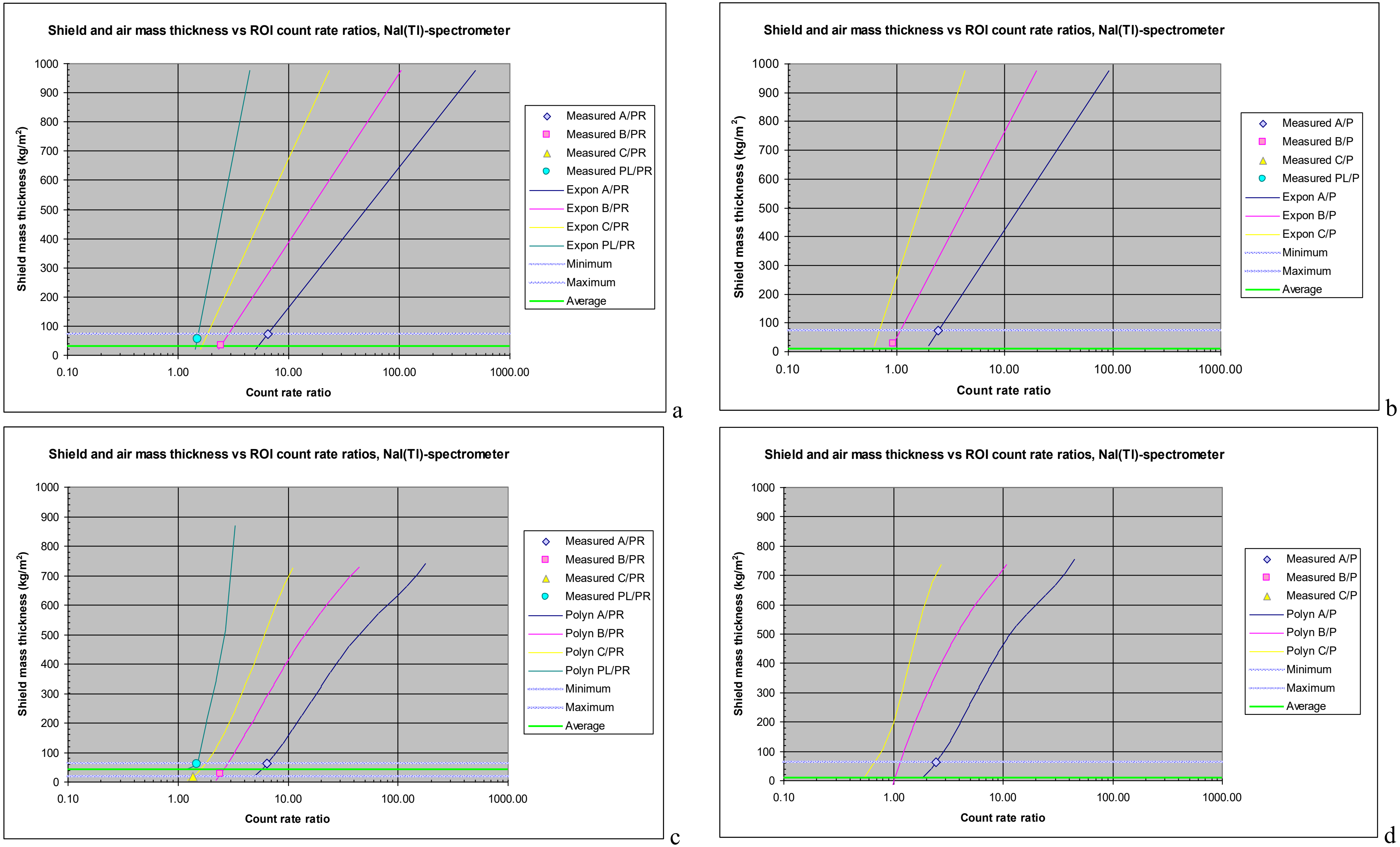

Fig B4-1-a-d (M1). Shield mass thickness determination by the DSA 4 litre NaI(Tl) spectrometer using the ROI count rate ratio method with exponential (a, b) and polynomial (c, d) models. The true shield mass thickness is 75.8 kg/m^2, including 61 m of air between the source and the detector.

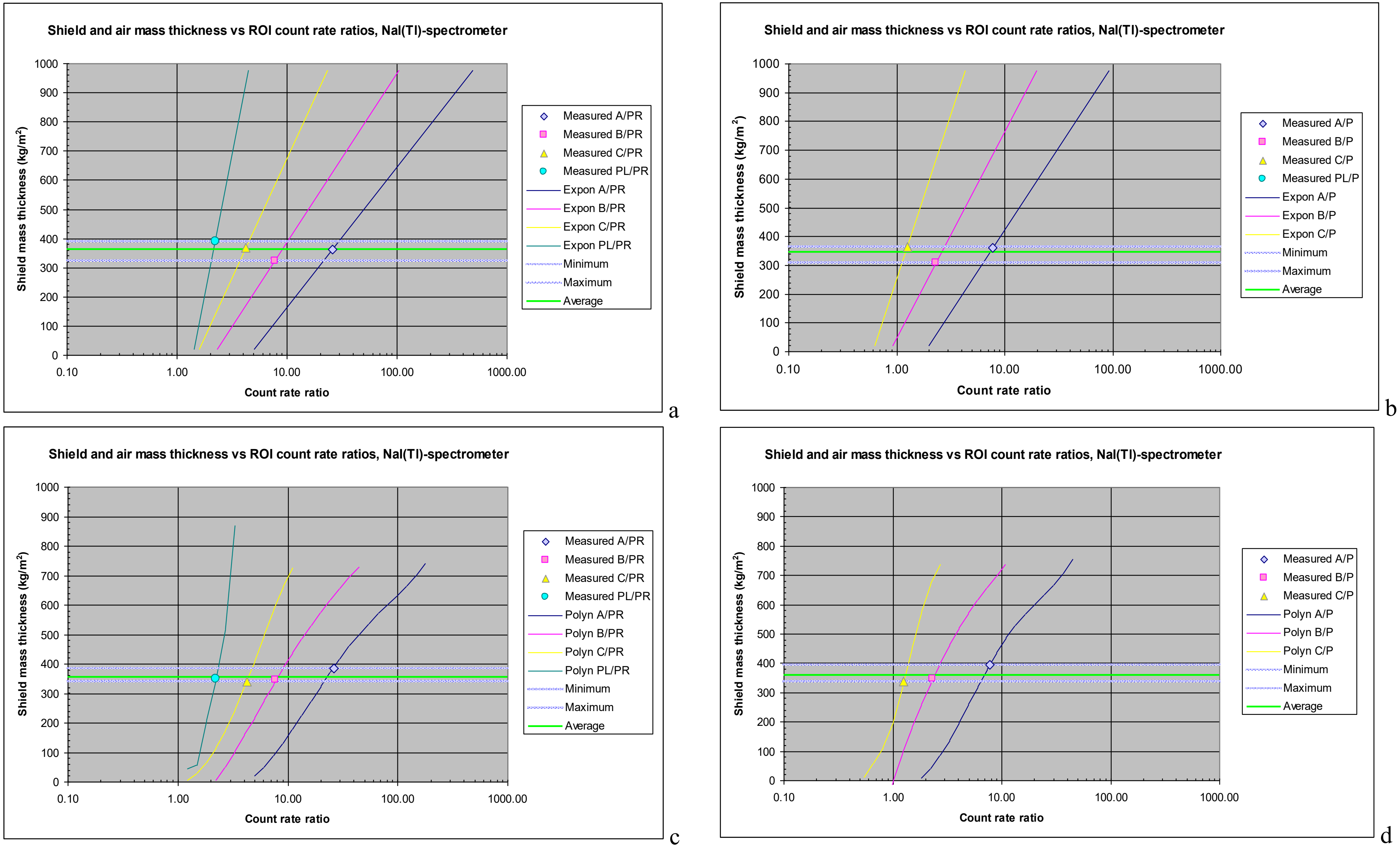

Fig B4-2-a-d (M2). Shield mass thickness determination by the DSA 4 litre NaI(Tl) spectrometer using the ROI count rate ratio method with exponential (a, b) and polynomial (c, d) models. The true shield mass thickness is 372 kg/m^2, including 31 m of air between the source and the detector.

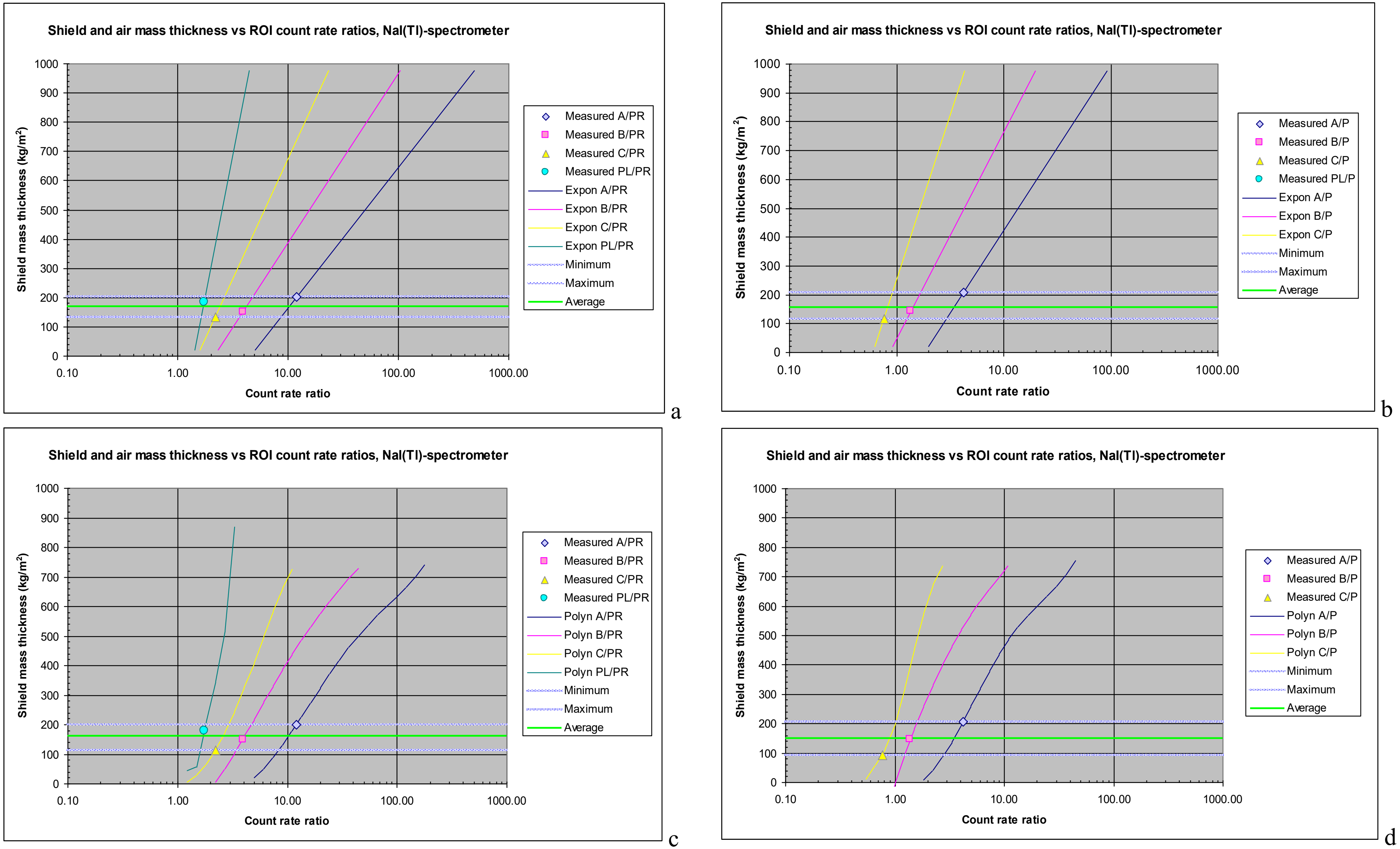

Fig B4-3-a-d (M3). Shield mass thickness determination by the DSA 4 litre NaI(Tl) spectrometer using the ROI count rate ratio method with exponential (a, b) and polynomial (c, d) models. The true shield mass thickness is 170 kg/m^2, including 61 m of air between the source and the detector.

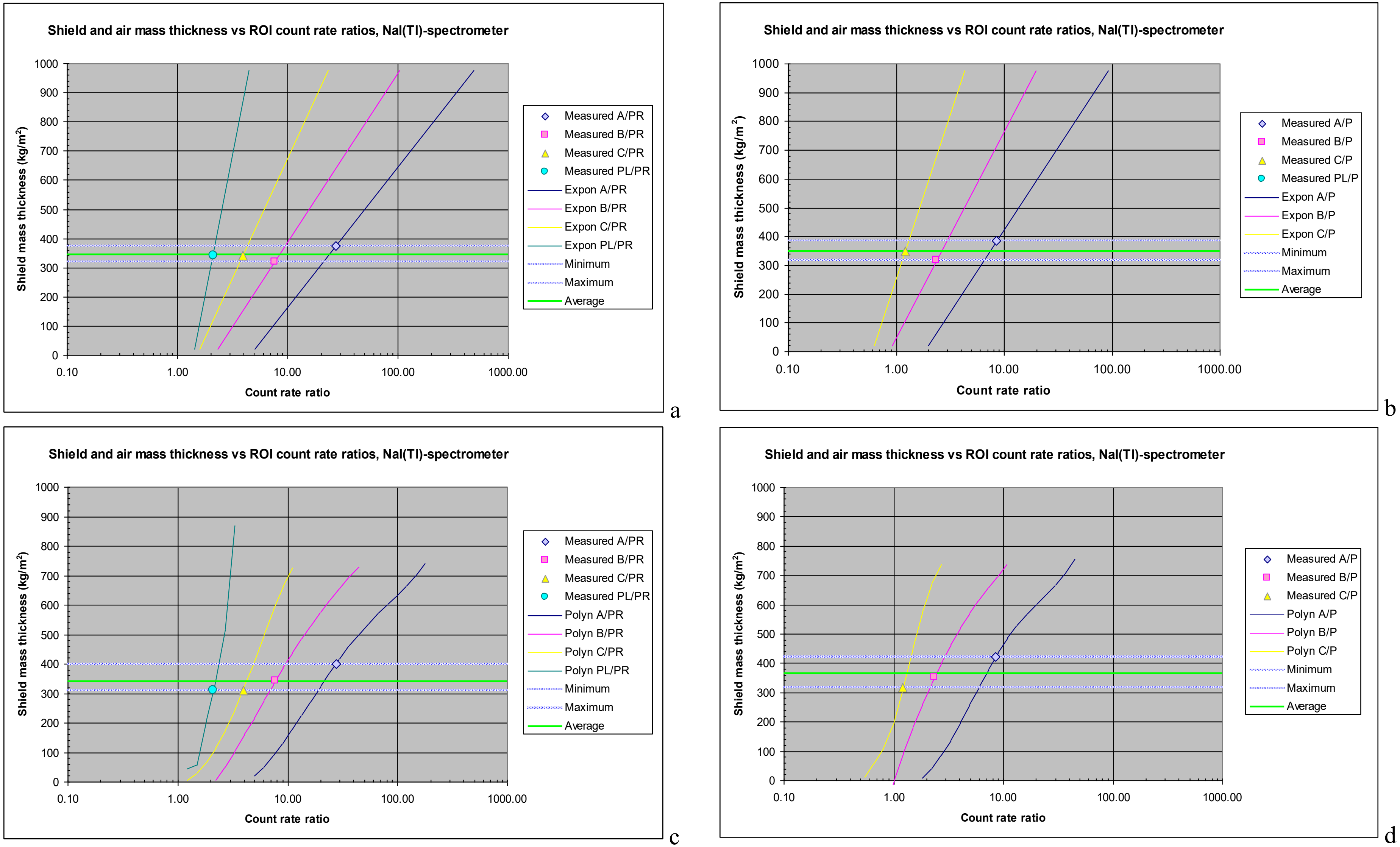

Fig B4-4-a-d (M4). Shield mass thickness determination by the DSA 4 litre NaI(Tl) spectrometer using the ROI count rate ratio method with exponential (a, b) and polynomial (c, d) models. The true shield mass thickness is 409 kg/m^2, including 61 m of air between the source and the detector.

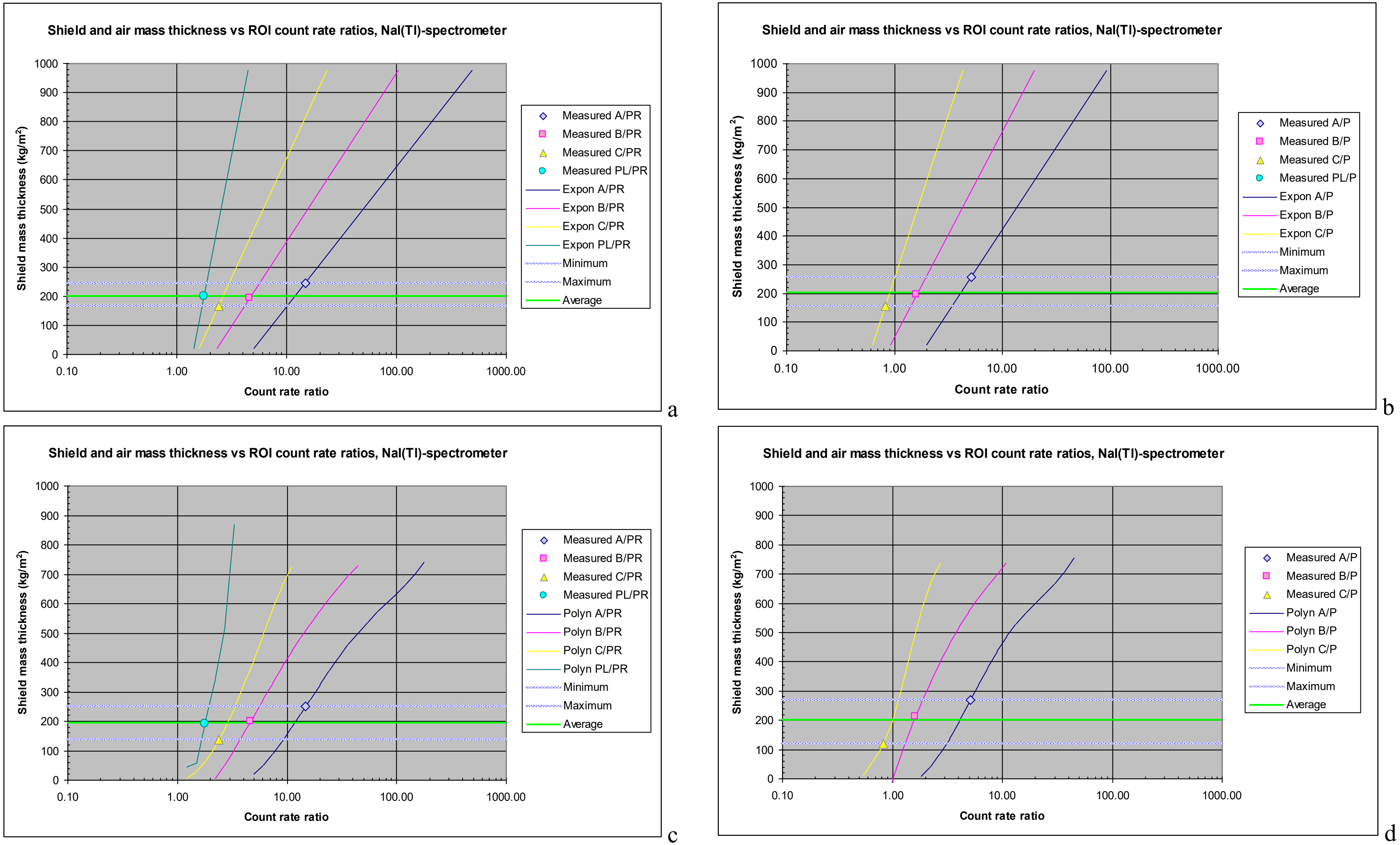

Fig B4-5-a-d (M5). Shield mass thickness determination by the DSA 4 litre NaI(Tl) spectrometer using the ROI count rate ratio method with exponential (a, b) and polynomial (c, d) models. The true shield mass thickness is 207 kg/m^2, including 91 m of air between the source and the detector.

B5. Results from source distance measurements, using SODAC

The distance to a Cs-137 point source was determined using the Excel program SODAC for five different setups with different distances and shielding (M1 - M5), as described in the main report. All measurements were made standing still (semi-stationary) at various locations along the road that passes the radiation source.

We had some issues with the assessment part at distances ±10 meters and ±20 meters along the road from the centre angle. This was due to bushes and small trees between the source and the detector, which the method does not consider. There were noticeable shielding effects from these obstacles. Therefore, we found distances where we had a clear view of the source (i.e. 15 m or 25 m). In these cases, we found the method to be OK, and we could fit a curve in the provided SODAC Excel routine.

Correcting the detector response for the angular dependence of the oblong detector for count rates from the source at different incident angles proved necessary during the analysis. How the correction is determined is reported in the text of the main report.

In the SODAC analysis, the actual shield thickness has been used in the distance determination (and not the one obtained through SSC) because it produces a more accurate picture of any distance determination deviations than a possibly distorted assumption of the shield thickness would do.

Results from the Excel program SODAC showing which "intensity curve" (primary photon fluence from the source as a function of distance along the road) best fits the measurement data along the road for the five setup distances are reproduced in figures B5-1 to B5-5.

Results from the distance and activity determination with SODAC are summarized in Table B5-1.

For setup M1 to M5, the distance determination was underestimated from 8% to 33% (rounded values) with an average underestimation of 18 ± 4%. On average, the calculated activity values at the underestimated distances were underestimated by 18 ± 13%. Using the actual distance values when determining the source activity, the activity was, on average, overestimated by 51 ± 19%.

The cause of the overestimation may be the low energy resolution in a NaI(Tl) detector and the increased distance to the source compared to the calibration distance for shield thickness. Photons scattered at small angles in front of the source are recorded as primary photons in the full-energy peak in the pulse height distribution of the detector. This photon scattering causes the count rate in ROI PR and ROI P to increase compared to primary-only photons, and it may affect distance and shield thickness determination at longer distances. Further experimental investigations of the detector's response at longer source distances and thicker shielding are needed to draw more definite conclusions.

Table B5-1. Results from the DSA 4 litre NaI(Tl) detector, applying the SODAC routine to obtain the source distance and activity for a Cs-137 point source. The distance is adjusted for the varying angular efficiency for horizontally oriented 4 litre NaI(Tl) detectors. The activity is calculated from the full energy peak count rate for the adjusted and the actual distance, using the actual shield thickness. The actual point source activity is 606 MBq in all setups.

Setup	Actual		SODAC obtained				Deviation	
	Distance to source m	Shield mass thickness kg/m^2	Distance m	Distance angular efficiency adjusted m	Activity at adjusted distance MBq	Activity at actual distance MBq	Distance at adjusted rounded %	Activity at adjusted (at actual) distance%
M1	61	air only	35	50	407	645	-17	-33 (6.4)
M2	31	333	20	25	714	1078	-17	18 (78)
M3	61	94	30	50	495	785	-17	-18 (30)
M4	61	333	50	55	*	*	-8	* (*)
M5	91	94	45	60	380	1142	-33	-37 (88)
Average							-18 ± 4	-18 ± 13 (51 ± 19)

* Uncertain background count rate value, activity not calculated.

SODAC source distance results, DSA 4 litre NaI(Tl)-detector

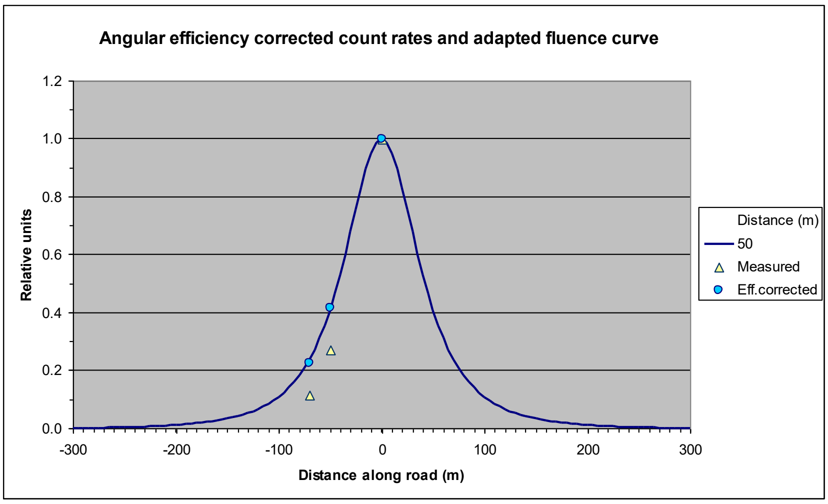

Fig B5-1. DSA. Setup M1 (M6). The true source distance is 61 m

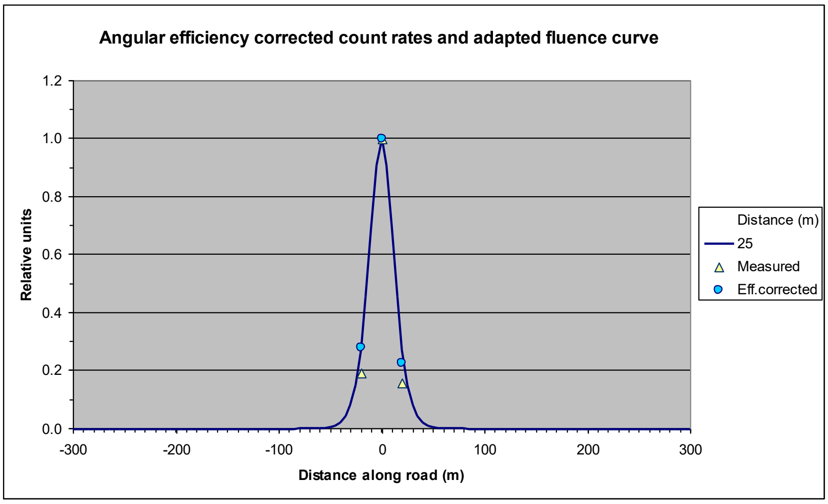

Fig B5-2. DSA. Setup M2 (M7). The true source distance is 31 m

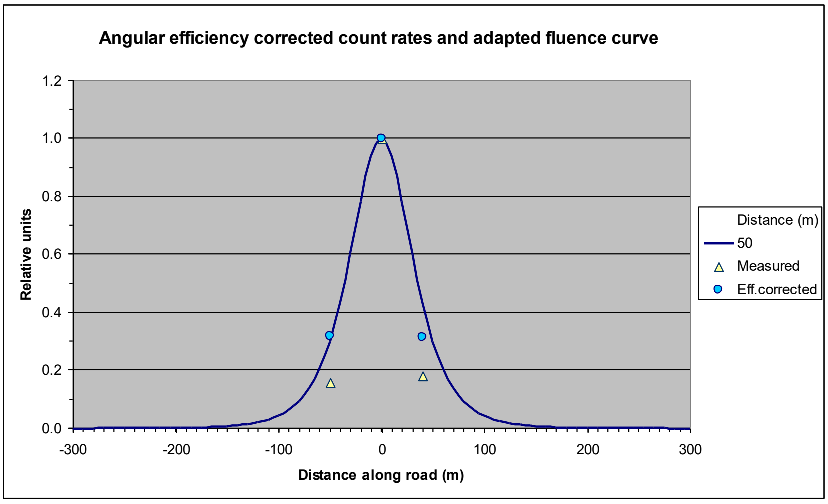

Fig B5-3. DSA. Setup M3 (M8). The true source distance is 61 m

The figures show SODAC determined source distance results for the DSA 4 litre NaI(Tl)-detector, corrected for varying angular efficiency. Tree-shielded measurement locations have been excluded.

SODAC source distance results, DSA 4 litre NaI(Tl)-detector

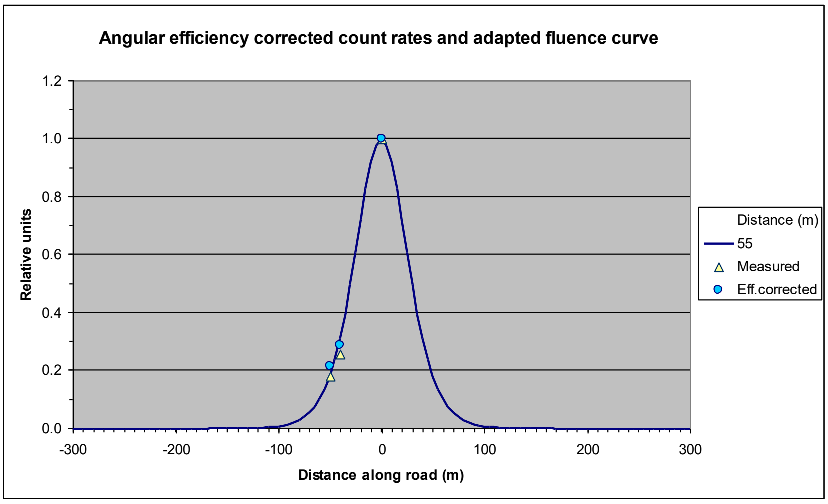

Fig B5-4. DSA. Setup M4 (M9). The true source distance is 61 m

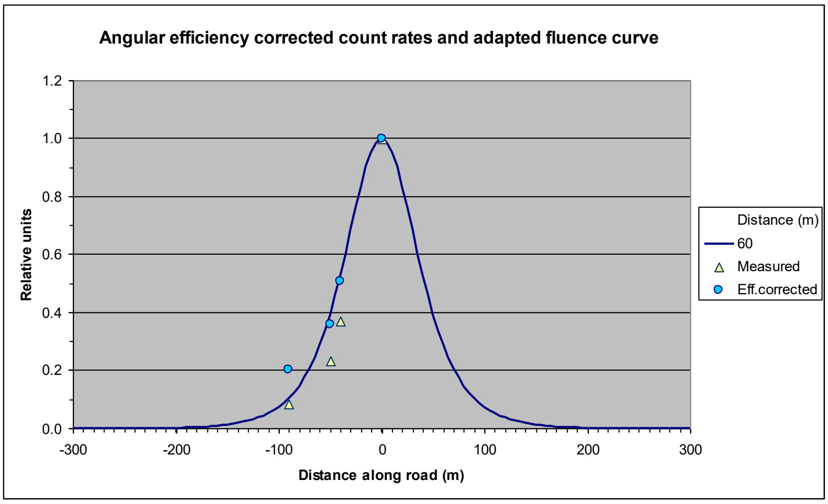

Fig B5-5. DSA. Setup M5 (M10). The true source distance is 91 m

The figures show SODAC determined source distance results for the DSA 4 litre NaI(Tl)-detector, corrected for varying angular efficiency. Tree-shielded measurement locations have been excluded.

B6. Summary and conclusion

Technically, all shield thickness calibrations (C1 to C10) and road assessments of the distance to the source, its shielding and activity (M1 to M5) went without problems.

In determining the mass thickness of the radiation shield with the SCC routine, two models have been used that describe the net count rate relationships between registrations from scattered radiation and primary radiation, an exponential model and a polynomial model. Both models give roughly the same results and underestimate the shield mass thickness by 20 ± 13% (standard error of the mean).

When determining the distance to a radiation source with the SODAC routine in five different cases with spacing from 30 to 90 m, the distances were, on average, underestimated by 18 ± 4%. The calculated activity was, on average, overestimated by 51 ± 19%. The reason for the deviations from actual values is not fully known.

Further experimental investigations of the detector's response at longer source distances and thicker shielding are needed to investigate the reason more in-depth.

To summarize, we think the present SSC and SODAC methods could roughly be used to estimate shielding material, distances and activity. The method applies to strict and controlled conditions with a clear view of the source-detector line. Nevertheless, using the method in an actual MORC situation would be beneficial and could disclose other factors that must be considered.

Appendix C. Results from team GR (Geislavarnir Ríkisins), Icelandic Radiation Safety Authority, Iceland

C1. Measuring equipment

The Icelandic team used a SPARCS mobile survey system. It comprises 2x2 litre NaI(Tl) detectors connected to an acquisition unit (ATU). The ATU is connected to a laptop computer with special software called AVID. The detector was placed in the back seat of a hired station wagon near the right door. This setup would be a typical configuration in case of a search for a lost or stolen radiation source.

C2. Detector efficiency calibration

The 2x2 litre NaI(Tl)-detector was calibrated for counting efficiency at 662 keV in an earlier NKS field experiment (NKS-AUTOMORC, 2018) using a Cs-137 point source with activity traceable to calibration sources from Eckert & Ziegler with 3% relative expanded uncertainty (k=2). When placed in measurement position in the car, the detector efficiency for 662 keV photons from the right side (the apparent detector area for total photon absorption) was 0.0299 m^2 with 8% relative expanded uncertainty (k=2).

C3. Detector calibration for shield mass thickness determination, using SSC

The response of the 2x2 litre NaI(Tl) detector as net count rates in ROI A, B, C and PL relative to ROI PR and ROI P was measured for different shield mass thicknesses described earlier in the report. The measurement data was entered into the Excel program SCC. The relationship between the net count rates for the ratios ROI A, B, C, and PL/PR for the exponential model is shown in Fig C3-1-a and the polynomial model in Fig C3-1-c. Corresponding relationships for the ratios ROI A, B, and C/P are shown in Figs C3-1-b and C3-1-d.

The coefficients for fitting the exponential model to observed data are given in Table C3-1. The coefficients for fitting the five-degree polynomial model to observed data are given in Table C3-2.

The exponential and five-degree polynomial models represent the measured net count rate ratios for the different shield mass thicknesses quite well.

Table C3-1. GR 2x2 litre NaI(Tl)-detector. Coefficients *a* and *b* in an exponential model for determining shield mass thickness according to the description in the main report. The unit of *b* is m^2/kg.

ROI ratio	*a*	*b*
ROI A/PR	4.28	0.00516
ROI B/PR	2.16	0.00448
ROI C/PR	1.38	0.00355
ROI PL/PR	1.21	0.00169
ROI A/P	1.89	0.00401
ROI B/P	0.953	0.00333
ROI C/P	0.612	0.00240

Table C3-2. GR 2x2 litre NaI(Tl)-detector. Coefficients a_0 - a_5 (kg/m^2) in the five-degree polynomial model for determining shield mass thickness according to Eqn 3 in the main report.

ROI ratio	a_5	a_4	a_3	a_2	a_1	a_0
ROI A/PR	2.465	-32.96	139.4	-162.9	37.26	0
ROI B/PR	2.747	-18.94	-3.988	227.6	-172.9	0
ROI C/PR	34.82	-251.5	569.6	-365.7	173.1	0
ROI PL/PR	3729	-15280	23050	-15750	5438	-654.9
ROI A/P	9.104	-72.58	148.0	51.77	-63.92	0
ROI B/P	1.168	44.20	-266.5	403.3	194.6	0
ROI C/P	572.5	-1021	-161.9	636.2	439.4	153.1

C4. Results from shield thickness measurements, using SSC

In connection with the experiment determining the source distance with the SODAC routine, a determination of the shield mass thickness in front of the Cs-137 point source was made using the SSC routine when the measuring car was directly opposite the source, i.e. at the road location with the shortest distance to the source. The results are given in tables C4-1 to C4-4.

The deviation in the calculated mass thickness from the actual value was between -8% and 53% for the exponential model, and the polynomial model's deviation was between -11% and 61%. It is impossible to say that one model gives better values than the other. On average, the models overestimated the mass thickness by 20 ± 12%.

The detailed result from SSC is also reproduced in Figs C4-1 to C4-5, where the individual net count rate ratios ROI A/PR, ROI B/PR Etc., are plotted along the lines of the exponential model and the polynomial model. The measurement data show relatively good agreement for the different ROI ratios for setup M1 and M2. There is a broader variation between the ROI ratios for setup M3, M4, and M5. These setups have combinations of more considerable distances and shielding, resulting in poorer counting statistics, which probably is the cause of the more significant variation.

Table C4-1. Result from the GR 2x2 litre NaI(Tl) detector determination of shield mass thickness by using ROI A, B, C, PL / PR net count rate ratios in an exponential model

Setup	Actual		Measured		Deviation
	Distance to source (m)	Shield mass thickness (kg/m^2)	Shield and air mass thickness (kg/m^2)	Shield mass thickness (kg/m^2)	of measured from actual value (%)
M1	61	0	69.7	-6.1	-8.0
M2	31	333	385	347	3.6
M3	61	94	227	151	33.8
M4	61	333	364	288	-11.1
M5	91	94	292	179	41.1
Average					11.9 ± 10.8

Table C4-2. Result from the GR 2x2 litre NaI(Tl) detector determination of shield mass thickness by using ROI A, B, C / P net count rate ratios in an exponential model

Setup	Actual		Measured		Deviation
	Distance to source (m)	Shield mass thickness (kg/m^2)	Shield and air mass thickness (kg/m^2)	Shield mass thickness (kg/m^2)	of measured from actual value (%)
M1	61	0	76.5	0.66	0.9
M2	31	333	393	355	5.8
M3	61	94	260	184	53.3
M4	61	333	382	306	-6.6
M5	91	94	308	195	48.6
Average					20.4 ± 12.6

Table C4-3. Result from the GR 2x2 litre NaI(Tl) detector determination of shield mass thickness by using ROI A, B, C, PL / PR net count rate ratios in a five-degree polynomial model

Setup	Actual		Measured		Deviation
	Distance to source (m)	Shield mass thickness (kg/m^2)	Shield and air mass thickness (kg/m^2)	Shield mass thickness (kg/m^2)	of measured from actual value (%)
M1	61	0	67.7	-8.1	-10.7
M2	31	333	435	396	17.0
M3	61	94	231	155	35.7
M4	61	333	405	329	-1.1
M5	91	94	311	198	50.3
Average					18.2 ± 11.3

Table C4-4. Result from the GR 2x2 litre NaI(Tl) detector determination of shield mass thickness by using ROI A, B, C / P net count rate ratios in a five-degree polynomial model

Setup	Actual		Measured		Deviation
	Distance to source (m)	Shield mass thickness (kg/m^2)	Shield and air mass thickness (kg/m^2)	Shield mass thickness (kg/m^2)	of measured from actual value (%)
M1	61	0	76.8	0.96	1.3
M2	31	333	454	415	22.1
M3	61	94	273	197	60.7
M4	61	333	428	352	4.6
M5	91	94	334	221	61.3
Average					30.0 ± 13.1

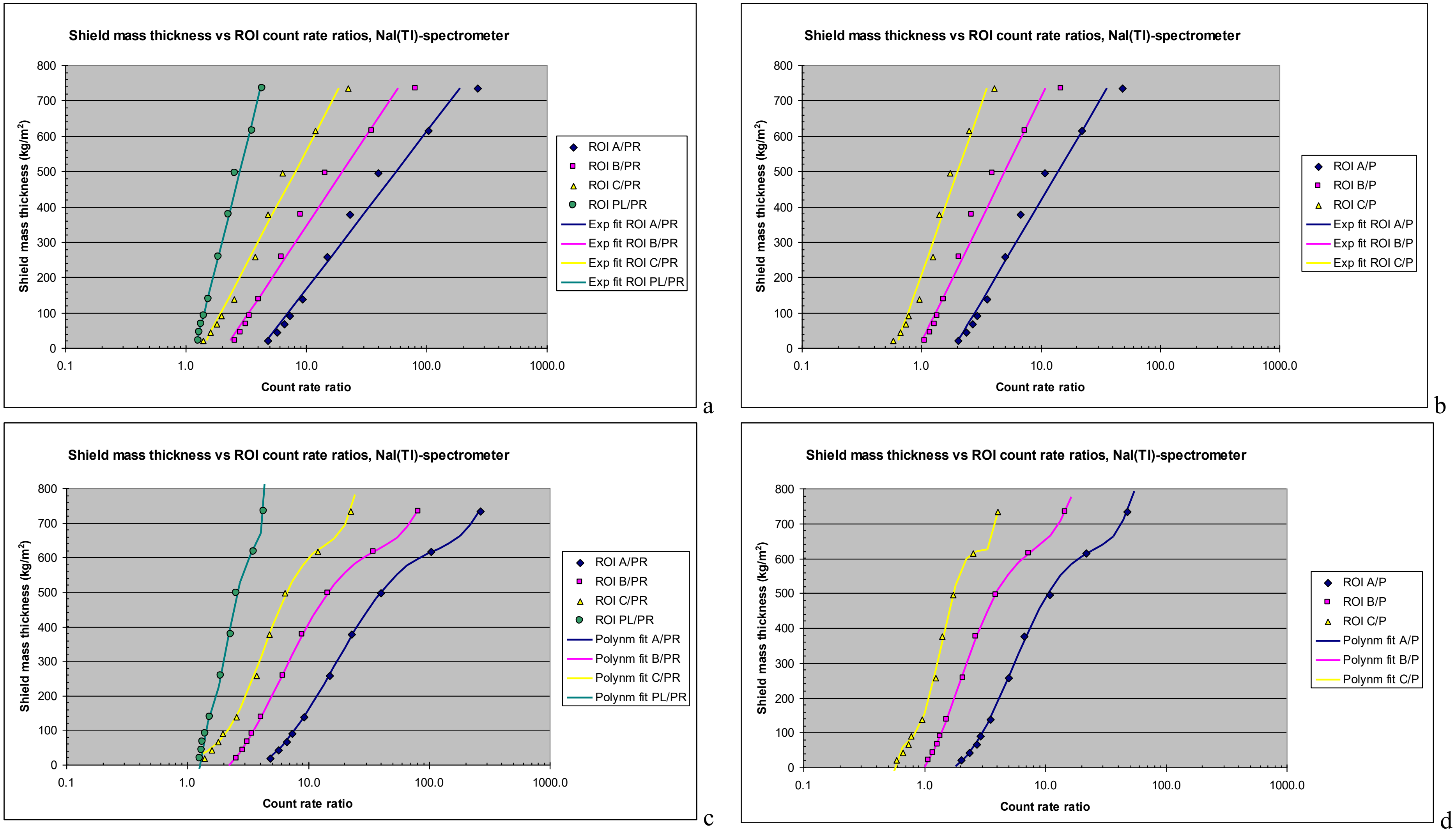

Fig C3-1-a-d. GR 2x2 litre NaI(Tl) spectrometer. Models of shield mass thickness as a function of ROI net count rate ratio obtained from fitting measured data to exponential functions (a, b) and five-degree polynomial functions (c, d), valid for Cs-137 point sources behind shields of standard building material (wood and concrete) with mass thickness between 20 and 730 kg/m^2. Values have been measured at a source-detector distance of 10 m.

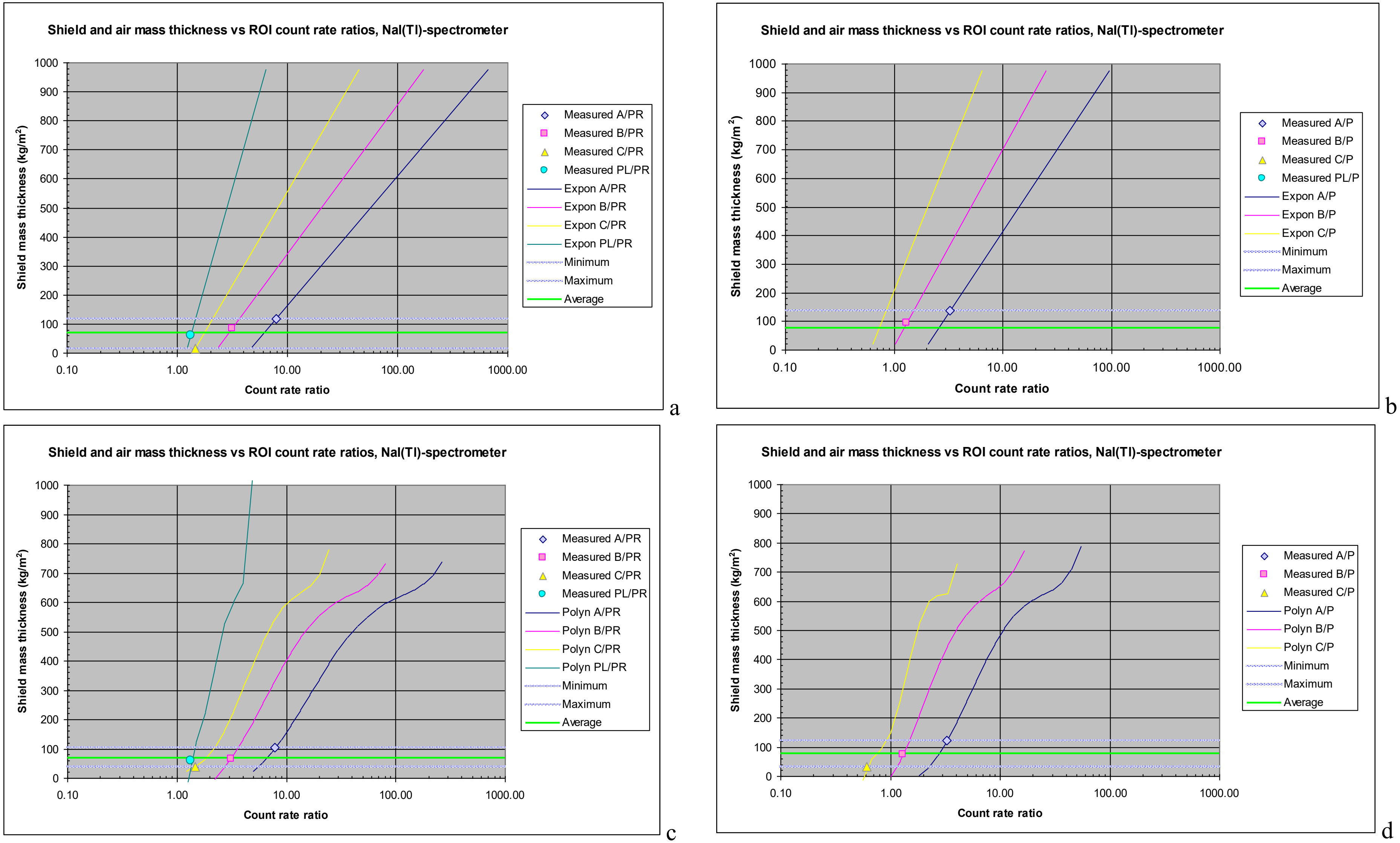

Fig C4-1-a-d (M1). Shield mass thickness determination by the GR 2x2 litre NaI(Tl) spectrometer using the ROI count rate ratio method with exponential (a, b) and polynomial (c, d) models. The true shield mass thickness is 75.8 kg/m^2, including 61 m of air between the source and the detector.

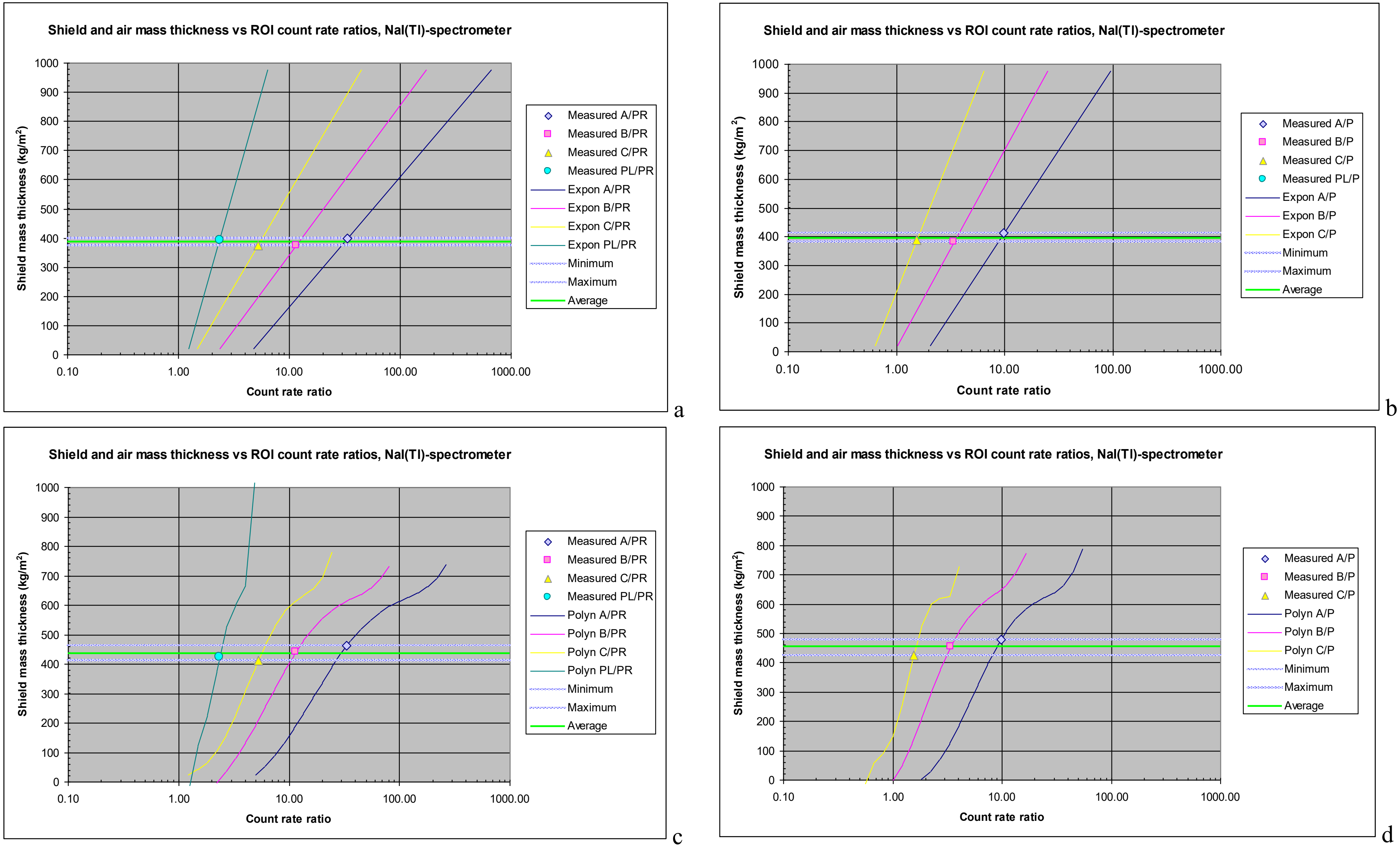

Fig C4-2-a-d (M2). Shield mass thickness determination by the GR 2x2 litre NaI(Tl) spectrometer using the ROI count rate ratio method with exponential (a, b) and polynomial (c, d) models. The true shield mass thickness is 372 kg/m^2, including 31 m of air between the source and the detector.

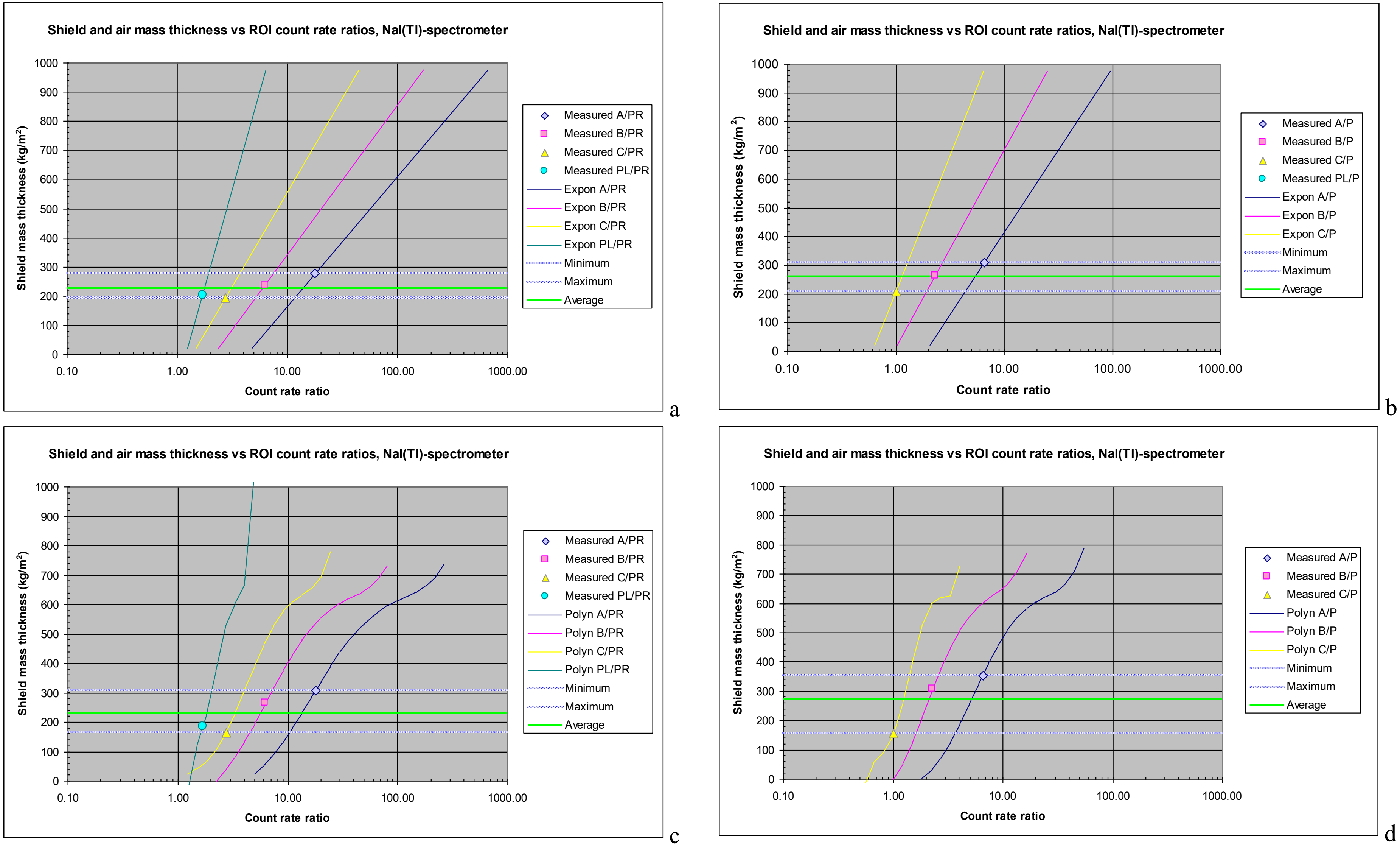

Fig C4-3-a-d (M3). Shield mass thickness determination by the GR 2x2 litre NaI(Tl) spectrometer using the ROI count rate ratio method with exponential (a, b) and polynomial (c, d) models. The true shield mass thickness is 170 kg/m^2, including 61 m of air between the source and the detector.

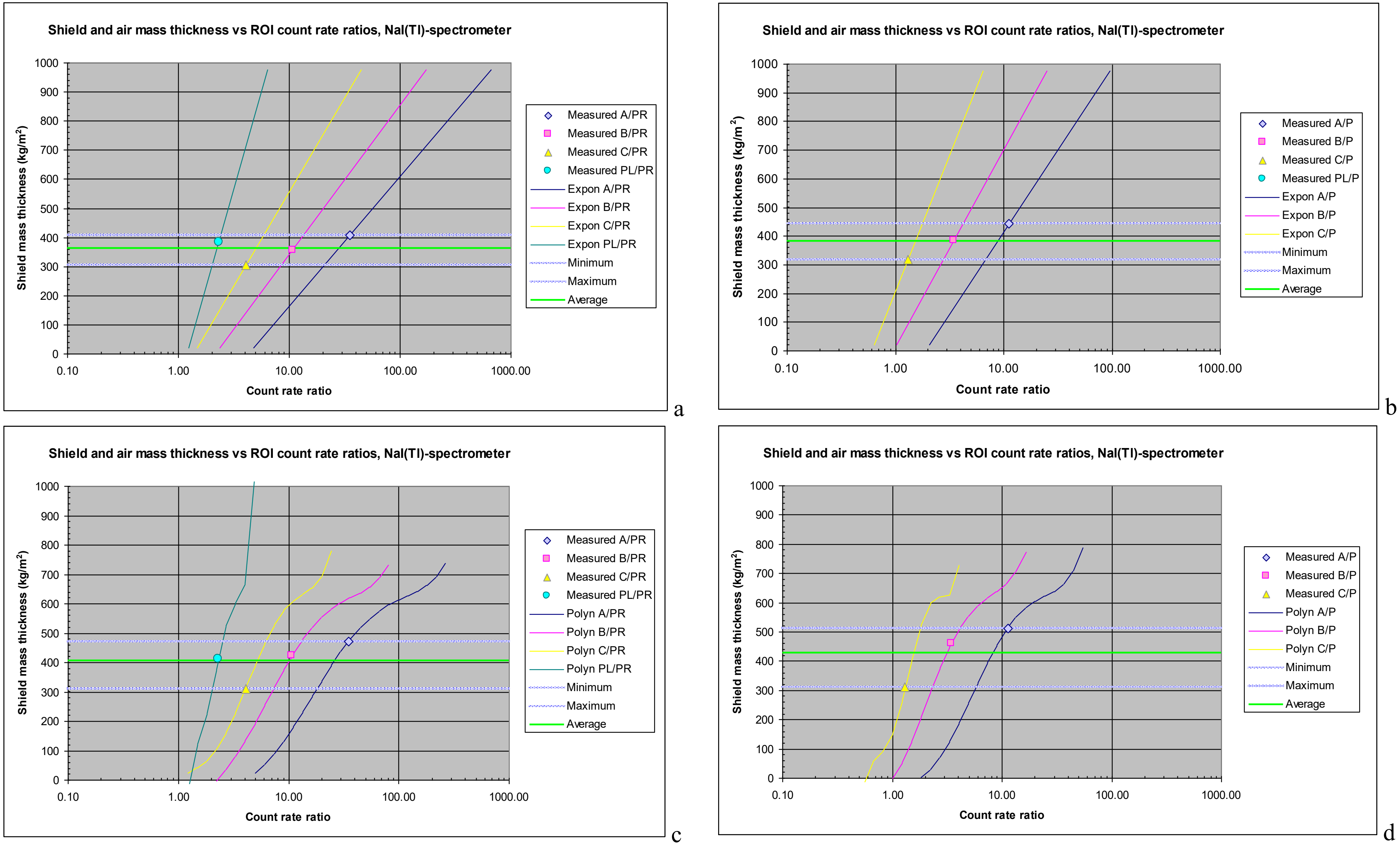

Fig C4-4-a-d (M4). Shield mass thickness determination by the GR 2x2 litre NaI(Tl) spectrometer using the ROI count rate ratio method with exponential (a, b) and polynomial (c, d) models. The true shield mass thickness is 409 kg/m^2, including 61 m of air between the source and the detector.

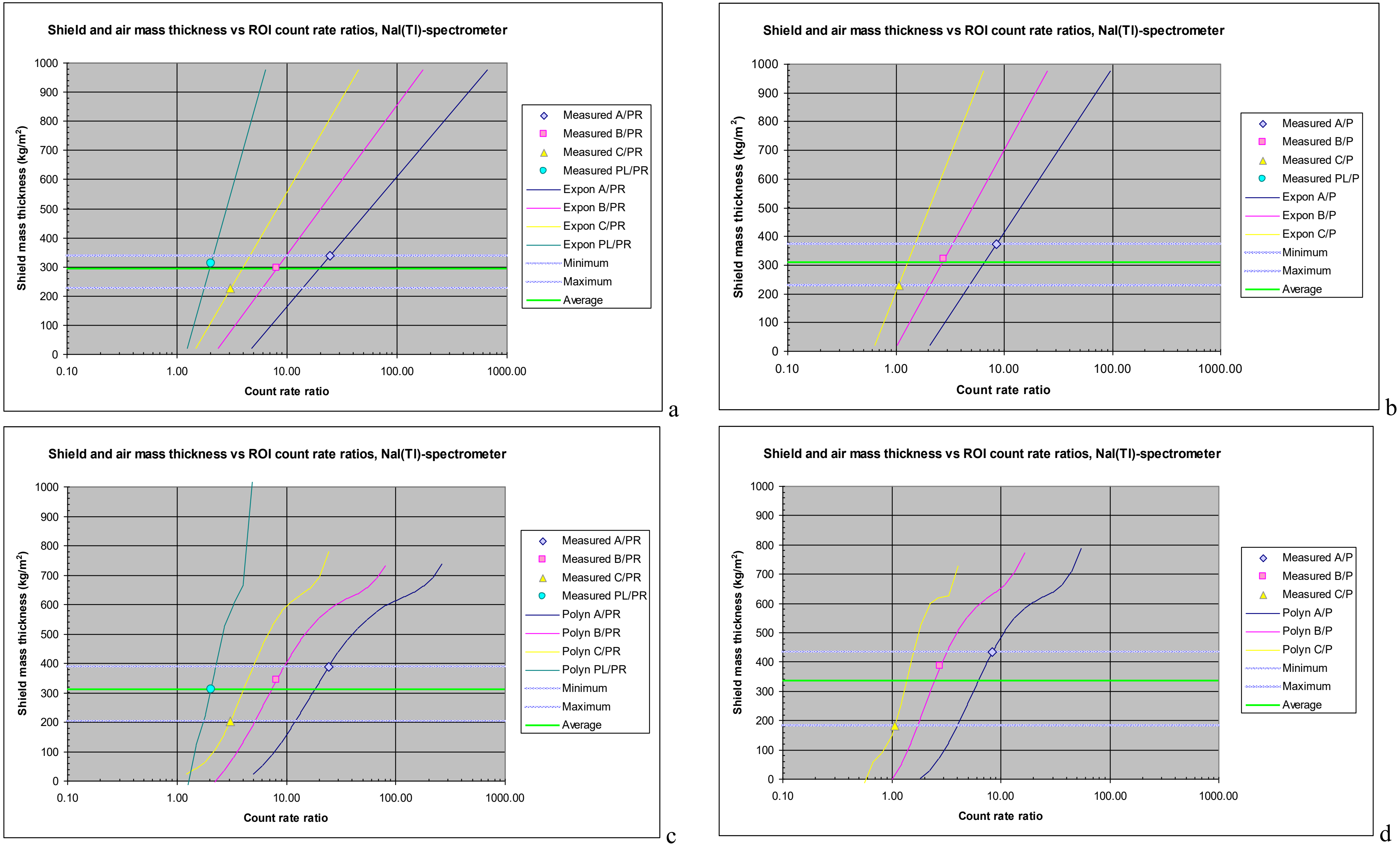

Fig C4-5-a-d (M5). Shield mass thickness determination by the GR 2x2 litre NaI(Tl) spectrometer using the ROI count rate ratio method with exponential (a, b) and polynomial (c, d) models. The true shield mass thickness is 207 kg/m^2, including 91 m of air between the source and the detector.

C5. Results from source distance measurements, using SODAC

The distance to a Cs-137 point source was determined using the Excel program SODAC for five different setups with different distances and shielding (M1 - M5), as described in the main report. All measurements were made standing still (semi-stationary) at various locations along the road that passes the radiation source. Unfortunately, it turned out that some trees between the radiation source and the measuring car shielded the photon fluence from the source at specific points along the road. These measurement points have been identified, and the data has been removed from the analysis.

Correcting the detector response for the angular dependence of the oblong detector for count rates from the source at different incident angles proved necessary during the analysis. How the correction is determined is reported in the text of the main report.

In the SODAC analysis, the actual shield thickness has been used in the distance determination (and not the one obtained through SSC) because it produces a more accurate picture of any distance determination deviations than a possibly distorted assumption of the shield thickness would do.

Results from the Excel program SODAC showing which "intensity curve" (primary photon fluence from the source as a function of distance along the road) best fits the measurement data along the road for the five setup distances are reproduced in Figures C5-1 to C5-5.

Results from the distance and activity determination with SODAC are summarized in Table C5-1. The source distances for four setups (M1, M2, M3, M5) were underestimated from 8% to 33% with an average underestimation of 23 ± 6%, and the source activity was overestimated by 22 ± 12%.

The reason for the deviations from actual values is unknown, but the low energy resolution in a NaI(Tl) detector may be one cause. Photons scattered at small angles in front of the source register in the full-energy peak in the pulse height distribution of the detector. These photons cause the count rate in ROI PR and ROI P to increase compared to primary-only photons, which may affect distance and shield thickness determination at longer distances. Further experimental investigations of the detector's response at longer source distances and thicker shielding are needed to draw more definite conclusions.

Table C5-1. Results from the GR 2x2 litre NaI(Tl) detector, applying the SODAC routine to obtain the source distance and activity for a Cs-137 point source. The distance is adjusted for the varying angular efficiency for horizontally oriented 4 litre NaI(Tl) detectors. The activity is calculated from the full energy peak count rate for the adjusted and the actual distance, using the actual shield thickness. The actual point source activity is 606 MBq in all setups.

Setup	Actual		SODAC obtained				Deviation	
	Distance to source m	Shield mass thickness kg/m^2	Distance m	Distance angular efficiency adjusted m	Activity at adjusted distance MBq	Activity at actual distance MBq	Distance at adjusted rounded %	Activity at adjusted (at actual) %
M1	61	air only	35	55	495	618	-8	-18.3 (2.0)
M2	31	333	25	25	628	949	-17	3.6 (56.6)
M3	61	94	35	40	254	692	-33	-58.1 (14.2)
M4	61	333	*	*	*	*	*	* (*)
M5	91	94	50	60	228	686	-33	-62.4 (13.2)
Average							-23 ± 6	-34 ± 16 (22 ± 12)

* Not enough measurement data available to determine the distance and activity.

SODAC source distance results, GR 2x2 litre NaI(Tl)-detector

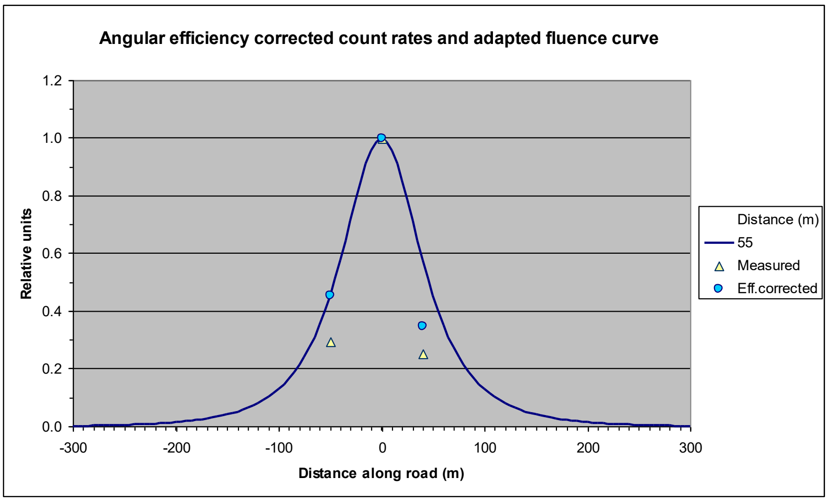

Fig C5-1. GR. Setup M1. The true source distance is 61 m

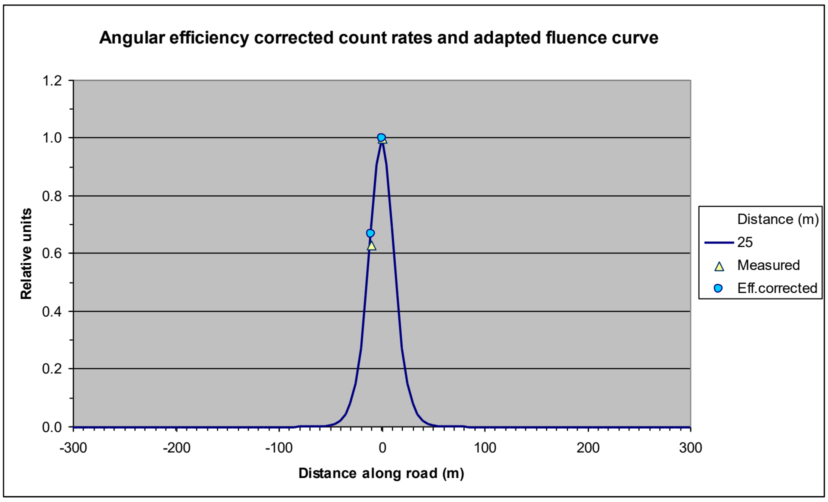

Fig C5-2. GR. Setup M2. The true source distance is 31 m

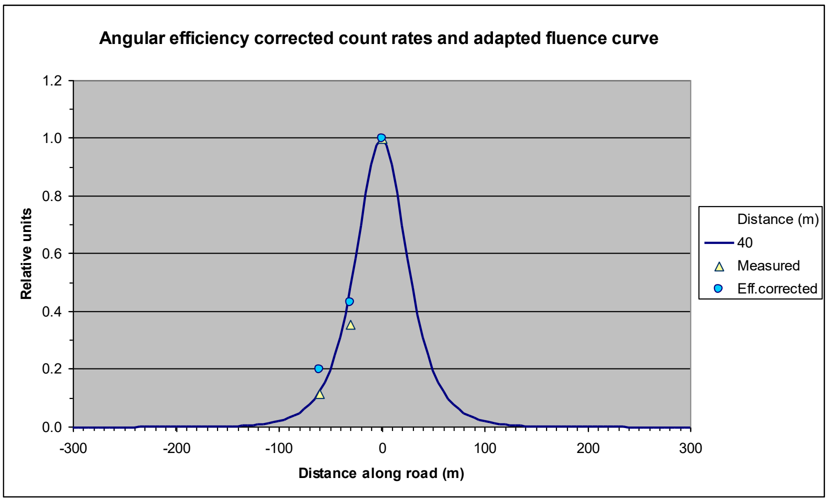

Fig C5-3. GR. Setup M3. The true source distance is 61 m

The figures show SODAC determined source distance results for the GR 2x2 litre NaI(Tl)-detector, corrected for varying angular efficiency. Tree-shielded measurement locations have been excluded.

SODAC source distance results, GR 2x2 litre NaI(Tl)-detector

For Setup M4, not enough measurement data was available to enable determination of the source distance by the SODAC routine.

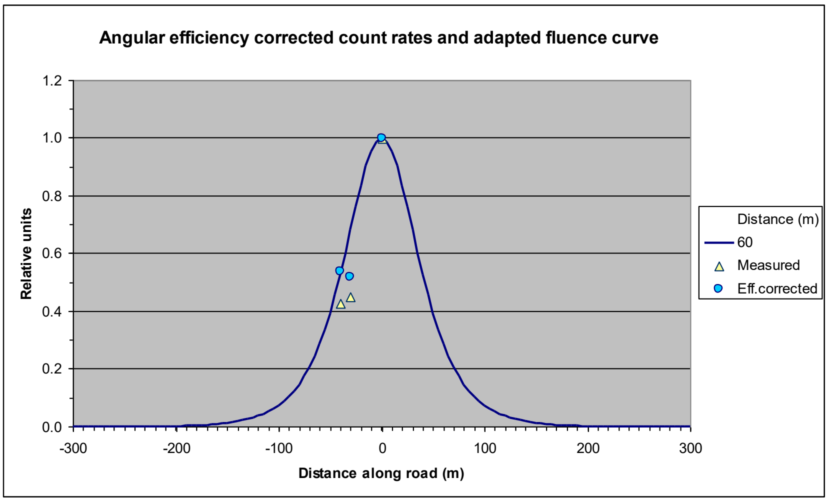

Fig C5-5. GR. Setup M5. The true source distance is 91 m

The figures show SODAC determined source distance results for the GR 2x2 litre NaI(Tl)-detector, corrected for varying angular efficiency. Tree-shielded measurement locations have been excluded.

C6. Summary and conclusion

In determining the mass thickness of the radiation shield with the SCC routine, two models have been used that describe the net count rate relationships between registrations from scattered radiation and primary radiation, an exponential model and a polynomial model. Both models give roughly the same results and overestimate the shield mass thickness by 20 ± 12% (standard error of the mean).

When determining the distance to a radiation source with the SODAC routine in four different cases with spacing from 30 to 90 m, the distances were, on average, underestimated by 23 ± 6%. The calculated activity was, on average, overestimated by 22 ± 12%. The reason for the deviations from actual values is not fully known. Further experimental investigations of the detector's response at longer source distances and thicker shielding are needed to investigate the reason more in-depth.

Appendix D. Results from team LU, Lund University, Sweden

D1. Measuring equipment

The LU mobile spectrometry vehicle was based on a Chevrolet Silverado pickup with the detector and electronics mounted in the back compartment (Fig. D1-1). The vehicle and equipment are owned by the Swedish Radiation Safety Authority and deployed at Lund University under a contract.

The spectrometric system consisted of four detectors; two 4 litre NaI(Tl) detectors with the dimensions 430 x 102 x 102 mm, one 76.2x76.2 mm (3"x3") cylindrical NaI(Tl) detector and one electrically cooled high purity germanium detector, HPGe (DetectiveX). The two 4-litre NaI(Tl) detectors were attached to the ceiling of the back compartment 1.67 meters above the ground (to the detector centre). The HPGe detector was mounted 1.1 m above ground on the right-hand side of the compartment and facing backwards. The 3"x3" NaI(Tl) detector was placed in the back 0.8 m above ground (to the detector centre). The detectors had a free line of sight at 90 degrees relative to the driving direction, except for the plastic doors covering the back compartment's sides.

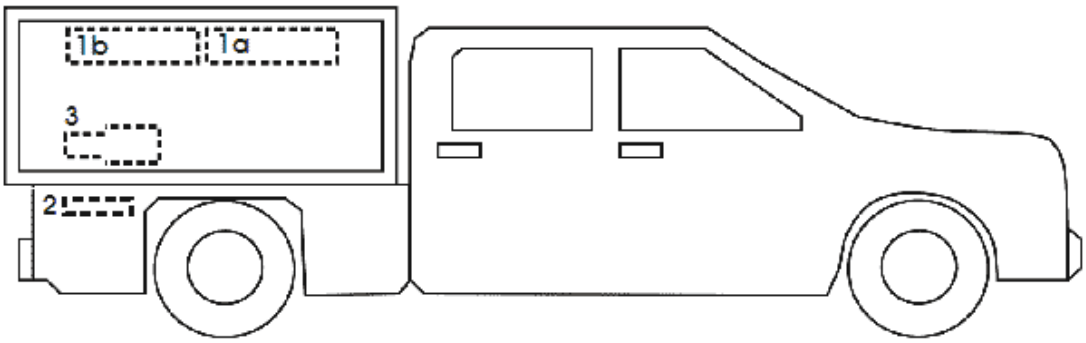

Fig D1-1. Schematic view of the mobile gamma spectrometry vehicle showing the position of the 2 x 4 litre NaI(Tl) detectors (1a and 1b), the 3"x3" NaI(Tl) detector (2) and the HPGe detector (3).

D2. Detector efficiency calibration

The counting efficiencies for the detectors at 662 keV were determined in separate calibration measurements using Cs-137 point sources with activity traceable to calibration sources from Eckert & Ziegler with 3% relative expanded uncertainty (k=2). The 4 litre NaI(Tl) detector efficiency for 662 keV photons incident from the right side (the apparent detector area for total photon absorption) was 0.0254 m^2 (front detector) and 0.0261 m^2 (rear detector). The 3"x3" NaI(Tl) detector efficiency for 662 keV photons from the right-hand side was 0.00236 m^2, and the HPGe detector efficiency was 0.000758 m^2. The efficiency uncertainties are estimated to be 8% relative expanded uncertainty (k=2).

D3. Detector calibration for shield mass thickness determination, using SSC

The response of the right side 4 litres NaI(Tl) detector as net count rates in ROI A, B, C and D relative to ROI PR and ROI P was measured for different shield mass thicknesses described in the main report. The measurement data was entered into the Excel program SCC.

The mass shield thickness as a function of the net count rates ratios ROI A, B, C, and PL/PR is shown in Fig B3-11 for the front 4 litres NaI(Tl)-detector, in Fig B3-21 for the rear 4 litres NaI(Tl)-detector, and in Fig B3-31 for the 3"x3" NaI(Tl)-detector.

The mass shield thickness as functions of net count rate ratios ROI A, B, C, D/P is shown in Fig B3-41 for the HPGe-detector.

The coefficients for fitting the exponential function model to observed data are given in Table D3-11 for the front 4 litres NaI(Tl)-detector, in Table D3-21 for the rear 4 litres NaI(Tl)-detector, in Table D3-31 for 3"x3" NaI(Tl)-detector, and in Table D3-41 for the DetectiveX HPGe-detector.

The coefficients for fitting the five-degree polynomial function model to observed data are given in Table D3-12 for the front 4 litres NaI(Tl)-detector, in Table D3-22 for the rear 4 litres NaI(Tl)-detector, in Table D3-32 for 3"x3" NaI(Tl)-detector, and in Table D3-42 for the DetectiveX HPGe-detector.

The exponential and five-degree polynomial models represent the measured net count rate ratios for the different detectors and shield mass thicknesses quite well.

Table D3-11. LU front 4 litres NaI(Tl)-detector. Coefficients *a* and *b* in an exponential model for determining shield mass thickness according to the description in the main report. The unit of *b* is m^2/kg.

ROI ratio	*a*	*b*
ROI A/PR	3.69	0.00398
ROI B/PR	1.98	0.00334
ROI C/PR	1.35	0.00231
ROI PL/PR	1.21	0.000392
ROI A/P	1.61	0.00377
ROI B/P	0.862	0.00313
ROI C/P	0.590	0.00210

Table D3-12. LU front 4 litres NaI(Tl)-detector. Coefficients a_0 - a_5 (kg/m^2) in the five-degree polynomial model for determining shield mass thickness according to Eqn 3 in the main report.

ROI ratio	a_5	a_4	a_3	a_2	a_1	a_0
ROI A/PR	5.410	-57.14	187.9	-137.5	-21.35	0
ROI B/PR	-0.7971	31.87	-230.4	606.6	-318.9	0
ROI C/PR	108.8	-577.3	931.1	-311.7	135.6	0
ROI PL/PR	6331000	-11190000	7503000	-2377000	356500	-20300
ROI A/P	3.091	-6.931	-84.48	347.3	-128.6	0
ROI B/P	-14.46	76.10	-118.9	-32.89	500.9	0
ROI C/P	505.4	-495.1	-543.8	391.4	605.2	223.0

Table D3-21. LU rear 4 litres NaI(Tl)-detector. Coefficients *a* and *b* in an exponential model for determining shield mass thickness according to the description in the main report. The unit of *b* is m^2/kg.

ROI ratio	*a*	*b*
ROI A/PR	3.45	0.00416
ROI B/PR	1.90	0.00349
ROI C/PR	1.33	0.00247
ROI PL/PR	1.30	0.000560
ROI A/P	1.43	0.00384
ROI B/P	0.787	0.00318
ROI C/P	0.552	0.00215

Table D3-22. LU rear 4 litres NaI(Tl)-detector. Coefficients a_0 - a_5 (kg/m^2) in the five-degree polynomial model for determining shield mass thickness according to Eqn 3 in the main report.

ROI ratio	a_5	a_4	a_3	a_2	a_1	a_0
ROI A/PR	7.617	-86.50	321.2	-383.6	138.8	0
ROI B/PR	10.15	-65.07	62.57	253.1	-173.98	0
ROI C/PR	168.7	-924.0	1605	-818.3	243.4	0
ROI PL/PR	-882400	1829000	-1449000	552800	-100800	7036
ROI A/P	5.579	-23.12	-54.32	322.5	-90.250	0
ROI B/P	-175.8	965.8	-1774	1109	328.90	0
ROI C/P	724.4	-491.7	-857.1	355.3	684.50	254.7

Table D3-31. LU 3"x3" NaI(Tl)-detector. Coefficients *a* and *b* in an exponential model for determining shield mass thickness according to the description in the main report. The unit of *b* is m^2/kg.

ROI ratio	*a*	*b*
ROI A/PR	6.14	0.00400
ROI B/PR	2.59	0.00309
ROI C/PR	1.43	0.00230
ROI PL/PR	1.22	0.000599
ROI A/P	2.65	0.00367
ROI B/P	1.11	0.00276
ROI C/P	0.616	0.00197

Table D3-32. LU 3"x3" NaI(Tl)-detector. Coefficients a_0 - a_5 (kg/m^2) in the five-degree polynomial model for determining shield mass thickness according to Eqn 3 in the main report.

ROI ratio	a_5	a_4	a_3	a_2	a_1	a_0
ROI A/PR	6.202	-85.13	403.4	-719.8	428.4	0
ROI B/PR	12.08	-95.27	200.5	54.57	-156.8	0
ROI C/PR	44.13	-333.1	703.0	-314.4	136.8	0
ROI PL/PR	-59400	-240701	123900	-76000	17290	-1265
ROI A/P	10.10	-91.21	247.6	-118.8	-34.82	0
ROI B/P	-67.10	453.1	-1134	1207	-90.58	0
ROI C/P	368.3	-394.6	-421.2	408.6	574.0	202.5

Table D3-41. LU DetectiveX HPGe-detector. Coefficients *a* and *b* in an exponential model for determining shield mass thickness according to the description in the main report. The unit of *b* is m^2/kg.

ROI ratio	a	b
ROI A/P	4.80	0.00467
ROI B/P	2.20	0.00354
ROI C/P	1.30	0.00231
ROI D/P	0.259	0.00246

Table D3-42. LU DetectiveX HPGe-detector. Coefficients a_0 - a_5 (kg/m^2) in the five-degree polynomial model for determining shield mass thickness according to Eqn 3 in the main report.

ROI ratio	a_5	a_4	a_3	a_2	a_1	a_0
ROI A/P	2.779	-35.67	148.8	-181.0	47.69	0
ROI B/P	5.402	-32.65	7.164	256.5	-184.0	0
ROI C/P	71.49	-321.9	411.7	42.72	90.96	0
ROI D/P	344.0	1474	2275	1619	854.2	494.3

D4. Results from shield thickness measurements, using SSC

In connection with the experiment determining the source distance with the SODAC routine, a determination of the shield mass thickness in front of the Cs-137 point source was made using the SSC routine when the measuring car was directly opposite the source, i.e. at the road location with the shortest distance to the source. The results are given in Tables B4-11 to B4-44.

The detailed result from SSC is also reproduced in Figs B4-11 to B4-55, where the individual net count rate ratios ROI A/PR, ROI B/PR Etc., are plotted along the lines of the exponential model and the polynomial model.

For the two 4-litre NaI(Tl)-detectors, the deviation in the calculated mass thickness from the actual value was between -131% and 37% for the exponential model and between -65% and 133% for the polynomial model. The average deviation was -26 ± 19% for the exponential model and -4 ±18% for the polynomial model.

For the 3"x3" NaI(Tl)-detector, the deviation in the calculated mass thickness from the actual value was between -78% and 45% for the exponential model and between -136% and 44% for the polynomial model. The average deviation was 4 ± 16% for the exponential model and -4 ±22% for the polynomial model.

For the HPGe-detector, the deviation in the calculated mass thickness from the actual value was between 15% and 92% for the exponential model and between 4% and 92% for the polynomial model. The average deviation was 47 ± 19% for the exponential model and 40 ±20% for the polynomial model.

For the NaI(Tl)-detectors, the mass shield thickness obtained from the ratio ROI PL/PR (area of the left part to the right part of the full energy peak) shows much more significant variations than obtained from the ratios ROI A/PR, B/PR, and C/PR. The considerable variation is because the function (both the exponential and the polynomial function) has a very steep slope. A slight variation in the count rate ratio results in a significant variation in apparent shield thickness obtained from the model. Even a tiny gain drift in the pulse height distribution accentuates the problem, which affects the count rate ratio ROI PL/PR. Thus, if the gain cannot be kept under perfect control, using the ROI PL/PR ratio for NaI(Tl) detectors is less appropriate.

If ROI P (the entire full energy peak) is used instead of ROI PR, the variations in the resulting shield thickness for the count rate ratios ROI A/P, B/P, and C/P are more limited. Using ROI P in the denominator is thus preferable to ROI PR.

Excluding the calculation with the ROI PL/PR ratio for NaI(Tl) detectors and ROI D/P for HPGe-detectors, there is no significant difference in the obtained shield thickness result between the exponential model and the polynomial model. Since the exponential model is computationally more straightforward, it is preferable.

For the HPGe detector, the obtained shield thickness appears to be increasingly overestimated as the distance to the shielded source increases. Why the SSC model shows, such an overestimation remains to be investigated.

Table D4-11. Result from the LU 4 litre NaI(Tl) front detector determination of shield mass thickness by using ROI A, B, C, PL / PR net count rate ratios in an exponential model.

Setup	Actual		Measured		Deviation
	Distance to source (m)	Shield mass thickness (kg/m^2)	Shield and air mass thickness (kg/m^2)	Shield mass thickness (kg/m^2)	of measured from actual value (%)
M1	61	0	12.1*	-63.8*	-84.0*
M2	31	333	392*	353*	5.44*
M3	61	94	198*	123*	16.8*
M4	61	333	-	-	
M5	91	94	231	117	11.3
Average					-12.6 ± 23.9

* ROI PL/PR not included due to uncontrolled peak gain drift during measurement

Table D4-12. Result from the LU 4 litre NaI(Tl) front detector determination of shield mass thickness by using ROI A, B, C / P net count rate ratios in an exponential model

Setup	Actual		Measured		Deviation

	Distance to source (m)	Shield mass thickness (kg/m^2)	Shield and air mass thickness (kg/m^2)	Shield mass thickness (kg/m^2)	of measured from actual value (%)
M1	61	0	49.1	-26.7	-35.2
M2	31	333	319	280	-14.3
M3	61	94	174	98.4	2.6
M4	61	333	-	-	
M5	91	94	236	122	13.7
Average					-8.3 ± 10.7

Table D4-13. Result from the LU 4 litre NaI(Tl) front detector determination of shield mass thickness by using ROI A, B, C, PL / PR net count rate ratios in a five-degree polynomial model

Setup	Actual		Measured		Deviation
	Distance to source (m)	Shield mass thickness (kg/m^2)	Shield and air mass thickness (kg/m^2)	Shield mass thickness (kg/m^2)	of measured from actual value (%)
M1	61	0	29.9*	-45.9*	-60.6*
M2	31	333	430*	382*	13.1*
M3	61	94	190*	114*	11.8*
M4	61	333	-	-	
M5	91	94	181	67.8	-12.6
Average					-12.1 ± 17.2

* ROI PL/PR not included due to uncontrolled peak gain drift during measurement

Table D4-14. Result from the LU 4 litre NaI(Tl) front detector determination of shield mass thickness by using ROI A, B, C / P net count rate ratios in a five-degree polynomial model

Setup	Actual		Measured		Deviation
	Distance to source (m)	Shield mass thickness (kg/m^2)	Shield and air mass thickness (kg/m^2)	Shield mass thickness (kg/m^2)	of measured from actual value (%)
M1	61	0	42.3	33.6	-44.3
M2	31	333	345	306	-7.2
M3	61	94	163	87.4	-3.9
M4	61	333	-	-	
M5	91	94	239	126	15.4
Average					-10.0 ± 12.5

Table D4-21. Result from the LU 4 litre NaI(Tl) rear detector determination of shield mass thickness by using ROI A, B, C, PL / PR net count rate ratios in an exponential model

Setup	Actual		Measured		Deviation

	Distance to source (m)	Shield mass thickness (kg/m^2)	Shield and air mass thickness (kg/m^2)	Shield mass thickness (kg/m^2)	of measured from actual value (%)
M1	61	0	-23.5	-99.4	-131
M2	31	333	508	470	36.7
M3	61	94	-15.6	-91.4	-109
M4	61	333	389	313	-4.9
M5	91	94	52.5	-60.4	-74.7
Average					-56.6 ± 31.6

Table D4-22 Result from the LU 4 litre NaI(Tl) rear detector determination of shield mass thickness by using ROI A, B, C / P net count rate ratios in an exponential model

Setup	Actual		Measured		Deviation
	Distance to source (m)	Shield mass thickness (kg/m^2)	Shield and air mass thickness (kg/m^2)	Shield mass thickness (kg/m^2)	of measured from actual value (%)
M1	61	0	37.4	-38.5	-50.7
M2	31	333	344	305	-7.4
M3	61	94	97.4	21.5	-42.7
M4	61	333	263	187	-35.7
M5	91	94	226	113	9.1
Average					-25.5 ± 11.3

Table D4-23. Result from the LU 4 litre NaI(Tl) rear detector determination of shield mass thickness by using ROI A, B, C, PL / PR net count rate ratios in a five-degree polynomial model

Setup	Actual		Measured		Deviation
	Distance to source (m)	Shield mass thickness (kg/m^2)	Shield and air mass thickness (kg/m^2)	Shield mass thickness (kg/m^2)	of measured from actual value (%)
M1	61	0	57.2	-18.6	-24.5
M2	31	333	469	431	26.2
M3	61	94	217	141	27.7
M4	61	333	489	413	19.7
M5	91	94	482	369	133
Average					36.4 ± 26.0

Table D4-24. Result from the LU 4 litre NaI(Tl) rear detector determination of shield mass thickness by using ROI A, B, C / P net count rate ratios in a five-degree polynomial model

Setup	Actual		Measured		Deviation

	Distance to source (m)	Shield mass thickness (kg/m^2)	Shield and air mass thickness (kg/m^2)	Shield mass thickness (kg/m^2)	of measured from actual value (%)
M1	61	0	26.7	-49.1	-64.8
M2	31	333	397	358	6.8
M3	61	94	58.1	-17.7	-65.8
M4	61	333	266	190	-34.9
M5	91	94	232	119	12.0
Average					-29.3 ± 16.8

Table D4-31. Result from the LU 3"x3" NaI(Tl) detector determination of shield mass thickness by using ROI A, B, C, PL / PR net count rate ratios in an exponential model

Setup	Actual		Measured		Deviation
	Distance to source (m)	Shield mass thickness (kg/m^2)	Shield and air mass thickness (kg/m^2)	Shield mass thickness (kg/m^2)	of measured from actual value (%)
M1	61	0	70.1	-5.71	-7.5
M2	31	333	500	461	34.5
M3	61	94	247	171	45.3
M4	61	333	-	-	-
M5	91	94	46.6	-66.5	-77.5
Average					-1.3 ± 27.8

Table D4-32. Result from the LU 3"x3" NaI(Tl) detector determination of shield mass thickness by using ROI A, B, C / P net count rate ratios in an exponential model

Setup	Actual		Measured		Deviation
	Distance to source (m)	Shield mass thickness (kg/m^2)	Shield and air mass thickness (kg/m^2)	Shield mass thickness (kg/m^2)	of measured from actual value (%)
M1	61	0	83.1	7.31	9.6
M2	31	333	391	352	5.3
M3	61	94	202	126	19.1
M4	61	333	-	-	-
M5	91	94	211	98.1	2.0
Average					9.0 ± 3.7

Table D4-33. Result from the LU 3"x3" NaI(Tl) detector determination of shield mass thickness by using ROI A, B, C, PL / PR net count rate ratios in a five-degree polynomial model

Setup	Actual		Measured		Deviation

	Distance to source (m)	Shield mass thickness (kg/m²)	Shield and air mass thickness (kg/m²)	Shield mass thickness (kg/m²)	of measured from actual value (%)
M1	61	0	80.2	4.40	5.8
M2	31	333	537	498	44.4
M3	61	94	201	125	18.5
M4	61	333	-	-	-
M5	91	94	-73.5	-187	-136
Average					-16.8 ± 40.5

Table D4-34. Result from the LU 3"x3" NaI(Tl) detector determination of shield mass thickness by using ROI A, B, C / P net count rate ratios in a five-degree polynomial model

Setup	Actual		Measured		Deviation
	Distance to source (m)	Shield mass thickness (kg/m²)	Shield and air mass thickness (kg/m²)	Shield mass thickness (kg/m²)	of measured from actual value (%)
M1	61	0	123	47.0	7.7
M2	31	333	423	384	13.8
M3	61	94	193	118	14.2
M4	61	333	-	-	-
M5	91	94	207	94.3	0.1
Average					8.95 ± 3.30

Table D4-41. Result from the LU DetectiveX HPGe detector determination of shield mass thickness by using ROI A, B, C / P net count rate ratios in an exponential model

Setup	Actual		Measured		Deviation
	Distance to source (m)	Shield mass thickness (kg/m²)	Shield and air mass thickness (kg/m²)	Shield mass thickness (kg/m²)	of measured from actual value (%)
M1	61	0	87.2	11.3	15.0
M2	31	333	438	400	17.9
M3	61	94	175	199	61.9
M4	61	333	-	-	-
M5	91	94	398	285	92.1
Average					46.7 ± 18.5

Table D4-42. Result from the LU DetectiveX HPGe detector determination of shield mass thickness by using ROI A, B, C / P net count rate ratios in a five-degree polynomial model

Setup	Actual		Measured		Deviation

	Distance to source (m)	Shield mass thickness (kg/m^2)	Shield and air mass thickness (kg/m^2)	Shield mass thickness (kg/m^2)	of measured from actual value (%)
M1	61	0	78.5	2.71	3.6
M2	31	333	429	390	15.4
M3	61	94	249	174	47.2
M4	61	333	-	-	-
M5	91	94	397	284	91.6
Average					39.5 ± 19.7

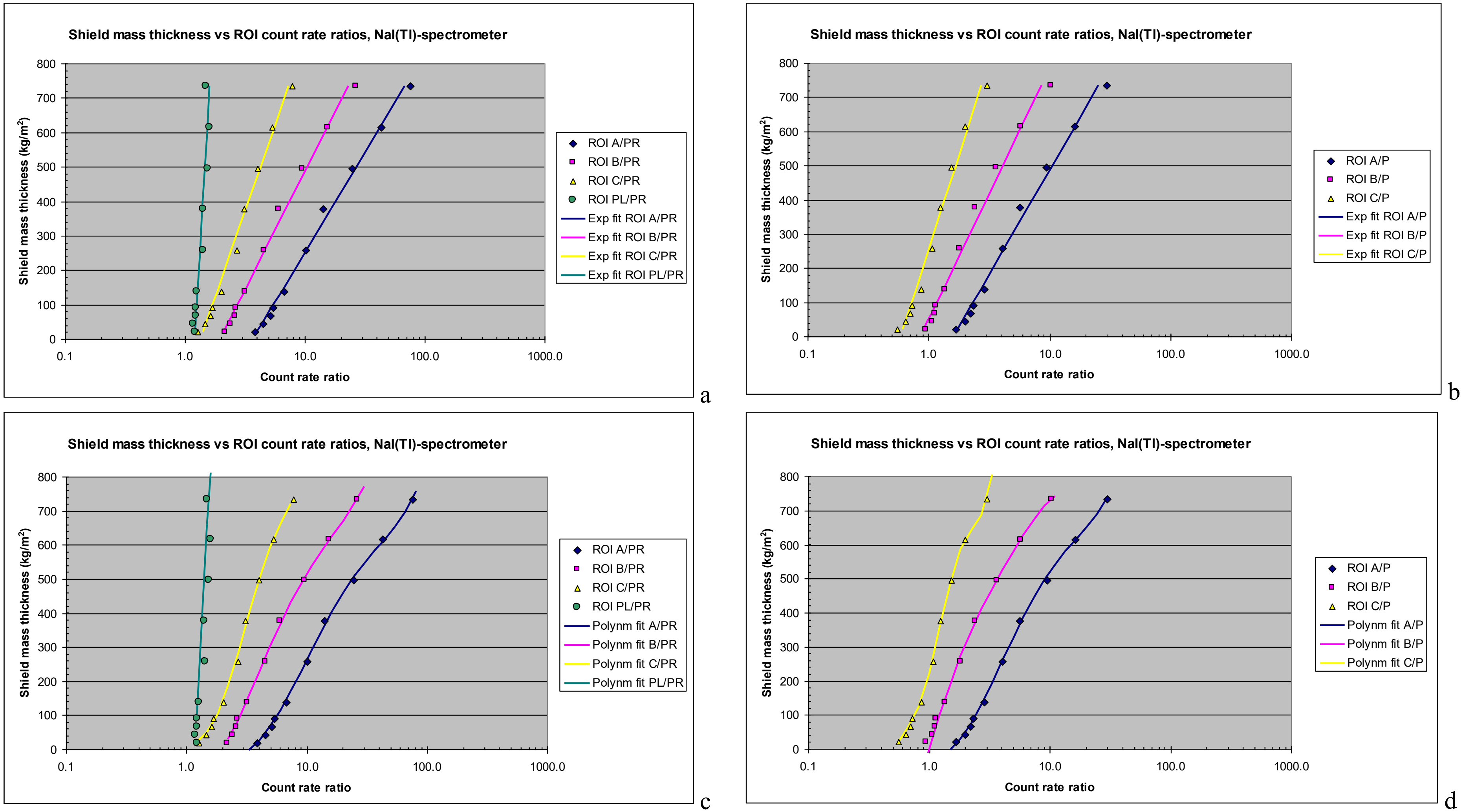

Fig D3-11-a-d. LU 4 litre (front) NaI(Tl) spectrometer. Models of shield mass thickness as a function of ROI net count rate ratio obtained from fitting measured data to exponential functions (a, b) and five-degree polynomial functions (c, d), valid for Cs-137 point sources behind shields of standard building material (wood and concrete) with mass thickness between 20 and 730 kg/m^2. Values have been measured at a source-detector distance of 10 m.

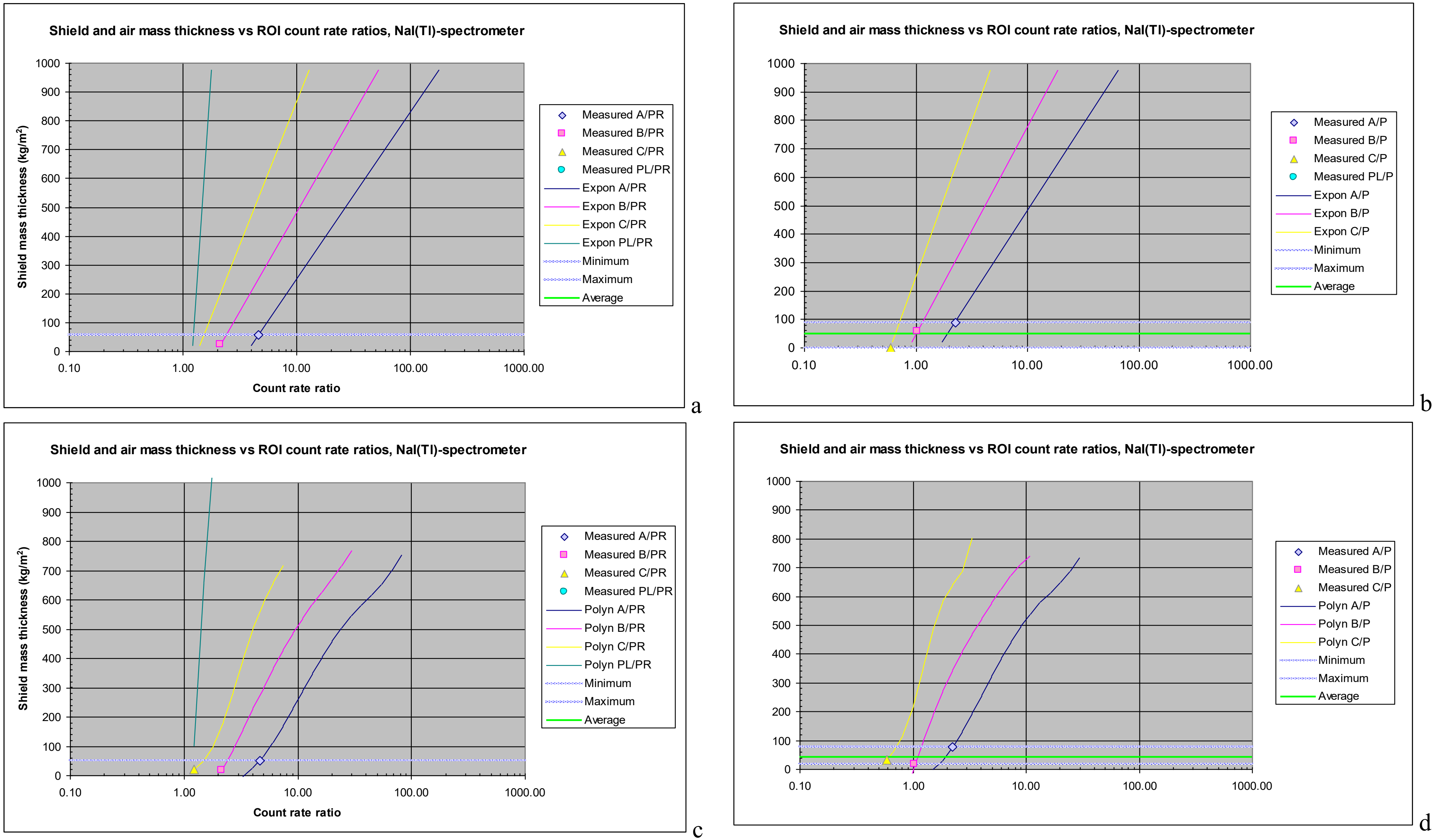

Fig D4-11-a-d (M1). Shield mass thickness determination by the LU 4 litre (front) NaI(Tl) spectrometer using the ROI count rate ratio method with exponential (a, b) and polynomial (c, d) models. The true shield mass thickness is 75.8 kg/m^2, including 61 m of air between the source and the detector.

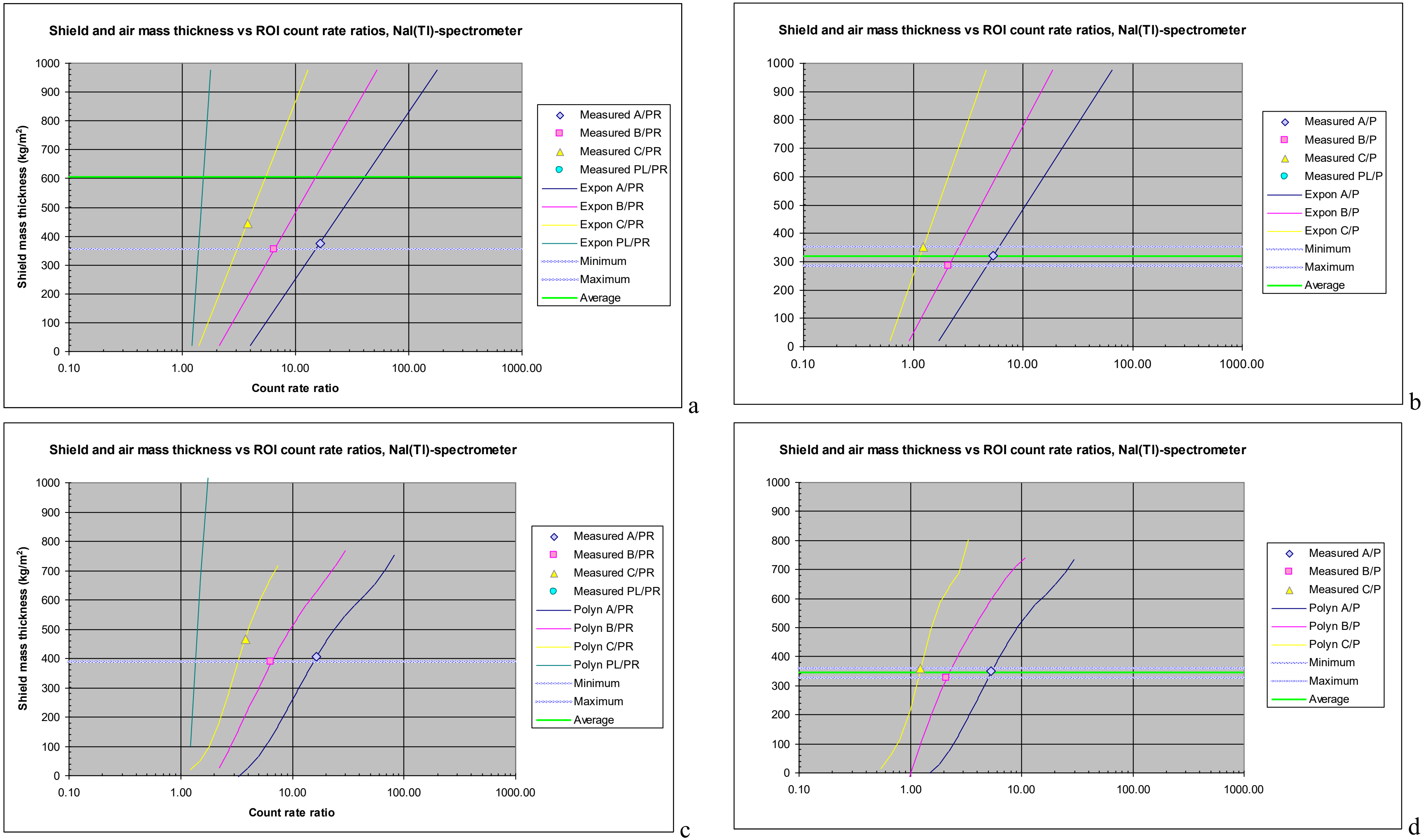

Fig D4-12-a-d (M2). Shield mass thickness determination by the LU 4 litre (front) NaI(Tl) spectrometer using the ROI count rate ratio method with exponential (a, b) and polynomial (c, d) models. The true shield mass thickness is 372 kg/m^2, including 31 m of air between the source and the detector.

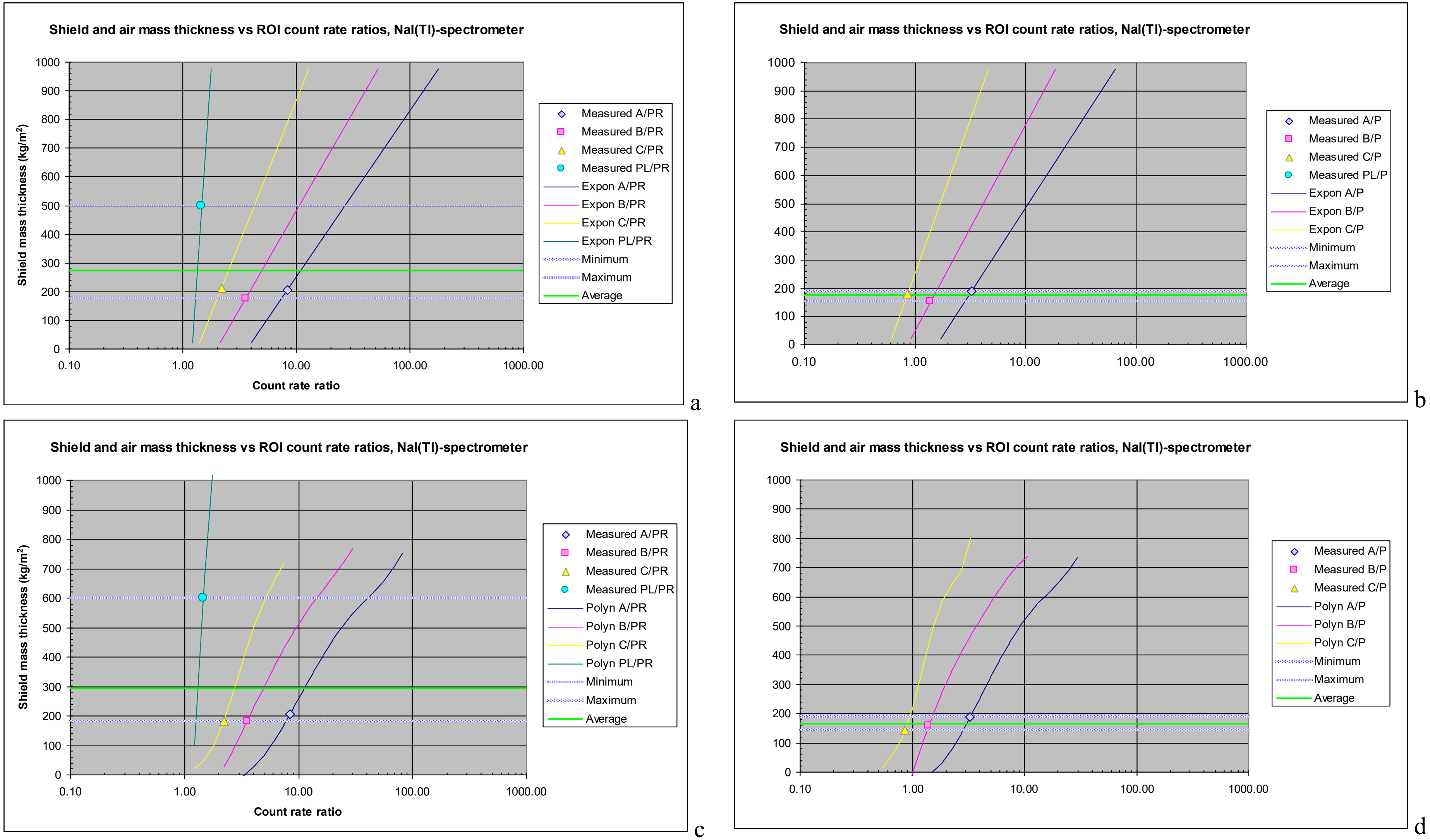

Fig D4-13-a-d (M3). Shield mass thickness determination by the LU 4 litre (front) NaI(Tl) spectrometer using the ROI count rate ratio method with exponential (a, b) and polynomial (c, d) models. The true shield mass thickness is 170 kg/m^2, including 61 m of air between the source and the detector.

Setup M4 was not measured due to technical problems with the detector.

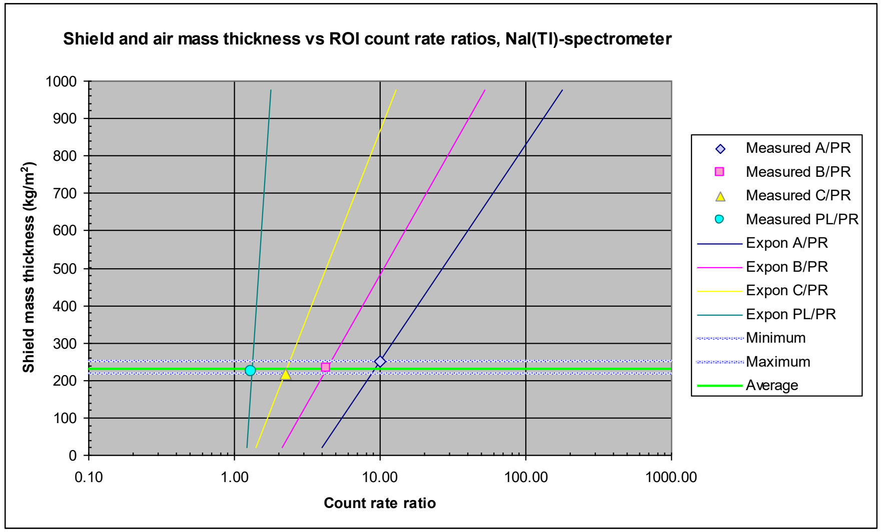

a

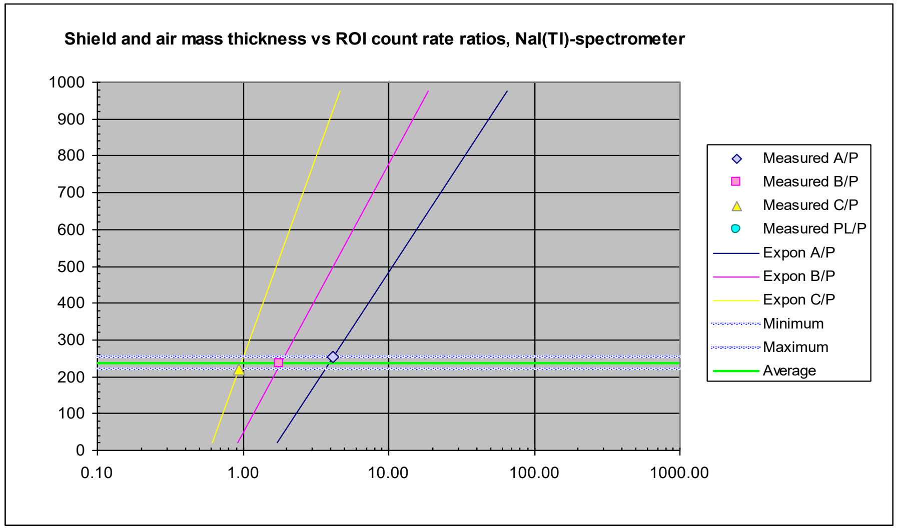

b

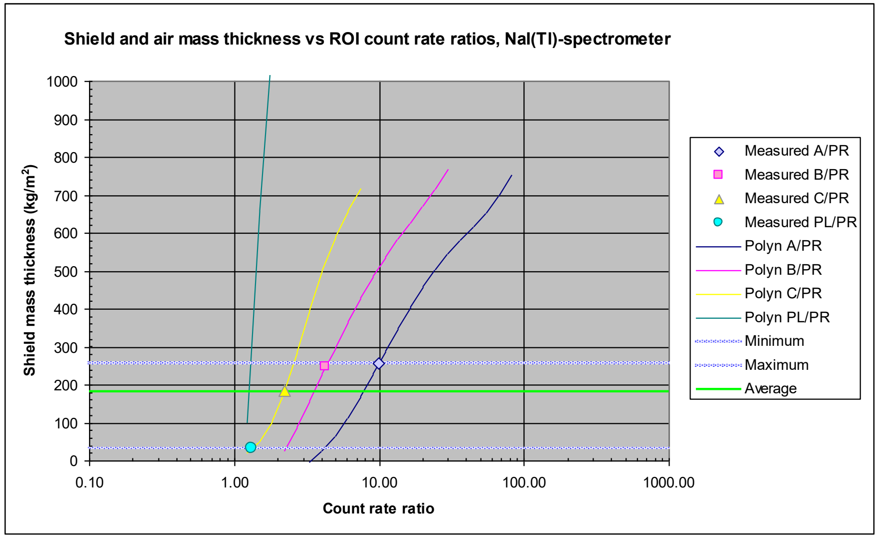

c

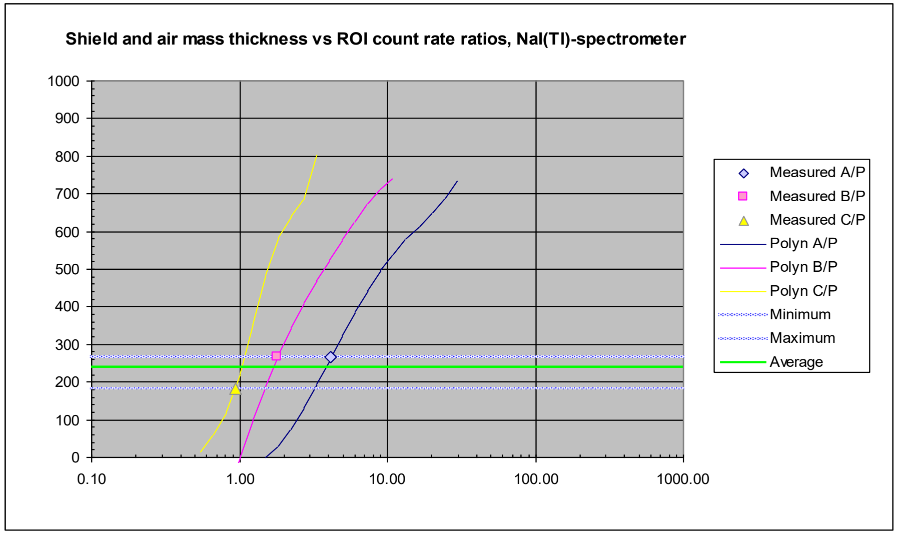

d

Fig D4-15-a-d (M5). Shield mass thickness determination by the LU 4 litre (front) NaI(Tl) spectrometer using the ROI count rate ratio method with exponential (a, b) and polynomial (c, d) models. The true shield mass thickness is 207 kg/m^2, including 91 m of air between the source and the detector.

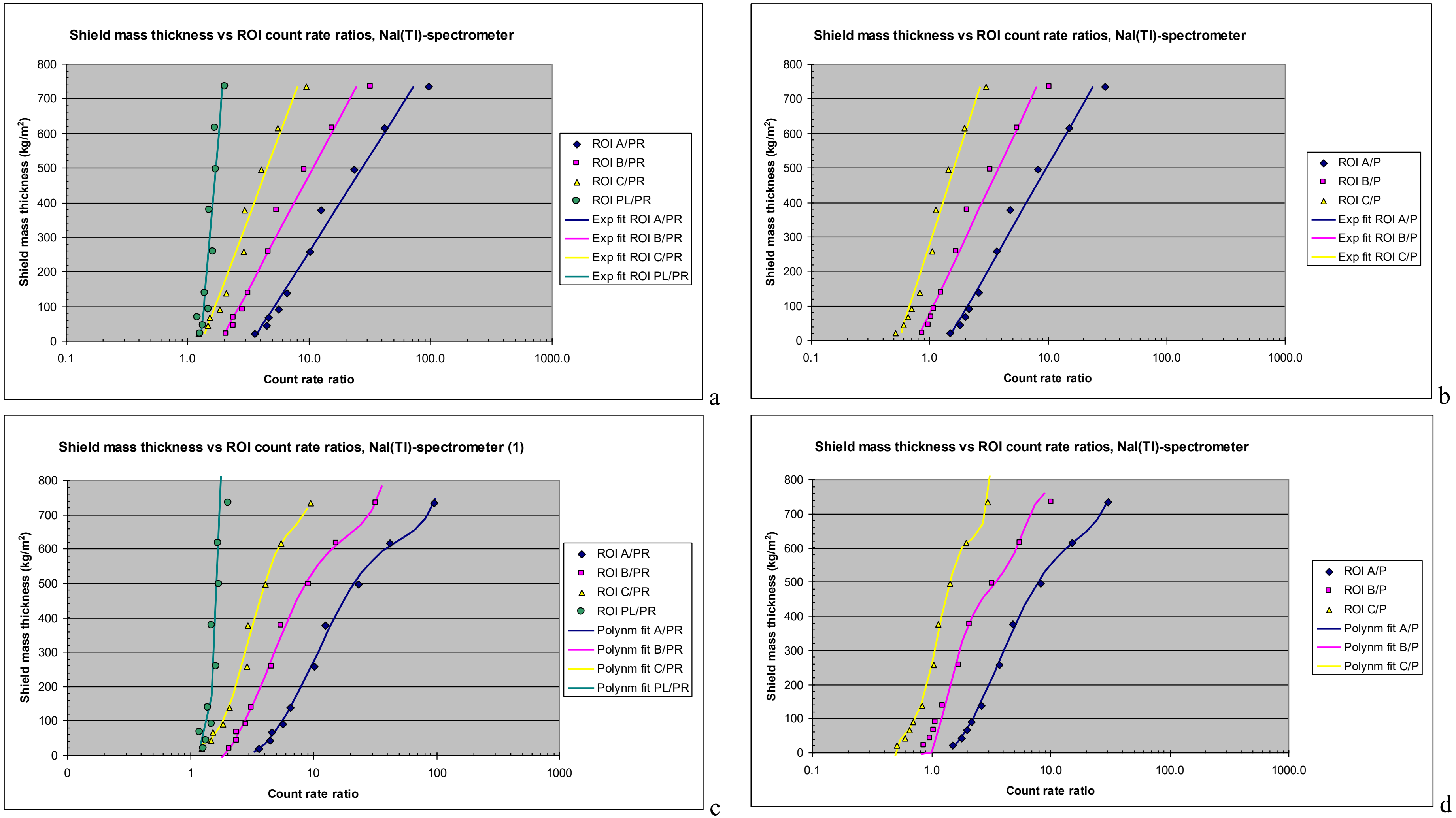

Fig D3-21-a-d. LU 4 litre (rear) NaI(Tl) spectrometer. Models of shield mass thickness as a function of ROI net count rate ratio obtained from fitting measured data to exponential functions (a, b) and five-degree polynomial functions (c, d), valid for Cs-137 point sources behind shields of standard building material (wood and concrete) with mass thickness between 20 and 730 kg/m^2. Values have been measured at a source-detector distance of 10 m.

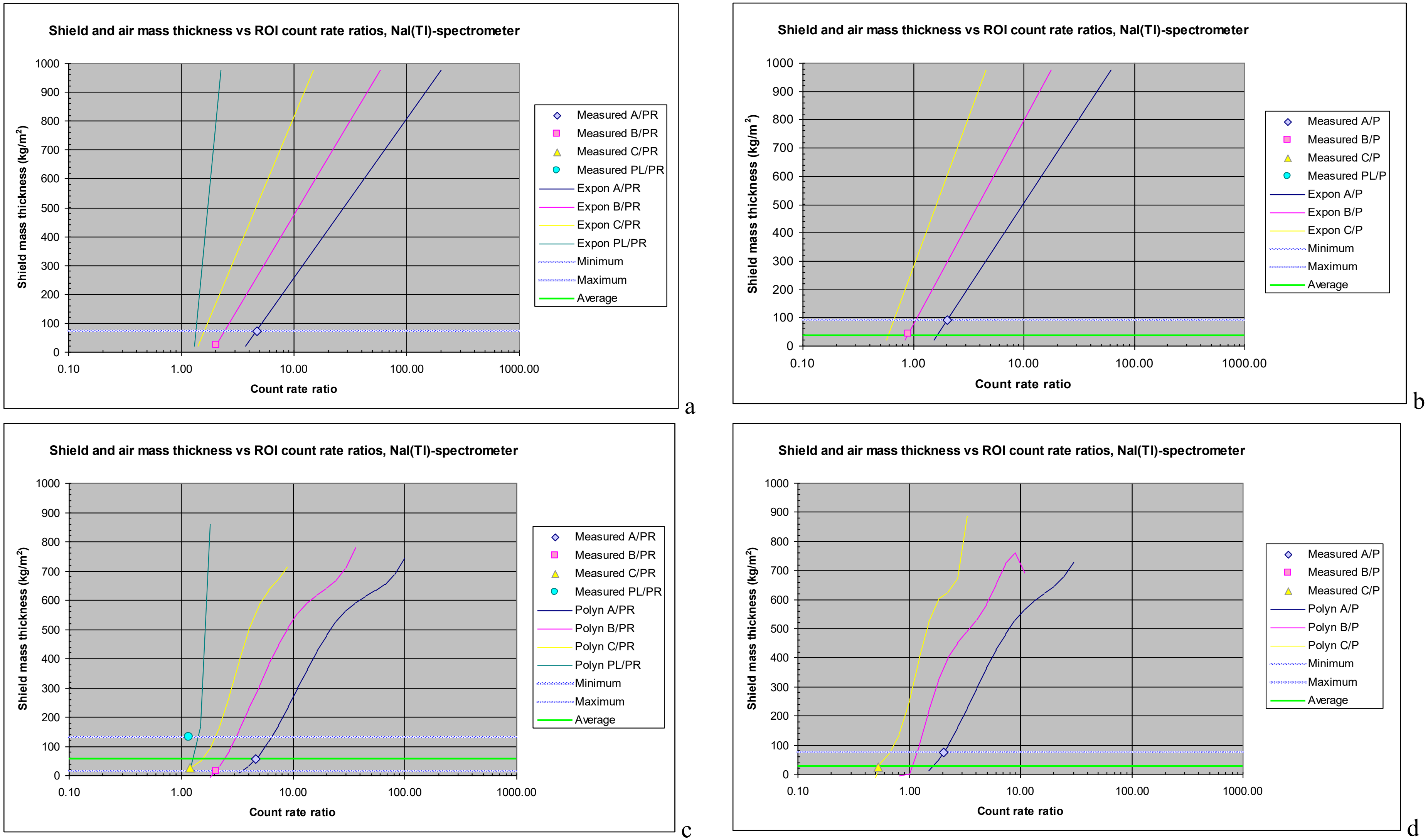

Fig D4-21-a-d (M1). Shield mass thickness determination by the LU 4 litre (rear) NaI(Tl) spectrometer using the ROI count rate ratio method with exponential (a, b) and polynomial (c, d) models. The true shield mass thickness is 75.8 kg/m^2, including 61 m of air between the source and the detector.

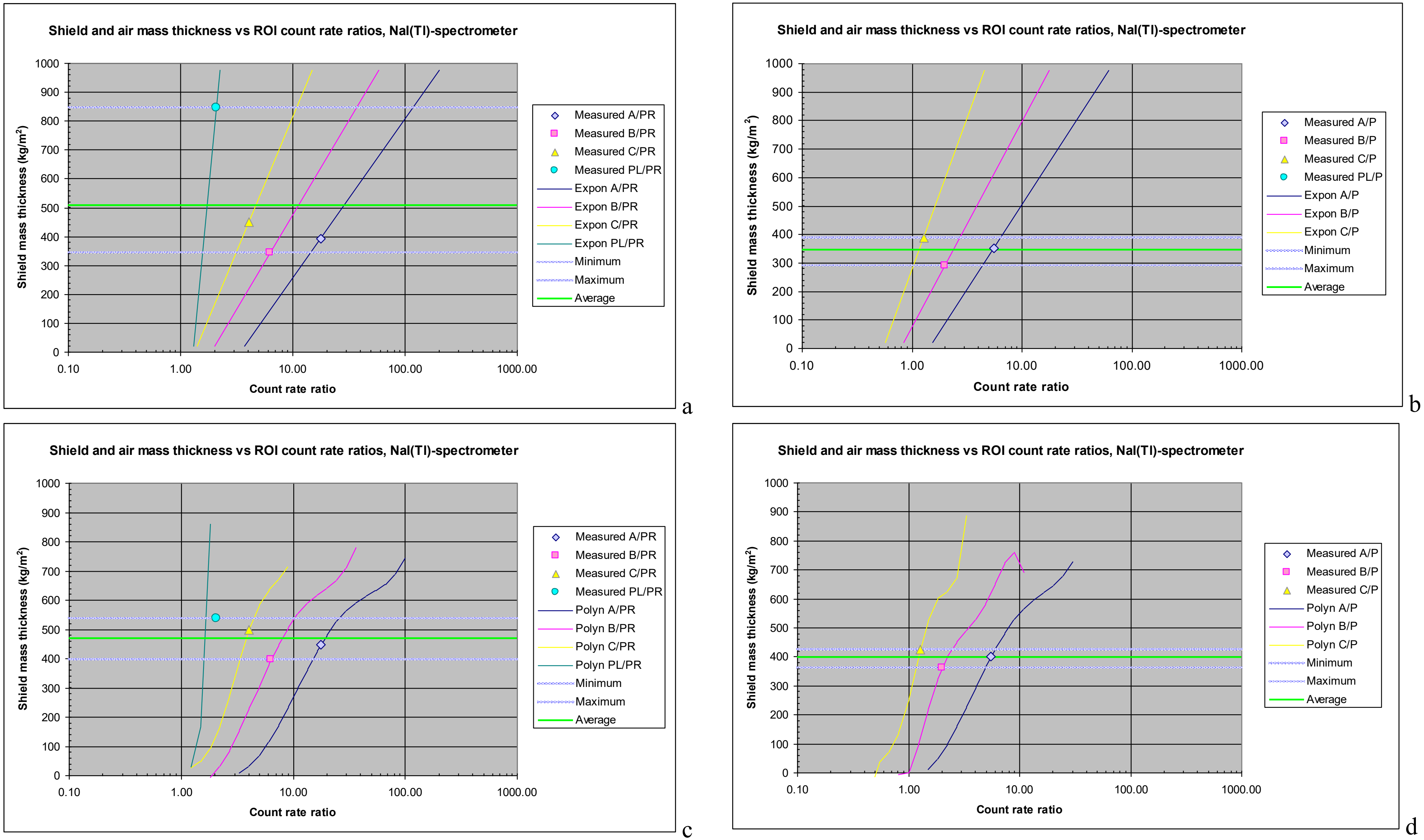

Fig D4-22-a-d (M2). Shield mass thickness determination by the LU 4 litre (rear) NaI(Tl) spectrometer using the ROI count rate ratio method with exponential (a, b) and polynomial (c, d) models. The true shield mass thickness is 372 kg/m^2, including 31 m of air between the source and the detector.

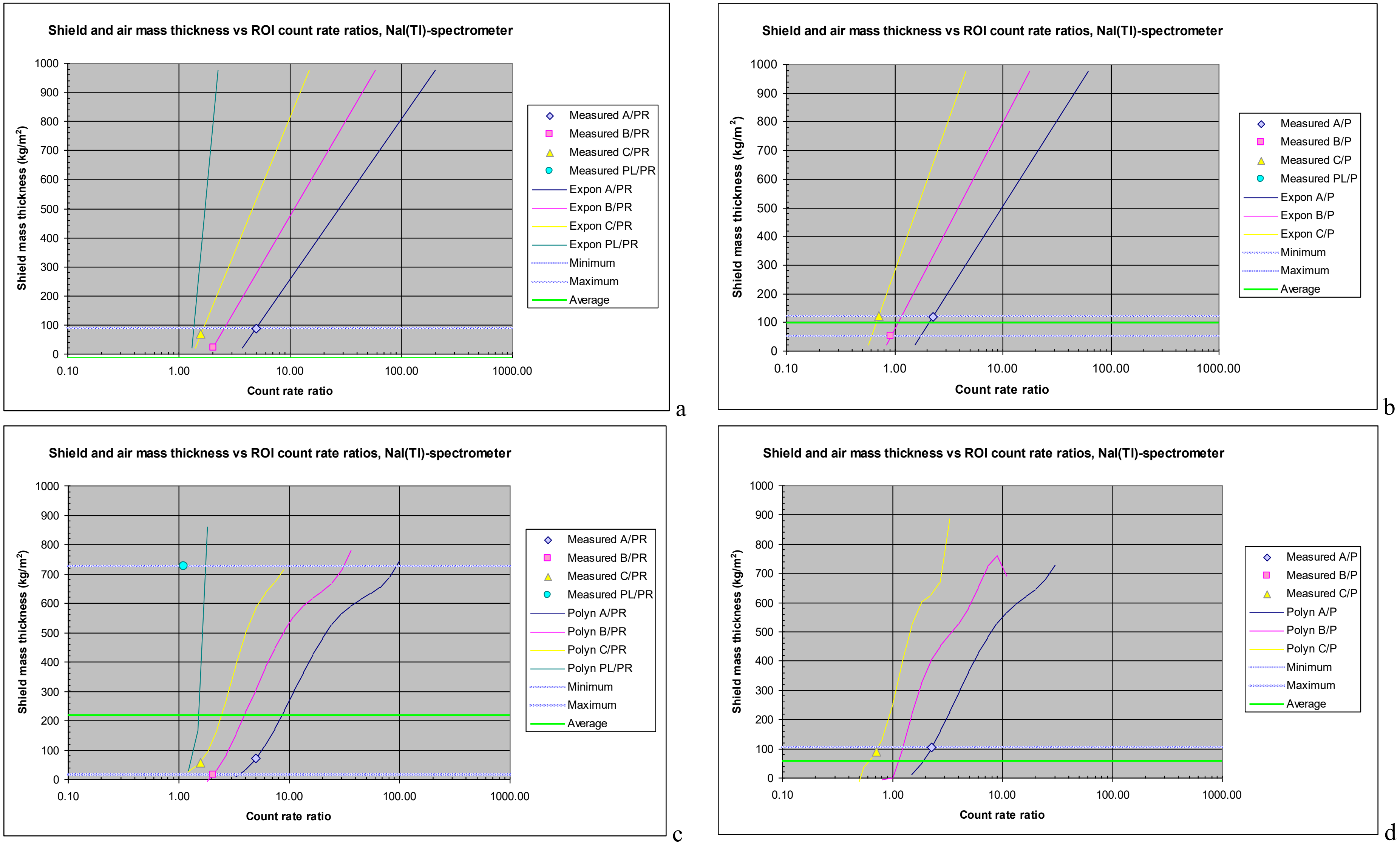

Fig D4-23-a-d (M3). Shield mass thickness determination by the LU 4 litre (rear) NaI(Tl) spectrometer using the ROI count rate ratio method with exponential (a, b) and polynomial (c, d) models. The true shield mass thickness is 170 kg/m^2, including 61 m of air between the source and the detector.

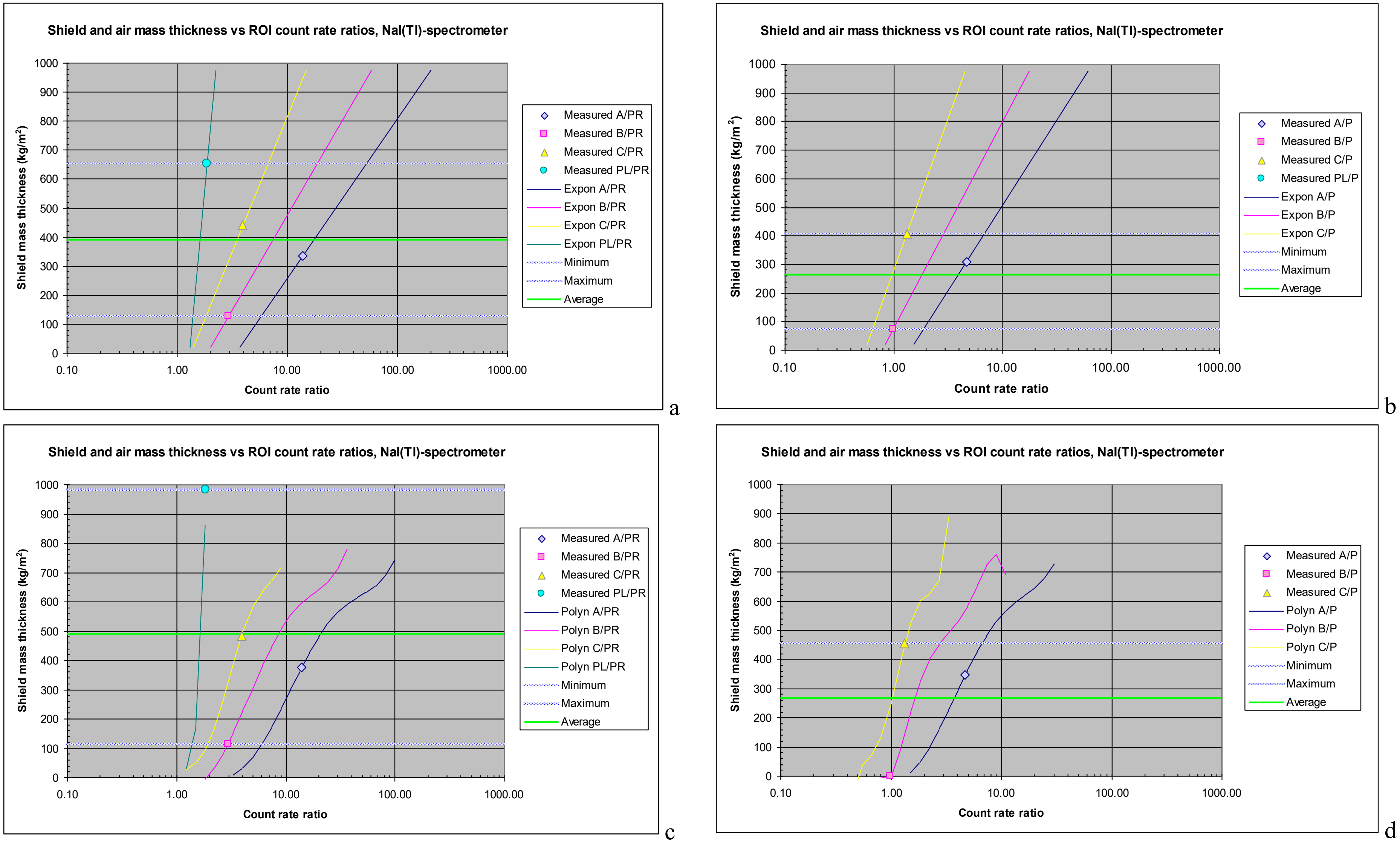

Fig D4-24-a-d (M4). Shield mass thickness determination by the LU 4 litre (rear) NaI(Tl) spectrometer using the ROI count rate ratio method with exponential (a, b) and polynomial (c, d) models. The true shield mass thickness is 409 kg/m^2, including 61 m of air between the source and the detector.

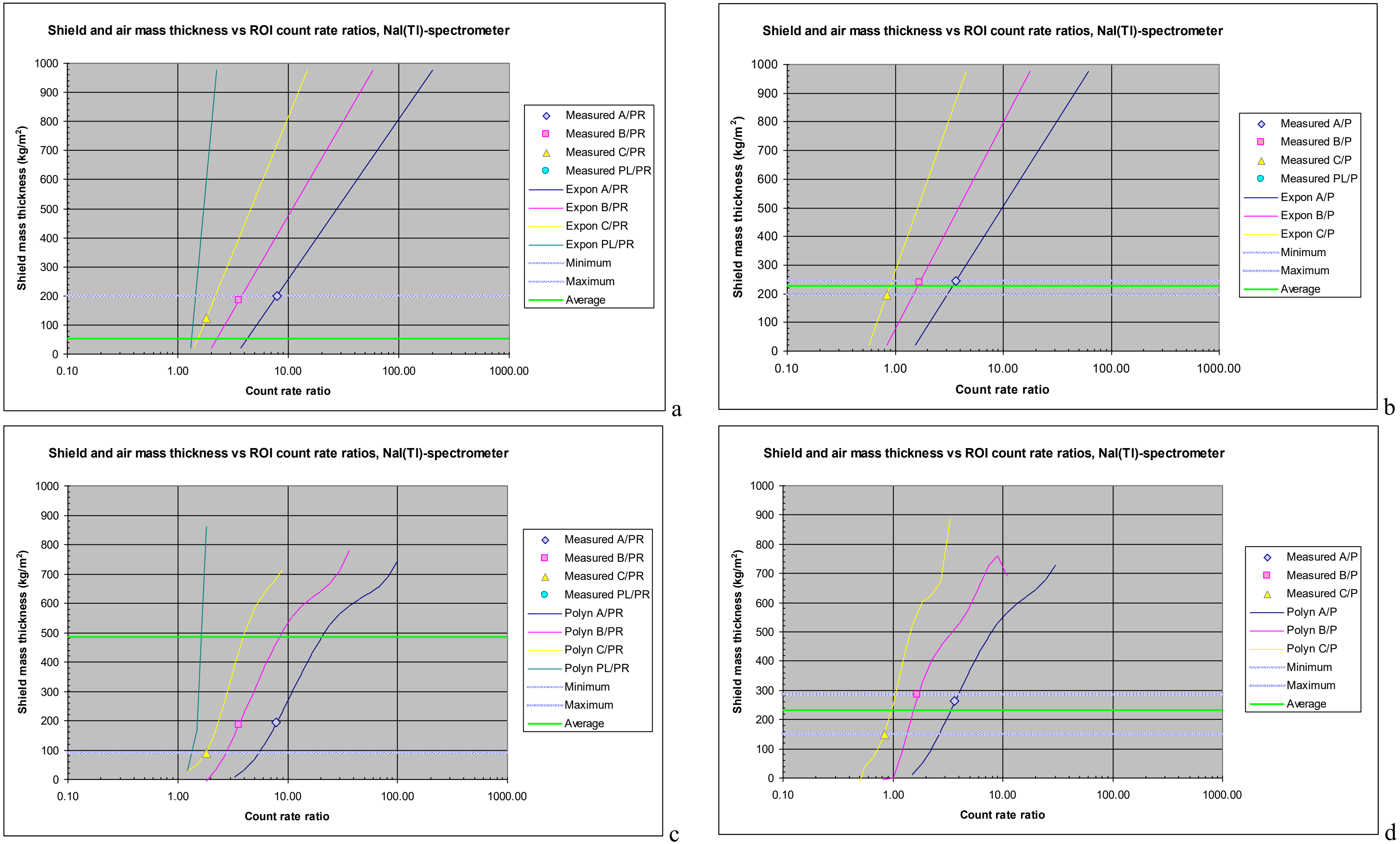

Fig D4-25-a-d (M5). Shield mass thickness determination by the LU 4 litre (rear) NaI(Tl) spectrometer using the ROI count rate ratio method with exponential (a, b) and polynomial (c, d) models. The true shield mass thickness is 207 kg/m^2, including 91 m of air between the source and the detector.

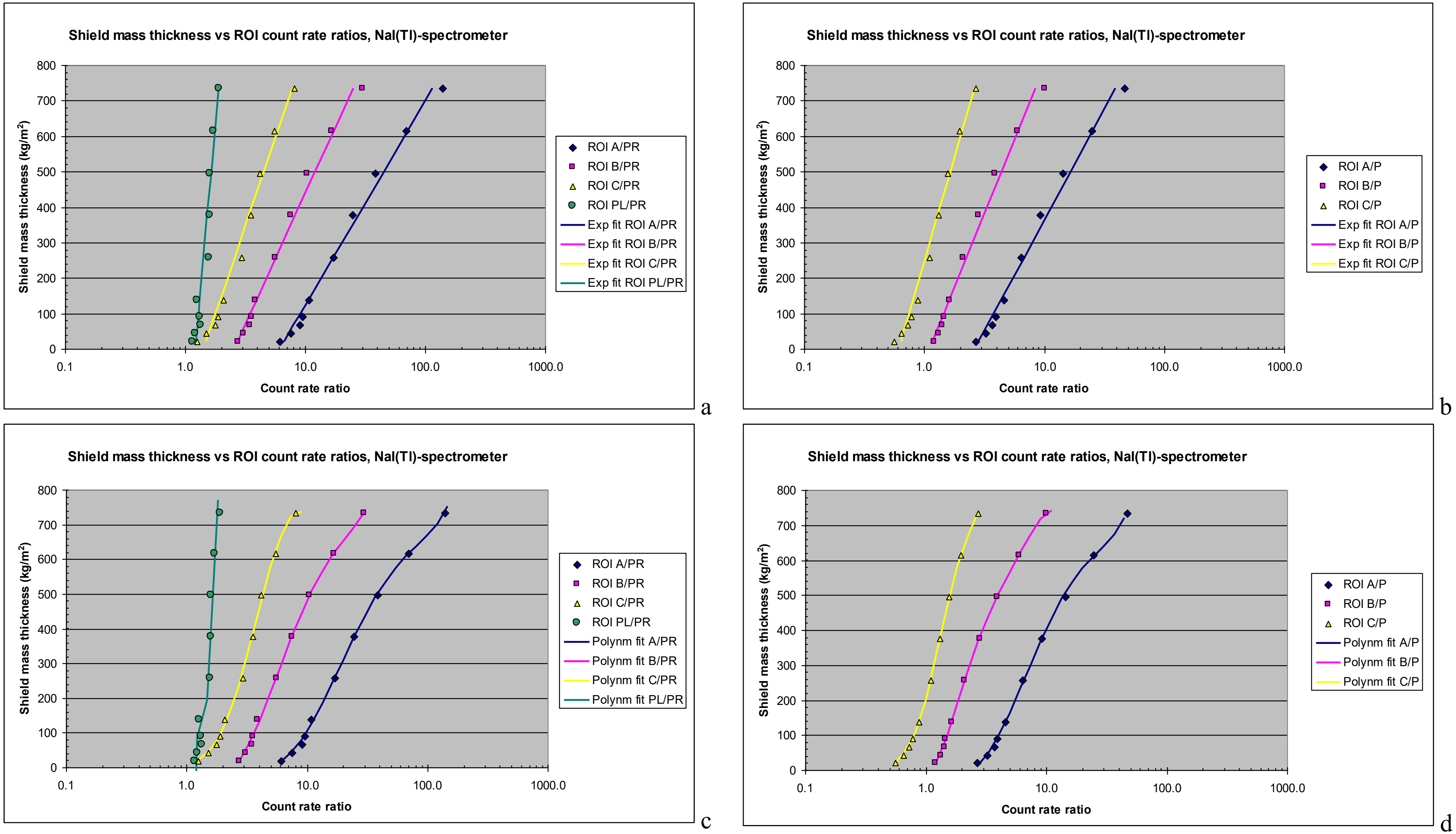

Fig D3-31-a-d. LU 3"x3" NaI(Tl) spectrometer. Models of shield mass thickness as a function of ROI net count rate ratio obtained from fitting measured data to exponential functions (a, b) and five-degree polynomial functions (c, d), valid for Cs-137 point sources behind shields of standard building material (wood and concrete) with mass thickness between 20 and 730 kg/m^2. Values have been measured at a source-detector distance of 10 m.

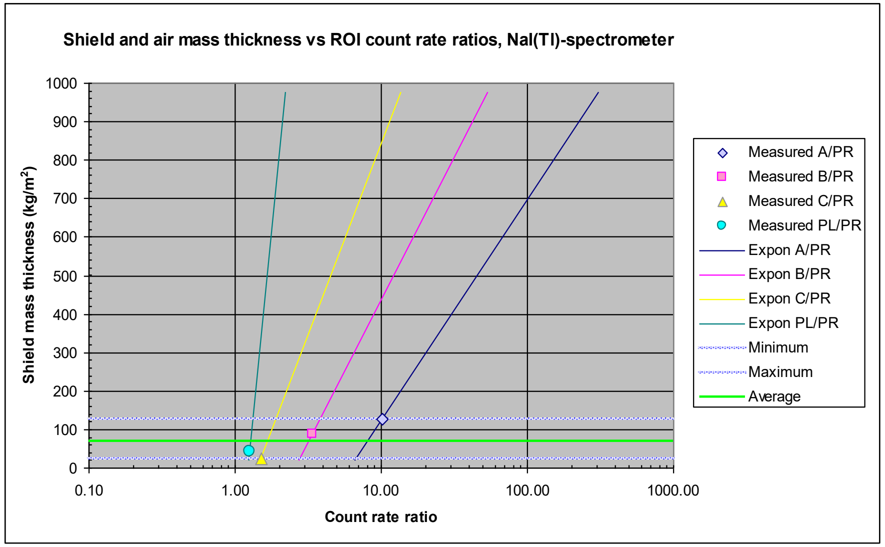

a

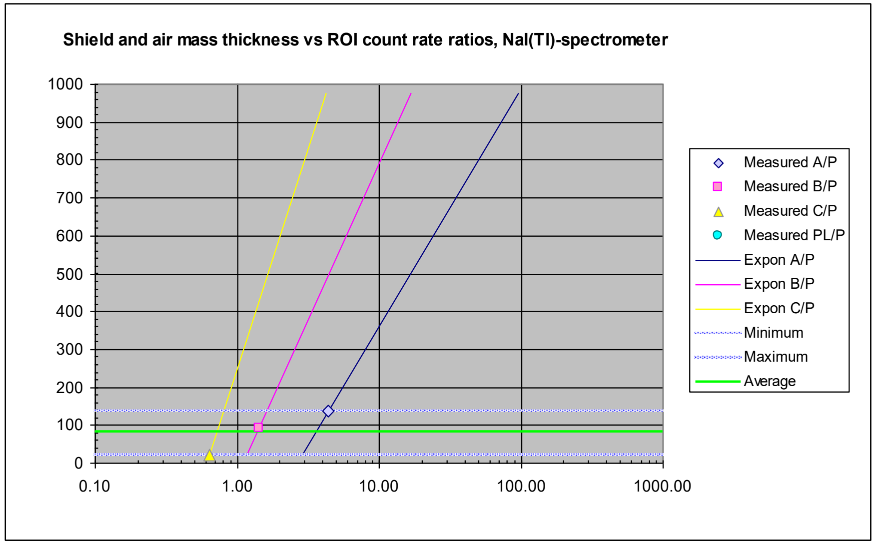

b

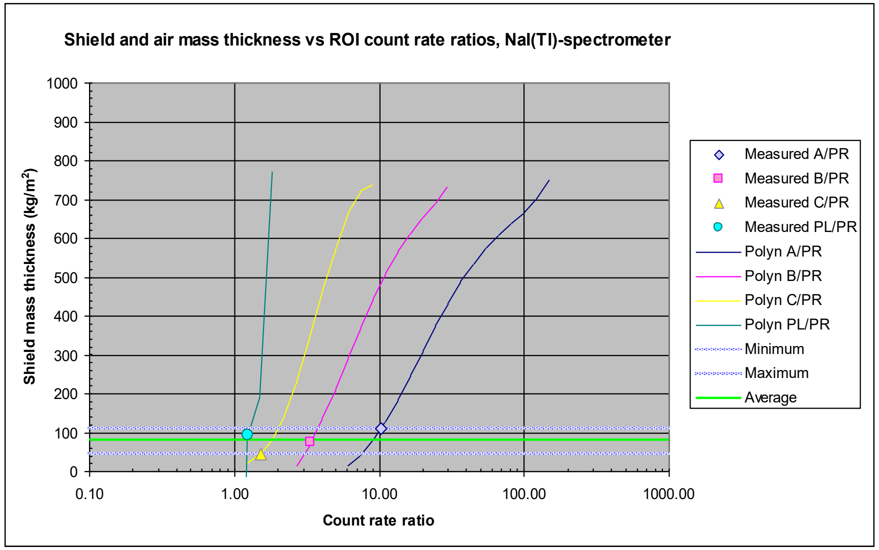

c

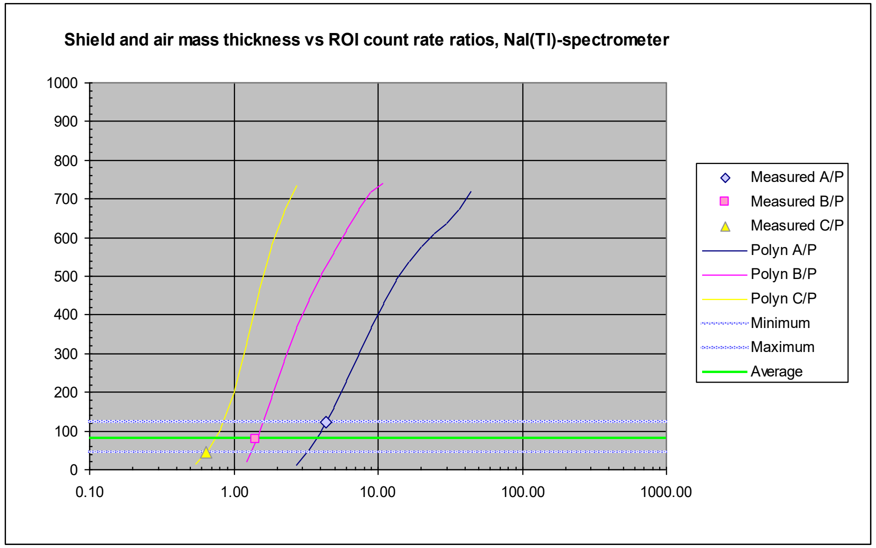

d

Fig D4-31-a-d (M1). Shield mass thickness determination by the LU 3"x3" NaI(Tl) spectrometer using the ROI count rate ratio method with exponential (a, b) and polynomial (c, d) models. The true shield mass thickness is 75.8 kg/m^2, including 61 m of air between the source and the detector.

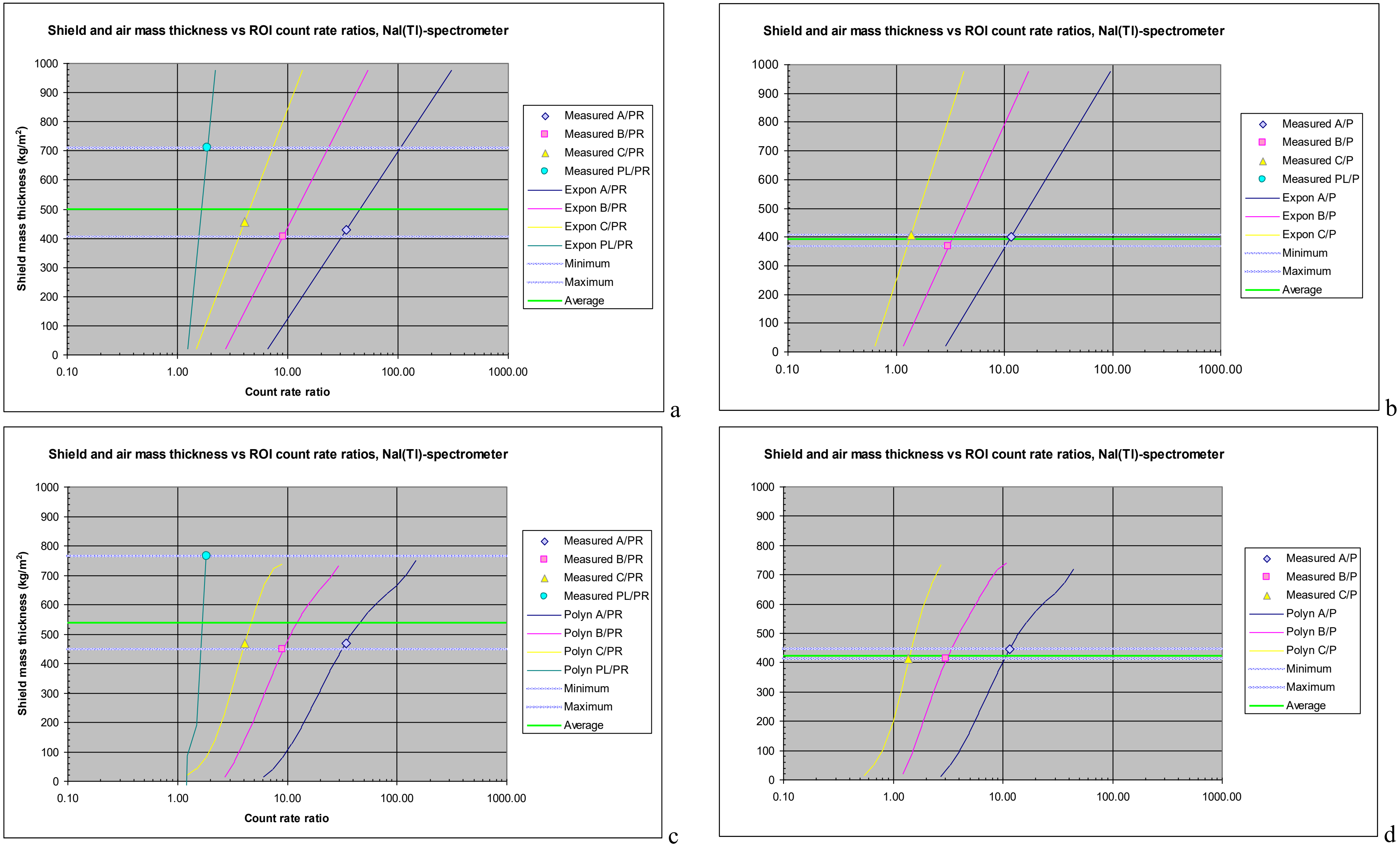

Fig D4-32-a-d (M29. Shield mass thickness determination by the LU 3"x3" NaI(Tl) spectrometer using the ROI count rate ratio method with exponential (a, b) and polynomial (c, d) models. The true shield mass thickness is 372 kg/m^2, including 31 m of air between the source and the detector.

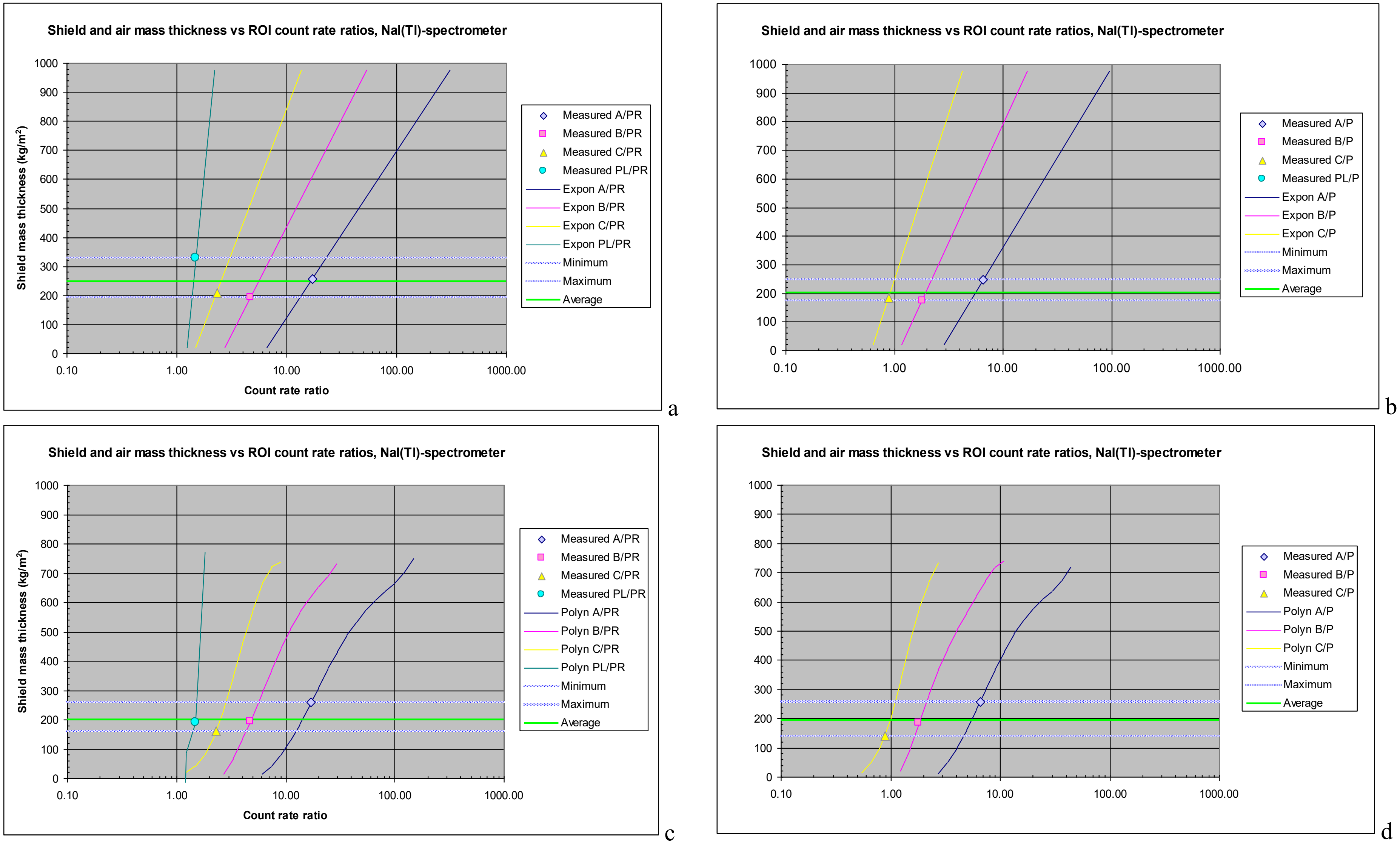

Fig D4-33-a-d (M3). Shield mass thickness determination by the LU 3"x3" NaI(Tl) spectrometer using the ROI count rate ratio method with exponential (a, b) and polynomial (c, d) models. The true shield mass thickness is 170 kg/m^2, including 61 m of air between the source and the detector.

Setup M4 was not measured due to technical problems with the detector.

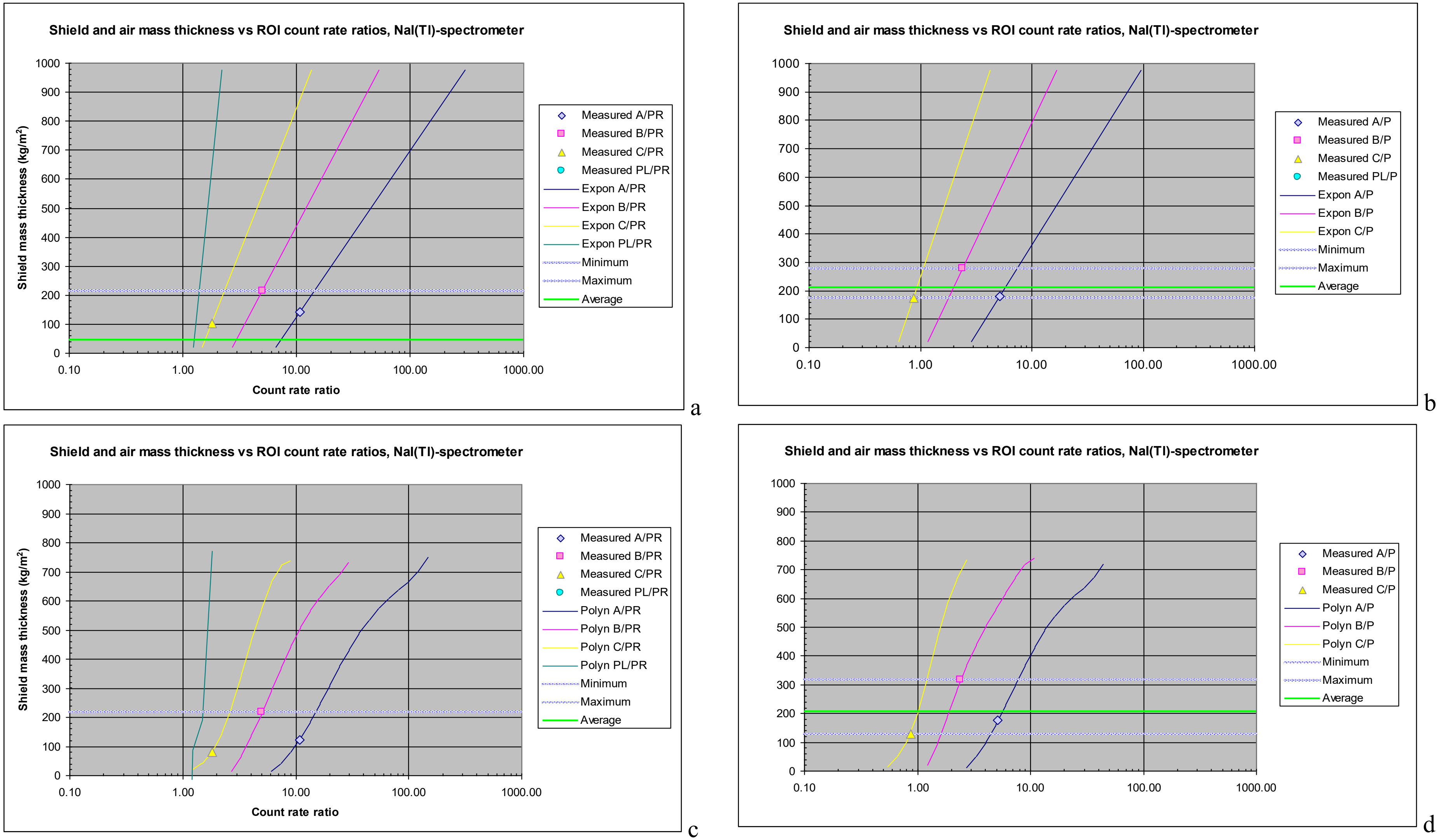

Fig D4-35-a-d (M5). Shield mass thickness determination by the LU 3"x3" NaI(Tl) spectrometer using the ROI count rate ratio method with exponential (a, b) and polynomial (c, d) models. The true shield mass thickness is 207 kg/m^2, including 91 m of air between the source and the detector.

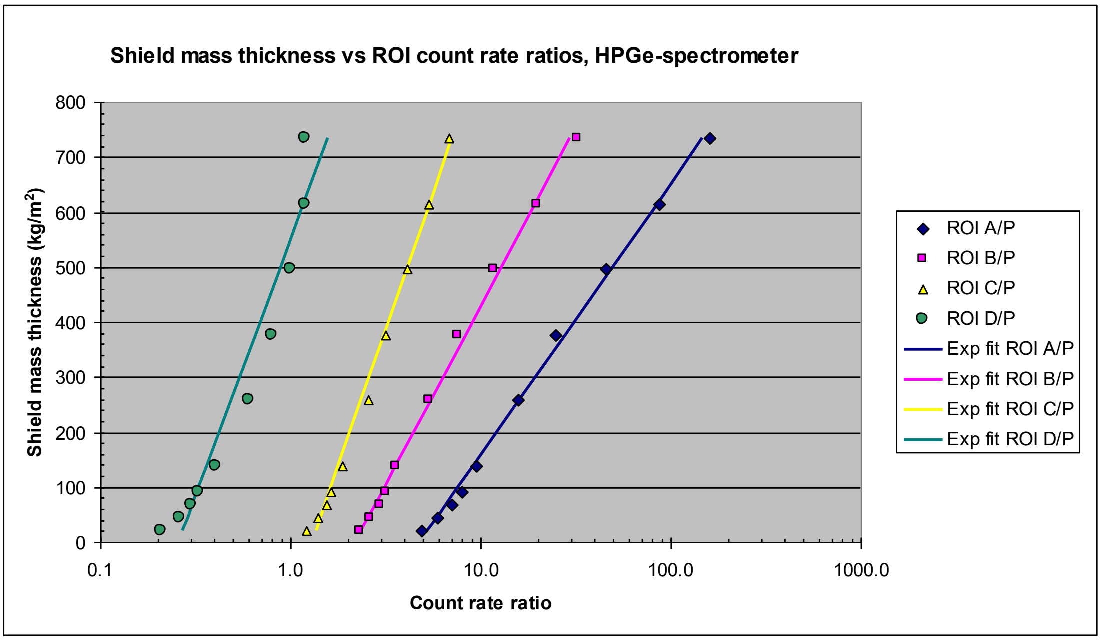

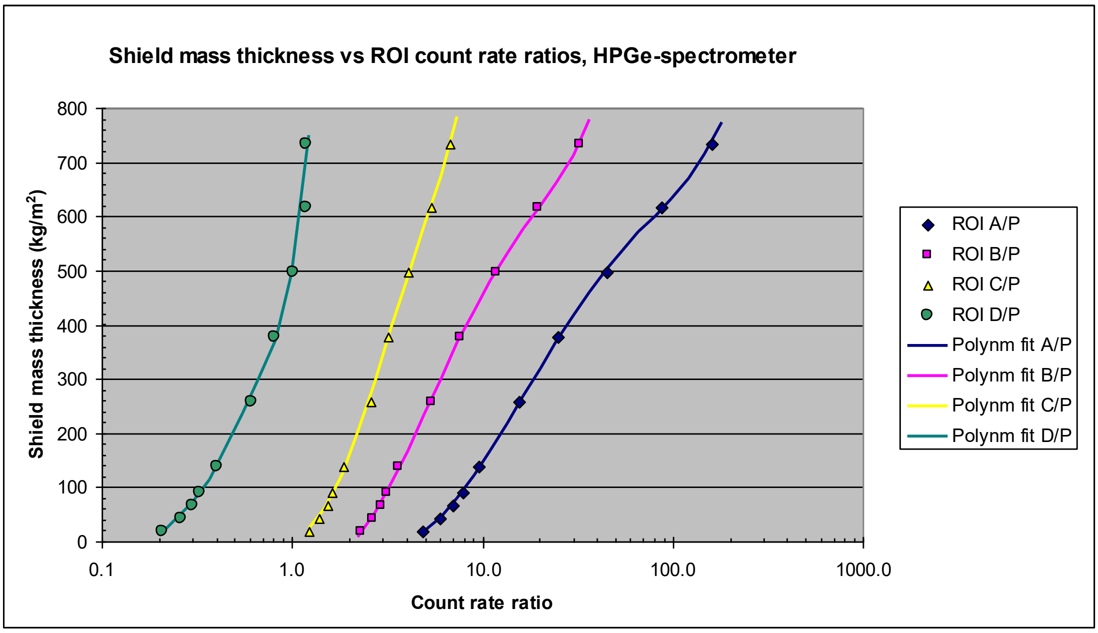

Fig D3-41. LU DetectiveX HPGe spectrometer. Models of shield mass thickness as a function of ROI net count rate ratio obtained from fitting measured data to exponential functions (top diagram) and five-degree polynomial functions (bottom diagram), valid for Cs-137 point sources behind shields of standard building material (wood and concrete) with mass thickness between 20 and 730 kg/m^2. Values have been measured at a source-detector distance of 10 m.

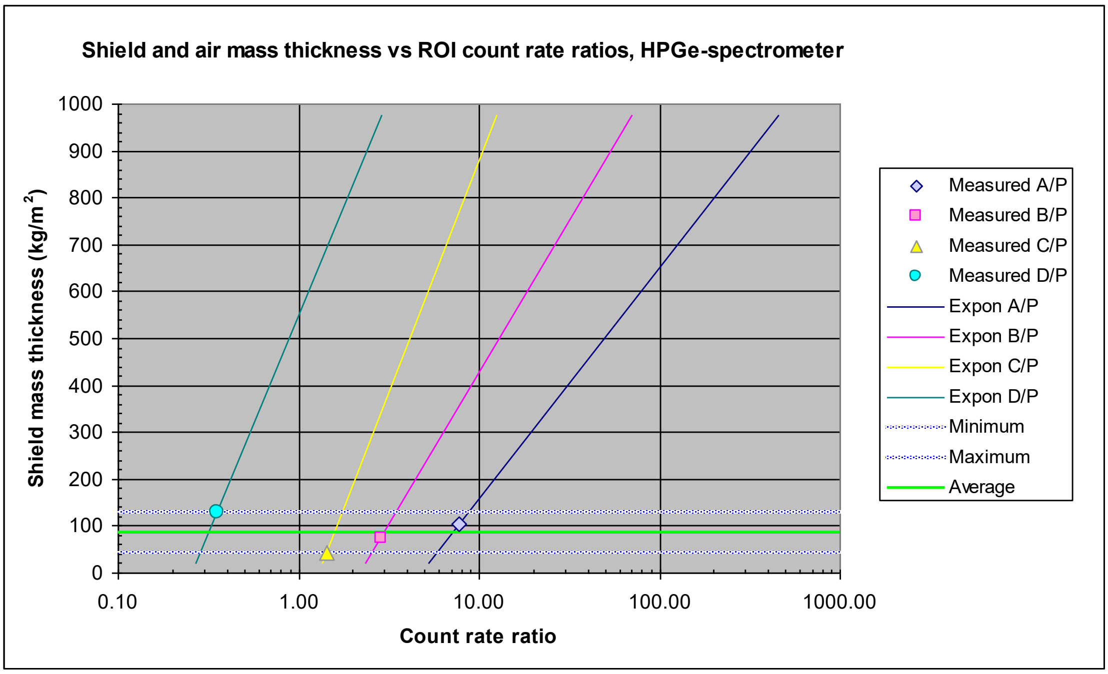

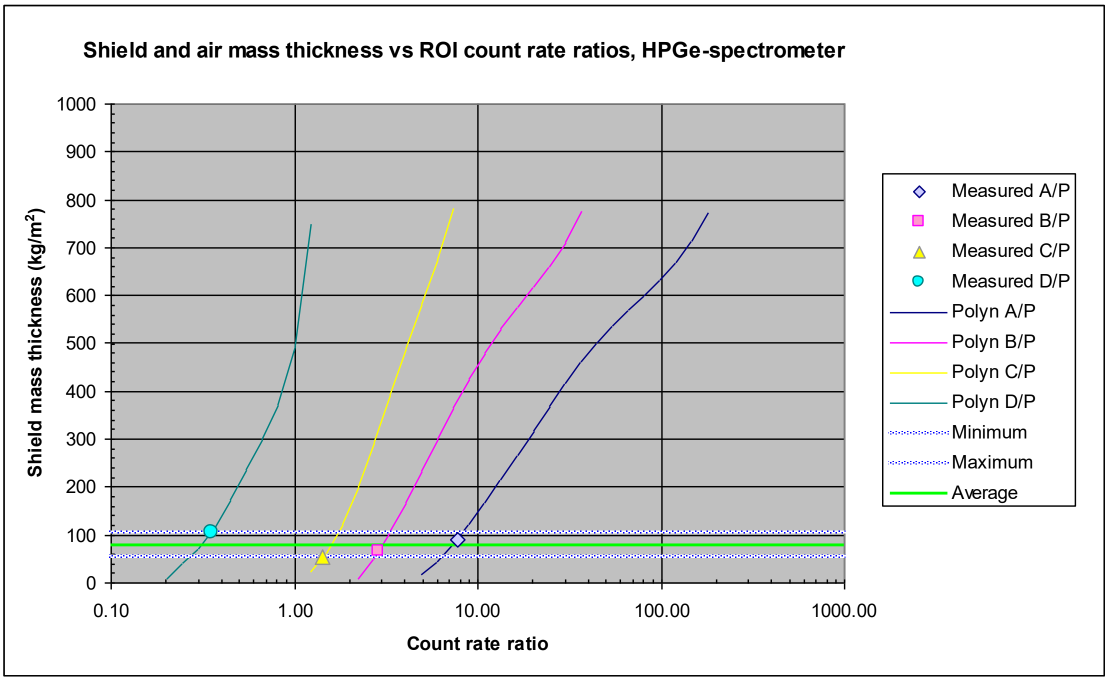

Fig D4-41 (M1). Shield mass thickness determination by the LU DetectiveX HPGe spectrometer using the ROI count rate ratio method with exponential (top diagram) and polynomial (bottom diagram) models. The true shield mass thickness is 75.8 kg/m^2, including 61 m of air between the source and the detector.

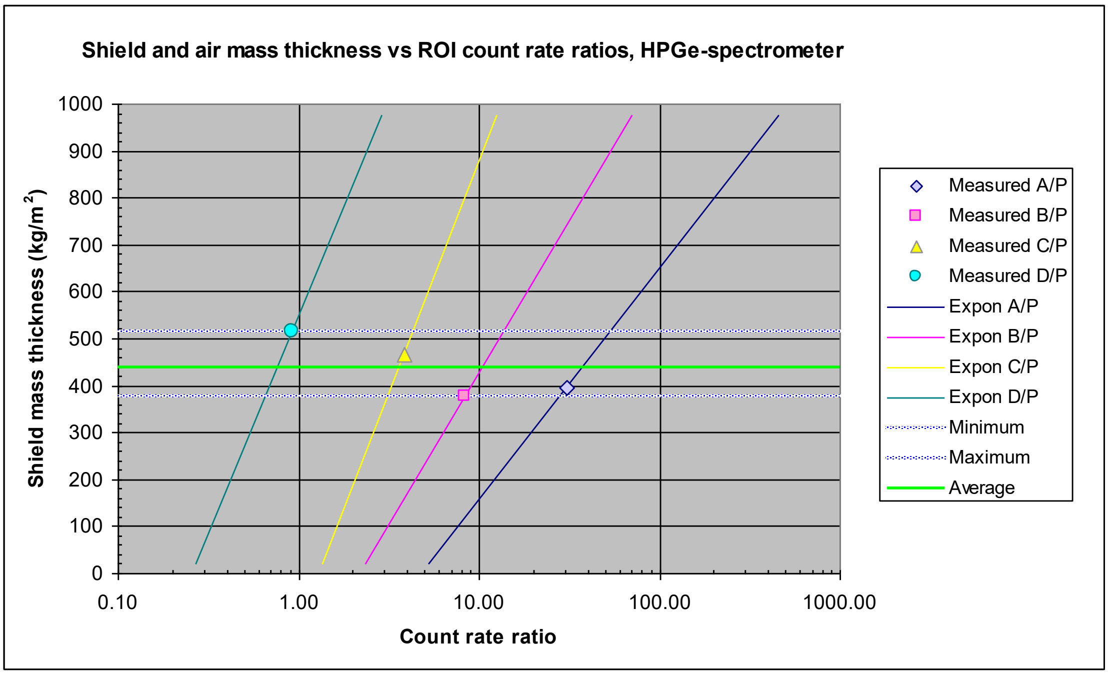

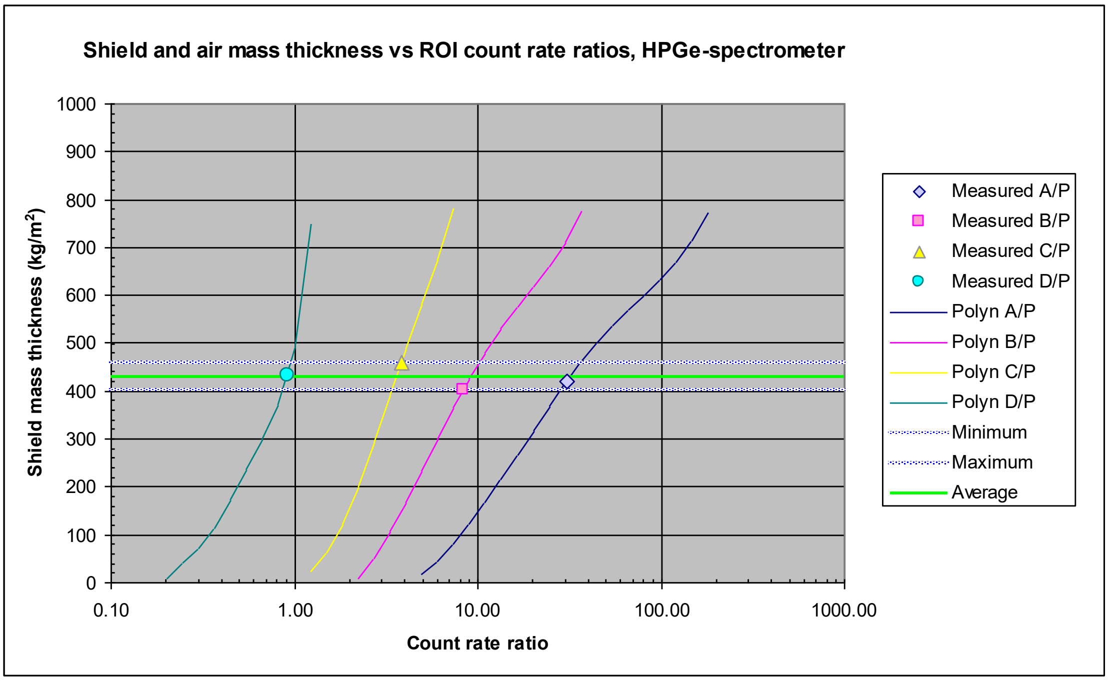

Fig D4-42 (M2). Shield mass thickness determination by the LU DetectiveX HPGe spectrometer using the ROI count rate ratio method with exponential (top diagram) and polynomial (bottom diagram) models. The true shield mass thickness is 372 kg/m^2, including 31 m of air between the source and the detector.

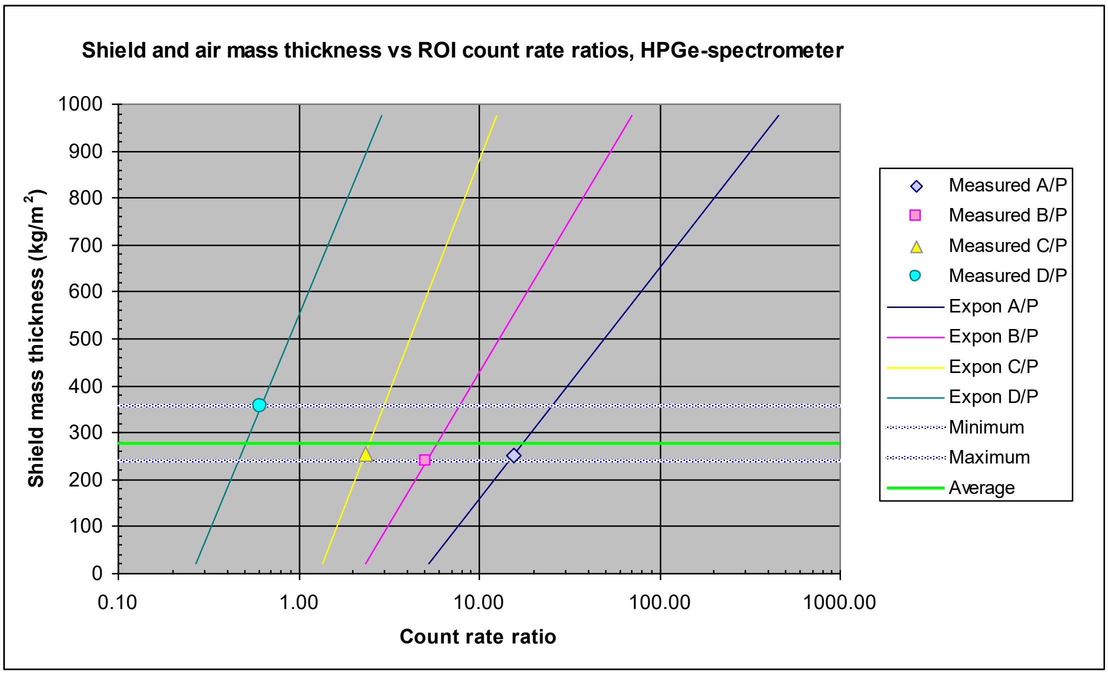

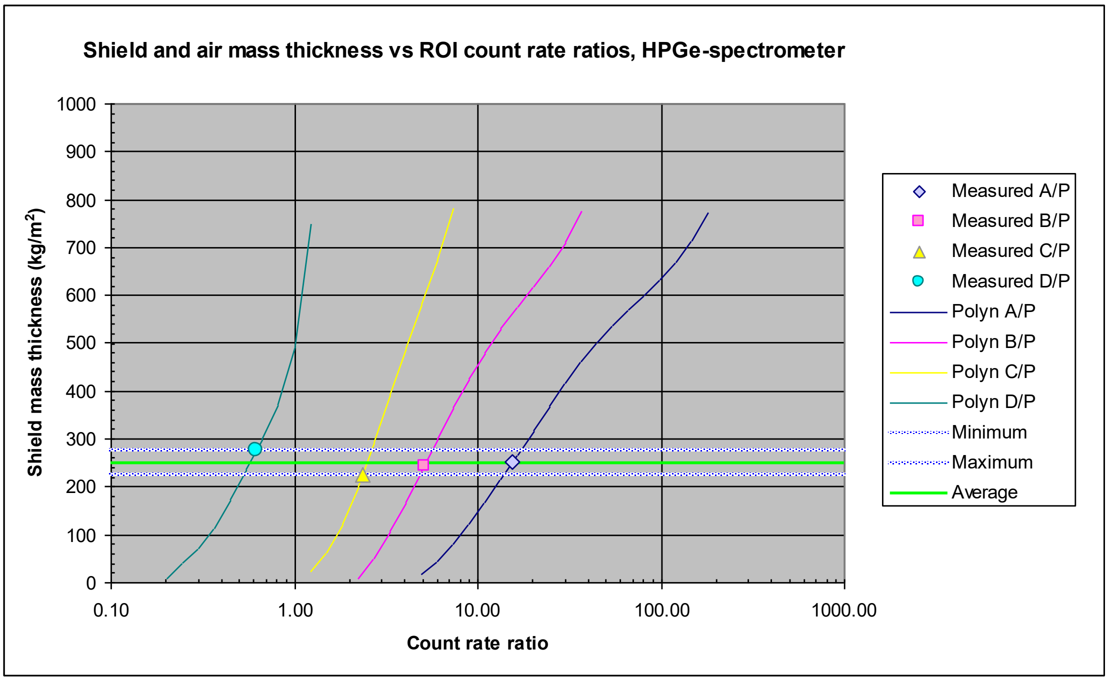

Fig D4-43 (M3). Shield mass thickness determination by the LU DetectiveX HPGe spectrometer using the ROI count rate ratio method with exponential (top diagram) and polynomial (bottom diagram) models. The true shield mass thickness is 170 kg/m^2, including 61 m of air between the source and the detector.

Setup M4 was not measured due to technical problems with the detector

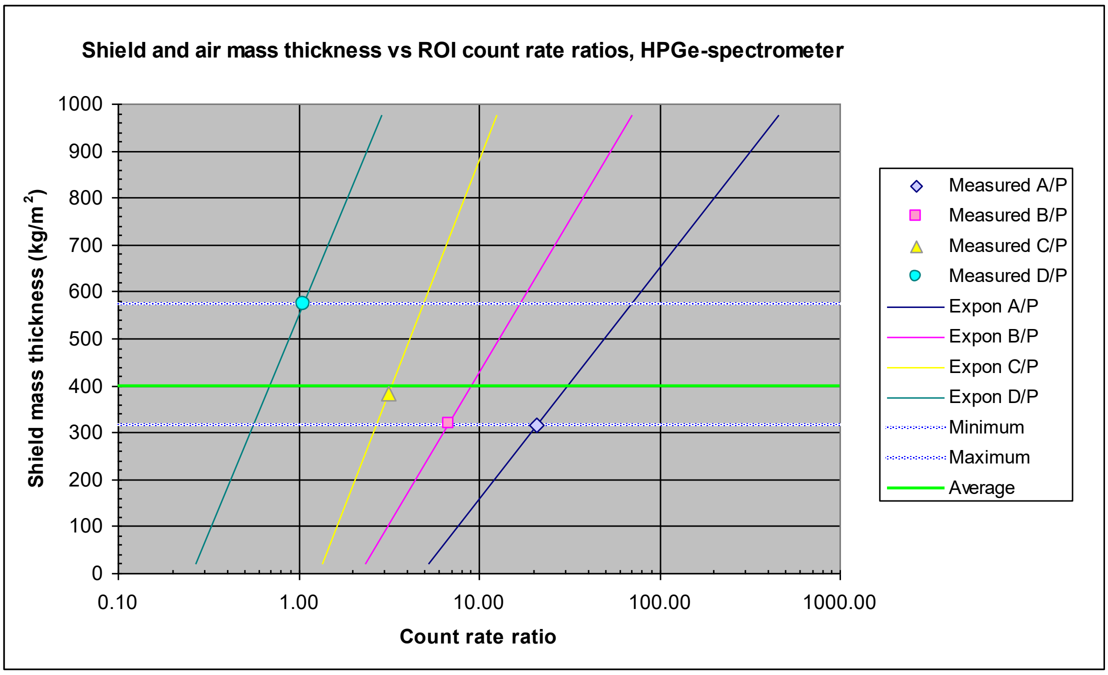

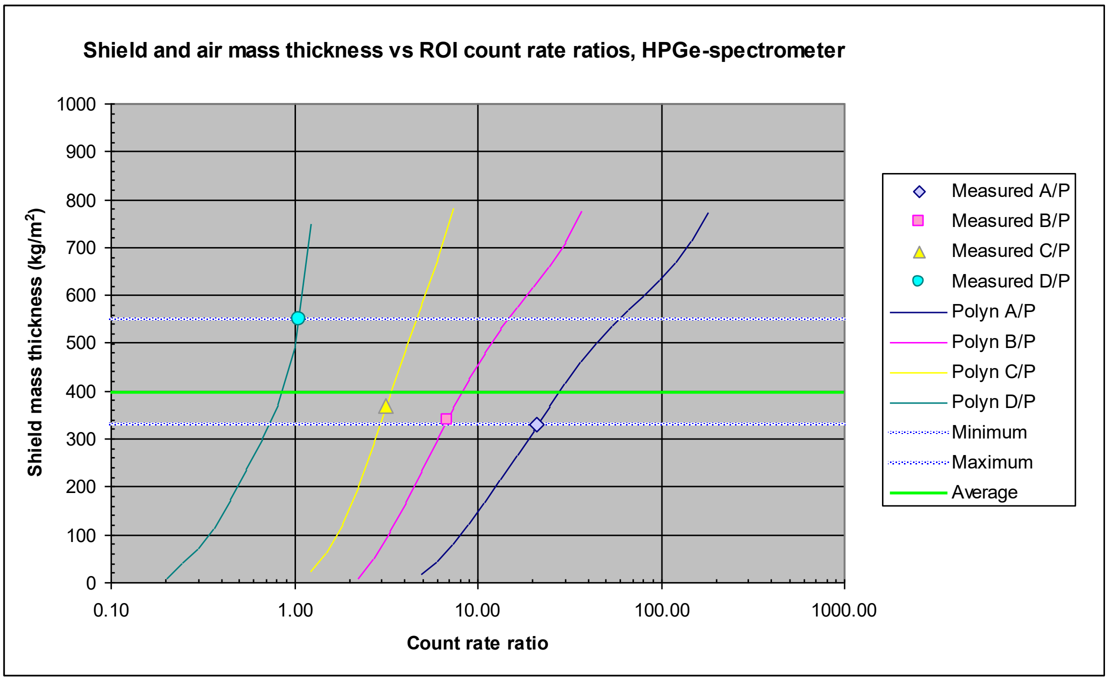

Fig D4-45 (M5). Shield mass thickness determination by the LU DetectiveX HPGe spectrometer using the ROI count rate ratio method with exponential (top diagram) and polynomial (bottom diagram) models. The true shield mass thickness is 207 kg/m^2, including 91 m of air between the source and the detector.

D5. Results from source distance measurements, using SODAC

The distance to a Cs-137 point source was determined using the Excel program SODAC for five different setups with different distances and shielding (M1 - M5), as described in the main report. All measurements were made standing still (semi-stationary) at various locations along the road that passes the radiation source.

It turned out that some trees between the radiation source and the measuring car shielded the photon fluence from the source at specific points along the road. These measurement points have been identified, and the data has been removed from the analysis.

Correcting the two 4-litre NaI(Tl)-detectors response for the angular dependence of the oblong detector for count rates from the source at different incident angles proved necessary during the analysis. How the correction is determined is reported in the text of the main report.

Measurement data from two detectors, the 3x3 NaI(Tl)- detector and the DetectiveX HPGe-detector, were not corrected for varying angular response since the length and width of their active volumes are approximately equal. The near-equal dimensions result in an approximately uniform angular response for source photons that is important for assessing the source distance.

In the SODAC analysis, the actual shield thickness has been used in the distance determination (and not the one obtained through SSC) because it produces a more accurate picture of any distance determination deviations than a possibly distorted assumption of the shield thickness would do.

Results from the Excel program SODAC showing which "intensity curve" (primary photon fluence from the source as a function of distance along the road) best fits the measurement data along the road for the five setup distances are reproduced in the following figures:

4 litre front NaI(Tl)-detector	Fig A5-11 to A5-15
4 litre rear NaI(Tl) detector	Fig A5-21 to A5-25
3"x3" NaI(Tl)-detector	Fig A5-31 to A5-35
DetectiveX HPGe-detector	Fig A5-41 to A5-45

Results from the distance and activity determination with SODAC are summarized in the following tables:

4 litre front NaI(Tl)-detector	Table A5-1
4 litre rear NaI(Tl) detector	Table A5-2
3"x3" NaI(Tl)-detector	Table A5-3
DetectiveX HPGe-detector	Table A5-4

For the front and rear 4 litre NaI(Tl)-detectors, the distance determination for setup M1 to M5 (except M4) deviated from the actual distance by -50% to 0% (rounded values) with an average deviation of -21 ± 11%. When calculated for the actual distances, the source activity was, on average, overestimated by 70 ± 23%.

For the 3"x3" NaI(Tl)-detector, the distance determination for setup M1 to M5 (except M4) deviated from the actual distance by -61% to -17% (rounded values) with an average deviation of -34 ± 11%. When calculated for the actual distances, the source activity was, on average, overestimated by 81 ± 30%.

For the DetectivX HPGe-detector, the distance determination for setup M1 to M5 (except M4) deviated from the actual distance by -28% to 0% (rounded values) with an average deviation of -13 ± 6%. When calculated for the actual distances, the source activity was, on average, overestimated by 18 ± 7%.

Table D5-1. Results from the LU 4 litre NaI(Tl) front detector, applying the SODAC routine to obtain the source distance and activity for a Cs-137 point source. The distance is adjusted for the varying angular efficiency for the detector. The activity is calculated from the full energy peak count rate for the adjusted and the actual distance, using the actual shield thickness. The actual point source activity is 606 MBq in all setups.

Setup	Actual		SODAC obtained				Deviation	
	Distance to source m	Shield mass thickness kg/m^2	Distance m	Distance angular efficiency adjusted m	Activity at adjusted distance MBq	Activity at actual distance MBq	Distance at adjusted rounded %	Activity at adjusted (at actual) distance %
M1	61	air only	40	60	286	779	0	-52.8 (28.6)
M2	31	333	25	30	938	1417	0	54.8 (134)
M3	61	94	45	60	481	987	0	-20.6 (62.9)
M4	61	333	-	-	-	-	-	- (-)
M5	91	94	45	55	351	1316	-39	-42.1 (117)
Average							-10 ± 10	-15 ± 24 (86 ± 24)

- Not measured

Table D5-2. Results from the LU 4 litre NaI(Tl) rear detector, applying the SODAC routine to obtain the source distance and activity for a Cs-137 point source. The distance is adjusted for the varying angular efficiency for the detector. The activity is calculated from the full energy peak count rate for the adjusted and the actual distance, using the actual shield thickness. The actual point source activity is 606 MBq in all setups.

Setup	Actual		SODAC obtained				Deviation	
	Distance to source m	Shield mass thickness kg/m^2	Distance m	Distance angular efficiency adjusted m	Activity at adjusted distance MBq	Activity at actual distance MBq	Distance at adjusted rounded %	Activity at adjusted (at actual) distance %
M1	61	air only	35	60	761	761	0	25.6 (25.6)
M2	31	333	20	20	392	971	-33	-35.3 (60.2)
M3	61	94	25	35	190	710	-42	-68.7 (17.1)
M4	61	333	-	-	-	-	-	- (-)
M5	91	94	35	45	209	1292	-50	-65.5 (113)
Average							-32 ± 11	-36 ± 22 (54 ± 22)

- Not measured

Table D5-3. Results from the LU 3"x3" NaI(Tl) detector, applying the SODAC routine to obtain the source distance and activity for a Cs-137 point source. No adjustment for photon angles of incidence is made in the distance determination. The activity is calculated from the full energy peak count rate for the obtained and the actual distance, using the actual shield thickness. The actual point source activity is 606 MBq in all setups.

Setup	Actual		SODAC obtained			Deviation	
	Distance to source m	Shield mass thickness kg/m^2	Distance m	Activity at obtained distance MBq	Activity at actual distance MBq	Distance rounded %	Activity at obtained (at actual) distance %
M1	61	air only	35	201	756	-42	-66.8 (24.8)
M2	31	333	25	796	1204	-17	31.4 (98.7)
M3	61	94	50	551	874	-17	-9.1 (44.2)
M4	61	333	-	-	-	-	- (-)
M5	91	94	35	139	1564	-61	-77 (158)
Average						-34 ± 11	-30 ± 25 (81 ± 30)

- Not measured

Table D5-4. Results from the LU DetectiveX HPGe detector, applying the SODAC routine to obtain the source distance and activity for a Cs-137 point source. No adjustment for photon angles of incidence is made in the distance determination. The activity is calculated from the full energy peak count rate for the obtained and the actual distance, using the actual shield thickness. The actual point source activity is 606 MBq in all setups.

Setup	Actual		SODAC obtained			Deviation	
	Distance to source m	Shield mass thickness kg/m^2	Distance m	Activity at obtained distance MBq	Activity at actual distance MBq	Distance rounded %	Activity at obtained (at actual) distance %
M1	61	air only	55	531	663	-8	-12.4 (9.4)
M2	31	333	30	745	745	0	22.9 (22.9)
M3	61	94	50	397	628	-17	-34.5 (3.6)
M4	61	333	-	-	-	-	- (-)
M5	91	94	65	333	813	-28	-45.0 (34.2)
Average						-13 ± 6	-17 ± 15 (18 ± 7)

- Not measured

SODAC source distance results, LU 4 litre NaI(Tl)-detector (front)

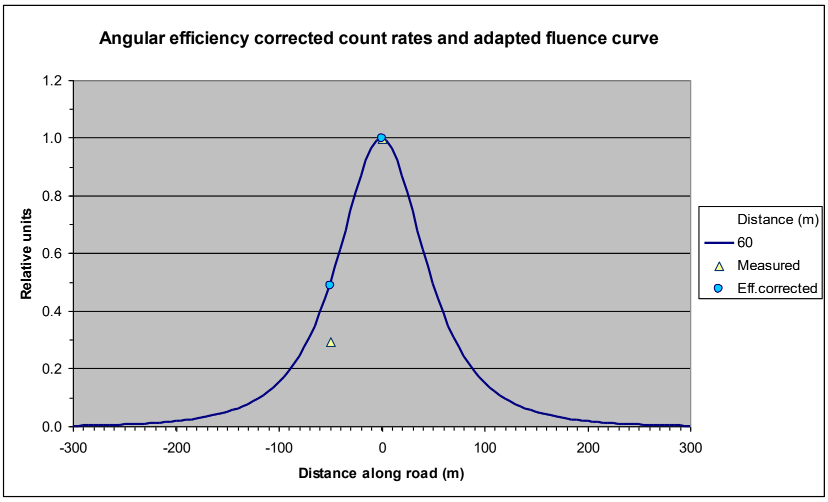

Fig D5-11. LU. Setup M1. The true source distance is 61 m

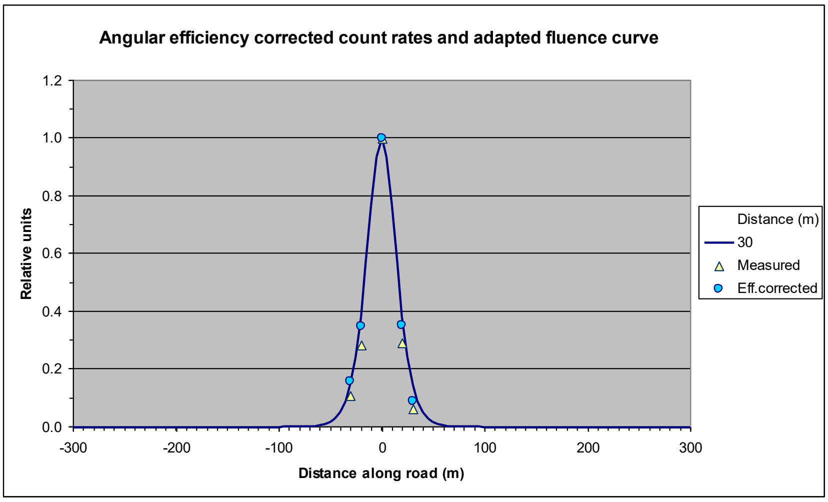

Fig D5-12. LU. Setup M2. The true source distance is 31 m

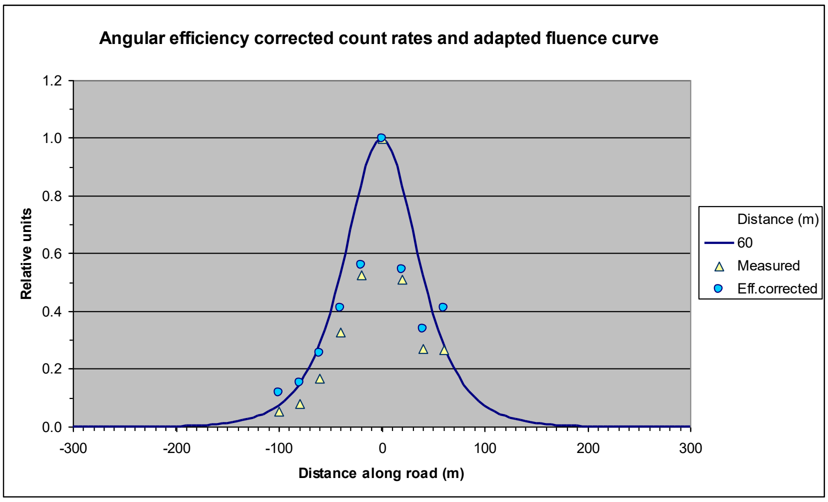

Fig D5-13. LU. Setup M3. The true source distance is 61 m

The figures show SODAC determined source distance results for the LU 4 litre NaI(Tl)-detector (front), corrected for varying angular efficiency. Tree-shielded measurement locations have been excluded.

SODAC source distance results, LU 4 litre NaI(Tl)-detector (front)

For Setup M4, not enough measurement data was available to enable determination of the source distance by the SODAC routine.

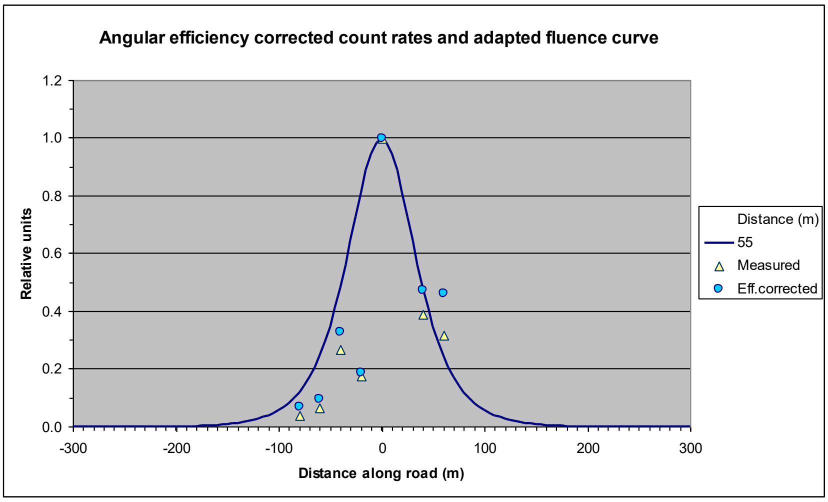

Fig D5-15. LU. Setup M5. The true source distance is 91 m

The figures show SODAC determined source distance results for the LU 4 litre NaI(Tl)-detector (front), corrected for varying angular efficiency. Tree-shielded measurement locations have been excluded.

SODAC source distance results, LU 4 litre NaI(Tl)-detector (rear)

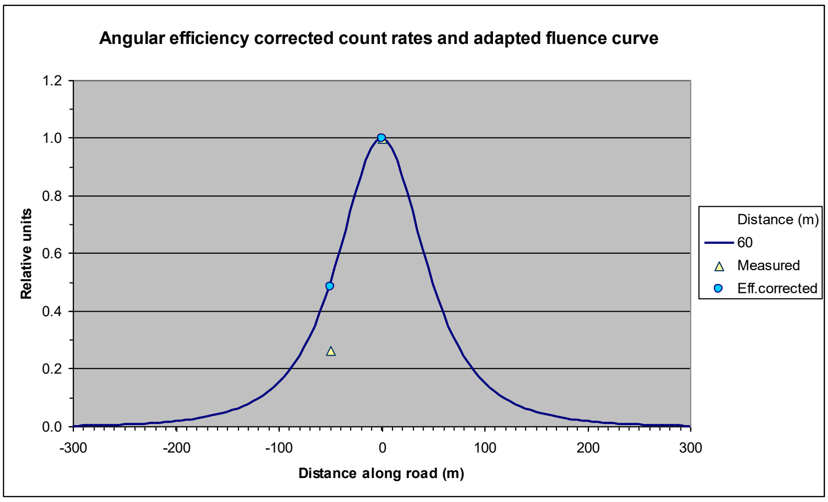

Fig D5-21. LU. Setup M1. The true source distance is 61 m

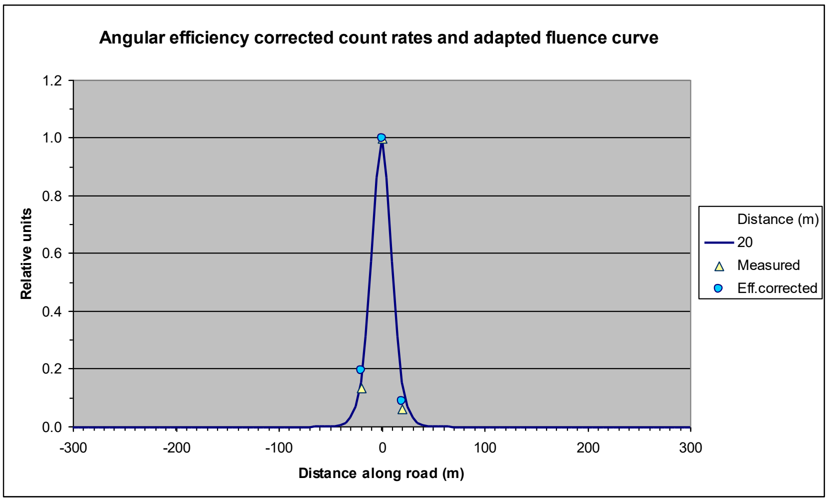

Fig D5-22. LU. Setup M2. The true source distance is 31 m

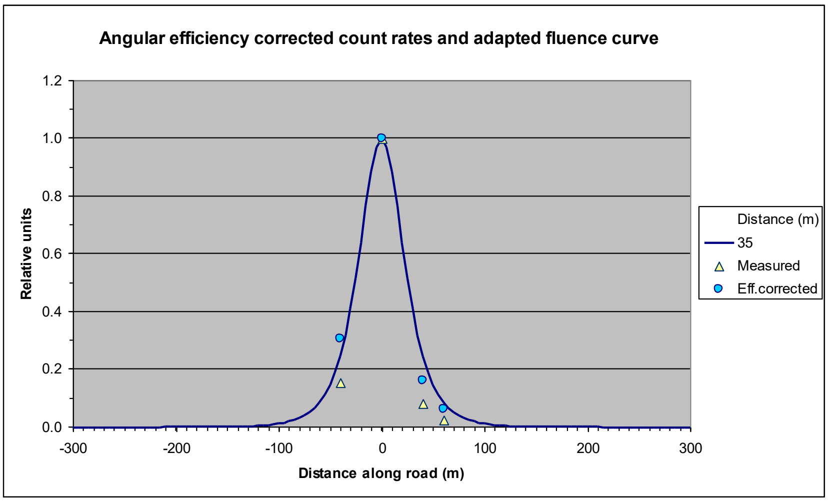

Fig D5-23. LU. Setup M3. The true source distance is 61 m

The figures show SODAC determined source distance results for the LU 4 litre NaI(Tl)-detector (rear), corrected for varying angular efficiency. Tree-shielded measurement locations have been excluded..

SODAC source distance results, LU 4 litre NaI(Tl)-detector (rear)

For Setup M4, not enough measurement data was available to enable determination of the source distance by the SODAC routine.

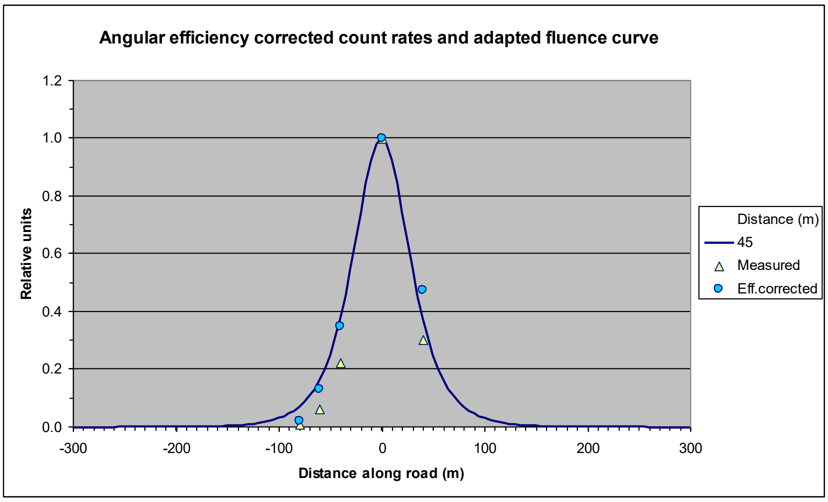

Fig D5-25. LU. Setup M5. The true source distance is 91 m

The figures show SODAC determined source distance results for the LU 4 litre NaI(Tl)-detector (rear), corrected for varying angular efficiency. Tree-shielded measurement locations have been excluded.

SODAC source distance results, LU 3"x3" NaI(Tl)-detector

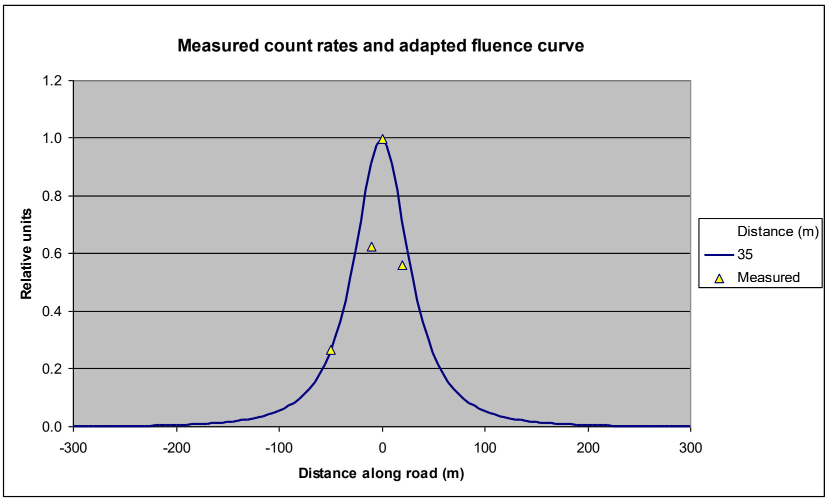

Fig D5-31. LU. Setup M1. The true source distance is 61 m

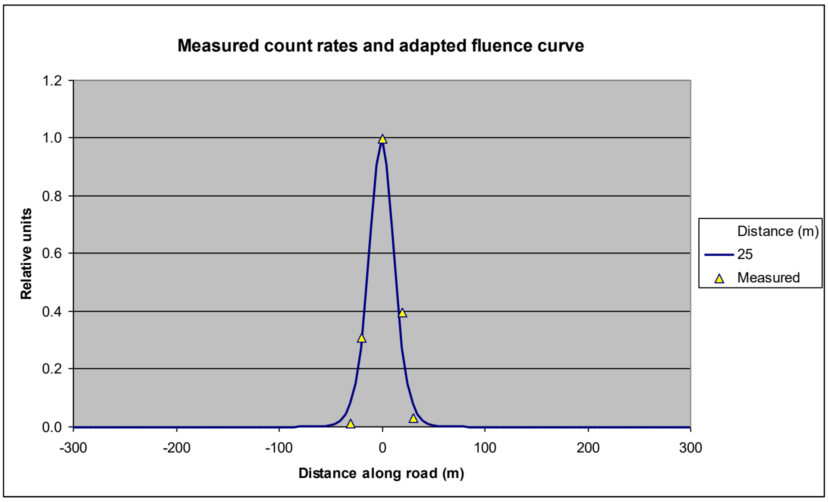

Fig D5-32. LU. Setup M2. The true source distance is 31 m

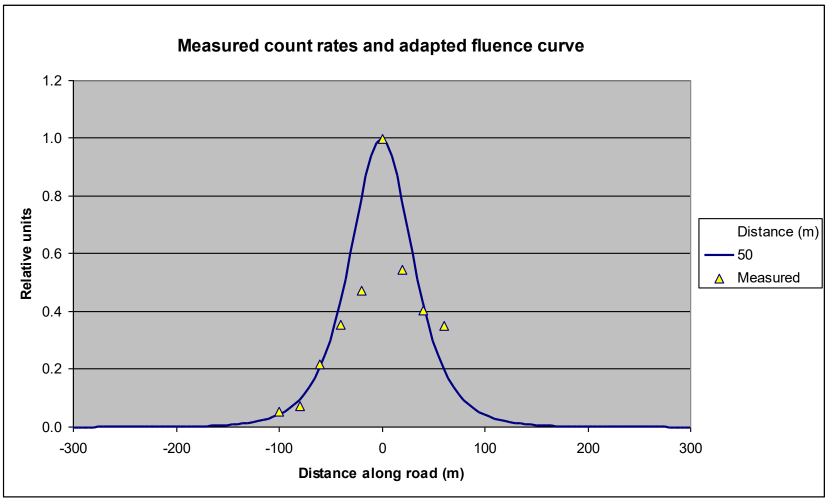

Fig D5-33. LU. Setup M3. The true source distance is 61 m

The figures show SODAC determined source distance results for the LU 3"x3" NaI(Tl)-detector. Tree-shielded measurement locations have been excluded.

SODAC source distance results, LU 3"x3" NaI(Tl)-detector

Setup M4 was not measured with the 3"x3" NaI(Tl)-detector.

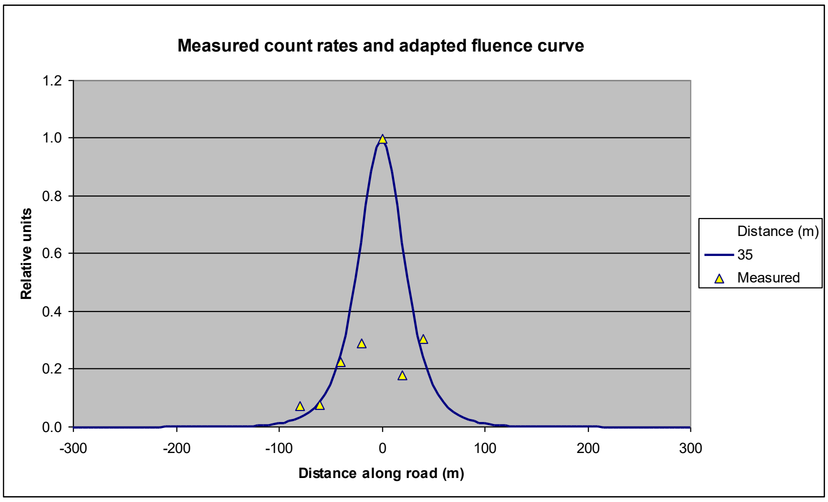

Fig D5-35. LU. Setup M5. The true source distance is 91 m

The figures show SODAC determined source distance results for the LU 3"x3" NaI(Tl)-detector. Tree-shielded measurement locations have been excluded.

SODAC source distance results, LU DetectivX HPGe-detector

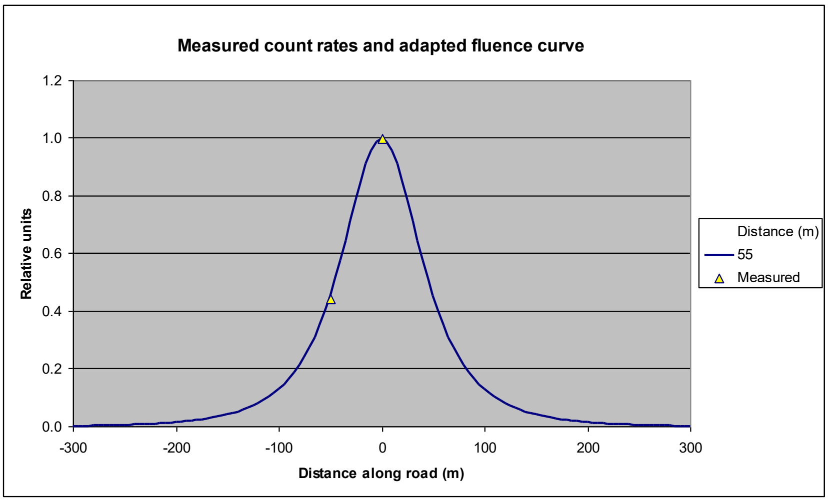

Fig D5-41. LU. Setup M1. The true source distance is 61 m

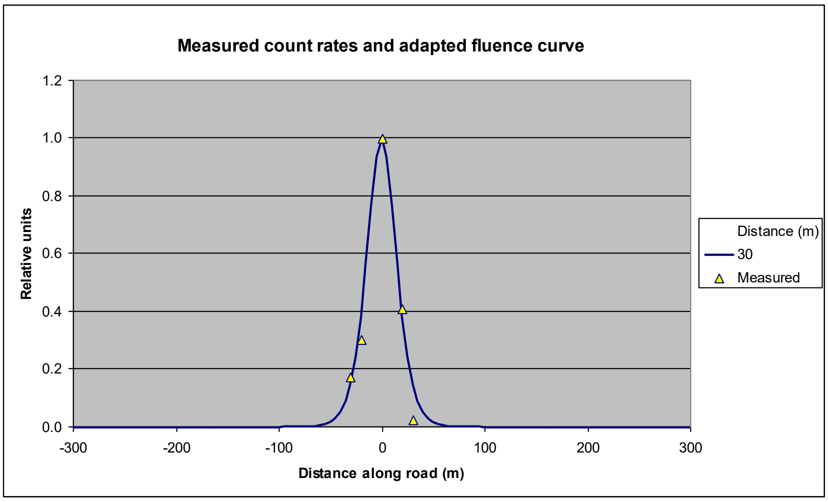

Fig D5-42. LU. Setup M2. The true source distance is 31 m

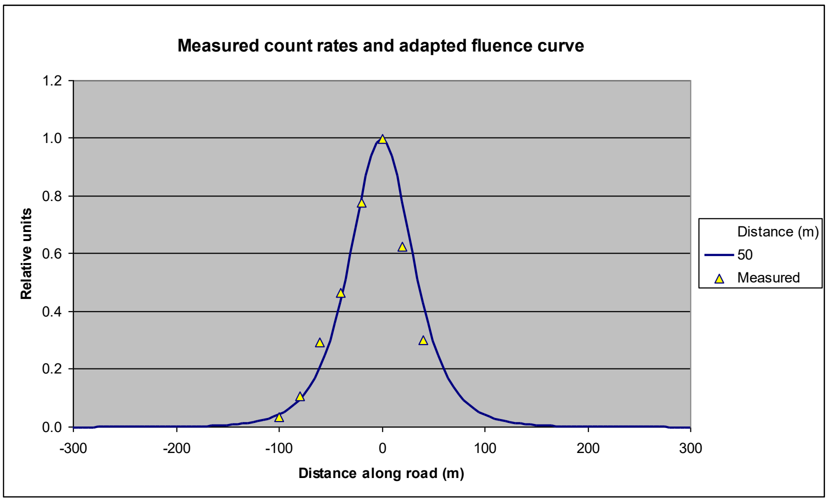

Fig D5-43. LU. Setup M3. The true source distance is 61 m

The figures show SODAC determined source distance results for the LU DetectiveX HPGe-detector. Tree-shielded measurement locations have been excluded.

SODAC source distance results, LU DetectivX HPGe-detector

Setup M4 was not measured with the DetectiveX HPGe-detector

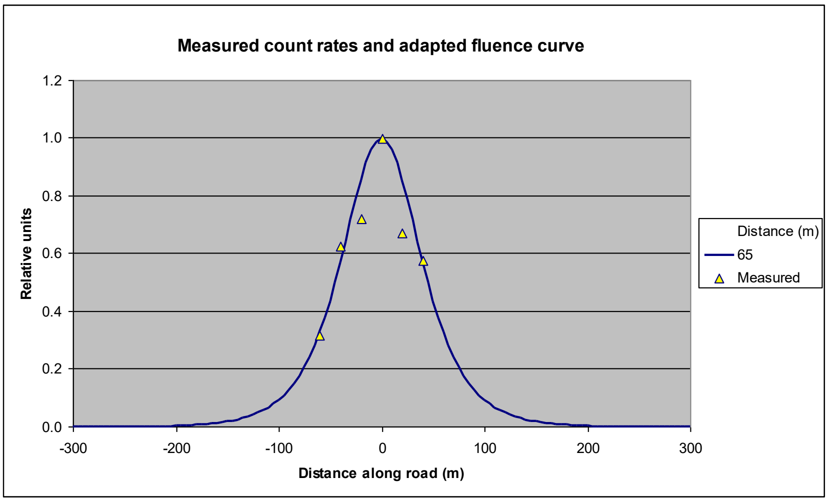

Fig D5-45. LU. Setup M5. The true source distance is 91 m

The figures show SODAC determined source distance results for the LU DetectiveX HPGe-detector. Tree-shielded measurement locations have been excluded.

D6. Summary and conclusion

Overall, it can be concluded that the NaI(Tl) detectors, when applying the SODAC routine, underestimate the distance to the radiation source by 20 - 30% and overestimate the activity of the source by 70 - 80%.

The deviations from actual values increase as the shield thickness increases and the distance to the radiation source increases. These deviations may be caused by the low energy resolution in a NaI(Tl) detector. Photons scattered at small angles in the shield in front of the source are recorded as primary photons in the full-energy peak in the pulse height distribution of the detector. Compared to primary-only photons, this small-angle Compton scattering causes the count rate in ROI PR and ROI P to increase, leading to calculated shorter distances and higher activity when applying the SODAC routine. The deviations may be corrected by introducing a distance modification factor in the SODAC routine when the measuring instrument is a NaI(Tl) detector. Further experiments are needed to investigate the effects of longer source distances.

The high-resolution HPGe detector registers almost no Compton-scattered photons in the full-energy peak. The absence of Compton photons in the full energy peak implies that the detector should give a more accurate result for primary photons from the radiation source (net count rate in ROI P), which should lead to a more limited deviation in determining the distance and activity of the radiation source with the SODAC routine. That is also the case. When using the HPGe-detector, the source distance is underestimated on average by 13 ± 6%, and the activity is overestimated by 18 ± 7%. Why these residual deviations exist should be investigated in future well-controlled experiments.

Appendix E. Results from team NGU, Geological Survey of Norway, Norway

E1. Measuring equipment

The measuring system was a Radiation Solutions (Canada) RSX-5 gamma spectrometer with 4x4 litre NaI(Tl) crystals. The spectrometer was mounted inside a Toyota HiAce van and positioned behind the front right passenger seat in the rear compartment. It was oriented vertically, as shown in Figure E1-1, with the four “downward” crystals facing the right side of the car. One “upward” crystal was situated on the other side of the four downward crystals, facing left, so the four “downward” crystals mostly shielded it from radiation from the right side. In the analysis, the summed signals from the four “downward” crystals with 16 litres were used for shielding, distance and activity assessments (detector 1). The “upward” (left) crystal (detector 2) was not used in the experiment. The signals from all the crystals were processed in an onboard spectrometer and exported via TCP/IP to a laptop in the front cabin of the vehicle, running RadAssist (RSI) software. The RadAssist software controls data acquisition, monitoring, and analysis of measured data and allows secondary software packages to access the same live data stream from the device.

Fig E1-1: Mobile gamma spectrometry car used by NGU and placement of the RSX-5 detector system inside the car. The four 4-litre NaI(Tl) crystals (usually referred to as “downward” when used in an aeroplane) were placed sideways so that the most sensitive part of the crystals was facing to the right. A fifth 4-litre NaI(Tl) crystal (usually referred to as “upward”) was facing the left side of the car.

E2. Detector efficiency calibration

The 4x4 litre NaI(Tl)-detector was calibrated for counting efficiency at 662 keV in an earlier NKS field experiment (NKS-AUTOMORC, 2018) using a Cs-137 point source with activity traceable to calibration sources from Eckert & Ziegler with 3% relative expanded uncertainty (k=2). When placed in measurement position in the car, the detector efficiency for 662 keV photons from the right side (the apparent detector area for total photon absorption) was 0.104 m^2 with 8% relative expanded uncertainty (k=2).

E3. Detector calibration for shield mass thickness determination, using SSC

The response of the 4x4 litre NaI(Tl) detector as net count rates in ROI A, B, C and PL relative to ROI PR and ROI P was measured for different shield mass thicknesses described earlier in the report. The measurement data was entered into the Excel program SCC. The relationship between the net count rates for the ratios ROI A, B, C, and PL/PR for the exponential model is shown in Fig E3-1-a and the polynomial model in Fig E3-1-c. Corresponding relationships for the ratios ROI A, B, and C/P are shown in Figs E3-1-b and E3-1-d.

The coefficients for fitting the exponential model to observed data are given in Table E3-1. The coefficients for fitting the five-degree polynomial model to observed data are given in Table E3-2.

The exponential and five-degree polynomial models represent the measured net count rate ratios for the different shield mass thicknesses quite well.

Table E3-1. NGU 4x4 litre NaI(Tl)-detector. Coefficients *a* and *b* in an exponential model for determining shield mass thickness according to the description in the main report. The unit of *b* is m^2/kg.

ROI ratio	*a*	*b*
ROI A/PR	3.54	0.00454
ROI B/PR	2.16	0.00366
ROI C/PR	1.57	0.00256
ROI PL/PR	1.53	0.000879
ROI A/P	1.34	0.00397
ROI B/P	0.822	0.00310
ROI C/P	0.597	0.00199

Table E3-2. NGU 4x4 litre NaI(Tl)-detector. Coefficients a_0 - a_5 (kg/m^2) in the five-degree polynomial model for determining shield mass thickness according to Eqn 3 in the main report.

ROI ratio	a_5	a_4	a_3	a_2	a_1	a_0
ROI A/PR	2.008	-24.48	89.94	-54.43	-14.18	0
ROI B/PR	0.1464	6.985	-92.45	350.23	-210.8	0
ROI C/PR	-25.54	62.37	14.84	63.50	51.75	0
ROI PL/PR	-39330	128300	-160800	97720	-28370	3155
ROI A/P	1.152	2.448	-80.02	269.9	-26.16	0
ROI B/P	-188.9	965.4	-1625	903.1	374.9	0
ROI C/P	110.6	-276.1	-267.0	386.6	565.6	215.2

E4. Results from shield thickness measurements, using SSC

The shield mass thickness measurements in front of the Cs-137 point source for setups M1 to M5 are not analyzed with SSC, but the SSC models are shown in Fig E3-1-a-d.

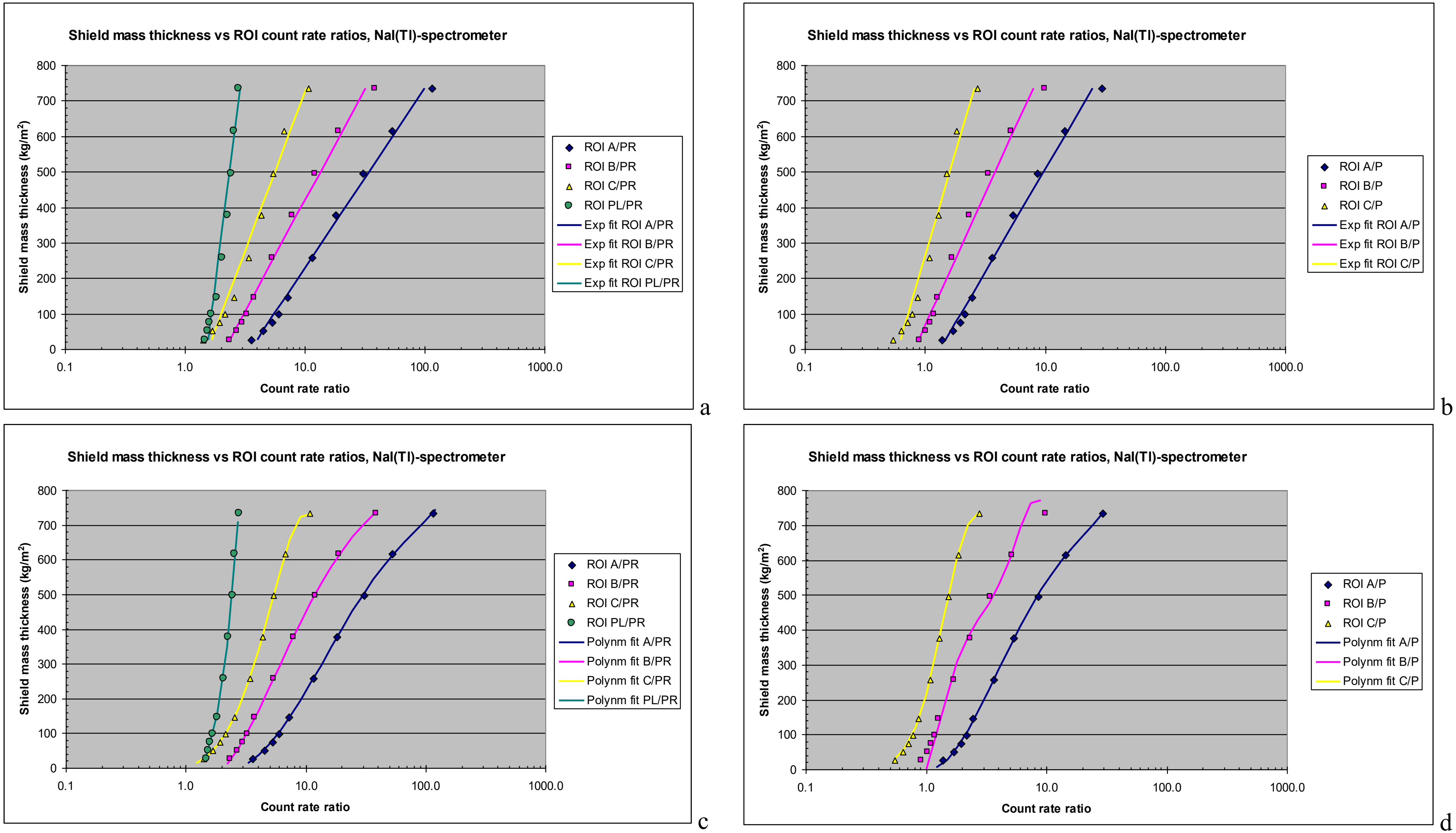

Fig E3-1-a-d. NGU 4x4 litre NaI(Tl) spectrometer. Models of shield mass thickness as a function of ROI net count rate ratio obtained from fitting measured data to exponential functions (a, b) and five-degree polynomial functions (c, d), valid for Cs-137 point sources behind shields of standard building material (wood and concrete) with mass thickness between 20 and 730 kg/m^2. Values have been measured at a source-detector distance of 10 m.

E5. Results from source distance measurements, using SODAC

The distance to a Cs-137 point source was determined using the Excel program SODAC for five different setups with different distances and shielding (M1 - M5), as described in the main report. All measurements were made standing still (semi-stationary) at various locations along the road that passes the radiation source. Unfortunately, it turned out that some trees between the radiation source and the measuring car shielded the photon fluence from the source at specific points along the road. These measurement points have been identified, and the data has been removed from the analysis.

Correcting the detector response for the angular dependence of the oblong detector for count rates from the source at different incident angles proved necessary during the analysis. How the correction is determined is reported in the text of the main report.

In the SODAC analysis, the actual shield thickness has been used in the distance determination (and not the one obtained through SSC) because it produces a more accurate picture of any distance determination deviations than a possibly distorted assumption of the shield thickness would do.

Results from the Excel program SODAC showing which "intensity curve" (primary photon fluence from the source as a function of distance along the road) best fits the measurement data along the road for the five setup distances are reproduced in Figures E5-1 to E5-5.

Results from the distance and activity determination with SODAC are summarized in Table E5-1. The source distances for four setups (M1, M2, M3, M5) were underestimated from 8% to 33% with an average underestimation of 17 ± 6%, and the source activity was overestimated by 104 ± 41%.

The reason for the deviations from actual values is not fully understood. The low energy resolution in a NaI(Tl) detector and the increased distance to the source compared to the calibration distance for shield thickness may be the cause. Photons scattered at small angles in the shield in front of the source register in the full-energy peak in the pulse height distribution of the detector. These photons cause the count rate in ROI PR and ROI P to increase compared to primary-only photons, which may affect distance and shield thickness determination at longer distances. Further experimental investigations of the detector's response at longer source distances and thicker shielding are needed to understand the deviations better.

Table E5-1. Results from the NGU 4x4 litre NaI(Tl) detector, applying the SODAC routine to obtain the source distance and activity for a Cs-137 point source. The distance is adjusted for the varying angular efficiency for horizontally oriented 4 litre NaI(Tl) detectors. The activity is calculated from the full energy peak count rate for the adjusted and the actual distance, using the actual shield thickness. The actual point source activity is 606 MBq in all setups.

Setup	Actual		SODAC obtained				Deviation	
	Distance to source m	Shield mass thickness kg/m^2	Distance m	Distance angular efficiency adjusted m	Activity at adjusted distance MBq	Activity at actual distance MBq	Distance at adjusted rounded %	Activity at adjusted (at actual distance) %
M1	61	air only	30	40	258	704	-33	-57.4 (16.2)
M2	31	333	25	30	1234	1234	0	104 (104)
M3	61	94	40	55	687	858	-8	13.4 (41.6)
M4	61	333	45	50	1337	2121	-17	120 (250)
M5	91	94	50	65	519	1266	-28	-14.4 (109)
Average							-17 ± 6	33 ± 34 (104 ± 41)

SODAC source distance results, NGU 4x4 litre NaI(Tl)-detector

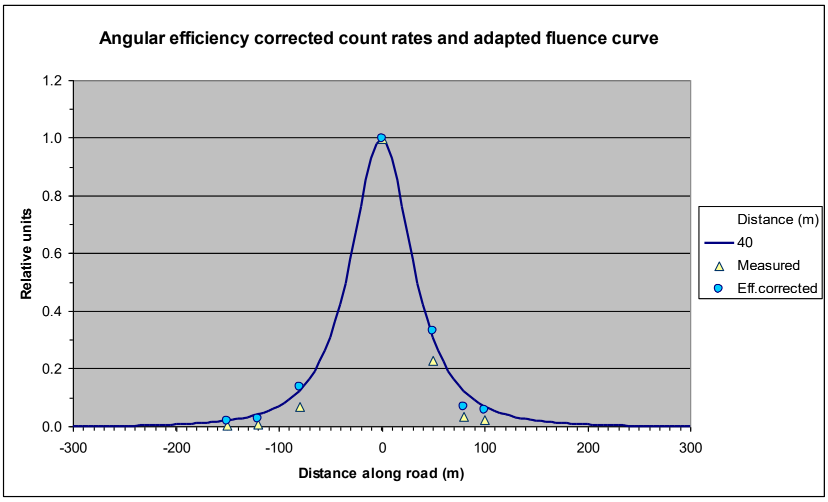

Fig E5-1. NGU. Setup M1. The true source distance is 61 m

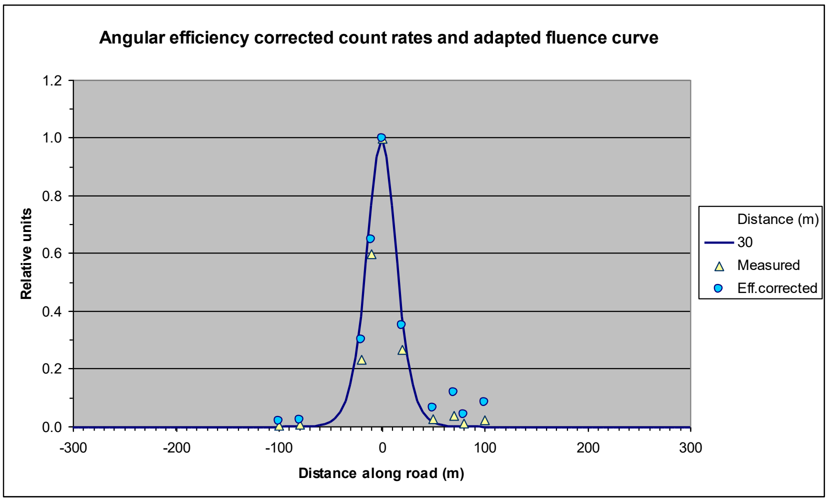

Fig E5-2. NGU. Setup M2. The true source distance is 31 m

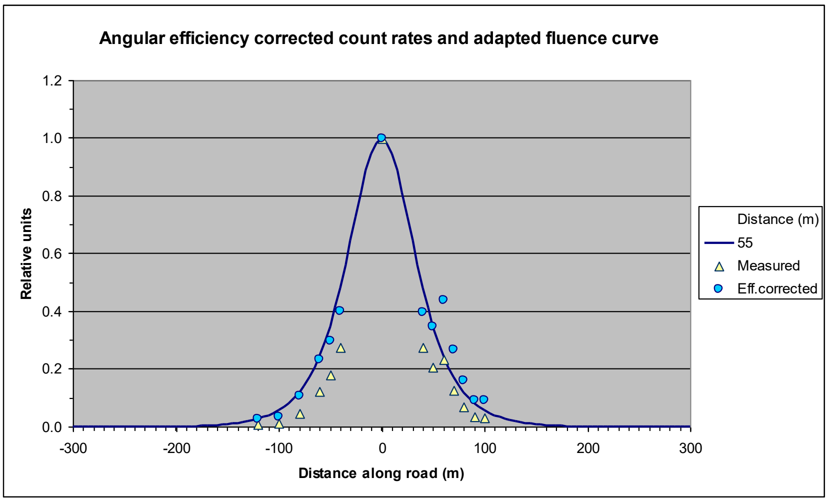

Fig E5-3. NGU. Setup M3. The true source distance is 61 m

The figures show SODAC determined source distance results for the NGU 4x4 litre NaI(Tl)-detector, corrected for varying angular efficiency. Tree-shielded measurement locations have been excluded.

SODAC source distance results, NGU 4x4 litre NaI(Tl)-detector

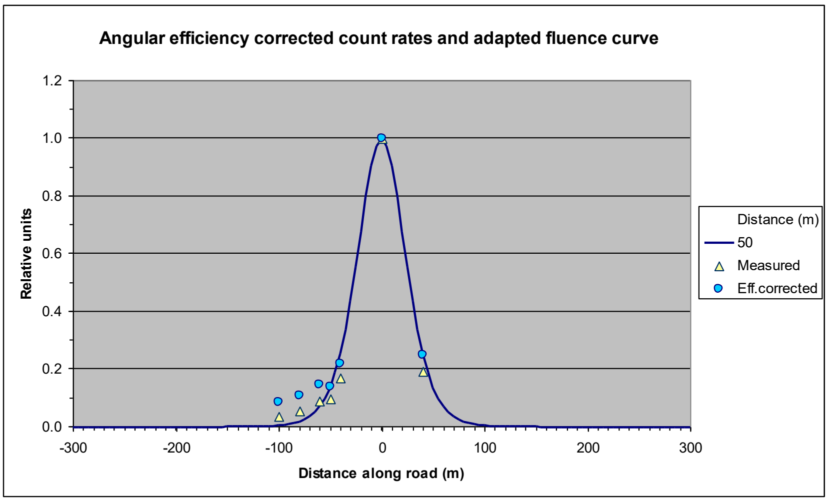

Fig E5-4. NGU. Setup M4. The true source distance is 61 m

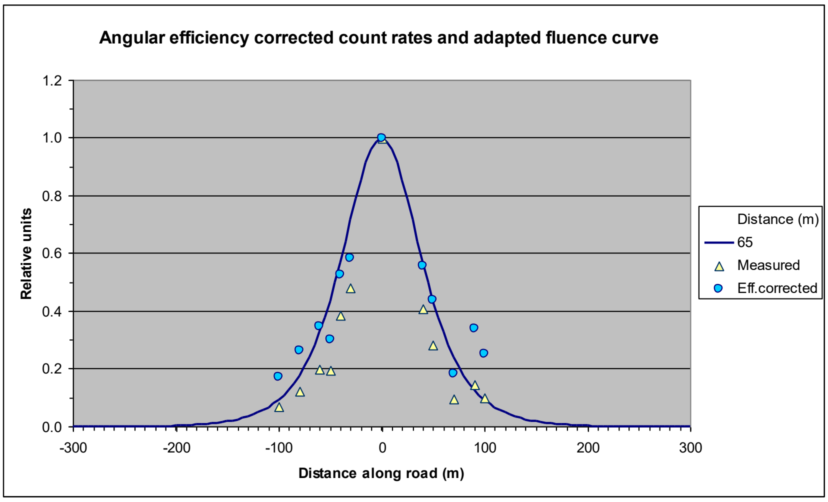

Fig E5-5 NGU. Setup M5. The true source distance is 91 m

The figures show SODAC determined source distance results for the NGU 4x4 litre NaI(Tl)-detector, corrected for varying angular efficiency. Tree-shielded measurement locations have been excluded.

E6. Summary and conclusion

The 4x4 litre NaI(Tl) detector system was calibrated for determining shield mass thickness using ten setups with Cs-137 point sources and varying shield thicknesses. Four ROI-models were used, two exponential and two five-degree polynomial models. The models, programmed in the SSC Excel routine, represent the measured net count rate ratios for the different shield mass thicknesses quite well.

When determining the distance to a radiation source with the SODAC routine in four different cases with spacing from 30 to 90 m, the distances were, on average, underestimated by 17 ± 6%. The calculated activity was, on average, overestimated by 104 ± 41%. The reason for the deviations from actual values is not fully known. Further experimental investigations of the detector's response at longer source distances and thicker shielding are needed to investigate the reason more in-depth.

Appendix F. Results from team STUK, Radiation and Nuclear Safety Authority, Finland

F1. Measuring equipment

Team STUK used two four-litre NaI(Tl) detectors mounted inside an MB Sprinter van called SONNI2, a radiological emergency response vehicle developed by STUK. The vehicle has identical detector packages (Environics RanidPort Mobile) mounted vertically on the floor near the opposing walls of the vehicle (Fig. F1-1). The detectors are moderately collimated with 20 mm steel plates that cover the 180-degree view facing the inside of the vehicle. This type of collimation gives a distinct difference between the signals from the two detectors, and the radiation source can be localized to either the right or left side of the vehicle. However, the COMBMORC experiments only used Cs-137 sources on the right side of the measuring vehicles, so all data reported here are from the right-hand side detector.

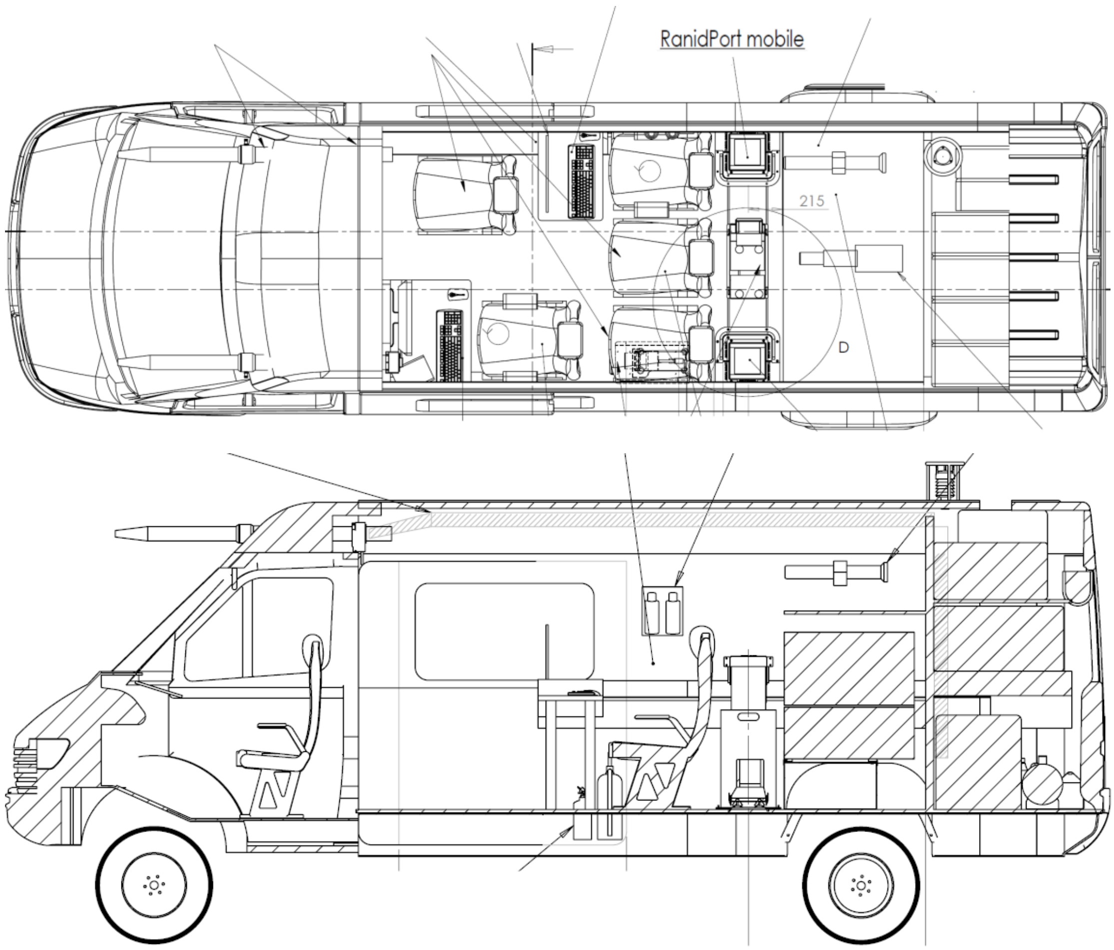

Figure F1-1. Two four-liter NaI(Tl) detectors mounted inside the MB Sprinter van marked as RanidPort Mobile on the top view. Three optional seats are shown in the pictures that were not installed on the vehicle during measurements.

F2. Detector efficiency calibration

The two 4 litre NaI(Tl)-detectors were calibrated for counting efficiency at 662 keV in an earlier NKS field experiment (NKS-AUTOMORC, 2018) using a Cs-137 point source with activity traceable to calibration sources from Eckert & Ziegler with 3% relative expanded uncertainty (k=2). When placed in measurement position in the car, the right side detector efficiency for 662 keV photons from the right side (the apparent detector area for total photon absorption) was 0.0229 m^2 with 8% relative expanded uncertainty (k=2).

F3. Detector calibration for shield mass thickness determination, using SSC

The response of the right side 4 litre NaI(Tl) detector as net count rates in ROI A, B, C and PL relative to ROI PR and ROI P was measured for different shield mass thicknesses described earlier in the report. The measurement data was entered into the Excel program SCC. The relationship between the net count rates for the ratios ROI A, B, C, and PL/PR for the exponential model is shown in Fig F3-1-a and the polynomial model in Fig F3-1-c. Corresponding relationships for the ratios ROI A, B, and C/P are shown in Figs F3-1-b and F3-1-d.

The coefficients for fitting the exponential model to observed data are given in Table F3-1. The coefficients for fitting the five-degree polynomial model to observed data are given in Table F3-2.

The exponential and five-degree polynomial models represent the measured net count rate ratios for the different shield mass thicknesses quite well.

Table F3-1. STUK 4 litre NaI(Tl)-detector (right side). Coefficients *a* and *b* in an exponential model for determining shield mass thickness according to the description in the main report. The unit of *b* is m^2/kg.

ROI ratio	*a*	*b*
ROI A/PR	3.85	0.00430
ROI B/PR	2.05	0.00361
ROI C/PR	1.33	0.00281
ROI PL/PR	1.33	0.00118
ROI A/P	1.56	0.00356
ROI B/P	0.833	0.00287
ROI C/P	0.540	0.00208

Table F3-2. STUK 4 litre NaI(Tl)-detector (right side). Coefficients a_0 - a_5 (kg/m^2) in the five-degree polynomial model for determining shield mass thickness according to Eqn 3 in the main report.

ROI ratio	a_5	a_4	a_3	a_2	a_1	a_0
ROI A/PR	5.614	-68.74	281.4	-392.9	186.0	0
ROI B/PR	9.2284	-73.09	155.4	30.94	-55.02	0
ROI C/PR	33.344	-248.1	573.0	-367.3	213.7	0
ROI PL/PR	12700	-44400	59760	-37980	11930	-1409
ROI A/P	21.59	-155.00	321.4	-90.32	36.16	0
ROI B/P	-202.2	1036	-1815	1146	294.7	0
ROI C/P	602.83	-504.9	-683.4	450.1	645.7	244.39

F4. Results from shield thickness measurements, using SSC

In connection with the experiment determining the source distance with the SODAC routine, a determination of the shield mass thickness in front of the Cs-137 point source was made using the SSC routine when the measuring car was directly opposite the source, i.e. at the road location with the shortest distance to the source. The results are given in tables F4-1 to F4-4.

The deviation in the calculated mass thickness from the actual value was between -5% and 65% for the exponential model, and the polynomial model's deviation was between -21% and 73%. It is impossible to say that one model gives better values than the other. On average, the models overestimated the mass thickness by 23 ± 12%.

The detailed result from SSC is also reproduced in Figs F4-1 to F4-5, where the individual net count rate ratios ROI A/PR, ROI B/PR Etc., are plotted along the lines of the exponential model and the polynomial model. The measurement data show relatively good agreement for the different ROI ratios for setup M1 and M2. There is a broader variation between the ROI ratios for setup M3, M4, and M5. These setups have combinations of more considerable distances and shielding, resulting in poorer counting statistics, which probably is the cause of the more significant variation.

Table F4-1. Result from the STUK 4 litre NaI(Tl) detector determination of shield mass thickness by using ROI A, B, C, PL / PR net count rate ratios in an exponential model

Setup	Actual		Measured		Deviation
	Distance to source (m)	Shield mass thickness (kg/m^2)	Shield and air mass thickness (kg/m^2)	Shield mass thickness (kg/m^2)	of measured from actual value (%)
M1	61	0	77.5	1.70	2.2
M2	31	333	372	333	0.1
M3	61	94	220	144	29.6
M4	61	333	328	253	19.7
M5	91	94	306	193	47.9
Average					19.9 ± 8.9

Table F4-2. Result from the STUK 4 litre NaI(Tl) detector determination of shield mass thickness by using ROI A, B, C / P net count rate ratios in an exponential model

Setup	Actual		Measured		Deviation
	Distance to source (m)	Shield mass thickness (kg/m^2)	Shield and air mass thickness (kg/m^2)	Shield mass thickness (kg/m^2)	of measured from actual value (%)
M1	61	0	112	35.8	47.1
M2	31	333	377	339	1.6
M3	61	94	258	182	52.1
M4	61	333	389	313	-4.9
M5	91	94	339	225	63.5
Average					31.9 ± 14.0

Table F4-3. Result from the STUK 4 litre NaI(Tl) detector determination of shield mass thickness by using ROI A, B, C, PL / PR net count rate ratios in a five-degree polynomial model

Setup	Actual		Measured		Deviation
	Distance to source (m)	Shield mass thickness (kg/m^2)	Shield and air mass thickness (kg/m^2)	Shield mass thickness (kg/m^2)	of measured from actual value (%)
M1	61	0	78.6	2.8	3.7
M2	31	333	370	331	-0.6
M3	61	94	201	126	18.6
M4	61	333	322	246	-21.3
M5	91	94	294	191	42.2
Average					8.52 ± 10.6

Table F4-4. Result from the STUK 4 litre NaI(Tl) detector determination of shield mass thickness by using ROI A, B, C / P net count rate ratios in a five-degree polynomial model

Setup	Actual		Measured		Deviation
	Distance to source (m)	Shield mass thickness (kg/m^2)	Shield and air mass thickness (kg/m^2)	Shield mass thickness (kg/m^2)	of measured from actual value (%)
M1	61	0	93.8	18.0	23.8
M2	31	333	408	369	9.8
M3	61	94	254	178	49.3
M4	61	333	419	343	2.4
M5	91	94	358	245	72.9
Average					31.6 ± 13.1

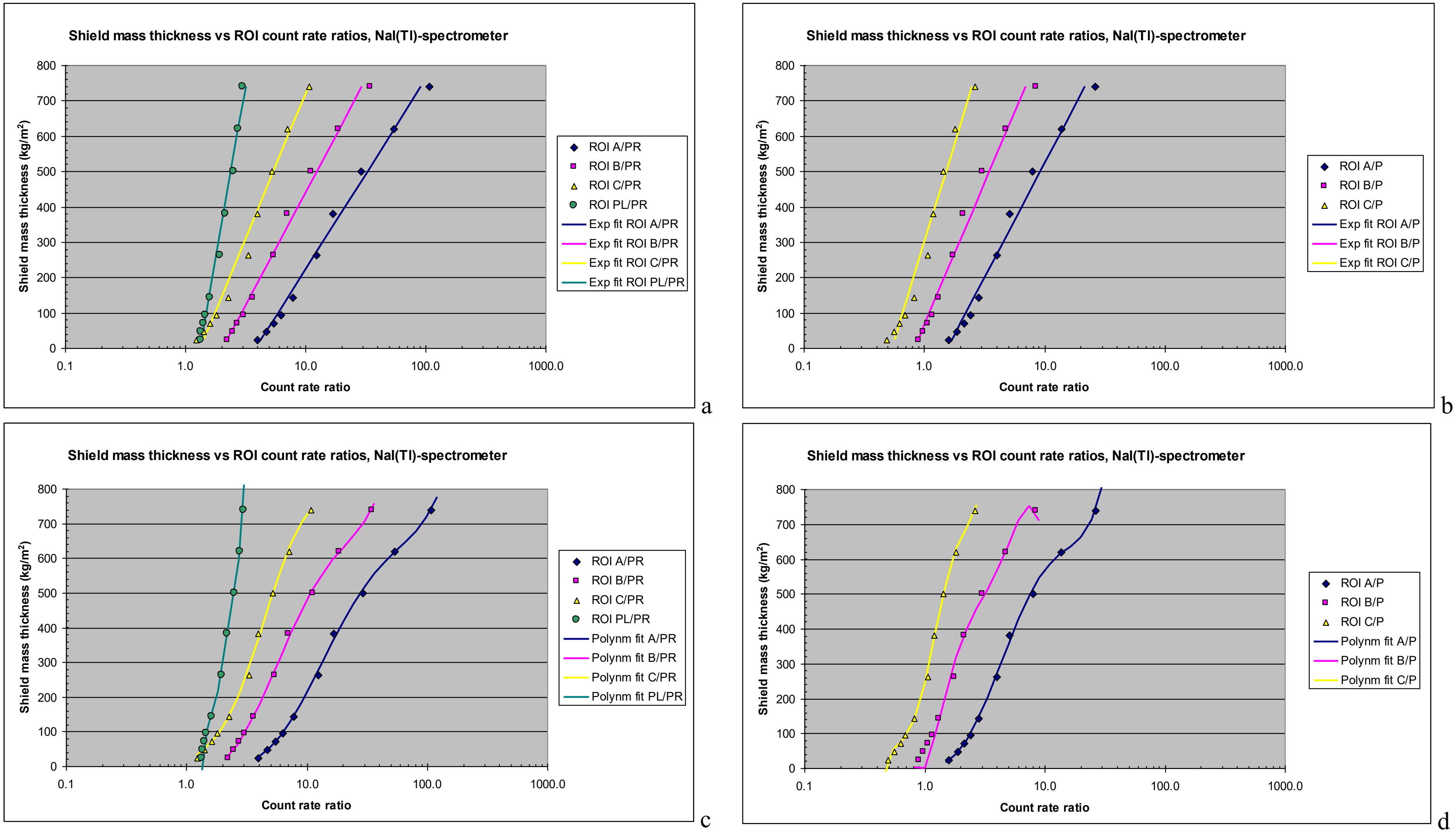

Fig F3-1-a-d. STUK 4 litre NaI(Tl) spectrometer. Models of shield mass thickness as a function of ROI net count rate ratio obtained from fitting measured data to exponential functions (a, b) and five-degree polynomial functions (c, d), valid for Cs-137 point sources behind shields of standard building material (wood and concrete) with mass thickness between 20 and 730 kg/m^2. Values have been measured at a source-detector distance of 10 m.

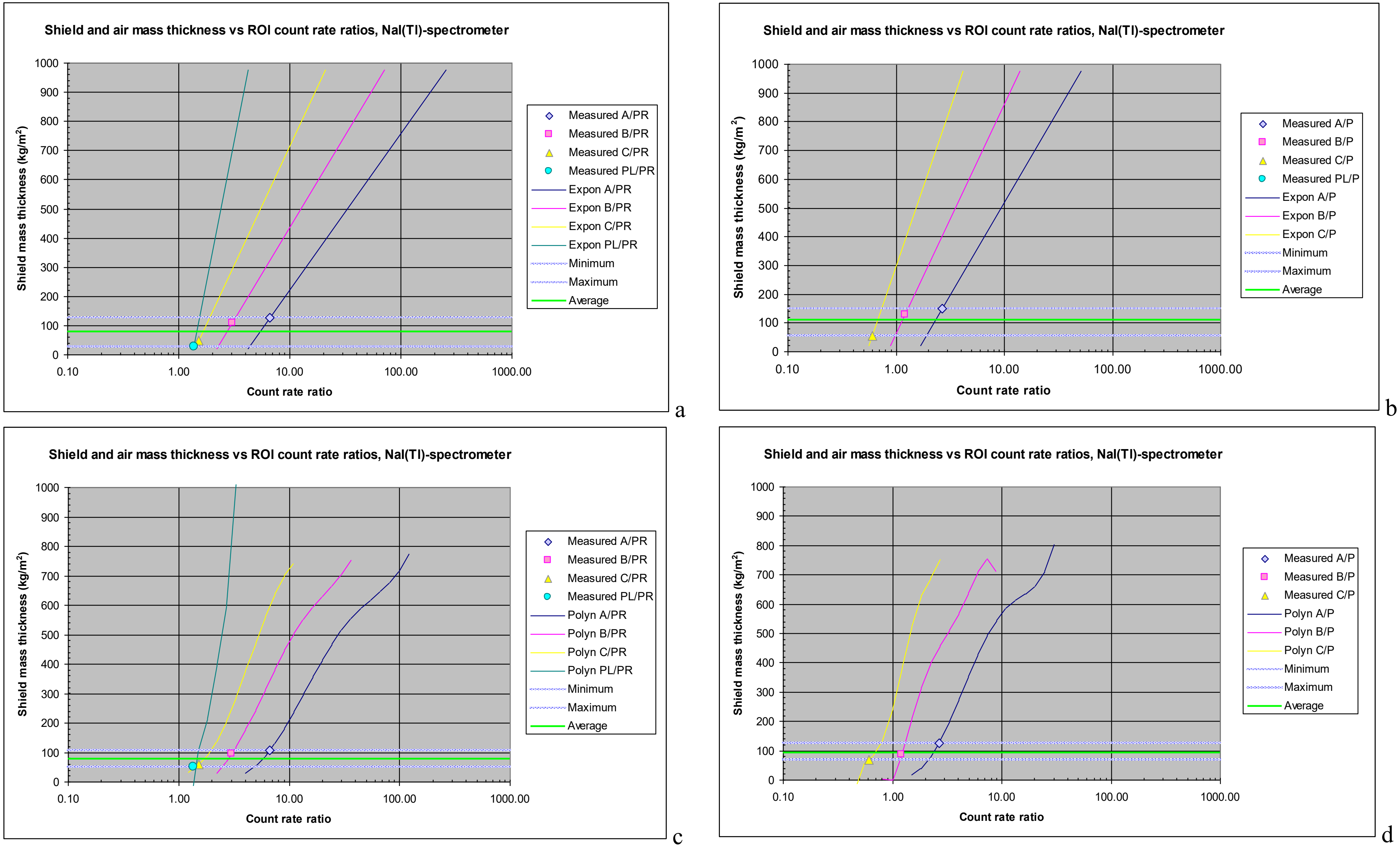

Fig F4-1-a-d (M1). Shield mass thickness determination by the STUK 4 litre NaI(Tl) spectrometer using the ROI count rate ratio method with exponential (a, b) and polynomial (c, d) models. The true shield mass thickness is 75.8 kg/m^2, including 61 m of air between the source and the detector.

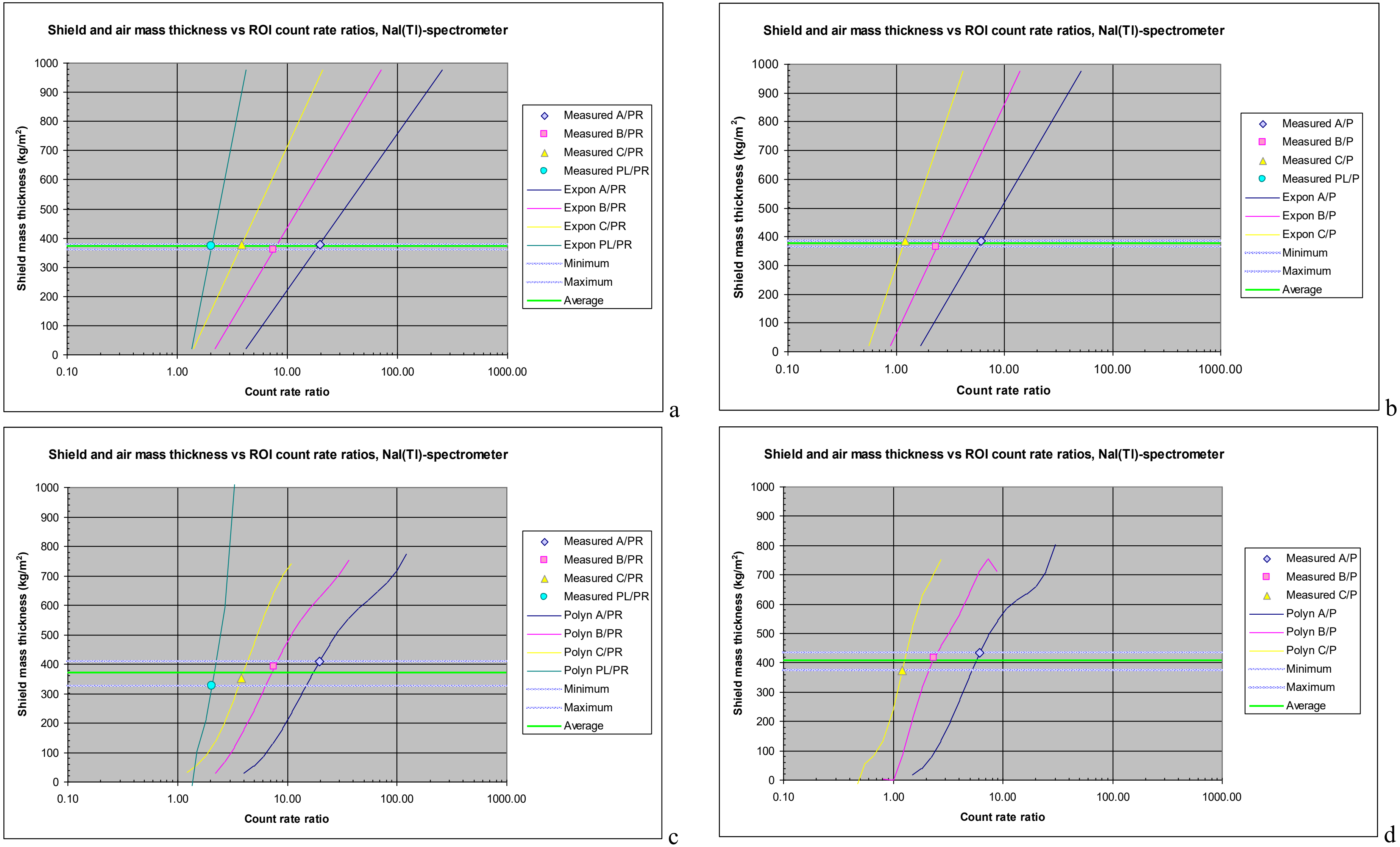

Fig F4-2-a-d (M2). Shield mass thickness determination by the STUK 4 litre NaI(Tl) spectrometer using the ROI count rate ratio method with exponential (a, b) and polynomial (c, d) models. The true shield mass thickness is 372 kg/m^2, including 31 m of air between the source and the detector.

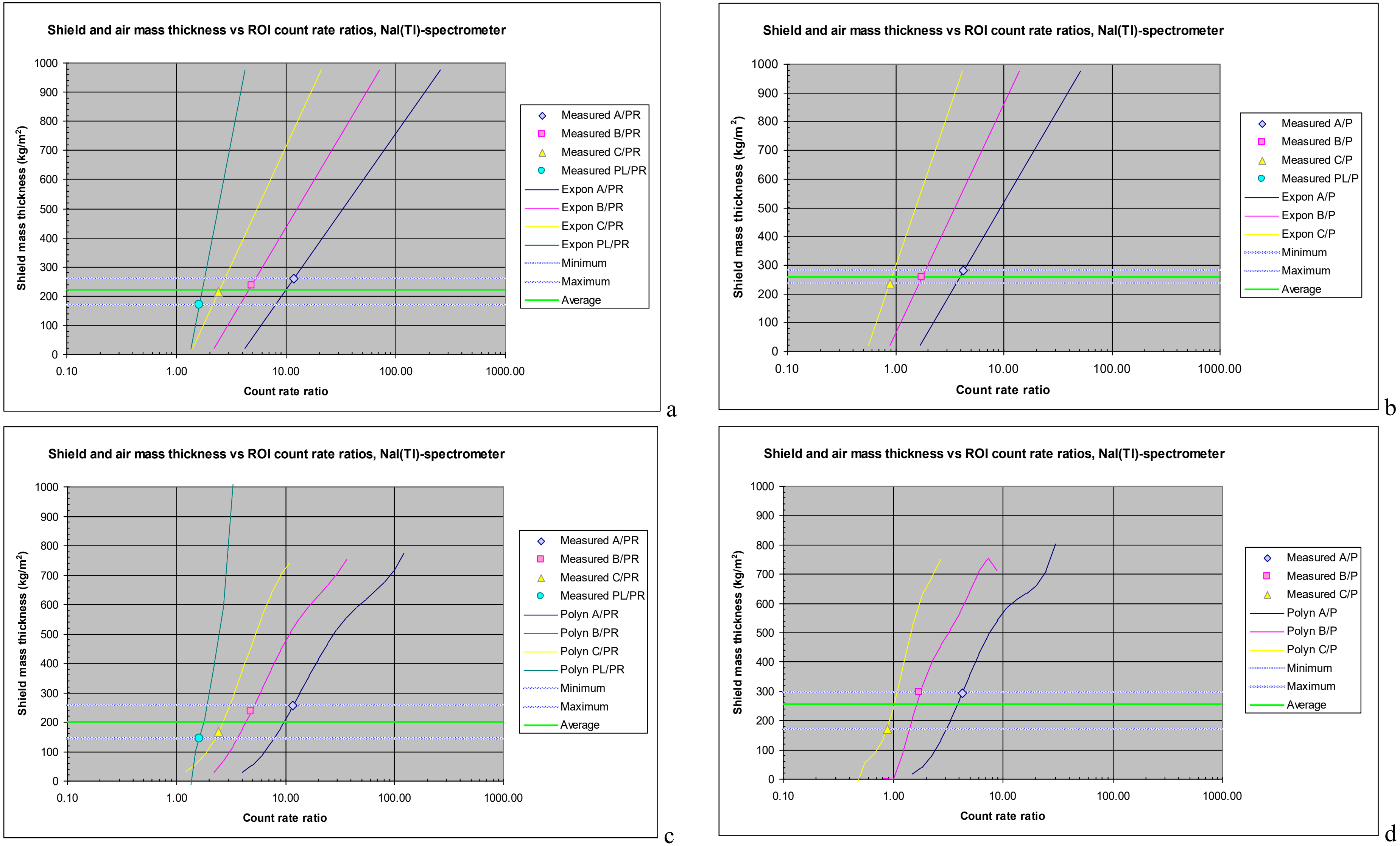

Fig F4-3-a-d (M3). Shield mass thickness determination by the STUK 4 litre NaI(Tl) spectrometer using the ROI count rate ratio method with exponential (a, b) and polynomial (c, d) models. The true shield mass thickness is 170 kg/m^2, including 61 m of air between the source and the detector.

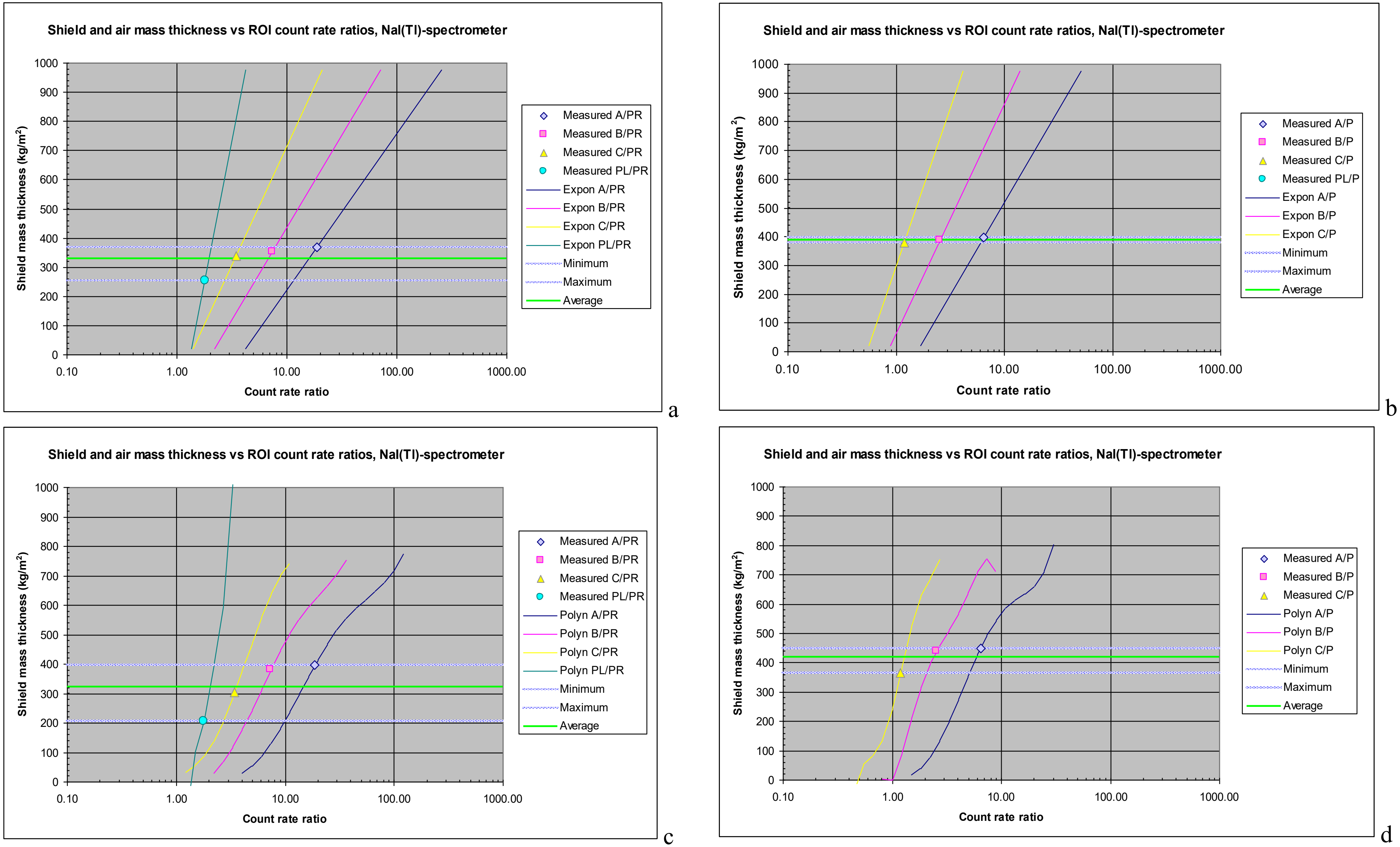

Fig F4-4-a-d (M4). Shield mass thickness determination by the STUK 4 litre NaI(Tl) spectrometer using the ROI count rate ratio method with exponential (a, b) and polynomial (c, d) models. The true shield mass thickness is 409 kg/m^2, including 61 m of air between the source and the detector.

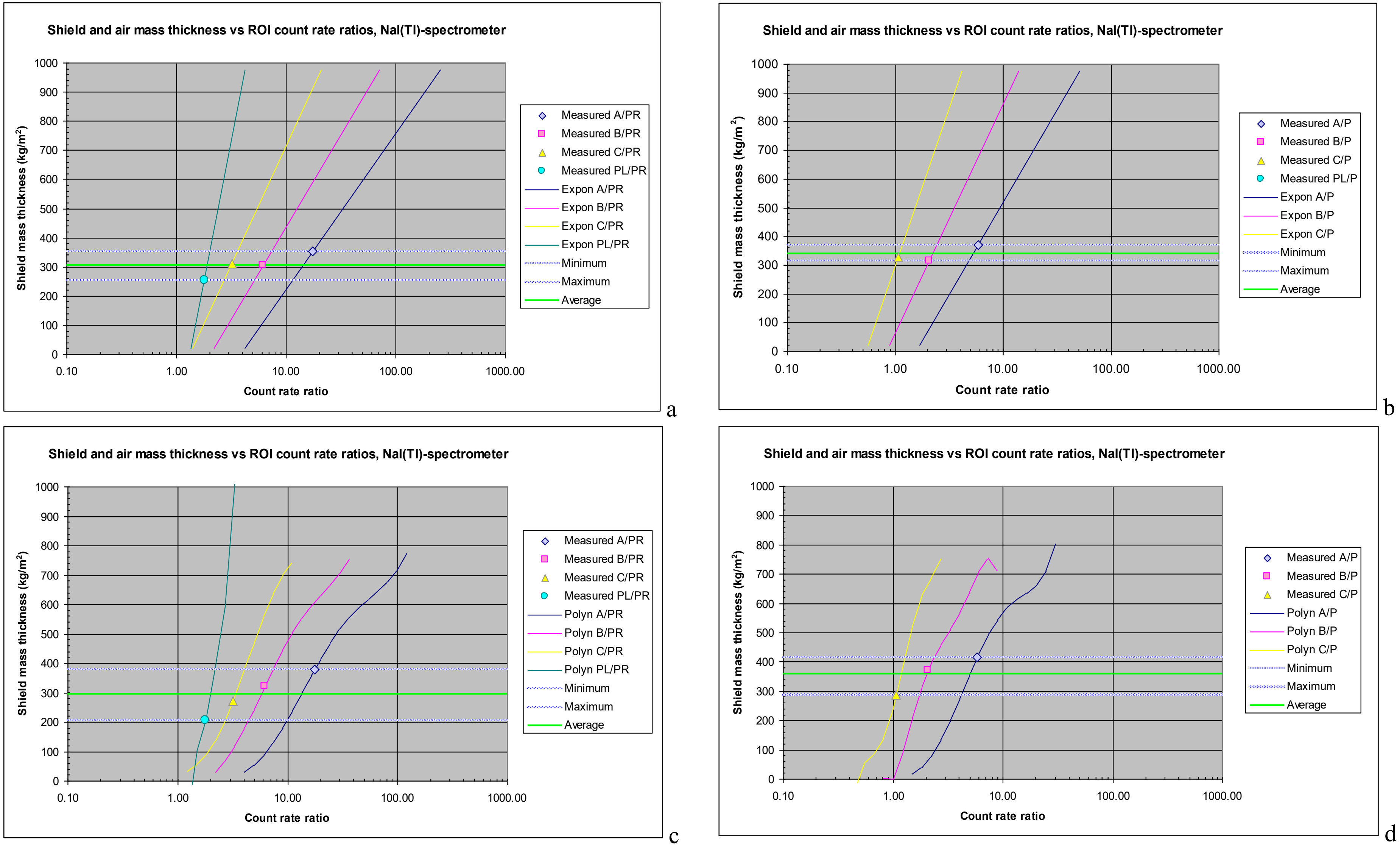

Fig F4-5-a-d (M5). Shield mass thickness determination by the STUK 4 litre NaI(Tl) spectrometer using the ROI count rate ratio method with exponential (a, b) and polynomial (c, d) models. The true shield mass thickness is 207 kg/m^2, including 91 m of air between the source and the detector.

F5. Results from source distance measurements, using SODAC

The distance to a Cs-137 point source was determined using the Excel program SODAC for five different setups with different distances and shielding (M1 to M5), as described in the main report. All measurements were made standing still (semi-stationary) at various locations along the road that passes the radiation source. Unfortunately, it turned out that some trees between the radiation source and the measuring car shielded the photon fluence from the source at specific points along the road. These measurement points have been identified, and the data has been removed from the analysis.

The detectors in the STUK vehicle are mounted vertically. Vertical mounting implies that the detectors' sensitivity is approximately the same for all angles in the horizontal plane (except in the direction towards the vehicle where there is lead shielding). No correction, therefore, needs to be made for different incident angles of photons from the outside of the vehicle, as is necessary for horizontal (horizontally oriented) 4 litre NaI(Tl) detectors.

In the SODAC analysis, the actual shield thickness has been used in the distance determination (and not the one obtained through SSC) because it produces a more accurate picture of any distance determination deviations than a possibly distorted assumption of the shield thickness would do.

Results from the Excel program SODAC showing which "intensity curve" (primary photon fluence from the source as a function of distance along the road) best fits the measurement data along the road for the five setup distances are reproduced in Figures F5-1 to F5-5.

Results from the distance and activity determination with SODAC are summarized in Table F5-1. The source distances for the five setups (M1 to M5) were correct for setup M2 (30 m) and underestimated from 8% to 33% for the other four setups, with an average underestimation of 18 ± 7%. The source activity was overestimated by 181 ± 70%.

The reason for the deviations from actual values is not fully known. It may be due to the low energy resolution in a NaI(Tl) detector and the increased distance to the source compared to the calibration distance for shield thickness. Photons scattered at small angles between the source and the detector are recorded as primary photons in the full-energy peak in the pulse height distribution of the detector. These photons cause the count rate in ROI PR and ROI P to increase compared to primary-only photons, which may affect the calculation of distance and shield thickness for longer distances. Further experimental investigations of the detector's response at longer source distances and thicker shielding are needed to draw more definite conclusions.

Table F5-1. Results from the STUK 4 litre NaI(Tl) detector, applying the SODAC routine to obtain the source distance and activity for a Cs-137 point source. The NaI(Tl) detector is vertically mounted and the angular efficiency variation is small. Therefore, no adjustment for photon angles of incidence is made in the distance determination. The activity is calculated from the full energy peak count rate for the measured and the actual distance, using the actual shield thickness. The actual point source activity is 606 MBq in all setups.

Setup	Actual		SODAC obtained			Deviation	
	Distance to source m	Shield mass thickness kg/m^2	Distance m	Activity at obtained distance MBq	Activity at actual distance MBq	Distance rounded %	Activity at obtained (at actual distance) %
M1	61	air only	50	535	848	-17	-11.7 (39.9)
M2	31	333	30	1564	1564	0	158 (158)
M3	61	94	55	886	1108	-8	46 (82.8)
M4	61	333	40	1212	3307	-33	100 (446)
M5	91	94	60	562	1687	-33	-7.2 (178)
Average						-18 ± 7	57 ± 32 (181 ± 70)

SODAC source distance results, STUK 4 litre NaI(Tl)-detector

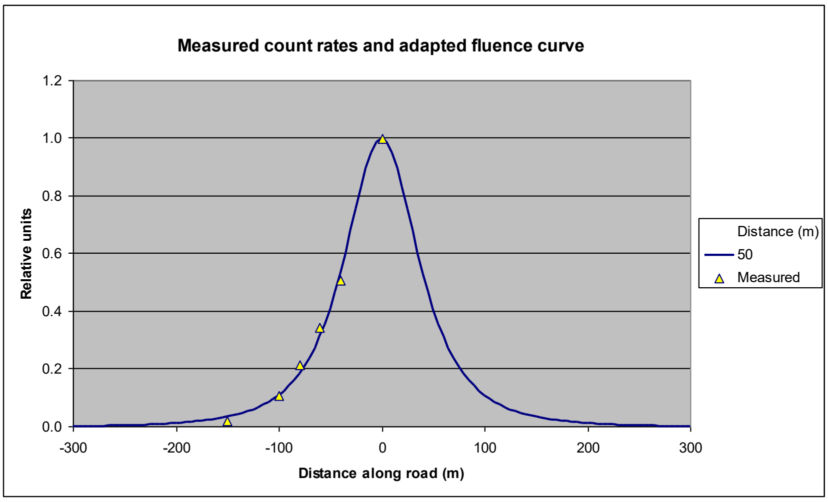

Fig F5-1. STUK. Setup M1 (M6). The true source distance is 61 m

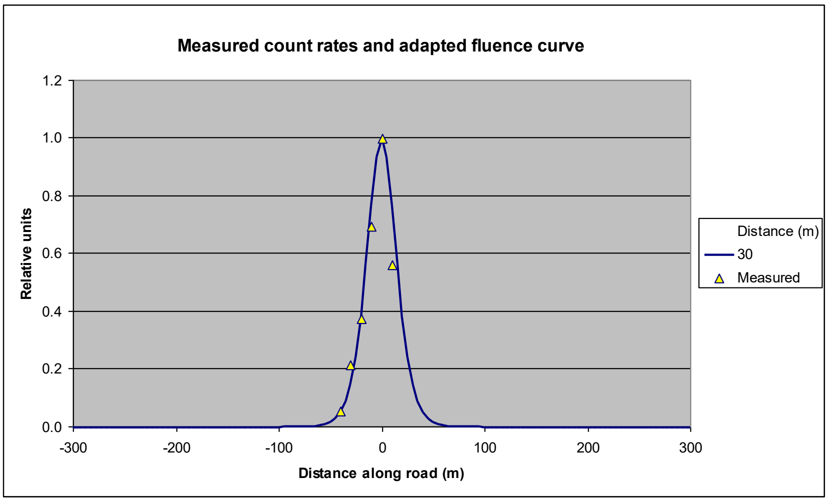

Fig F5-2. STUK. Setup M2 (M7). The true source distance is 31 m

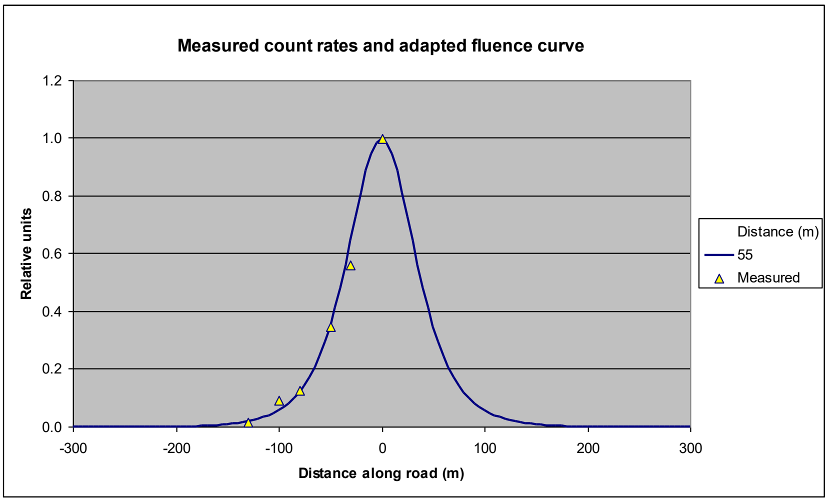

Fig F5-3. STUK. Setup M3 (M8). The true source distance is 61 m

The figures show SODAC determined source distance results for the STUK 4 litre NaI(Tl)-detector. Tree-shielded measurement locations have been excluded.

SODAC source distance results, STUK 4 litre NaI(Tl)-detector

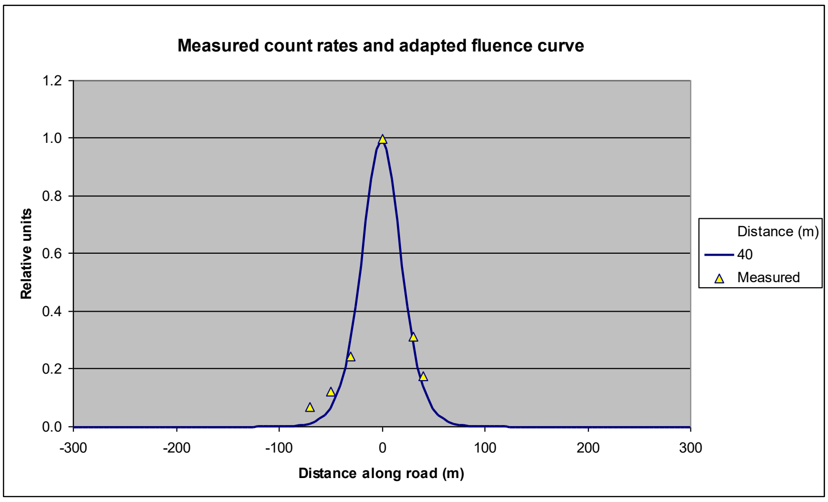

Fig F5-4. STUK. Setup M4 (M9). The true source distance is 61 m

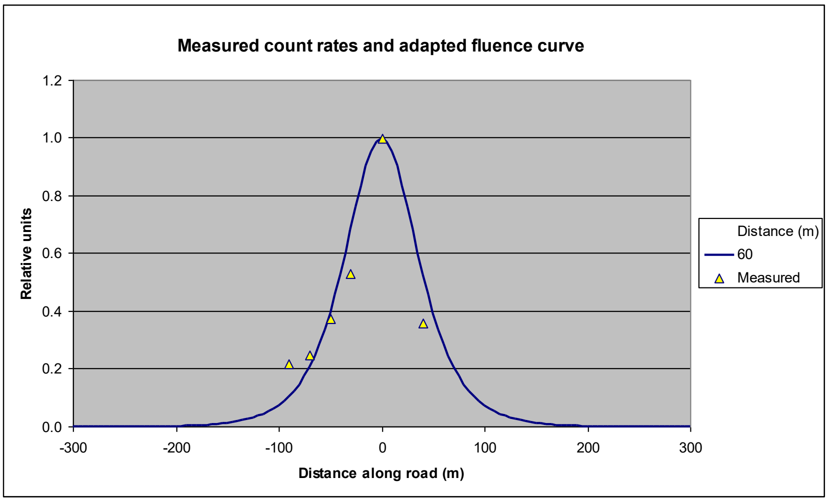

Fig F5-5. STUK. Setup M5 (M10). The true source distance is 91 m

The figures show SODAC determined source distance results for the STUK 4 litre NaI(Tl)-detector. Tree-shielded measurement locations have been excluded.

F6. Summary and conclusion

In determining the mass thickness of the radiation shield with the SCC routine, two models have been used that describe the net count rate relationships between registrations from scattered radiation and primary radiation, an exponential model and a polynomial model. Both models give roughly the same results and overestimate the shield mass thickness by 23 ± 12% (standard error of the mean).

When determining the distance to a radiation source with the SODAC routine in four different cases with spacing from 30 to 90 m, the distances were, on average, underestimated by 18 ± 7%. The calculated activity was, on average, overestimated by 181 ± 70%. The reason for the deviations from actual values is not fully known. Further experimental investigations of the detector's response at longer source distances and thicker shielding are needed to investigate the reason more in-depth.

Appendix G. Setup of detector response calibration for shielded sources

G1. Shielding configuration

As the first part of COMBMORC 2022, a response calibration for Cs-137 point sources was performed to determine the mass thickness of a radiation shield from the pulse height distributions of gamma spectrometers. The net count rates in regions of interest ROI A, B, C, PL, PR and P, as described in the main report, were measured for Cs-137 sources behind ten setups with different shield thicknesses. The measurement data was entered into the Excel routine SSC, where it constituted a "knowledge library", which was used to determine the mass thickness of unknown radiation shields in setup M1 to M5 using the ROI method described in the main report.

The distance between the source and detector in the response calibration was 10 m. The SSC routine adds the air mass thickness for the 10 m distance to the mass thickness of the shield, and the air distance corresponds to 12.43 kg/m^2. However, there is also a 1 mm steel plate in the trailer sidewall, which in mass corresponds to 6 m of air. To correct for the steel wall, 10 + 6 = 16 m was input to the SSC calibration sheet at the line "Input distance to source (m)". The steel wall is included in the mass thickness given in Table G1 for the calibration setup.

Pictures of the shielding construction for response calibration are shown in Fig G1 to G3.

An example of input data to the SSC routine from a 4-litre NaI(Tl) detector is shown in Fig G4.

Table G1. The shielding configuration in the detector response calibration for determining the pulse height distribution energy regions ROI A, B, C, PL/PR and ROI A, B, C/P net count rate ratios valid for a Cs-137 point source with 662 keV primary photons as a function of shield mass thickness. The mass thickness given in the table includes the air between the source and the detector and 1 mm of steel plate in the sidewall of the trailer.

Setup number	Material	Mass thickness (kg/m^2)
C1	Air only	19.89
C2	4.5 cm wood	43.38
C3	9 cm wood	66.87
C4	13.5 cm wood	90.36
C5	5 cm concrete	139.0
C6	10 cm concrete	258.1
C7	15 cm concrete	377.2
C8	20 cm concrete	496.3
C9	25 cm concrete	615.4
C10	30 cm concrete	734.5

Fig G1. Setup C4 for shield thickness calibration of the different team's mobile gamma spectrometers. The setup is mounted on a trailer showing the shielding material from the side. The Cs-137 source is inside the clay brick cave. The shield consists of three layers of 4.5 cm wooden beams producing a wall thickness of 135 mm in two directions, left and right. The mass thickness of the wooden wall is 70.7 kg/m^2. The sidewalls of the trailer consist of 1 mm steel.

Fig G2. Setup C10 for shield thickness calibration of the different team's mobile gamma spectrometers. The Cs-137 source is placed inside the clay brick cave. The shield consists of six layers of 5 cm concrete blocks producing a wall thickness of 300 mm in two directions, left and right. The mass thickness of the concrete wall is 714.6 kg/m^2.

Fig G3. Setup C10 for shield thickness calibration of the different team's mobile gamma spectrometers. View obliquely from behind and above. The source is placed in the cave below the clay bricks. The shield consists of six layers of 5 cm concrete blocks producing a wall thickness of 300 mm in two directions, left and right. The mass thickness of the concrete wall is 714.6 kg/m^2.

Known shield material	Air only	Wood	Wood	Wood	Concrete	Concrete	Concrete	Concrete	Concrete	Concrete
Known shield thickness (cm)	0	4.5	9	13.5	5	10	15	20	25	30
Known shield density (kg/m3)	0	522	522	522	2382	2382	2382	2382	2382	2382
Mass thickness (kg/m2)	0	23.49	46.98	70.47	119.1	238.2	357.3	476.4	595.5	714.6
Input distance to source (m)	16	16	16	16	16	16	16	16	16	16
Total mass thickness (kg/m2)	19.888	43.378	66.868	90.358	138.988	258.088	377.188	496.288	615.388	734.488
Input measured background (cps)										
ROI A	940.168	940.168	940.168	940.168	940.168	940.168	940.168	940.168	940.168	940.168
ROI B	350.9333	350.9333	350.9333	350.9333	350.9333	350.9333	350.9333	350.9333	350.9333	350.9333
ROI C	164.6626	164.6626	164.6626	164.6626	164.6626	164.6626	164.6626	164.6626	164.6626	164.6626
ROI PL	65.27293	65.27293	65.27293	65.27293	65.27293	65.27293	65.27293	65.27293	65.27293	65.27293
ROI PC	1.78895	1.78895	1.78895	1.78895	1.78895	1.78895	1.78895	1.78895	1.78895	1.78895
ROI PR	42.92891	42.92891	42.92891	42.92891	42.92891	42.92891	42.92891	42.92891	42.92891	42.92891
ROI P	109.9908	109.9908	109.9908	109.9908	109.9908	109.9908	109.9908	109.9908	109.9908	109.9908
Input measured gross (cps)										
ROI A	1974.278	1974.457	1935.207	1880.995	4258.132	3101.23	5686.233	4498.303	3910.459	3665.67
ROI B	950.7978	907.8957	869.1307	821.2758	1941.657	1334.564	2416.265	1751.951	1437.697	1270.278
ROI C	518.9547	506.9434	494.2725	469.578	1218.064	778.0625	1283.766	783.7453	552.1091	432.1909
ROI PL	433.3828	379.2853	325.7564	314.7804	771.7684	412.1687	638.0333	328.7744	185.2303	123.6178
ROI PC	36.19115	29.48315	25.57516	22.5796	58.44444	25.85353	40.16041	17.67116	8.58723	4.903827
ROI PR	330.515	275.2909	259.0508	208.8338	550.0538	255.8454	421.8782	195.5565	113.4701	71.3332
ROI P	800.089	684.0594	610.3823	546.1937	1380.267	693.8677	1100.072	542.0021	307.2876	199.8548

Fig G4. Example of input response calibration data to the Excel SSC routine for assessing shield mass thickness from ROI count rate data from a gamma spectrometer. The data is for Lund University 4 litre NaI(Tl) rear detector.

Appendix H. Setup for source distance determination

H1. Source configuration

Part of COMBMORC included the experiment in determining the distance, shielding and activity of a Cs-137 radiation source based on semi-stationary measurements along a path that runs past the source. In the experiment, the radiation source was placed in a trailer with two radiation shields of different thicknesses in diametrically opposite directions. Moving and turning the trailer achieved five different combinations of distances from the road and shield thicknesses. Table H1 shows the combinations (setup M1 to M5) used in the experiment. The setups M6 to M10 are identical to M1 to M5.

Table H1. Data for setup M1 to M5 for determining Cs-137 source distance, shield mass thickness and source activity in semi-mobile gamma spectrometry when applying the Excel routines SODAC and SSC.

Setup	Distance (m)	Shield material	Mass thickness (kg/m^2)	Activity (MBq)
M1, M6	60	60 m air	74.58	606
M2, M7	30	13 cm concrete 4.5 cm wood 30 m air	309.7 23.5 37.3 Σ 370.5	606
M3, M8	60	18 cm wood 60 m air	94.0 74.6 Σ 168.6	606
M4, M9	60	13 cm concrete 4.5 cm wood 60 m air	309.7 23.5 74.6 Σ 407.8	606
M5, M10	90	18 cm wood 90 m air	94.0 111.9 Σ 205.9	606

H2. Source obstruction by vegetation

The small side road where the trailer with the radiation source was placed had smaller trees and bushes on the sides. In the subsequent measurement data analysis along the main road, the teams discovered that primary photons from the radiation source in some measurement points showed lower photon fluence rates than expected. The cause was identified as shielding in the vegetation along the sides of the side road. Determining where the free line of sight between the radiation source and detector along the main road was obstructed has identified the measurement points affected by tree shielding. Data from these measurement points were sorted out before the analysis with the Excel routine SODAC was carried out. Table H2 indicates which points along the main road were affected by the tree shielding.

Table H2. Road locations where trees or bushes obstruct the line of sight between the source and the detector. Measurement data from these locations were removed from the distance analysis in the Excel routine SODAC.

	Source distance (m)		
Road location (m)	30	60	90
-150			
-140			
-130			
-120			
-110			
-100			
-90	Uncertain		
-80	Uncertain		
-70	Uncertain		
-60	Uncertain		
-50	Uncertain		Tree
-40	Tree	Busch	
-30	Tree	Tree	
-20	Tree	Uncertain	Busch
-10	Tree	Tree	Tree
0			
10	Tree	Tree	Tree
20		Tree	Tree
30	Tree	Tree	Bushes
40	Bushes	Bushes	Bushes
50	Bushes	Bushes	Bushes
60	Bushes	Bushes	Bushes
70	Bushes	Bushes	Bushes
80	Bushes	Bushes	Bushes
90	Bushes	Bushes	Bushes
100	Bushes	Bushes	Bushes

The lines of sight between the source and the detector in the measurement car (i.e. the paths of primary photons from the source to the detector) are shown in Fig H2-1 and H2-2 for the three source distances along the side road that was used in the experiment.

The lines of sight in the ground view for the source-road distance 30 m, 60 m, and 90 m are shown in Figs H2-3 to H2-5, respectively.

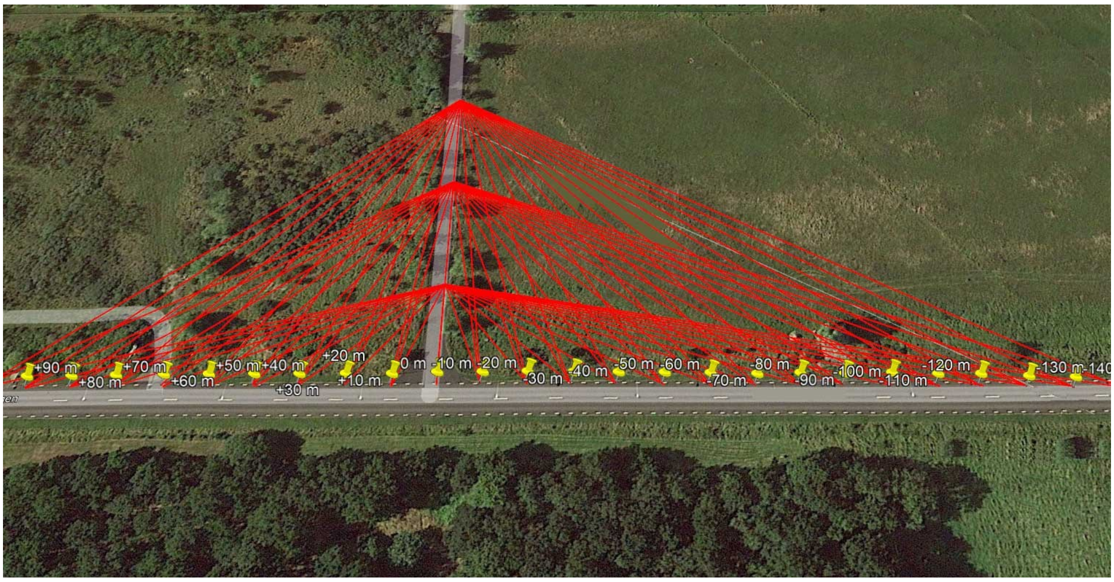

Fig H2-1. Bird's view of locations along the main road for semi-stationary gamma spectrometry in determining source distance, shielding and activity. Measurement locations are interspaced by 10 m along the main road. Source locations are at distances 30 m (setup M2), 60 m (setup M1, M3, M4), and 90 m (setup M5) along the side road perpendicular to the main road. Lines of sight between the source and measurement locations are indicated with red lines. (Map from Google Earth).

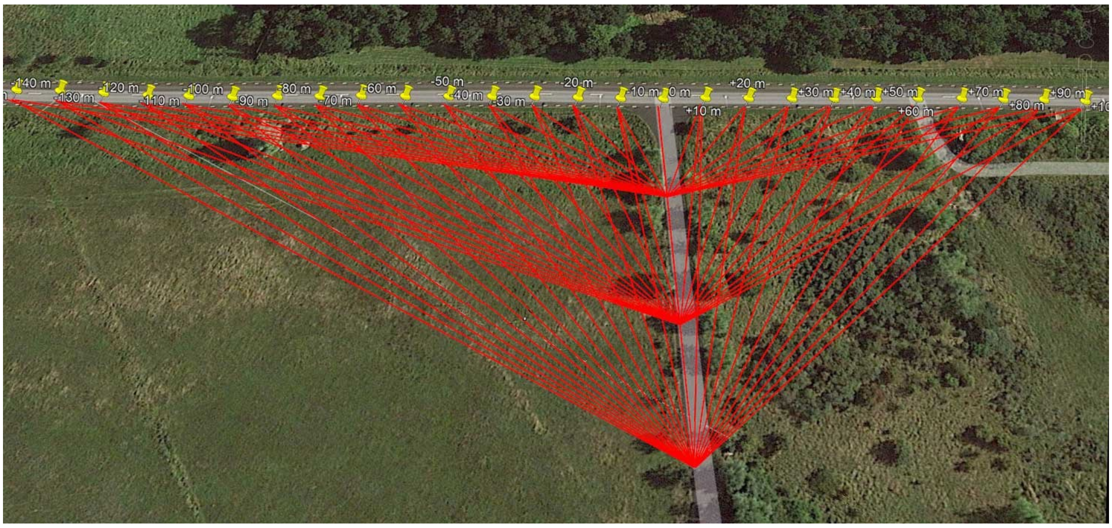

Fig H2-2. Bird's view of road locations for semi-stationary mobile gamma spectrometry when determining source distance, shielding and activity, seen from the source locations at 30, 60 and 90 m on the side road. (Map from Google Earth).

Fig H2-3. Source location at 30 m from the main road. Red lines indicate the lines of sight between the source and measurement locations along the main road with 10 m interspacing. Trees and bushes obstruct the line of sight for some locations, listed in Table H2. (Photo from Google Earth).

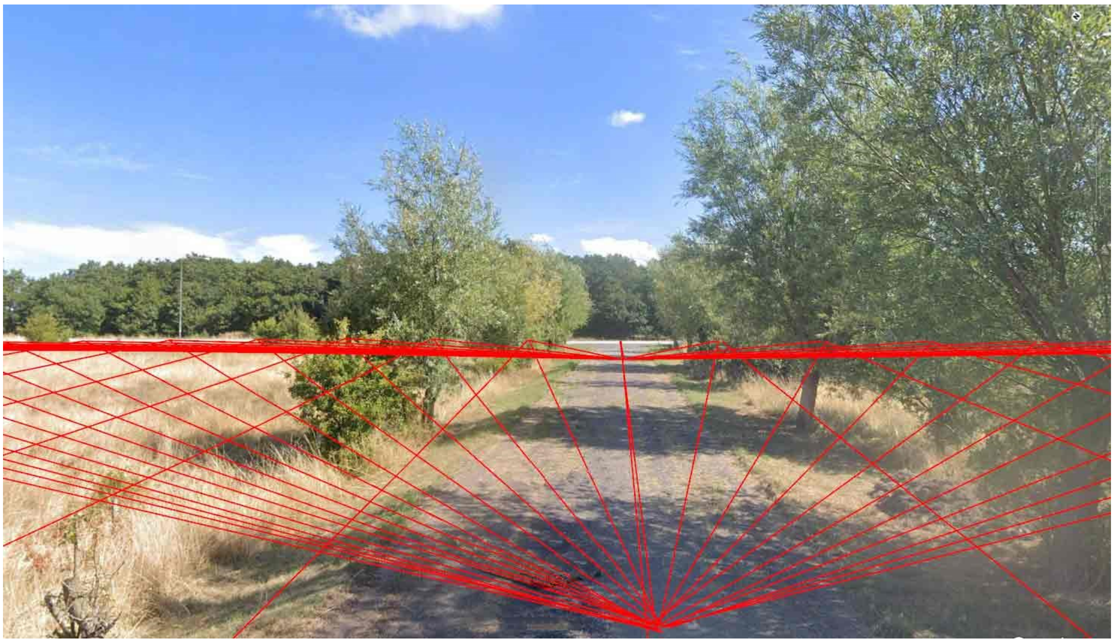

Fig H2-4. Source location at 60 m from the main road. Red lines indicate the lines of sight between the source and measurement locations along the main road with 10 m interspacing. Trees and bushes obstruct the line of sight for some locations, listed in Table H2. (Photo from Google Earth).

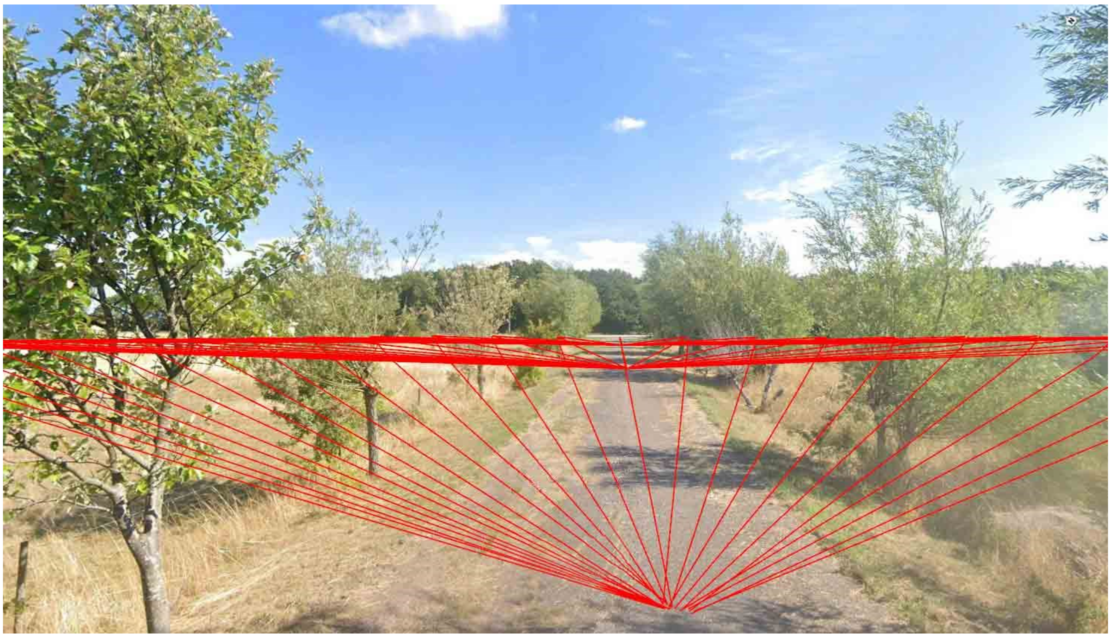

Fig H2-5. Source location at 90 m from the main road. Red lines indicate the lines of sight between the source and measurement locations along the main road with 10 m interspacing. Trees and bushes obstruct the line of sight for some locations, listed in Table H2. (Photo from Google Earth).

Appendix I. ROI regions for gamma spectrometers and teams

Here are reported the settings of regions-of-interest, ROIs, used by participating teams for their gamma spectrometers.

I1. Generic ROI

Generic ROI is meant to guide how the different ROIs should be chosen for gamma spectrometers with different conversion gains so that the respective energy intervals cover roughly the same width.

Table I1 provides examples of ROI selections for different conversion gains and energy width per channel.

Table I1. Suggested ROIs with energy interval limits given in keV for detecting primary and scattered photons measured by a gamma spectrometer having 1024, 512 or 256 channels corresponding to channel widths of 3, 6 or 12 keV/channel. The peak area ROI is suitable for a NaI(Tl) spectrometer and is divided into three sub-components: left peak area (PL), centre channel (PC) and right peak area (PR), which together constitute the full energy peak area (P).

ROI	Energy node (keV)	Compton scattered degree	3 keV/ch (keV)	ROI width chs	6 keV/ch (keV)	ROI width chs	12 keV/ch (keV)	ROI width ch
	74							
A			77-239	55	80-236	27	86-230	13
	242	110						
B			245-407	55	248-404	27	254-398	13
	410	58						
C			413-575	55	416-572	27	422-566	13
	578	27						
PL			581-659	27	584-656	13	590-650	6
PC			662	1	662	1	662	1
PR			665-743	27	668-740	13	674-734	6
P			581-743	55	584-740	27	590-734	13

I2. DEMA

Table I2. The ROI setup for the DEMA shielding experiment in SHIELDMORC 2020 and COMBMORC 2021-22

ROI	Energy node (keV)	Energy interval (keV)	Channel interval	Number of channels
	74			
A		75 - 240	25 - 80	55
	242			
B		243 - 408	81 - 136	55
	410			
C		441 - 576	137 - 192	55
	578			
PL		579 - 660	193 - 220	27
PC	662	663	221	1
PR		666 - 747	222 - 249	27

I3. IRSA/GR

Table I3. The ROI setup for the IRSA/GR shielding experiment in SHIELDMORC 2020 and COMBMORC 2021-22.

ROI	Energy node (keV)	Energy interval (keV)	Channel interval	Number of channels
	74			
A		79 - 238	32 - 84	53
	242			
B		247 - 405	87 - 139	53
	410			
C		415 - 573	142 - 194	53
	578			
PL		582 - 659	197 - 222	26
PC	662	662	223	1
PR		665 - 741	224 - 249	26

I4. Lund University

Table I4-1. ROI application for the Lund University 4 litre NaI(Tl) spectrometer system (Ortec Digibase) using a conversion gain of 1024 channels and setting the energy calibration for Cs-137, 661.66 keV in channel 231 and for K-40, 1460.66 keV in channel 500.

ROI	Compton scattered degree	Channel numbers	Photon energy keV	Number of channels
Node		32	74.1	1
ROI A		33-88	77.0-239.1.0	56
Node	110	89	242.1	1
ROI B		90-145	245.0-407.4	56
Node	58	146	410.3	1
ROI C		147-202	413.3-575.8	56
Node	27	203	578.8	1
ROI PL		204-230	581.8-658.7	27
ROI PC	0	231	661.7	1
ROI PR		232-258	664.6-741.6	27
Node		259	744.6	1

Table I4-2. ROI application for the Lund University 3"x3" NaI(Tl) spectrometer system (Ortec Digibase) using a conversion gain of 1024 channels and setting the energy calibration for Cs-137, 661.66 keV in channel 231 and for K-40, 1460.86 keV in channel 500.

ROI	Compton scattered degree	Channel numbers	Photon energy keV	Number of channels
Node		36	75.9	1
ROI A		37-91	78.9-240.4	55
Node	110	92	243.4	1
ROI B		93-147	246.4-407.7	55
Node	58	148	410.7	1
ROI C		149-203	413.7-575.0	55
Node	27	204	578.0	1
ROI PL		205-231	581.0-658.6	27
ROI PC	0	232	661.7	1
ROI PR		233-259	664.6-742.2	27
Node		260	745.2	1

Table I4-3. ROI application for the Lund University DetectiveX HPGe spectrometer system using a conversion gain of 16383 channels and setting the energy calibration for Cs-137 661.66 keV in channel 3615.87, K-40 1460.86 keV in channel 7979.71, and Tl-208 2614.53 keV in channel 14278.57. (A, B, C, D (PLNaI), P - variant).

ROI	Compton scattered degree	Channel numbers	Photon energy keV	Number of channels
Node		412	74.92	1
ROI A		413-1330	75.11-243.04	918
Node	109.2	1331	243.22	1
ROI B		1332-2249	243.40-411.34	918
Node	57.96	2250	411.52	1
ROI C		2251-3168	411.70-579.64	918
Node	27.0	3169	579.82	1
ROI D (PLNaI)		3170-3598	580.00-658.38	429
Node	4.89	3599	658.57	1
ROI PL		3600-3615	658.75-661.50	16
ROI PC		3616	661.68	1
ROI PR		3617-3633	661.86-664.61	16
ROI P		3600-3632	658.75-664.61	33
Node		3633	664.79	1

I5. NGU

Table I5. The ROI setup for the NGU shielding experiment in SHIELDMORC 2020 and COMBMORC 2021-22

ROI	Energy node (keV)	Energy interval (keV)	Channel interval	Number of channels
	74			
A		77 - 239	26 - 80	55
	242			
B		245 - 407	82 - 136	55
	410			
C		413 - 575	138 - 192	55
	578			
PL		581 - 659	194 - 220	27
PC	662	662	221	1
PR		665 - 743	222 - 248	27
	746			

I6. SSM

Table I6-1. The ROI setup for the SSM shielding experiment in SHIELDMORC 2020 using a 4 liter NaI(Tl) detector (L).

ROI	Energy node (keV)	Energy interval (keV) ± 1.5 keV	Channel interval	Number of channels
	74		34	
A		78 – 238	35 - 90	56
	242		91	
B		244 – 408	92 - 148	57
	410		149	
C		414 – 576	150 - 205	56
	578		206	
PL		582 – 659	207 - 233	27
PC	662	662	234	1
PR		665 – 742	235 - 261	27
	745			

Table I6-2. The ROI setup for the SSM shielding experiment in SHIELDMORC 2020 using a 4 liter NaI(Tl) detector (R).

ROI	Energy node (keV)	Energy interval (keV) ± 1.5 keV	Channel interval	Number of channels
	74		34	
A		76 – 240	35 - 91	57
	242		92	
B		246 – 407	93 - 148	56
	410		149	
C		413 – 575	150 - 205	56
	578		206	
PL		581 – 658	207 - 233	27
PC	662	661	234	1
PR		664 – 741	235 - 261	27
	745			

Table I6-3. The ROI setup for the SSM shielding experiment in SHIELDMORC 2020 using a 120% HPGe detector.

ROI	Energy node (keV)	Energy interval (keV) ± 1.5 keV	Channel interval	Number of channels
	74.1		204	
A		74.5 – 241.8	205 - 663	459
	242.2		664	1
B		242.6 – 409.5	665 - 1122	458
	409.9		1123	1
C		410.2 – 577.6	1124 – 1582	459
	577.9		1583	1
P		653.5 -669.6	1790 - 1834	45

I7. STUK

Table I7. The ROI setup for the STUK shielding experiment in SHIELDMORC 2020 and COMBMORC 2021-22. The channel values represent photon energies with an uncertainty of ± 1.5 keV in relation to the energy nodes recommended by for Lund University model.

ROI	Energy node (keV)	Energy interval (keV) ± 1.5 keV	Channel interval	Number of channels
	74			
A		74 - 242	22 - 69	48
	242			
B		242 - 410	69 - 116	68
	410			
C		410 - 578	116 – 163	48
	578			
PL		578 - 662	163-186	24
PC	662	662	1	1
PR		662 - 746	186 – 209	24
	746			

Appendix J. Instructions for the Source Shielding Calculator, SSC

J1. About SSC

SSC is used in mobile gamma spectrometry to calculate the mass thickness of a shield in front of a Cs-137 point source from count rates in regions of interest (ROI) in a pulse height distribution (measured gamma spectrum). The gamma spectrometer can be of type NaI(Tl) or HPGe. SSC is an Excel application developed by Lund University for the NKS/COMBMORC activity. The application is written in Excel 2000. It contains macrocode, which Excel must allow to obtain full functionality. The application can run on all Windows systems from Windows XP to Windows 10 with any Excel version. It can also run on all open-source applications Libre Office Calc versions.

J2. Method in short

SSC uses a “knowledge library” describing how the net (background subtracted) count rate ratios for scattered to primary radiation vary with the mass thickness of a shield in front of a Cs-137 point source. The principle of obtaining shield thickness is based on measurements of count rates in different energy intervals, representing Compton single and multi-scattering photons in the shield. Count rates from scattered photons are divided by count rates from primary photons that have passed through the shield. The ratio increases exponentially with shield thickness. The parameters in the exponential function can be determined by “calibration” measurements for known shield thicknesses. The shield material must have atomic numbers between 3 and 25 to allow the principle to work. The ordinary building material used in the Nordic countries has atomic numbers within this range. SSC can do both the “calibration” assessment of the exponential parameters given to the “knowledge library” and the calculation of shield mass thickness from a measured pulse height distribution in an actual situation using the “knowledge library”.

J3. Regions of interest (ROI) for shield thickness determination

The analysis of mobile gamma spectrometric measurement data from both primary and scattered radiation uses the relatively simple method of defining a few regions of interest (ROI) over large energy areas instead of using the entire spectrum (in the form of all individual channels in the pulse height distribution). It is relatively easy to implement because all software for gamma spectrometry can output sums of count rates for selectable energy intervals.

For COMBMORC, six ROIs have been used, which represents Compton scattered and primary radiation from a Cs-137 point source. Table J1 gives the selected ROI subdivisions into energy intervals and which photon interaction they generally represent. The exact selection of ROI regions for each team’s gamma spectrometer is given in Appendix I.

For a NaI(Tl) spectrometer, there is always a substantial spread of photon energies into adjacent ROIs because of the spectrometers’ low energy resolution.

For an HPGe spectrometer, the higher energy resolution produces less overlap between primary and Compton scattered photons. The full energy peak ROI P is used in its entity and not divided. The NaI(Tl) energy region ROI PL contains only scattered photons and is for HPGe spectrometers called ROI PLN or ROI D.

Table J1. Generic information on energy regions for NaI(Tl) spectrometers in the COMB-MORC experiments, assuming a channel width of 3 keV. For other channel widths the energy regions may have to be somewhat adjusted to the channel division. The energy intervals guide each gamma spectrometer's final selection of channel regions.

Region designation	Energy interval (keV)	Detected photons from the source are mainly…
ROI A	77 – 239	Compton scattered 110 - 180 degrees and multiple scattered
ROI B	245 – 407	Compton scattered 27 - 58 degrees
ROI C	413 – 575	Compton scattered 0 - 27 degrees
ROI PL	581 – 659	Primary and small angle Compton scattered
ROI PR	665 – 743	Primary
ROI P	581 – 743	Primary and small angle Compton scattered

J4. Calibrating the gamma spectrometer for shield thickness assessment

SSC can accept ROI measurement data (count rates) for known shield thicknesses. After input of measured ROI data, SSC creates an exponential model of shield mass thickness versus ROI count rate ratios and stores the model parameters in a “knowledge library”. Three NaI(Tl) spectrometers and one HPGe spectrometer can be calibrated for shield thickness assessment. Another copy of the SSC Excel file must be used for the calibration of additional detectors.

Calibration input for up to three NaI(Tl) spectrometers uses worksheets InputCalib(1), InputCalib(2), and InputCalib(3), respectively. Calibration input for an HPGe spectrometer uses the worksheet InputCalib(4).

J5. Assessing a shield thickness from gamma spectrometric data

SSC can accept ROI measurement data (count rates) from a gamma spectrometer to assess the shield mass thickness in front of a point source, provided that the spectrometer calibration parameters have been stored in the SSC “knowledge library”.

Assessing the shield thickness from a NaI(Tl) spectrometer ROI count rate data uses the worksheet Shield(NaI). An HPGe spectrometer uses the worksheet Shield(HPGe).

J6. Dimensions and limitations of SSC

In the current version, SSC is programmed for calibration input from three NaI(Tl) spectrometers and one HPGe spectrometer. In addition, calibration parameters from previous measurements on shielded sources are stored in the “knowledge library”.

Shield thickness assessment presumes that the shield is of slab type with an atomic number between 3 and 25, where Compton scattering is the dominating effect for gamma radiation with energies between 100 and 1000 keV. The method does not work for lead shields.

SSC may give wrong shield thickness values if a source is far from a shield of non-uniform lateral extent. This source-shield geometry is, for example, the case if a source is in the middle of a house with windows toward the detector. Gamma radiation passing through the windows will not be Compton scattered to the same extent as in the thicker walls, and SSC will underestimate the wall thickness.

J7. Calibrating for shield thickness, example of input data

Fig J7-1 shows the SSC shield thickness calibration sheet “InputCalibNaI(1)”, which is for a NaI(Tl) detector. If more than one NaI(Tl) detector, you can also use “InputCalibNaI(2)” and “InputCalibNaI(3)”.

For an HPGe detector, use “InputCalibHPGe(4)”.

Inputs should be made in the blank fields close to the marked yellow fields.

Start by filling in “Team and detector”. The description will be stored in the “knowledge library”.

There are 13 possible calibration setups preprogrammed (marked in blue). At least two calibration measurements with different shield thicknesses must be input to generate an input to the “knowledge library”.

Input the distance from the detector to the source (within ± 1 m). It will be the same distance for all measurements if the detector is kept stationary during the calibration measurements.

Input the background count rates for all ROI representing the site. The background count rates will be valid for all measurements if the detector is kept stationary during all calibration measurements.

Input the measured gross count rates for all ROI for the specific shield thickness setup. SSC will automatically subtract the background count rate to obtain the net count rate from the source, and SSC calculates the net ROI ratios.

Valid for	Your NaI(Tl) detector (1) calibrated in COMBMORC					Team and detector:		Lund University 4 litre NaI(Tl)-detector, rear-(left)-right					
Detector number in database	1		Radionuclide:	Cs-137 point source									
Known shield material	Air only	Wood	Wood	Wood	Wood	Concrete	Concrete	Concrete	Concrete	Concrete	Concrete	Concrete	Concrete
Known shield thickness (cm)	0	4.5	9	13.5	18	5	10	15	20	25	30	35	40
Known shield density (kg/m3)	0	522	522	522	522	2382	2382	2382	2382	2382	2382	2382	2382
Mass thickness (kg/m2)	0	23.49	46.98	70.47	93.96	119.1	238.2	357.3	476.4	595.5	714.6	833.7	952.8
Input distance to source (m)	16	16	16	16		16	16	16	16	16	16		
Total mass thickness (kg/m2)	19.888	43.378	66.868	90.358		138.988	258.088	377.188	496.288	615.388	734.488		
Input measured background (cps)													
ROI A	940.167956	940.168	940.168	940.168		940.168	940.168	940.168	940.168	940.168	940.168		
ROI B	350.933333	350.9333	350.9333	350.9333		350.9333	350.9333	350.9333	350.9333	350.9333	350.9333		
ROI C	164.662615	164.6626	164.6626	164.6626		164.6626	164.6626	164.6626	164.6626	164.6626	164.6626		
ROI PL	65.2729282	65.27293	65.27293	65.27293		65.27293	65.27293	65.27293	65.27293	65.27293	65.27293		
ROI PC	1.78895028	1.78895	1.78895	1.78895		1.78895	1.78895	1.78895	1.78895	1.78895	1.78895		
ROI PR	42.9289134	42.92891	42.92891	42.92891		42.92891	42.92891	42.92891	42.92891	42.92891	42.92891		
ROI P	109.990792	109.9908	109.9908	109.9908		109.9908	109.9908	109.9908	109.9908	109.9908	109.9908		
Input measured gross (cps)													
ROI A	1974.27751	1974.457	1935.207	1880.995		4258.132	3101.23	5686.233	4498.303	3910.459	3665.67		
ROI B	950.797788	907.8957	869.1307	821.2758		1941.657	1334.564	2416.265	1751.951	1437.697	1270.278		
ROI C	518.954713	506.9434	494.2725	469.578		1218.064	778.0625	1283.766	783.7453	552.1091	432.1909		
ROI PL	433.382833	379.2853	325.7564	314.7804		771.7684	412.1687	638.0333	328.7744	185.2303	123.6178		
ROI PC	36.1911532	29.48315	25.57516	22.5796		58.44444	25.85353	40.16041	17.67116	8.58723	4.903827		
ROI PR	330.515008	275.2909	259.0508	208.8338		550.0538	255.8454	421.8782	195.5565	113.4701	71.3332		
ROI P	800.088994	684.0594	610.3823	546.1937		1380.267	693.8677	1100.072	542.0021	307.2876	199.8548		

Fig J7-1. SSC sheet for shield thickness calibration. Data should be written in the empty fields close to the marked yellow fields. The example shows input from ten calibration measurements. At least two measurements are needed to generate an input to the “knowledge library”.

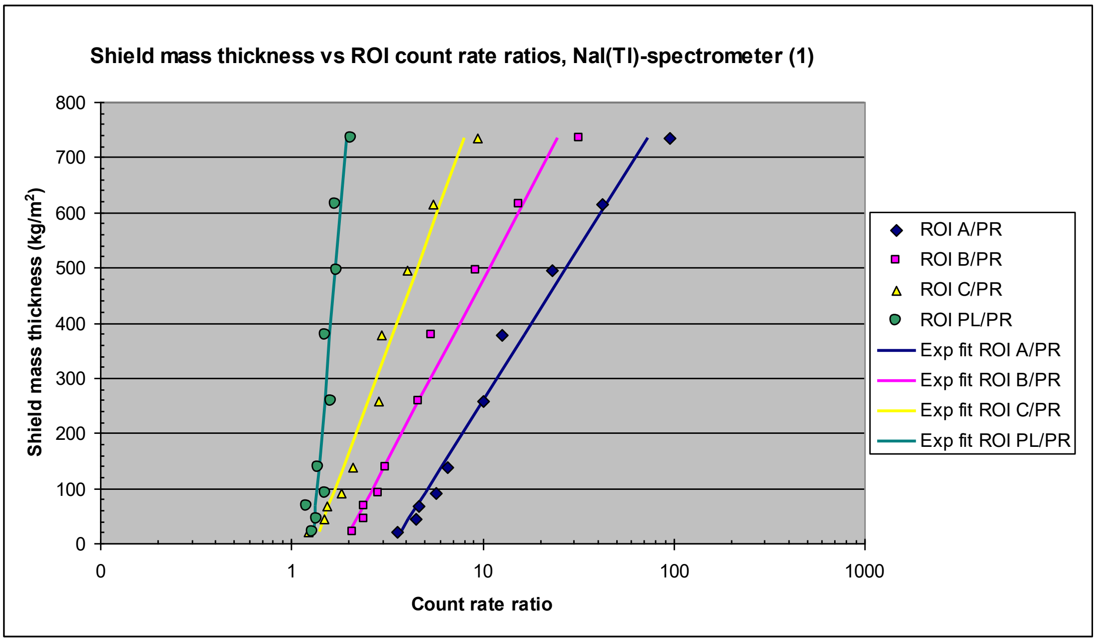

Fig J7-2. A plot of ROI quotas is automatically shown in the SSC “InputCalib” sheet diagram when at least two calibration measurements with different shield thicknesses have been written into the table’s fields. The straight lines show how the exponential function fits the given data. The exponential function’s parameters (slope and intercept in the logarithmic conversion) are stored in the “knowledge library”.

J8. Assessing a shield thickness from a measured pulse height distribution

Fig J8-1 shows a shield thickness calculation sheet. The three sheets “ShieldNaI(1), Shield NaI(2), and ShieldNaI(3)” are for measurements with NaI(Tl) spectrometers and the fourth sheet, “ShieldHPGe(4)” for HPGe spectrometers.

Provide input data at the yellow fields
Privide optional input, if the source-detector distance is known
Calculated shield mass thickness is obtained in the green and blue fields

Error messages

Team and setup	Lu, Setup M1, Location 0
Select detector	Your NaI(Tl) detector (3) calibrated in COMBMORC
Nr in database: 3	Lund University 3"x3" NaI(Tl)-detector

	Measured by gamma spectrometry			Method	Calculated by exponential model			Calculated by polynomial model		
ROI	Input background count rate (cps)	Input measured gross count rate (cps)	Net count rate (cps)	ROI */PR ratios	Shield and air mass thickness (kg/m^2)	Shield only mass thickness (kg/m^2)	Deviation from observed (%)	Shield and air mass thickness (kg/m^2)	Shield only mass thickness (kg/m^2)	Deviation from observed (%)
A	178.14	259.81	81.67	10.264	128.37	52.54	69.3	110.30	34.48	45.5
B	54.36	81.22	26.86	3.376	86.13	10.31	13.6	74.61	-1.21	-1.6
C	22.48	34.51	12.03	1.512	23.94	-51.88	-68.4	43.31	-32.51	-42.9
PL	8.99	18.97	9.97	1.253	42.01	-33.81	-44.6	92.66	16.84	22.2
PR	5.50	13.46	7.96	Average	70.11	-5.71	-7.5	80.22	4.40	5.8
P	14.72	33.44	18.72							

				Method	Calculated by exponential model			Calculated by polynomial model		
ROI	Background count rate (cps)	Measured gross count rate (cps)	Net count rate (cps)	ROI */P ratios	Shield and air mass thickness (kg/m^2)	Shield only mass thickness (kg/m^2)	Deviation from observed (%)	Shield and air mass thickness (kg/m^2)	Shield only mass thickness (kg/m^2)	Deviation from observed (%)
A	178.14	259.81	81.67	4.363	136.38	60.56	79.9	122.86	47.04	62.0
B	54.36	81.22	26.86	1.435	91.72	15.89	21.0	78.50	2.68	3.5
C	22.48	34.51	12.03	0.643	21.31	-54.51	-71.9	43.72	-32.11	-42.3
P	14.72	33.44	18.72	Average	83.14	7.31	9.6	81.69	5.87	7.7

Option: Observed without gamma spectrometry				Observed	
Source detector distance (m)	Air mass thickness (kg/m^2)	Optional-Shield thickness observed (cm)	Optional-Shield material density (kg/m^3)	Shield and air mass thickness (kg/m^2)	Shield only mass thickness (kg/m^2)
61.00	75.82			75.82	0.00

Fig J8-1.The SSC "ShieldNaI(3)" calculation sheet to assess shield mass thickness from count rates in different ROI in the pulse height distribution of a calibrated gamma spectrometer. The calculation uses the exponential function of shield thickness versus ROI count rate ratios with function parameters stored in the "knowledge library".

Input data in the blank fields near the marked yellow areas.

Input Team and Setup number (will only be stored on the same page)

Select detector in the drop-down combo box. If there is a calibration for the selected detector, data from the "knowledge library" will be shown. Parameters from the team's 2020 measurements at the home laboratory are stored in the "knowledge library".

Input the background count rates and the gross count rates for the ROIs. In COMB-MORC, the background is measured at the site when the source is absent. In an actual situation with a source present, the background must be estimated some other way, for example, by measuring far from a suspected source.

Input the estimated distance to the source to correct for Compton scattering in the air between the source and the detector.

SSC calculates the mass thickness of the shield, assessed individually for the four ROI ratios ROI A/PR, ROI B/PR, ROI C/PR, ROI PL/PR and for the three ROI ratios ROI A/P, ROI B/P, ROI C/P. These should, at best, produce approximately the same shield mass thickness. Suppose there is a significant deviation between the four ROI ratio assessments. Then, there is something deviant in assuming a uniform slab shield in front of the source, a wrong detector calibration or insufficient statistical accuracy in the measurement.

If the shield thickness and material are known (as they will be in COMBMORC), the correct observed thickness can be input at the marked green fields. The SSC will show the percentage deviation between the calculated and known shield thickness.

Fig J8-2 shows the four calculated versions of the shield mass thickness obtained from the four ROI count rate ratios using the exponential model related to ROI PR. In addition, the four exponential functions are shown as straight lines in the logarithmic diagram. Maximum and minimum values in the calculation are given as solid red lines, and the observed (actual) value is shown as a blue line.

The current version of SSC shows four result diagrams for NaI(Tl)- detectors, two for the exponential model (related to ROI PR and ROI P) and two for the five-degree polynomial model (related to ROI PR and ROI P). For an HPGe-detector, two diagrams are shown, one for the exponential model and one for the five-degree polynomial model (related to ROI P).

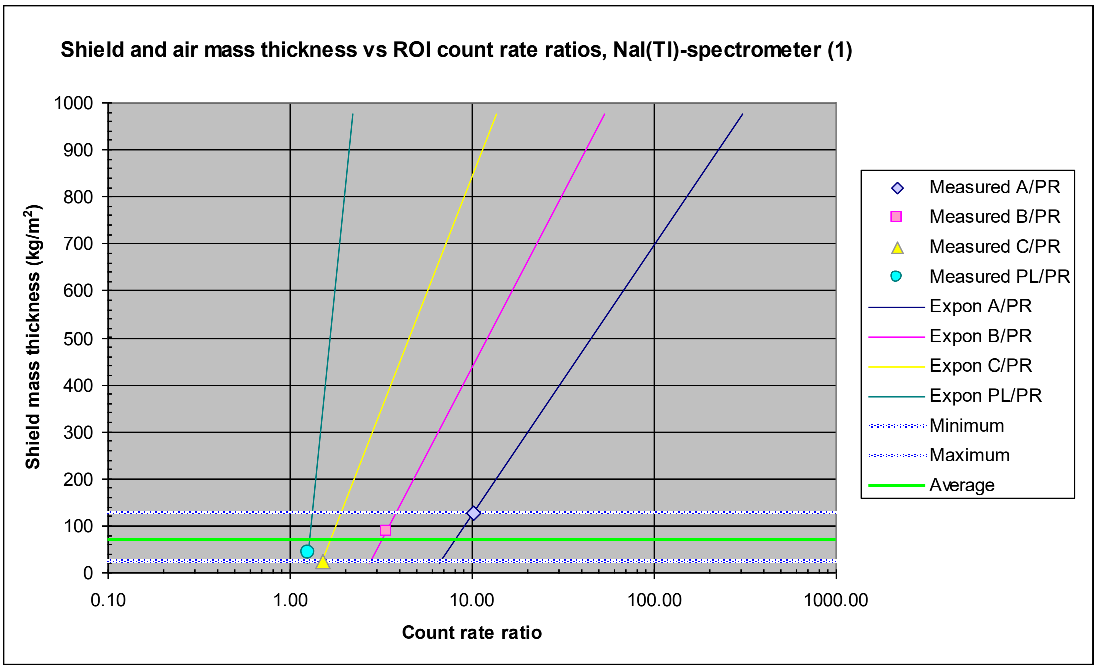

Fig J8-2. Diagram showing the calculated shield thickness result for the four ROI count rate ratios. Solid, differently coloured lines represent the four exponential functions with parameters from the “knowledge library”. Dotted white-blue lines mark the minimum and maximum thickness values, and the solid green line marks the average shield thickness from the four ROI ratios.

J9. Saving data from SSC

After inputting values to SSC and obtaining the calibration or a shield thickness, values can be saved in one of the following ways:

(1) On the Excel menu bar, choose “File” and “Save as”. Choose “Microsoft Excel 97-2003 Workbook (*.xls) and provide a file name according to the principle for COMBMORC, which saves the entire workbook. It is suitable for recalculation because measured data must not be input again. Note that if saving the workbook as a *.xlsx file, the macrocode is lost, and no drop-down menu will be available.

(2) On the Excel menu bar, choose “File” and “Save as”. Choose “Comma delimited” (*.csv) and provide a file name according to the principle for COMBMORC, which saves the current worksheet data as a comma-delimited file. It does not save the workbook, and this is suitable if you only want to save input data and the result in numeric form. The saved file will not display the diagrams.

(3) On the Excel menu bar, choose “File” and “Print”. Choose PDF and provide a file name according to the principle for COMBMORC, which saves the current worksheet as a PDF file. This way of saving data is suitable for documenting input data, the calculated result and the diagrams. However, for a recalculation, data must be input to SODAC again.

J10. Starting a new calculation

After saving all data, exit the current Excel program and start over again with the file “SSC.XLS”

Appendix K. Instructions for the Source Distance and Activity Calculator, SODAC

K1. About SODAC

SODAC is used in mobile gamma spectrometry to calculate the distance and activity of a Cs-137 point source from a set of count rate measurements in the full energy peak along a straight route past the source. The gamma spectrometer can be of type NaI(Tl) or HPGe. SODAC is an Excel application developed by Lund University for the NKS/COMBMORC activity. The application is written in Excel 2000. It contains macrocode, which Excel must allow to obtain full functionality. The application can run on all Windows systems from Windows XP to Windows 10 with any Excel version. It can also run on all open-source applications Libre Office Calc versions.

K2. Method in short

SODAC uses a “knowledge base” describing how the photon fluence (the “intensity”) curve varies along a straight route for different source distances. The curve that best fits the measured input data determines the distance. With knowledge of the distance and the detector efficiency (the effective detector area), the source activity is calculated, assuming the source is unshielded. If the source is shielded, SODAC underestimates the source activity. The shielding effect can be adapted by giving an estimated value of the shield thickness. The adoption presumes the shield is a plane slab of standard building materials.

K3. Unshielded sources

The input measurement data should be the gross count rate (cps) in the full energy peak measured at least at three locations along the route. In addition, an estimate of the background count rate (without the source) should be given.

Measurements points should be in a straight line along the route so that the maximum count rate is found and that measurement points lie before and after the maximum. Otherwise, the source distance and activity may be underestimated. If the measurement route is curved, wrong distance and activity values will be obtained.

Measurements should be made while standing still at the measurement points. Any movement during measurements will deteriorate the spatial resolution and impair the precision of the calculated source-distance value.

K4. Shielded sources

The shielding of a source can be obtained by measuring the net (background subtracted) count rate ratio of scattered to primary radiation. The SSC (Source Shielding Calculator) application can estimate the shielding thickness from measured scattered and primary components in the gamma spectrometer's pulse height distribution.

If it is assumed that a slab shield, such as a wall of wood, brick or concrete, shields the source, the estimated shield thickness can be input to SODAC. A slab shield alters the "intensity" curve and makes it narrower. The application looks for the most probable distance (further away) that fits the narrowed curve and then recalculates the (higher) activity that will produce the same count rate in the detector.

SODAC can estimate slab shield thicknesses from the variation in primary count rates along the route if enough well-spaced measurement points related to the source distance are obtained. An example is given in Fig K6-6 and K6-7.

In the shielding calculations, it is presumed that the slab shield is parallel with the measuring route. If that is not the case and the angle between the slab shield and the route is larger than 30 degrees, shielding values obtained by SSC or SODAC may be in error.

K5. Dimensions and limitations of SODAC

In the current version, SODAC is programmed for a route length of up to 600 m with measurement points interspaced at 5 m. The "knowledge base" contains intensity curves for source distances from 5 to 150 m in 5 m steps. The application will give wrong distance and activity values for sources closer than 5 m and farther away than 150 m from the road. In future versions, however, it may be possible to alter these limitations.

K6. Example of input data and calculations

Fig K6-1 shows the startup screen.

Start by choosing "Team and instrument" in the drop-down menu. This determines the efficiency value used for the activity calculation. Values are based on previous efficiency measurements from COMBMORC 2021 and AUTOMORC 2018. (Fig K6-2).

Input the background count rate (the full energy peak ROI P cps) representing the site. (Fig K6-2).

In column 2, start giving gross count rates (cps) from ROI P measured in chosen points along the road. Road coordinates run from - 300 m to +300 m in 5 m steps. Data can be input in column 2, starting anywhere, but the spacing between measurement points in steps of 5 m must be correct. The routine automatically adjusts the highest input value to the road coordinate zero and relocates the other coordinates accordingly. (Fig K6-3).

After input of the first cps value, an "intensity" curve for a distance of 5 m is shown in the diagram, which is the start guess. It is probably a wrong guess, but the routine cannot calculate better until the next measured value is given.

After input of the second cps value, an "intensity" curve for the best fit of the two values is shown. The road-source distance from the maximum cps point is shown in the diagram and given at the green marking. In addition, the calculated source activity is displayed. The calculated distance and activity values may have significant uncertainties, and more input data is needed.

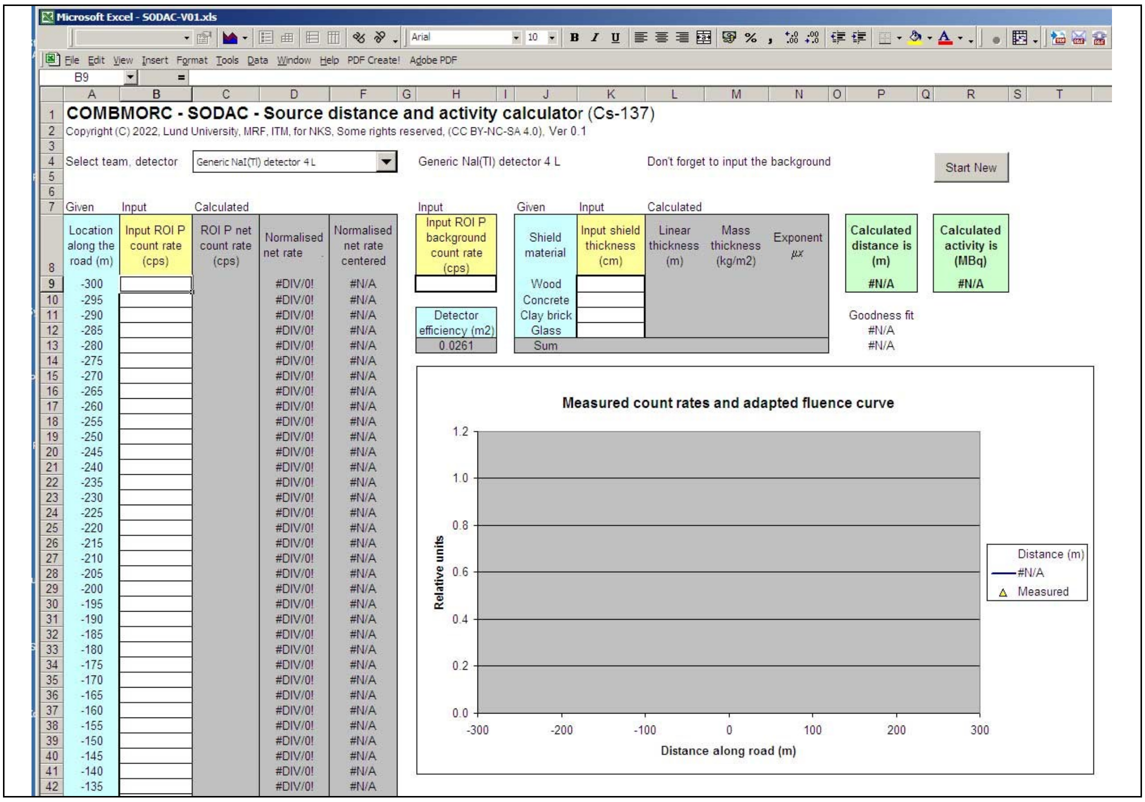

Fig K6-1. SODAC at startup. Input can be given at the drop-down menu "Select team and detector" and at the three columns marked with the yellow heading: "ROI P count rate (cps), ROI P background count rate (cps), and Shield thickness (cm)".

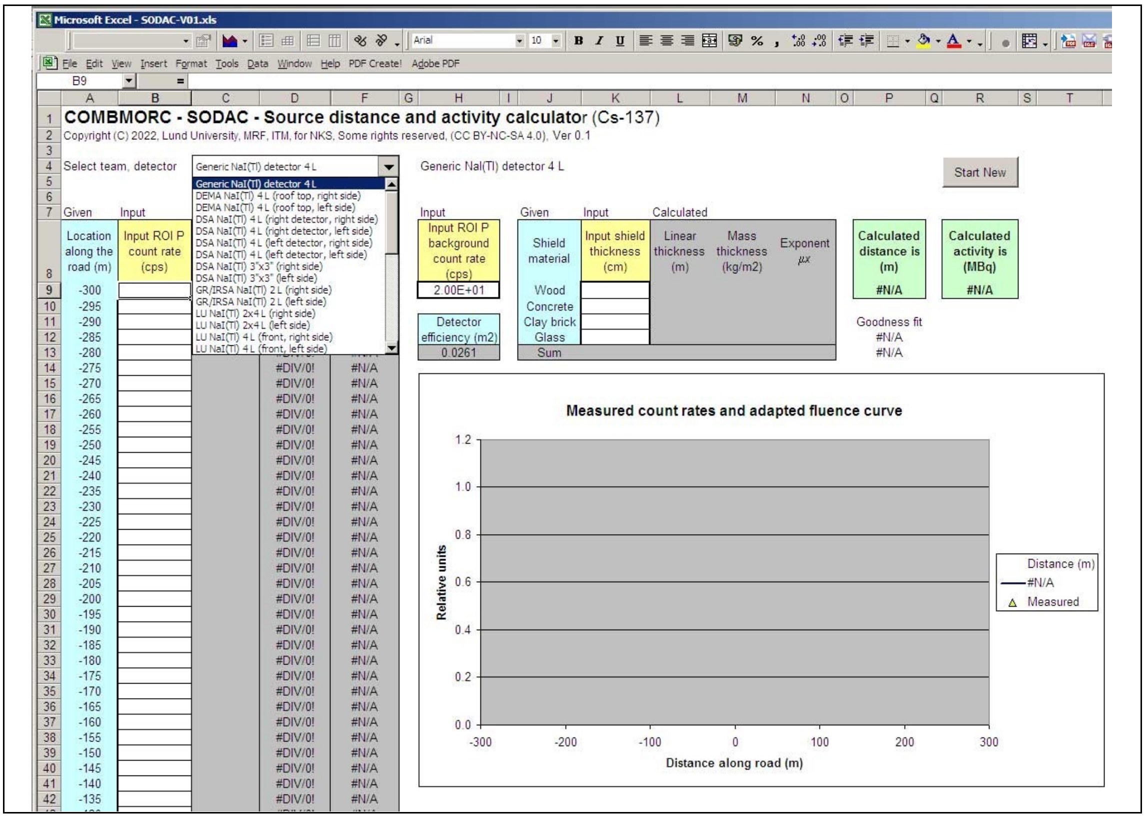

Fig K6-2. The drop-down menu for choosing team and detector. Example input of background count rate (20 cps) obtained in ROI P.

After inputting the third cps value (and additional values), a goodness of fit is displayed. The range is from 0 to 100 %. The rating of 100 % means that all measured cps values are precisely on the “intensity” curve. Ratings near zero imply a bad fit of all cps values except the maximum value forced to 1. The displayed distance and activity values are probably wrong with a bad fit.

Fig K6-3 shows the result of four cps values with 10 m spacing. The routine has corrected the maximum input value 250 at road coordinate -20 in column 2 to coordinate zero and normalized it to 1. The other coordinates are recalculated accordingly and displayed in column 5. The best fit to the data is the “intensity” curve for a source at 25 m from the maximum point at the road.

Fig K6-4 shows the source's distance and calculated activity in the green-marked areas up to the right. A goodness of fit is displayed if three or more cps measurement data have been input. In this figure, two additional cps values have been input, indicating that a maximum cps value has been found along the route and that the source likely is located at a 25 m distance perpendicular to the road from the maximum point.

Fig K6-5 shows the same cps measurement data as in Fig K6-4 but with a larger (double) interspaced distance between each measurement point, which produces a broader “intensity” curve. The broader curve indicates a longer distance to the source, here 35 m, and the longer distance results in a higher source activity, 1600 MBq.

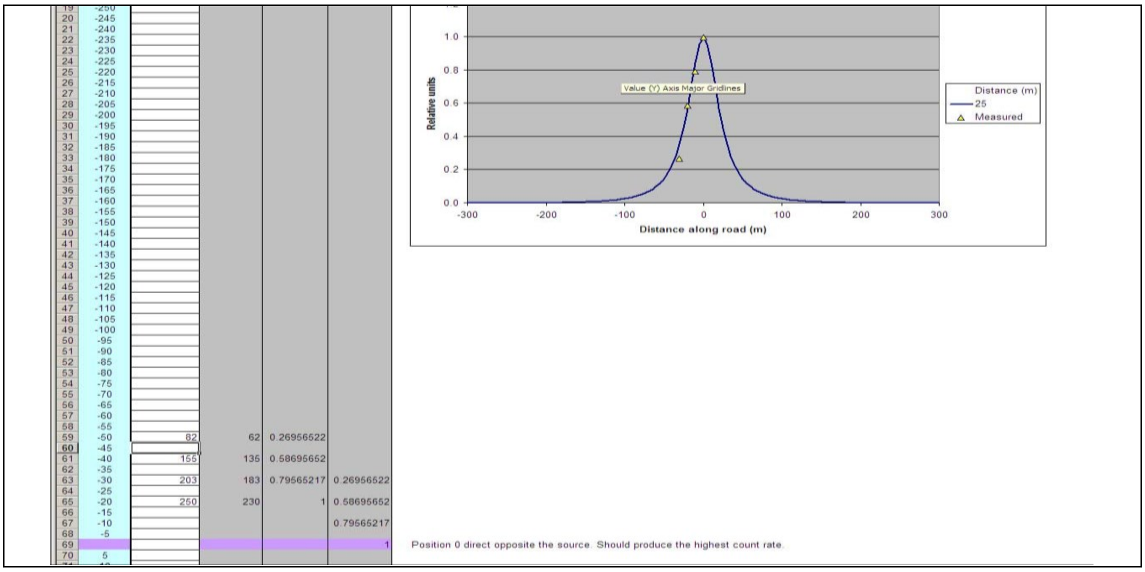

Fig K6-3. Input of cps values 82, 155, 203, and 25 at road coordinates -50, -40, -30, and -20 m. Input data is normalized, and the maximum value is adjusted to road coordinate zero. The diagram displays the “intensity” with the best fit of the data, which corresponds to a road-source distance of 25 m.

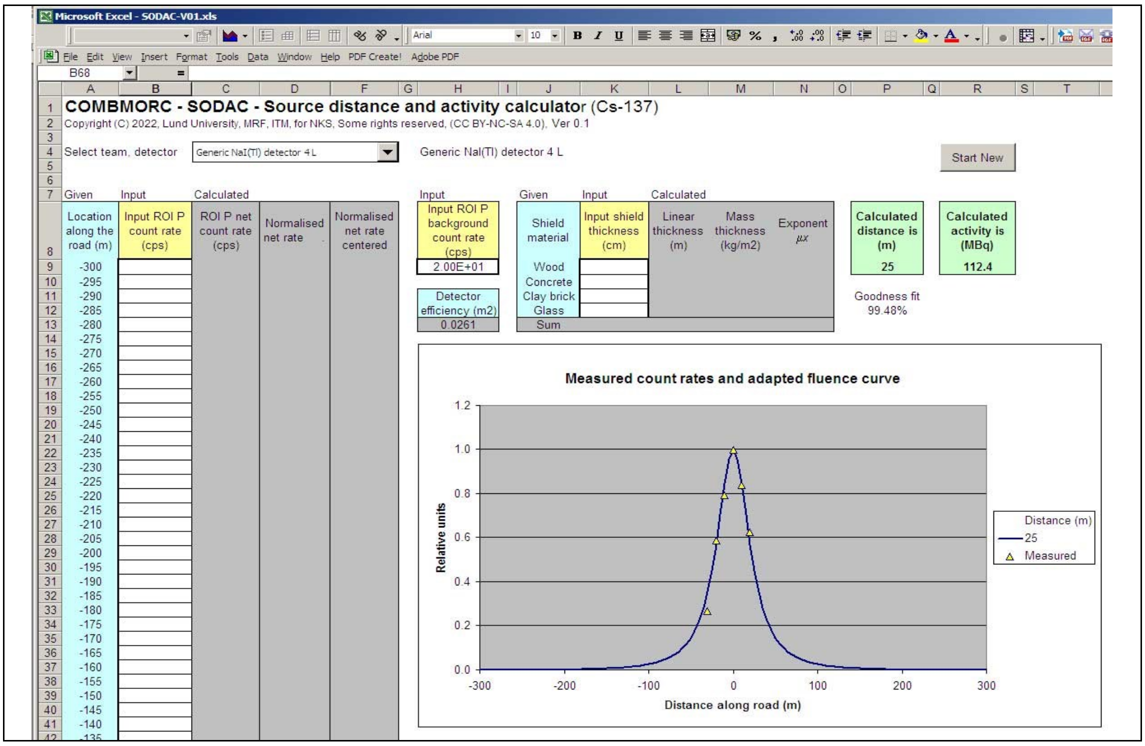

Fig K6-4. Two additional cps values along the road have been input, indicating that the point of maximum count rate has been found with an uncertainty of about ±5 m. The distance to the source is calculated to 25 ±5 m (Distances are calculated in 5 m steps).

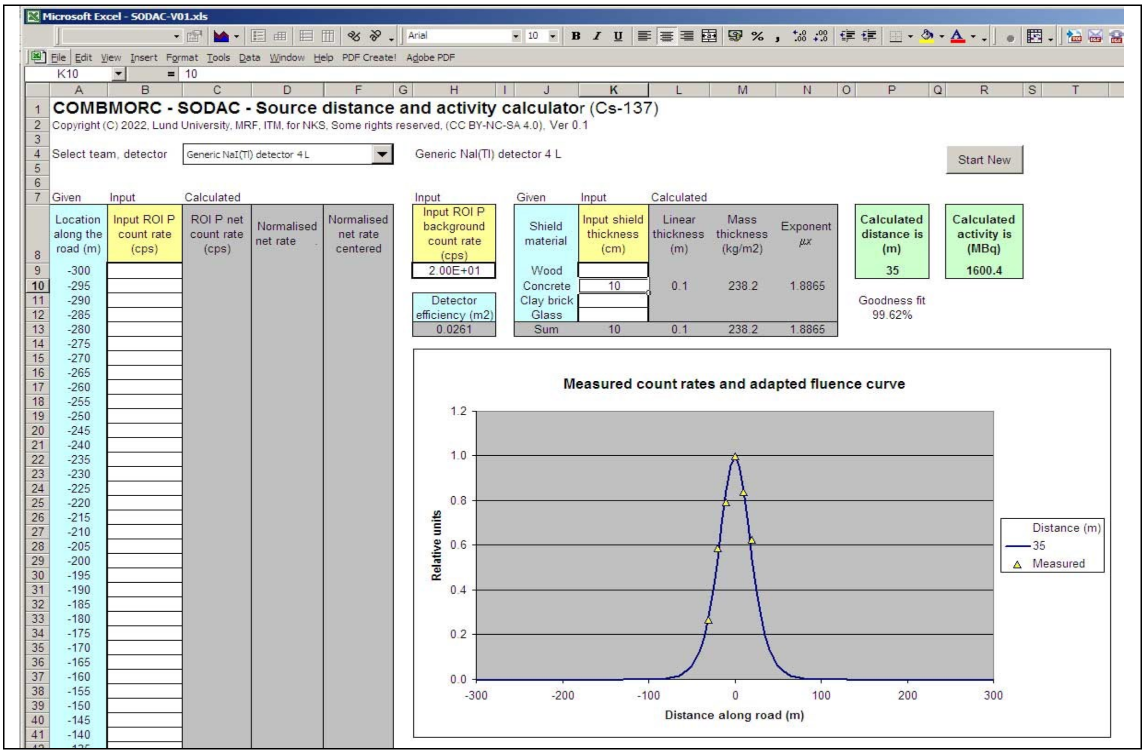

Fig K6-5. The same cps measurement data as in fig 4, but with a larger interspaced distance between each measurement, produces a broader “intensity” curve. The broader curve indicates a longer distance to the source; 35 m — the longer distance results in higher activity, 1600 MBq.

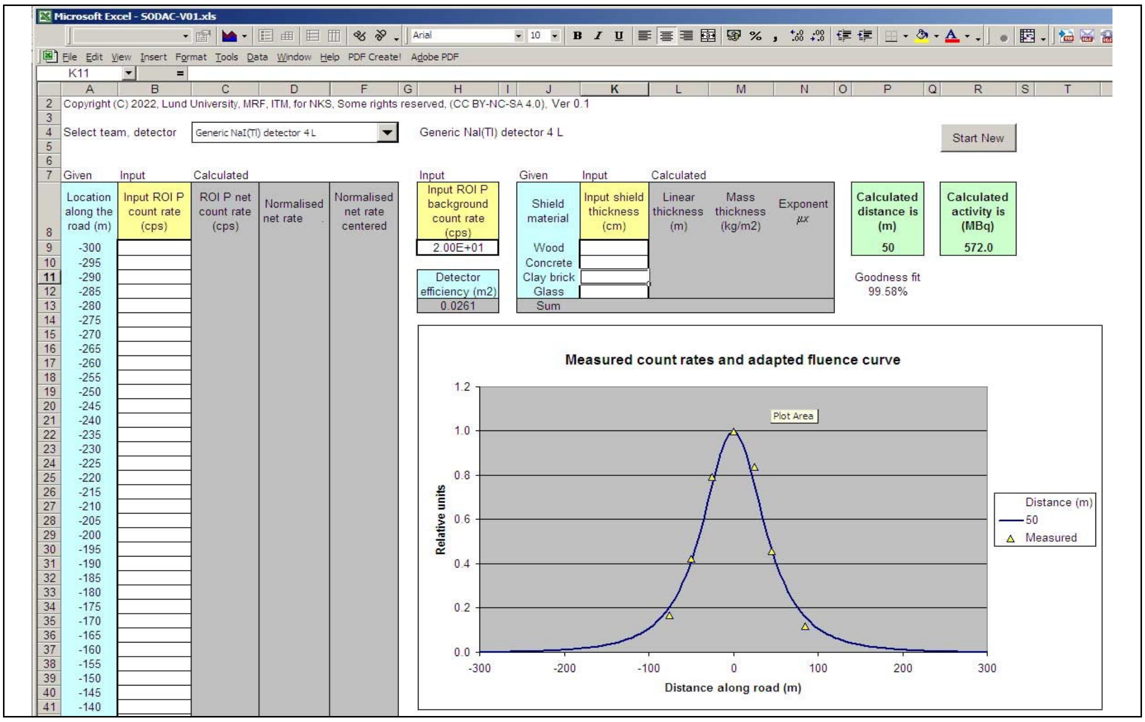

Fig K6-6. Count rate data at points along the measurement route indicate the presence of a shield in front of the source because measurement points at larger distances show decreased values below the fit to the "intensity" curve.

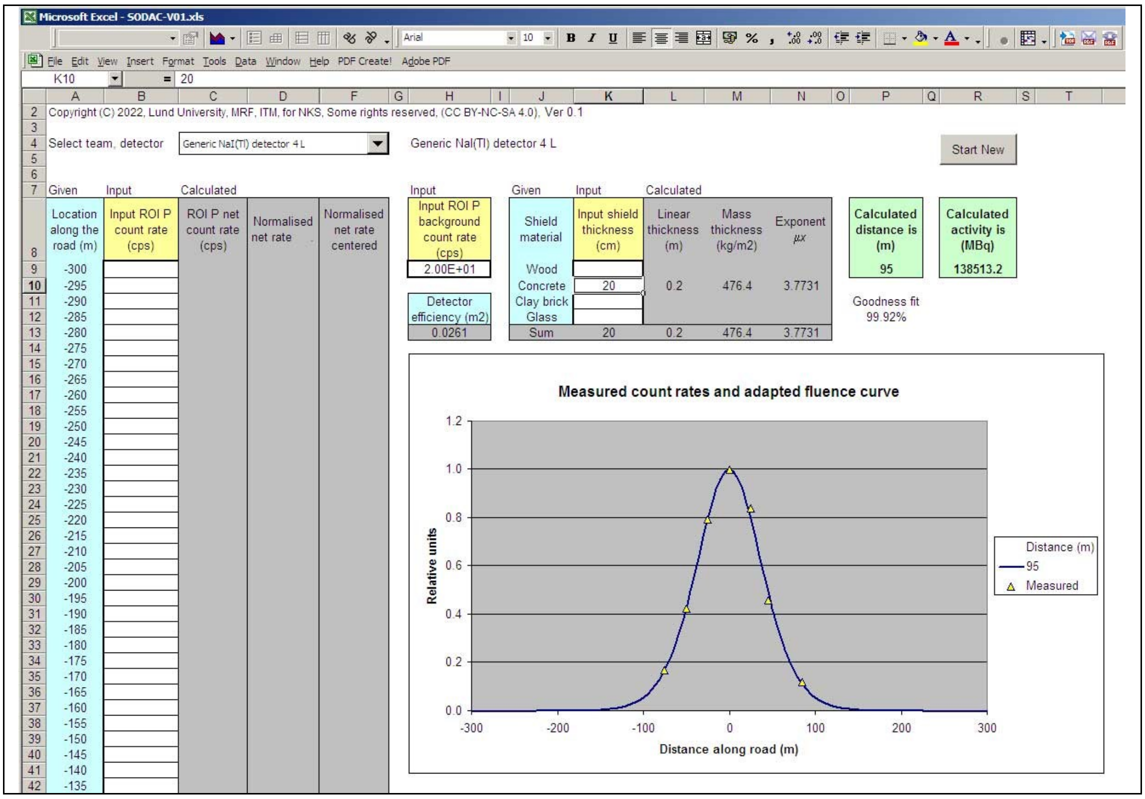

Fig K6-7. A better fit of the "intensity" curve may be obtained by testing different shield thicknesses. When the highest value of the goodness of fit is obtained, a value of the shield thickness is likely found.

K7. Correction for a detector's uneven angular efficiency

All participating teams in the COMBMORC experiments except STUK used horizontally oriented 4 litres, 2x2 litre or 4x4 litre NaI(Tl) detectors. These detectors all have a long shape, resulting in varying sensitivity for recording photons incident on the detector in the horizontal plane. The angle-dependent efficiency for a 4-litre NaI(Tl) detector was determined in connection with the NKS/AUTOMORC experiments in 2018. Fig K7-1 shows how the angular efficiency varies for different incidence angles relative to 90 degrees, i.e. directly to the right of the detector when mounted horizontally in the measuring vehicle. Suppose one does not correct the measurement data for the lower efficiency of obliquely incident photons relative to 90 degrees. In that case, the photon fluence from a point source will be underestimated when the source is not directly at 90 degrees. The underestimation can be significant if the source is in the 20 - 30 degree direction, but there will also be some underestimation in the 40 - 60 degree direction. Without correction, this underestimation of the photon fluence from the source makes the source appear closer to the measurement vehicle than in reality because the measured "intensity curve" (photon fluence rate) decays more rapidly on the sides of the maximum, as it would for a detector with uniform angular efficiency if the source were closer to the measurement vehicle.

A correction routine is introduced in SODAC to avoid underestimating the distance to a radiation source due to the varying angular efficiency of a horizontally oriented oblong NaI(Tl) detector. The routine recalculates the full energy peak areas ROI PL, PR and P at an assumed angle to the radiation source relative to 90 degrees. Table K7-1 and Fig K7-2 give values for this conversion for different photon incidence angles.

However, the angles of incidence are not known when the distance to the source is unknown. There are, thus, two unknown variables to the solution. In SODAC, there is an option to test distances (with the associated angle corrections) in order to find an "intensity curve" from the "knowledge library" that provides the best fit to the angular-corrected measurement data. This solution improves the distance determination but still entails some uncertainty in the distance at low count rates in the detector where the statistical variation in the measurement data may be significant.

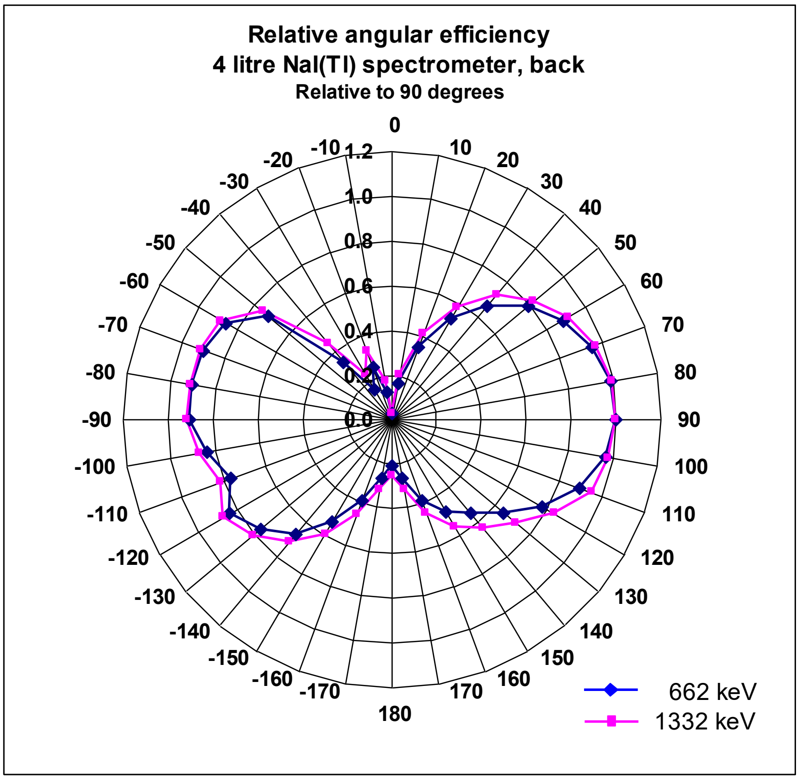

Fig K7-1. Relative angular efficiency for the 4 litre NaI(Tl)-detector (rear) used in mobile gamma spectrometry by Lund University, measured in the NKS/AUTOMORC experiments 2018.

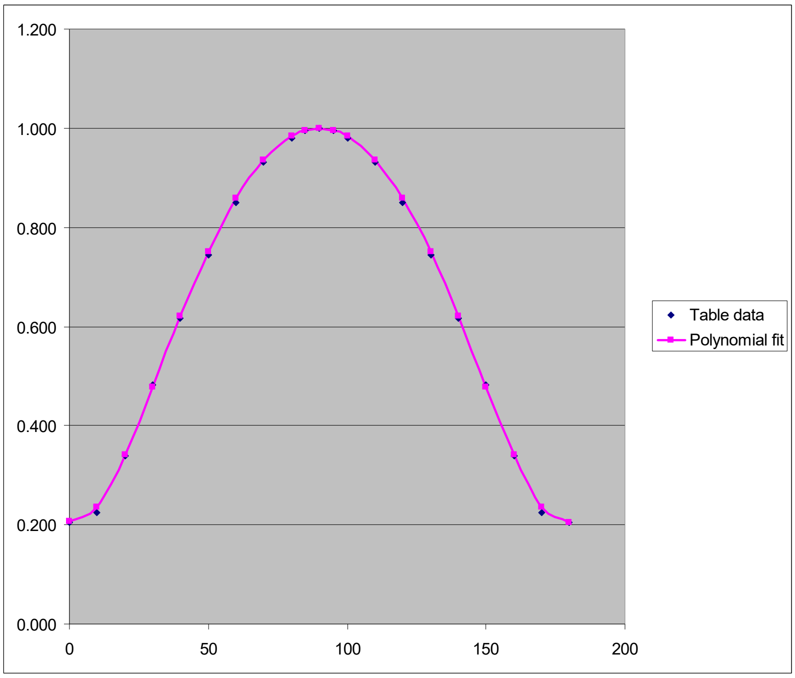

Fig K7-2. Relative angular efficiency for a horizontally oriented 4 litre NaI(Tl)-detector assumed in SODAC and based on angular calibration measurements in NKS/AUTOMORC 20218 (Fig K7-1).

Table K7-1 Assumed relative angular efficiency for a mobile 4 litre NaI(Tl)-detector with its short side facing forward in the driving direction. Data are based on angular calibration measurements made by Lund University 2018, here setting the efficiency at 90 degrees (direction to the right side of the vehicle and the detector) to 1 and assuming a symmetric distribution of the angular efficiency.

Angle of incidence for primary photons	Relative efficiency normalized to angel of incidence 90 degrees
0	0.205
10	0.215
20	0.350
30	0.483
40	0.616
50	0.745
60	0.850
70	0.932
80	0.980
90	1.000
100	0.980
110	0.932
120	0.850
130	0.745
140	0.616
150	0.483
160	0.350
170	0.215
180	0.205

K8. How to find the shield thickness by SODAC calculation

Suppose a slab shield of ordinary building material shields the source, and the shield is parallel with the measurement route. Then the thickness of the shield may be assessed by looking at the attenuation of primary photons at different angles from the source. A thick shield will attenuate more primary photons when penetrating the shield at large angles than a thin shield. The “intensity” curve caused by the shield can be identified by measuring the decrease in the count rate from primary photons (ROI P) at increased distances from the maximum value along the route. As a rule of thumb, this distance to a measurement point along the route to detect the reduction in the photon fluence (compared to air attenuation only) should be at least the same as the road-source distance at the maximum point (i.e. 45 degrees angle to the source).

A minimum of 6 measurement points with good statistics should be obtained on both sides of the maximum value to detect a reduction of the primary photon fluence due to a slab shield. At least two points should be chosen at 45 degrees or larger between the normal to the road and a line from the source to the gamma spectrometer.

It should be noted that the reduced photon fluence from the source at larger distances along the route from the maximum value needs longer measurement times to obtain the same statistical accuracy as at the maximum point. At 45 degrees, the measurement time should be about four times longer than at the maximum point.

Fig K6-6 shows an example of count rate data at points along the measurement route indicating, the presence of a shield in front of the source because measurement points at larger distances show decreased values below the fitted “intensity” curve.

Fig K6-7. Shield thickness values can be given under the yellow marking “Input shield thickness (cm)”. By testing how the “intensity” curve fits the data points for different shield thicknesses, a better fit of the “intensity” curve may be obtained. The shielding thickness is likely found when the highest goodness of fit is obtained.

K9. Saving data from SODAC

After inputting values to SODAC and obtaining the distance and activity of the source, values can be saved in one of the following ways:

(1) On the Excel menu bar, choose “File” and “Save as”. Choose “Microsoft Excel 97-2003 Workbook (*.xls) and provide a file name according to the principle for COMBMORC, which saves the entire workbook. It is suitable for recalculation because measured data must not be input again. Note that if saving the workbook as a *.xlsx file, the macrocode is lost, and there will be no drop-down menu.

(2) On the Excel menu bar, choose “File” and “Save as”. Choose “Comma delimited” (*.csv) and provide a file name according to the principle for COMBMORC, which saves the “Input” worksheet data as a comma-delimited file. It does not save the workbook. This alternative is suitable if one only wants to save input data and the result in numeric form. The saved file will not display the “intensity” curve.

(3) On the Excel menu bar, choose “File” and “Print”. Choose PDF and provide a file name according to the principle for COMBMORC, which saves the Input worksheet as a PDF file. It is suitable for documentation to save input data, the calculated result and the fitted “intensity” curve this was, but for a recalculation, data must be input to SODAC again.

K10. Starting a new calculation

A new calculation can be started in two ways

(1) Click “Start New” at the top-right of the Input worksheet. All input values are erased.

(2) Exit the current Excel program and start over again with the file “SODAC.XLS”.

Appendix L. Formats for measurement data reporting

Data should be given as comma separated values (csv), row by row, where a "," separates each value and a "." represents the decimal dot. Each file should contain measurements from one round. Rounds are to be numbered at the end of the file name.

The contents of a csv-file should follow this format:

Value number	Contains	Example:
1	Date (dd-mmm-yy)	13-oct-22
2	Time (hh:mm:ss)	11:35:23
3	Acquisition time interval in seconds	1
4	North coordinate in WGS84 decimal value	55.761982
5	East coordinate in WGS84 decimal value	12.931692
6	Counts in the ROI A	152
7	Counts in the ROI B	148
8	Counts in the ROI C	121
9	Counts in the ROI PL	135
10	Counts in the ROI PR	83
11	Counts in the ROI P	238
12	Additional comment, text	Location A+30m

The counts given as value numbers 6 - 11 should be the gross number of counts in the ROI (not the count rate) for the specific radionuclide without any background subtraction or other type of compensation. Value number 12 is and additional text comment, for example noting a marked location along the measurement road.

Appendix M. File naming in the COMBMORC 2022 experiment

The file naming principle for **SSC calibration** output should be the following:
AAAA_SSC_CAL_N

Where	is one of these
AAAA	DEMA, DSA, GR, LU, NGU, SSM, STUK
CAL	CAL
N	1, 2, 3, etc, optional, if more than one SSC calibration file output

The file naming principle for **SSC shield thickness assessment** output should be the following:
AAAA_SSC_DDDDD_M_N

Where	is one of these
AAAA	DEMA, DSA, GR, LU, NGU, SSM, STUK
DDDDD	HPGE, NAI3I, NAI2L, NAI4L, NAI8L, NAI16L
M	The setup number for the source placed at the measurement site "M"
N	1, 2, 3, etc, optional, if more than one measurement is made for the same detector and setup number

The file naming principle for **SODAC source distance and activity assessment** output should be the following:
AAAA_SODAC_DDDDD_M_N

Where	is one of these
AAAA	DEMA, DSA, GR, LU, NGU, SSM, STUK
DDDDD	HPGE, NAI3I, NAI2L, NAI4L, NAI8L, NAI16L
M	The setup number for the source placed at the measurement site "M"
N	1, 2, 3, etc, optional, if more than one measurement is made for the same detector and setup number

The file naming principle for **ROI data** output as csv-files from shield thickness calibration site C should be the following:
AAAA_CAL_DDDDD_ROI_M_N.csv

Where	is one of these
AAAA	DEMA, DSA, GR, LU, NGU, SSM, STUK
DDDDD	HPGE, NAI3I, NAI2L, NAI4L, NAI8L, NAI16L
M	The setup number for the source placed at the measurement site "C"
N	1, 2, 3, etc, optional, if more than one measurement is made for the same detector and setup number

The file naming principle for **ROI data** output as csv-files from road measurements should be the following:
AAAA_ROAD_DDDDD_ROI_SX_N.csv

Where	is one of these
AAAA	DEMA, DSA, GR, LU, NGU, SSM, STUK
DDDDD	HPGE, NAI3I, NAI2L, NAI4L, NAI8L, NAI16L
M	The setup number for the source placed at the measurement site “M”
SX	The road x-coordinate, which is the distance along the road with origo just opposite the source. S indicates negative (N) or positive (P) coordinates. Give NX for distance (m) before the source and PX after the source.
N	1, 2, 3, etc, optional, if more than one measurement is made for the same detector, position and setup number

The file naming principle for **Spectral data** output from shield thickness calibration site should be the following:
AAAA_CAL_DDDDD_SPECT_M_N

Where	is one of these
AAAA	DEMA, DSA, GR, LU, NGU, SSM, STUK
DDDDD	HPGE, NAI3I, NAI2L, NAI4L, NAI8L, NAI16L
M	The setup number for the source placed at the measurement site “C”
N	1, 2, 3, etc, optional, if more than one measurement is made for the same detector and setup number

The file naming principle for **Spectral data** output from road measurements should be the following:
AAAA_ROAD_DDDDD_SPECT_SX_N

Where	is one of these
AAAA	DEMA, DSA, GR, LU, NGU, SSM, STUK
DDDDD	HPGE, NAI3I, NAI2L, NAI4L, NAI8L, NAI16L
M	The setup number for the source placed at the measurement site “M”
SX	The road x-coordinate, which is the distance along the road with origo just opposite the source. S indicates negative (N) or positive (P) coordinates. Give NX for distance (m) before the source and PX after the source.
N	1, 2, 3, etc, optional, if more than one measurement is made for the same detector, position and setup number

The file naming principle for **Excel** output of SODAC results as xls-files from road measurements should be the following:
SODAC_AAAA_DDDDD_M.csv

Where	is one of these
AAAA	DEMA, DSA, GR, LU, NGU, SSM, STUK
DDDDD	HPGE, NAI3I, NAI2L, NAI4L, NAI8L, NAI16L
M	The setup number for the source placed at the measurement site “M”

The file naming principle for Excel output of SSC results as xls-files from shield thickness measurements at the road location opposite the source should be the following:
SSC_AAAA_DDDDD_M.csv

Where	is one of these
AAAA	DEMA, DSA, GR, LU, NGU, SSM, STUK
DDDDD	HPGE, NAI3I, NAI2L, NAI4L, NAI8L, NAI16L
M	The setup number for the source placed at the measurement site “C”

Appendix N. Participants in the COMBMORC 2022 experiment

Participants in the NKS COMBMORC 2022 field experiment in Barsebäck, October 11 - 13, 2022 are listed in Table N1. Fig N1 shows a photo of the participants outside the conference building "Grevinnan", which was used as headquarter and meeting place for the teams in the experiments.

Table N1. Participants in the NKS/COMBMORC field experiment in Barsebäck, October 11 - 13, 2022.

Country, Institution*	Name
Finland, STUK	Petri Smolander
Norway, DSA	Bredo Møller
Norway, DSA	Per Otto Hetland
Norway,DSA	Jon Drefvelin
Norway, NGU	Vikas Baranwal
Norway, NGU	Frode Ofstad
Iceland, GR	Gísli Jónsson
Iceland, GR	Kjartan Gudnason
Denmark, DEMA	Marie Lundegaard Davidsdóttir
Denmark, DEMA	Jan Gert Olsen
Denmark, DEMA	Charlotte Alfast Espensen
Sweden, LU	Mattias Jönsson
Sweden, LU	Marius-Catalin Dinca
Sweden, LU	Kerstin Lundmark
Sweden, LU	Christopher L. Rääf
Sweden, LU	Robert Finck

* SSM, Sweden did not participate in the COMBMORC 2022 field experiment as originally planned, because personnel resources could not be made available.

Fig C1. COMBMORC 2022 participants outside the headquarter “Grevinnan”. From left: Vikas Baranwal, Frode Ofstad, Jon Drefvelin, Bredo Möller, Per Otto Hetland, Petri Smolander, Kjartan Gudnason, Gísli Jónsson, Mattias Jönsson, Marius-Catalin Dinca, Robert Finck, Marie Lundegaard Davidsdóttir, Charlotte Alfast Espensen. Photo by Kerstin Lundmark.

Bibliographic Data Sheet **NKS-476**

Title	COMBMORC - Combined analysis of primary and scattered components in mobile gamma spectrometric data for detection of materials out of regulatory control, NKS-B COMBMORC Report 2022
Author(s)	Christopher L. Rääf[1] (chair), Robert R. Finck[1] (co-chair), Vikas C. Baranwal[5], Marius-Catalin Dinca[1], Jon Drefvelin[6], Charlotte Alfast Espensen[2], Kjartan Guðnason[4], Per Otto Hetland[6], Gísli Jónsson[4], Mattias Jönsson[1], Marie Lundgaard Davidsdóttir[2], Bredo Møller[6], Frode Ofstad[5], Jan Gert Olsen[2], Petri Smolander[3],
Affiliation(s)	[1]Medical Radiation Physics, ITM, Lund University, Sweden [2]Danish Emergency Management Agency, Denmark [3]Radiation and Nuclear Safety Authority, Finland [4]Icelandic Radiation Safety Authority, Iceland [5]Geological Survey of Norway, Norway [6]Norwegian Radiation and Nuclear Safety Authority, Norway
ISBN	978-87-7893-571-7
Date	August 2023
Project	NKS-B / COMBMORC, Contract: AFT/B(22)2
No. of pages	192
No. of tables	84
No. of illustrations	147
No. of references	13
Abstract max. 2000 characters	The NKS-supported research project COMBMORC 2021-2022 aimed to develop combined methods within mobile gamma spectrometry to search for radiation sources that have come out of the authorities' control (Material Out of Regulatory Control, MORC). In 2022, mobile gamma spectrometry teams from the Nordic countries conducted a joint field experiment in southern Sweden. The experiment was to test region-of-interest (ROI) based methods to determine ratios between detector recordings from Compton scattered and primary radiation along a road past a Cs-137 source to determine the distance, shielding and activity of the source. The assessment used two newly developed Excel applications (SSC and SODAC). On average, the distance determination was underestimated by 20 ± 3 per cent at source-detector distances of 30 - 90 m. The shield thickness

determination was overestimated on average by 4 ± 9 per cent for building material thicknesses 0 - 330 kg/m^2.

Key words Mobile gamma spectrometry, orphan sources, shielding